UNIVERSITAT DE BARCELONA

Biofilms microbianos: Virulencia e interacciones hongo-bacteria

Betsy Verónica Arévalo Jaimes

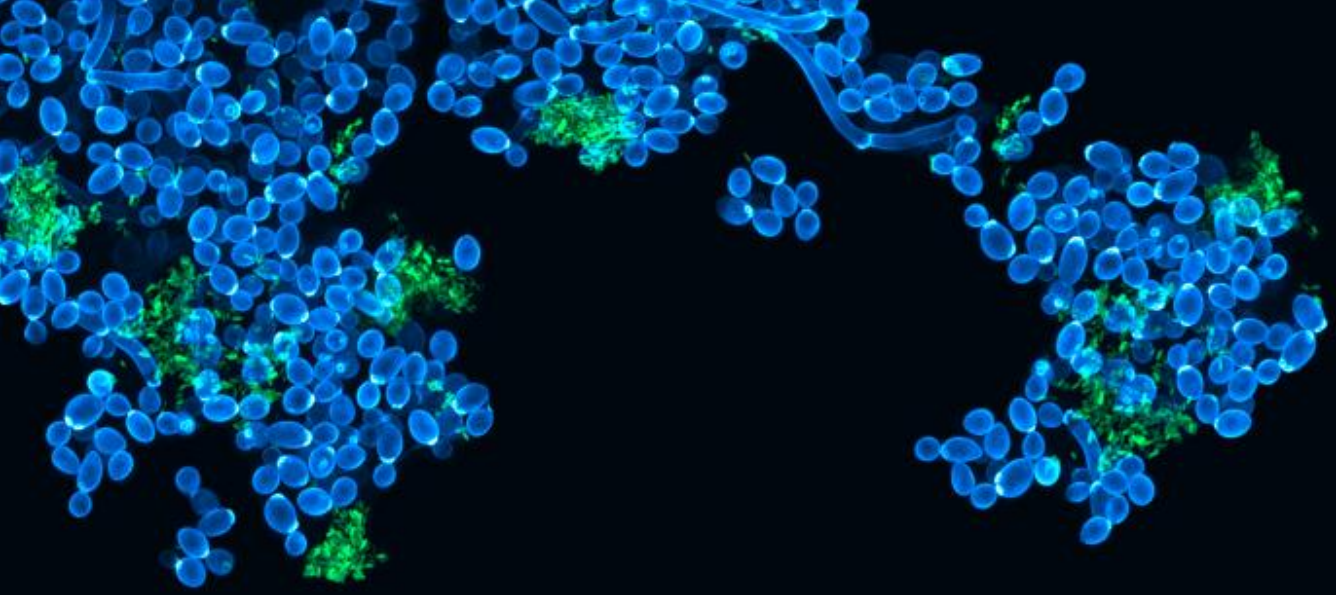

Biofilms microbianos: virulencia e interacciones hongo-bacteria

Tesis doctoral

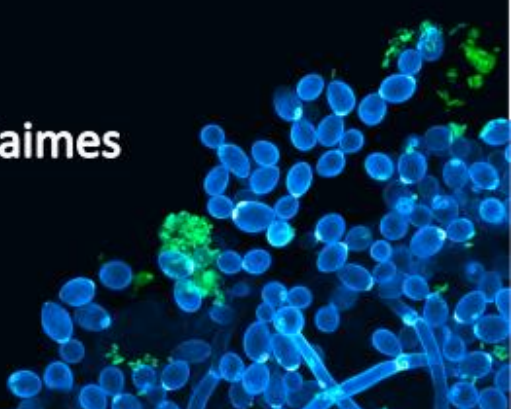

Betsy Verónica Arévalo Jaimes

UNIVERSITAT DE BARCELONA

FACULTAT DE BIOLOGIA

BIOFILMS MICROBIANOS: VIRULENCIA E INTERACCIONES HONGO-BACTERIA

Tesis doctoral

Betsy Verónica Arévalo Jaimes

Barcelona, 2024

Facultat de Biologia

Departament de Genètica, Microbiologia i Estadística

Programa de Doctorado en Biomedicina

BIOFILMS MICROBIANOS: VIRULENCIA E INTERACCIONES HONGO-BACTERIA

Memoria presentada por

Betsy Verónica Arévalo Jaimes

para optar al grado de

Doctora por la Universitat de Barcelona

Tesis dirigida y tutorizada por el Dr. Eduard Torrents Serra

Betsy Verónica Arévalo Jaimes

Doctoranda

A mi madre

“Búscate un amigo que te falle
un amor que te maldiga
busca un sueño que te estalle
pa’ que aprendas que de migas
se construye el porvenir,
y cuando estés
en el fondo de los fondos,
ya verás que no hay camino
que no sea el de subir…”

Resumen

En la naturaleza la mayoría de los microorganismos viven en comunidades protegidas por una matriz extracelular. Estas agrupaciones, denominadas biofilms, generalmente albergan múltiples especies de microorganismos que interactúan entre sí. En el contexto biomédico, los biofilms se asocian con infecciones comunes, infecciones causantes de morbilidad severa e incluso infecciones causantes de mortalidad. Una vez adquiridas, estas infecciones son difíciles de erradicar, generando típicamente enfermedades recurrentes y/o crónicas. La consecuente prolongación en las hospitalizaciones genera una carga económica considerable e impacta negativamente en la calidad de vida de los pacientes. A pesar de esto, actualmente existen varias limitaciones que dificultan el manejo adecuado de las infecciones causadas por biofilms.

La presente tesis estudió interacciones ambientales e inter-especies que influencian las características de los biofilms de hongos del género *Candida* y bacterias patógenas, siendo de particular interés aquellas relacionadas con la susceptibilidad y la virulencia.

En primer lugar, se evaluó el impacto de cuatro medios de cultivo comúnmente usados en las principales características patogénicas de *Candida parapsilosis*. Las variaciones obtenidas en la tasa de crecimiento, morfología, susceptibilidad y virulencia asociadas al medio de cultivo resaltan el papel de las adaptaciones metabólicas en la patogenicidad de esta levadura y señalan la importancia de elegir adecuadamente las condiciones de los diseños experimentales.

Luego, se estudiaron biofilms polimicrobianos de *Candida albicans* y *Pseudomonas aeruginosa*. Los resultados demuestran que el orden de colonización de las especies es un factor importante en el establecimiento de las interacciones entre estos microorganismos. En este escenario, los efectos de prioridad no sólo influencian la biomasa de las especies, sino también la estructura, susceptibilidad y virulencia del biofilm resultante.

Por otra parte, el estudio de las interacciones no físicas entre *C. albicans* y *Staphylococcus aureus* permitió identificar que cambios ambientales relacionados con el pH y la disponibilidad de recursos resultan en nuevos fenotipos de *S. aureus*. Estas variantes presentan cambios en la expresión de factores de virulencia pertenecientes al sistema *agr*, que impactan negativamente la supervivencia de larvas de *Galleria mellonella*.

Finalmente, conscientes de la necesidad de contar con métodos y plataformas confiables para la realización de pruebas de susceptibilidad de biofilms, se evaluó el uso de diferentes tinciones en el estudio de los biofilms de *C. parapsilosis*. De esta manera, se encontró que las tinciones Syto 9, Naranja de tiazol y Diacetato de fluoresceína tenían un bajo rendimiento en el marcaje de *C. parapsilopsis*, a diferencia de la tinción FUN-1. Adicionalmente, se diseñó un dispositivo de microfluídica para el estudio de biofilms bacterianos en condiciones dinámicas. El BiofilmChip permite la formación de biofilms partir de cepas de laboratorio, aislamientos clínicos y muestras de pacientes, proporcionando condiciones que se asemejan a las encontradas en infecciones naturales. Además, posee un método de lectura rápido y sencillo basado en la impedancia, que permite monitorear el crecimiento y los cambios de biomasa asociados a la efectividad del tratamiento.

En conclusión, el presente trabajo demuestra la importancia de caracterizar las respuestas de los microorganismos que crecen en biofilms frente a variaciones ambientales, para así definir mejores protocolos para su estudio. Además, resalta la necesidad de estudiar las coinfecciones hongo-bacteria como una comunidad, donde las interacciones físicas y químicas y los efectos de prioridad pueden aumentar el potencial patogénico de los microorganismos. Esto permitirá la formación de biofilms en condiciones más realistas, lo que se traducirá en avances de conocimiento en el campo. Por último, el desarrollo conjunto de métodos para la evaluación de susceptibilidad en biofilms, brindará las herramientas necesarias para ofrecer un tratamiento con mayor probabilidad de éxito en el manejo de las infecciones.

Abstract

In nature, most microorganisms live in communities protected by an extracellular matrix. These assemblies, known as biofilms, typically harbor multiple interacting species. In the biomedical context, biofilms are associated with infections that range from common to severe morbidity and even mortality. Once established, these infections are difficult to eradicate, often resulting in recurrent and/or chronic diseases. Consequently, the prolongation of hospital stays imposes a considerable economic burden and negatively impacts patients' quality of life. Despite this, several limitations currently hinder the proper management of biofilm-associated infections.

This thesis studied environmental and interspecies interactions that influence the characteristics of biofilms formed by fungi of the genus *Candida* and clinically relevant bacteria, with particular interest in those factors related to susceptibility and virulence.

First, recognizing the importance of the emergent pathogen *Candida parapsilosis*, culture media was identified as an important variable in biofilm formation, susceptibility, and virulence. Then, the performance of conventional fluorescent dyes for antifungal susceptibility testing of this yeast was evaluated, highlighting the necessity of optimal assessment of techniques before implementation.

Second, microbial interactions between *Candida albicans* and the bacteria *Pseudomonas aeruginosa* and *Staphylococcus aureus* were studied by two different approaches, showing that interkingdom interactions (physical, chemical and priority effects) can impact positively the virulence of co-infections.

Finally, the BiofilmChip, a microfluidic device that allows the formation and susceptibility testing of bacterial biofilms through impedance readings, was designed and validated as a versatile and easy- to-implement tool.

In conclusion, this work demonstrates the importance of characterizing the responses of microorganisms growing in biofilms to environmental variations to define better research protocols. Additionally, it highlights the need to study fungal-bacterial coinfections as a community, where interspecies interactions can increase the pathogenic potential of the microorganisms. Lastly, the development and validation of methods for biofilm susceptibility testing will improve the likelihood of success in managing infections.

Índice

Lista de tablas y figuras

Abreviaturas

ADNe	Ácido desoxirribonucleico extracelular
AmB	Anfotericina B
AMPs	*Antimicrobial peptides* - Péptidos antimicrobianos
BHI	*Brain Heart Infusion* - Infusión Corazón Cerebro
BQ	Bronquiectasia no asociada a fibrosis quística
BSIs	*Bloodstream infections* - Infecciones del torrente sanguíneo
CAS	Caspofungina
CA-UTIs	*Catheter-Associated Urinary Tract Infections* - Infecciones del Tracto Urinario Asociadas a Catéter
CDC	*Control Diseases Center* - Centro de Control de Enfermedades
CFUs	*Colony Forming Units* - Unidades Formadoras de Colonia
CLSM	*Confocal Laser Scanning Microscopy* - Microscopía Confocal de Escaneo Láser
CV	Cristal Violeta
CW	*Calcofluor white* - Blanco de calcoflúor
ECM	*Extracellular matrix* - Matriz extracelular
EIS	*Electrochemical Impedance Spectroscopy* - Espectroscopía de Impedancia Eléctrica
EPOC	Enfermedad Pulmonar Obstructiva Crónica
ESCMID	*European Society of Clinical Microbiology and Infectious Diseases* - Sociedad Europea de Microbiología Clínica y Enfermedades Infecciosas
FDA	*Fluorescein diacetate* – Diacetato de fluoresceína
FQ	Fibrosis Quística
GlcNAc	N-acetilglucosamina
HAIs	*Hospital Acquired Infections* - Infecciones Adquiridas en los Hospitales
LIPs	Lipasas
MER	Meropenem
MIC	*Minimal Inhibitory Concentration* - Concentración Mínima Inhibitoria
MRSA	*Methicillin-resistant* Staphylococcus aureus - *Staphylococcus aureus* Resistente a la Meticilina

MSCRAMM	*Microbial Surface Component Recognizing Adhesive Matrix Molecules* - Componentes de Superficie Microbiana que Reconocen Moléculas de Matriz Adhesivas
NETs	*Neutrophil Extracellular Traps* - Trampas Extracelulares de Neutrófilos
NIH	*National Health Institutes* - Institutos Nacionales de Salud
OMS	Organización Mundial de la Salud
PCR	*Polymerase Chain Reaction* - Reacción en Cadena de la Polimerasa
PDMS	Polidimetilsiloxano
PIA	*Polysaccharide Intercellular Adhesin* - Adesina Intercelular de Polisacáridos
ROS	*Reactive Oxygen Species* - Especies Reactivas de Oxígeno
RPMId	*Roswell Park Memorial Institute dextrose* - Roswell Park Memorial Institute dextrosa
SAgs	Superantígenos
Saps	*Secreted aspartyl proteinases* - Aspartil proteasas secretadas
SSIs	*Surgical Site Infection* - Infecciones de Sitio Quirúrgico
S9	Syto 9
TO	*Thiazole Orange* – Naranja de tiazol
TSB	*Trypticase Soy Broth* - Caldo de Triptona Soja
T3SS	*Type III Secretion system* - Sistema de Secreción Tipo III
UTIs	Urinary Tract Infections - Infecciones del Tracto Urinario
VAP	*Ventilator Associated Pneumonia* - Neumonía Asociada a Ventilador
YPD	*Yeast Peptone Dextrose* - Extracto de levadura Peptona Dextrosa

Introducción

1. Biofilms

A finales del siglo XVII, Anthony van Leeuwenhoek vio mediante su microscopio primitivo **agregados de microbios** en muestras de su propia boca [1]. Dos siglos después, Louis Pasteur observó agregados de bacterias que acidulaban el vino [2]. Pero no fue sino hasta el siglo XX, que **el crecimiento sésil de los microbios fue reconocido como un modo de vida ubicuo y predominante de ecosistemas naturales y artificiales, incluyendo interacciones comensales y patogénicas** [3]. Se estima que el 40-80% de los procariotas vive en este estado [4].

En la década de los 30, el término "*film*" (película) fue empleado en microbiología marina para describir la capa biológica de agregados bacterianos adheridos a las superficies de los barcos [5]. Posteriormente, gracias a estudios de microscopía, se descubrió que los "*biological films*" (película biológicas) no eran necesariamente capas planas uniformes, sino que su estructura era heterogénea, y los microorganismos podían estar presentes en distintas conformaciones [3].

En los años 70, se realiza la primera observación de agregados bacterianos en muestras de esputo de pacientes con fibrosis quística (FQ) infectados con *Pseudomonas aeruginosa* [6]. De esta forma, en los años 80 el término "*biofilm*" (biopelícula) es introducido en el campo de la microbiología clínica por John William Costerton [5]. Este hecho ocurrió de manera conjunta con el hallazgo de que los microbios en biofilms poseen **mayor resistencia al tratamiento con antimicrobianos que cuando están en estado plantónico** [7]. La palabra biofilm se establece entonces como el término para designar a "agregados de células microbianas adheridas a una superficie biótica o abiótica, contenidas en una matriz de sustancias poliméricas extracelulares de origen microbiano" [8].

Sin embargo, los biofilms también **pueden formarse en la interfaz de dos microambientes o como agregados en suspensión**. Por ejemplo, *P. aeruginosa* forma biofilms en el moco de las vías respiratorias [9]. Así mismo, **la matriz extracelular puede contener componentes derivados del huésped** [8]. Por estas razones, la definición de biofilm fue modificada, y se describió como el "consorcio estructurado de células microbianas rodeadas por una matriz polimérica autosecretada" [8]. No obstante, un nuevo modelo

conceptual más amplio, en el que los agregados microbianos adheridos o no a una superficie son considerados biofilms, fue propuesto recientemente [10]. En esta definición, **la agregación de los microorganismos es la característica principal de los biofilms**, por tanto comprende estructuras microbianas descritas previamente como flóculos, gránulos, tapetes (*mats* en inglés), etc. [10]. Los agregados se definen además como **heterogéneos**, **compuestos de múltiples microambientes que a su vez han sido producidos y modelados por factores ambientales** [10].

Adicionalmente, la visión tradicional del biofilm como una colección de células individuales que representa la etapa de vida sésil de los microorganismos ha empezado a ser cuestionada [11]. Diferentes características propias de los biofilm han llevado a considerar el paradigma opuesto. Esto resulta en la conceptualización de los biofilm como agregados multicelulares que usan el modo de vida unicelular como estadio intermedio de dispersión [11]. Aunque el debate actualmente permanece abierto, el rol de los biofilms en la naturaleza y los ambientes antropogénicos hace indiscutible la necesidad del estudio de este modo de vida. Tanto así, que hoy en día el término biofilm es ampliamente usado en la comunidad biomédica, y **se asocia con características propias y consecuencias clínicas relevantes en la profilaxis y el éxito de las estrategias terapéuticas en las infecciones crónicas** [3].

1.1 La comunidad microbiana

La comunidad microbiana de un biofilm puede estar compuesta por una sola especie, formando **biofilms monomicrobianos**, o múltiples especies, dando lugar a **biofilms polimicrobianos** [12]. En algunas ocasiones, especies bacterianas interactúan con arqueas y/o hongos, generando lo que se conoce como **biofilms inter-reino** (*interkingdom* en inglés) [13]. En la naturaleza, los biofilms por lo general albergan diferentes especies, siendo tan diversos como los microrganismos que los componen (Figura 1) [14]. La naturaleza polimicrobiana de los biofilms involucra la coexistencia de múltiples especies en un mismo espacio [15]. **Los comportamientos multicelulares dentro y entre las especies de estas comunidades organizadas son coordinados por diferentes interacciones físicas y químicas** [16]. Dichas interacciones pueden ser cooperativas o competitivas/antagonistas.

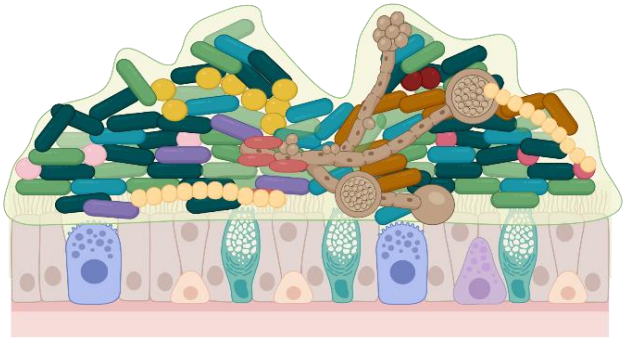

Figura 1. Representación de un biofilm polimicrobiano. Imagen creada en Biorender.

Las estrategias de cooperación se llevan a cabo cuando dos o más partes comparten un interés, mientras que **la competencia** favorece el crecimiento de una especie sobre la otra [15]. **Ambos tipos de interacción son necesarios para mantener el balance y la biodiversidad del biofilm** [11, 16]. Sin embargo, la homeóstasis de la comunidad microbiana requiere que los mecanismos de cooperación y sinergia superen los efectos antagónicos presentes [15]. Tanto el **medio ambiente** como el **orden de colonización** de las especies han sido identificados como factores importantes en la determinación del tipo de interacción que se establecerá en los biofilms polimicrobianos [15]. En la Tabla 1 se pueden consultar algunos ejemplos de mecanismos de sinergia y competencia/antagonismo descritos entre los microorganismos que conforman un biofilm.

Diversos procesos biológicos de las interacciones químicas microbianas están regulados mediante el sistema de comunicación célula-célula [16]. Este sistema, denominado ***quorum sensing***, se basa en la secreción, detección y respuesta a pequeñas moléculas de señalización difusibles [16]. Por ende, el *quorum sensing* **dirige actividades sociales de los microbios, jugando un papel importante en la virulencia a nivel poblacional** [16]. Además, las moléculas de este sistema de secreción son de gran importancia en la comunicación microbiana inter-reino, especialmente entre hongo y bacteria [13].

Otro tipo de interacción importante involucra a los bacteriófagos, los cuáles han demostrado tener un impacto en la ecología y evolución de las comunidades microbianas [13]. Por ejemplo, la inducción de profagos puede ocasionar lisis bacteriana, liberando moléculas y nutrientes que pueden favorecer positivamente la formación de biofilms.

Tabla 1. Principales interacciones de las comunidades microbianas de un biofilm.

	Mecanismo	Descripción	Ejemplo
Sinergia	Cohesión y Co-agregación	Los microbios producen diferentes componentes adhesivos e inducen interacciones intercelulares que permiten la formación de biofilms.	Colonizadores iniciales del biofilm oral de la placa dental proveen mecanismos específicos para la colonización de segundas especies.
	Interacciones metabólicas	Los subproductos del metabolismo de una especie son utilizados como fuentes de nutrientes por otra especie.	La simbiosis presente entre bacterias productoras de ácido láctico y bacterias que dependen del lactato como fuente de nutrientes.
	Interacciones vía *Quorum sensing*	Moléculas secretadas por algunos microorganismos inducen cambios en el comportamiento de otros.	Moléculas secretadas por *Streptococcus gordonii* promueven la filamentación de *Candida albicans.*
	Transferencia horizontal de genes	Intercambio de material genético entre las distintas especies.	Adquisición de plásmidos de resistencia.
	Producción de componentes benéficos	Microbios secretan moléculas que son utilizadas o benefician a otros.	Secreción de enzimas β-lactamasas protegen a microrganismos de la acción de antibióticos β-lactámicos
Competencia y antagonismo	Agotamiento de nutrientes y recursos	La habilidad de usar nutrientes de ciertos microorganismos promueve su crecimiento a expensas de los demás.	Poblaciones capaces de quelar hierro tiene una ventaja de crecimiento sobre las que no lo hacen.
	Producción de compuestos perjudiciales	Algunas especies secretan moléculas que tienen un efecto antimicrobiano en otras.	Producción de bacteriocinas y moléculas tóxicas.

La información presentada en esta tabla fue obtenida del artículo de revisión de Luo *et al*., 2022 [15].

Al final, la manera en que el conjunto de actores interactúe entre sí afectará profundamente la función, biomasa, estructura, diversidad y patogénesis del biofilm [13, 16, 17]. Así mismo, el costo de tales interacciones influirá en la coexistencia de las especies y la diversidad del biofilm [13].

1.2 La matriz extracelular

La matriz extracelular (ECM, por sus siglas en inglés) es el **conglomerado de diferentes tipos de biopolímeros, producidos en su mayoría por los microbios y que sirven de soporte a la estructura tridimensional** del biofilm [18]. La ECM rodea y embebe las células, por lo que representa el 90% de la biomasa total [18].

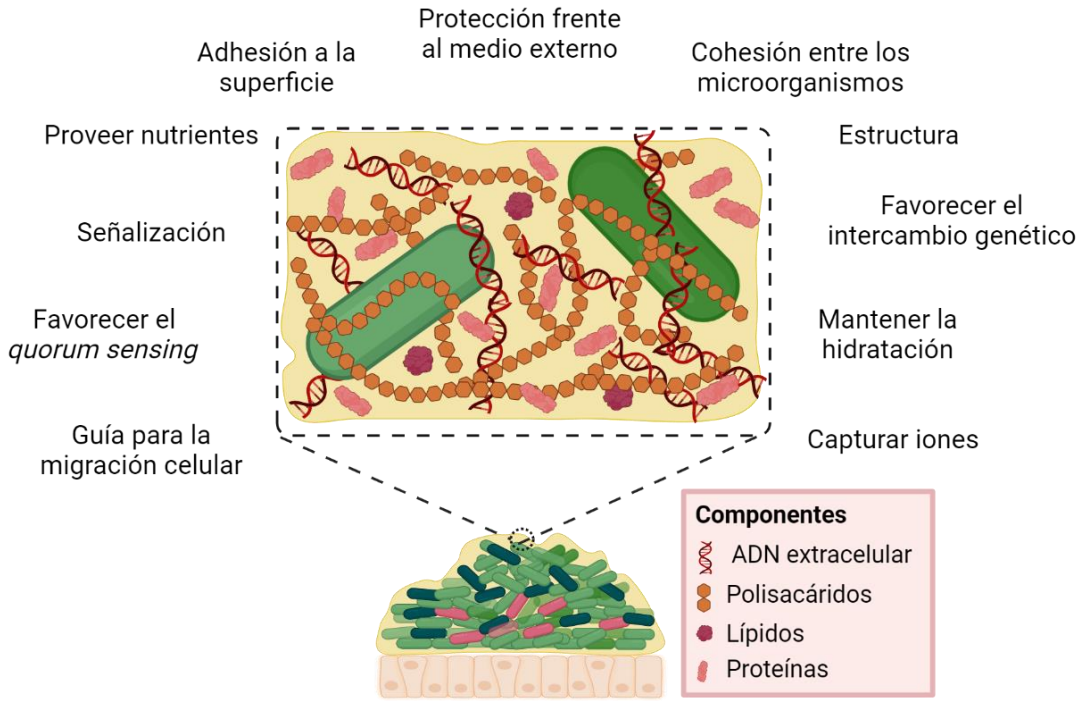

Figura 2. La matriz extracelular y sus funciones. Imagen creada en Biorender.

Además de **actuar como barrera física**, la ECM es la responsable de **mantener a la comunidad de microrganismos unida entre sí y a las superficies** [18, 19]. Dentro de las funciones de la ECM (Figura 2) también se encuentra **proveer nutrientes, capturar cationes y conservar un nivel de hidratación** adecuado [18, 20, 21]. La ECM contiene componentes propios, restos de lisis celular y enzimas extracelulares capaces de degradar partículas del medio externo, que aportan fuentes de carbono y energía a las células del biofilm [18]. A su vez, polímeros aniónicos presentes en la ECM pueden actuar como agentes quelantes de cationes [21].

El conjunto de biomoléculas que componen la ECM junto con su diversidad molecular, estructural y funcional, se conocen como **matrisoma** [22]. La composición de la ECM varía dependiendo de los microorganismos presentes, la temperatura, la disponibilidad de nutrientes y la hidrodinámica a la que el biofilm esté expuesto [18]. La constitución de la ECM es relevante en las infecciones clínicas pues influye en la respuesta inmune presentada por el huésped [23].

Por lo general, la ECM contiene:

- **Exopolisacáridos:** Son indispensables para la formación de biofilms, con funciones en el proceso de **adhesión**, la formación de **microcolonias** y el desarrollo de la **estructura tridimensional** (Sección 1.3) [18, 24].

- **Proteínas:** Los biofilms contienen cantidades considerables de **proteínas estructurales** que incluyen adhesinas de superficie celular, subunidades proteicas del flagelo o pili, fibras amiloides, proteínas secretadas extracelularmente y proteínas de la membrana externa de vesículas [18, 25]. Por otra parte, los biofilms contienen **enzimas** que pueden modular la estructura de la matriz mediante modificaciones localizadas, participar en el proceso de dispersión del biofilm y actuar como **factores de virulencia** [24].

- **ADN extracelular (ADNe):** Es una parte integral de la ECM y el modo de vida sésil. Participa en la adhesión y etapas iniciales de formación del biofilm, como **componente estructural**, en **procesos de transferencia genética**, reparación del ADN y como fuente de carbón, nitrógeno y fosfato [18, 24, 26]. El origen del ADNe es generalmente genómico y se relaciona principalmente con procesos de lisis, aunque mecanismos de secreción activa y liberación vía vesículas también han sido propuestos [24].

- **Lípidos y biosurfactantes:** Lípidos, lipopolisacáridos y biosurfactantes confieren a la ECM propiedades hidrofóbicas necesarias para la **adhesión** a ciertas superficies. Los biosurfactantes además poseen **propiedades antimicrobianas** [18]. Así mismo, vesículas de membrana pueden viajar a través de la ECM con material citoplásmico en su interior [24].

- **Agua:** Es por mucho el mayor componente por peso y volumen de la ECM y el biofilm, llegando a representar un 97% de la biomasa total [27, 28]. El agua forma estructuras dentro del biofilm descritas como poros o canales que **protegen a las células de la desecación** y permiten el **almacenamiento y transporte de nutrientes y desechos** [18, 27].

Estas biomoléculas interactúan entre sí y crean **microambientes heterogéneos dentro del biofilm sujetos a dinámicas temporales, con diferentes propiedades químicas y que influencian el metabolismo microbiano local** [22, 24]. La respuesta celular a los cambios

del ambiente extracelular hace que los componentes de la ECM actúen como **moléculas de señalización**, promoviendo cambios asociados al estilo de vida sésil, activando mecanismos de defensa y participando en el proceso de dispersión [21, 29, 30]. Además, la acumulación de ciertas biomoléculas de la ECM parecen servir como **guía para la migración celular**, favoreciendo la expansión de las colonias y una mayor colonización de las superficies [21].

1.3 El proceso de formación

El cambio del crecimiento plantónico al modo de vida sésil ocurre en respuesta a diferentes estímulos ambientales, como la disponibilidad de nutrientes, la temperatura y el pH [31]. El proceso de formación de un biofilm es complejo y dinámico, y en general, involucra tres grandes pasos [10, 32] (Figura 3).

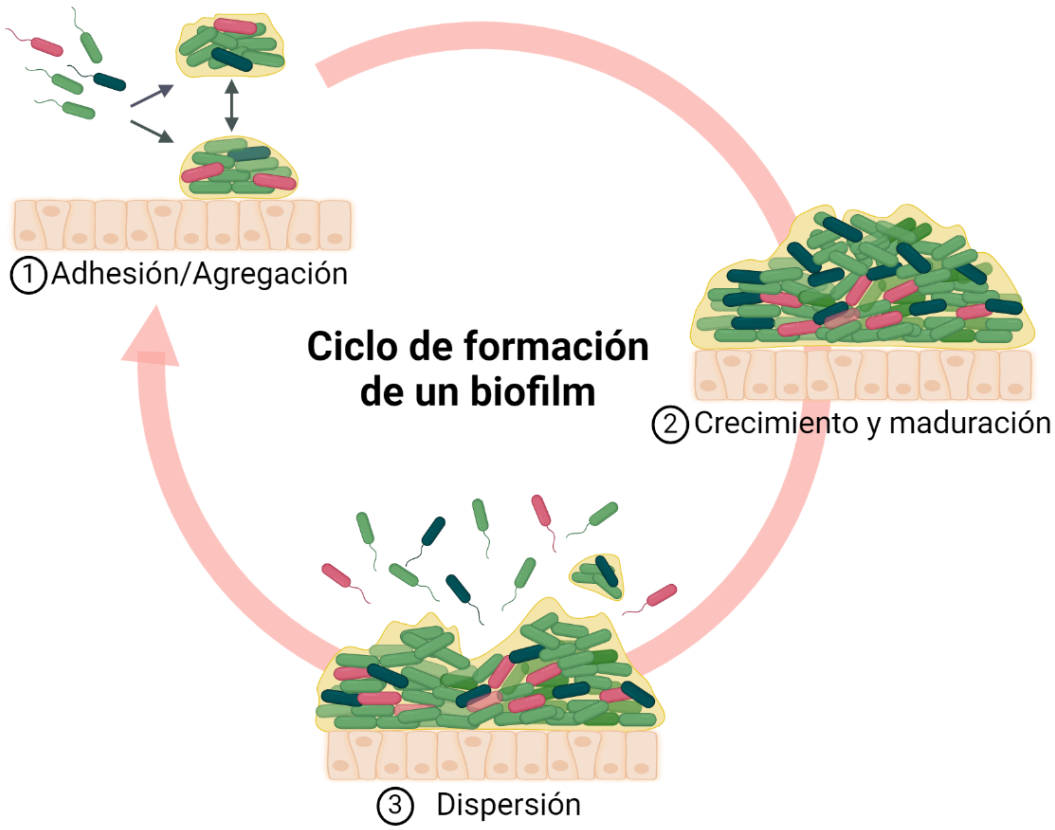

Figura 3. Proceso de formación de un biofilm. Imagen modificada de Blanco-Cabra *et al*. (2024) [33] en Biorender.

1.3.1 Adhesión/Agregación

Primero, los microorganismos se adhieren a una superficie o forman agregados entre ellos [10]. Esta unión conlleva **cambios transcripcionales** asociados al crecimiento sésil, como la perdida de flagelo y la producción de sustancias poliméricas, que vuelven la adhesión fuerte e irreversible.

1.3.2 Crecimiento y maduración

Posteriormente, la comunidad de microorganismos se expande mediante replicación y/o reclutamiento de células adyacentes [10]. El crecimiento de estas agrupaciones, denominadas microcolonias, va acompañado de la producción de la **ECM** hasta formar una estructura tridimensional compleja. La arquitectura y organización de los biofilms es especie dependiente y se ve afectada por condiciones ambientales [34]. Dentro de esta estructura se crean **gradientes de oxígeno, nutrientes, moléculas de señalización y productos de desecho** en dependencia de la profundidad del biofilm, siendo el centro el lugar con las condiciones más precarias [35-37]. Estas diferencias favorecen la aparición de **subpoblaciones con adaptaciones metabólicas**, donde las células de la capa más profunda tienen una tasa metabólica reducida y crecimiento lento [36].

1.3.3 Dispersión

Finalmente, células o pequeños agregados se desprenden del biofilm y se desplazan hasta encontrar un **nuevo lugar para colonizar** [10, 32]. Aunque las células de dispersión se encuentran en estado plantónico, estudios han mostrado que estas poseen un estado fisiológico diferente. Por ejemplo, en el caso de *P. aeruginosa*, las células de dispersión son más virulentas contra macrófagos y más sensibles a estrés por hierro [38]. Así mismo, las células de dispersión de *C. albicans* han sido descritas como pre-condicionadas para máxima virulencia [39]. Diferentes factores pueden causar la dispersión de los biofilms, por ejemplo alcanzar el límite poblacional, poca disponibilidad de nutrientes o las condiciones hidrodinámicas a las que el biofilm esté expuesto [31].

Durante la formación de biofilms el sistema ***quorum sensing*** es imprescindible [32]. En algunas especies bacterianas tiene un papel importante en la formación de la matriz extracelular. Además, permite monitorear la densidad celular y regular el comportamiento colectivo, siendo indispensables también en las etapas de maduración y dispersión [31, 34].

1.4 Los mecanismos de protección

Como hemos visto en las secciones anteriores, la formación de biofilms involucra procesos costosos energéticamente, como la producción de la ECM (Sección 1.2) y las interacciones microbianas (Sección 1.1) [13]. No obstante, en la mayoría de los escenarios naturales, los microbios viven en este estado. Esto se debe a que el modo de vida sésil ofrece a los microorganismos una serie de beneficios que compensa la inversión de recursos.

Se sabe que las bacterias pueden ser entre 10 a 1000 veces más tolerantes a los antibióticos creciendo en biofilms en comparación a su forma libre [36]. Esta disminución en la susceptibilidad se debe a distintos mecanismos (Figura 4) [40]. En primer lugar, los mecanismos de **resistencia genotípica** propios del crecimiento plantónico permanecen, como la selección de mutaciones que permiten evadir la acción de los antimicrobianos [20]. Sin embargo, algunas características propias del modo de vida de biofilm contribuyen en la disminución de la susceptibilidad de los microorganismos, lo que se denomina **resistencia fenotípica o tolerancia** [20].

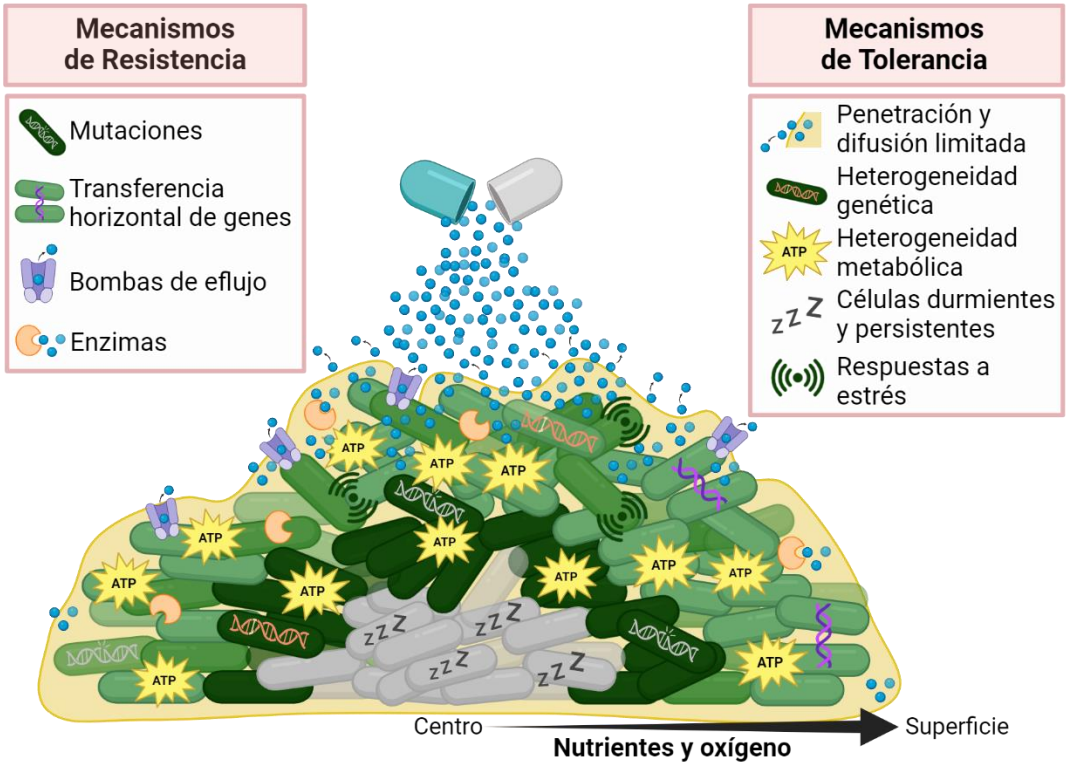

Figura 4. Principales mecanismos de resistencia y tolerancia al tratamiento antimicrobiano en microorganismos formando biofilms. Imagen creada en Biorender.

Dentro de los mecanismos que confieren a las células de los biofilms resistencia y tolerancia a los antimicrobianos se encuentran (Figura 4) [20, 30, 36, 41-44]:

- **La ECM:** Actúa como **una barrera física y química** frente los antimicrobianos y componentes del sistema inmune (Sección 1.2). La ECM puede adsorber, reaccionar y **limitar físicamente la penetración de las moléculas**. En algunas ocasiones enzimas extracelulares atrapadas en la ECM pueden **inactivar los compuestos químicos**. Además, la exposición a estrés oxidativo o concentraciones de antimicrobianos por debajo de la MIC puede inducir un aumento en la producción de la ECM.

- **La heterogeneidad poblacional**: Dentro de un biofilm, las células del interior poseen una **tasa metabólica y de replicación reducida** (células durmientes o persistentes), que les permite escapar frente a agentes antimicrobianos cuya actividad depende del crecimiento. Por otra parte, el hecho de ser una comunidad de microorganismos provee a los biofilms de **diversidad genética**. Esto, junto a la proximidad de las células y la abundancia de ADNe en la ECM, favorece la adquisición de genes de resistencia vía transferencia horizontal. Finalmente, diferentes **interacciones entre los microorganismos** (Sección 1.1) pueden traducirse en beneficios poblacionales que generan tolerancia. Por ejemplo, la secreción de metabolitos por una especie puede generar cambios en la pared celular de la otra. Así mismo, componentes de la ECM secretados por una especie sirven de protección para los demás miembros de la comunidad.

- **Factores protectores específicos:** Los microorganismos en biofilms pueden expresar **bombas de eflujo multidroga** como respuesta adaptativa frente condiciones ambientales adversas. Así mismo, la expresión de **regulones de respuesta a estrés**, como la respuesta estricta (*stringent response* en inglés) y la respuesta SOS, pueden conferir tolerancia y resistencia a los antimicrobianos. Por otra parte, las **propiedades viscoelásticas** de los biofilms dificultan su remoción mecánica, facilitando su persistencia.

La existencia de estos mecanismos de protección puede exponer a las células a **concentraciones sub-inhibitorias** de los agentes antimicrobianos, favoreciendo la aparición de **microrganismos multirresistentes** [36].

No obstante, la protección que el biofilm confiere a los microorganismos va más allá de la recalcitrancia a los agentes antimicrobianos. Este modo de vida les permite **colonizar nichos competitivos y sobrevivir a ambientes estresantes**. Las células que componen un biofilm tienen una **mayor tolerancia frente a diferentes condiciones ambientales hostiles**, como el pH y las temperatura extremas, alta salinidad, alta presión, radiación ultravioleta, desecación y escasez de nutrientes [37, 41]. E incluso, los biofilms son más **tolerantes a los ataques externos** de bacteriófagos, depredadores y los mecanismos de defensa del huésped [36, 37, 41].

2. Biofilms en el laboratorio

2.1 Modelos *in vitro* para el estudio de biofilms

El entendimiento de las características y propiedades de los biofilms permite el desarrollo de nuevas estrategias terapéuticas. Los modelos *in vitro* para el estudio de biofilms son indispensables en esta tarea, ya que propician el crecimiento de los microorganismos en este modo de vida en el entorno controlado del laboratorio. Dependiendo de la frecuencia en que el medio de cultivo es suministrado, los modelos *in vitro* se dividen en dos grandes grupos: estáticos y dinámicos (Figura 5).

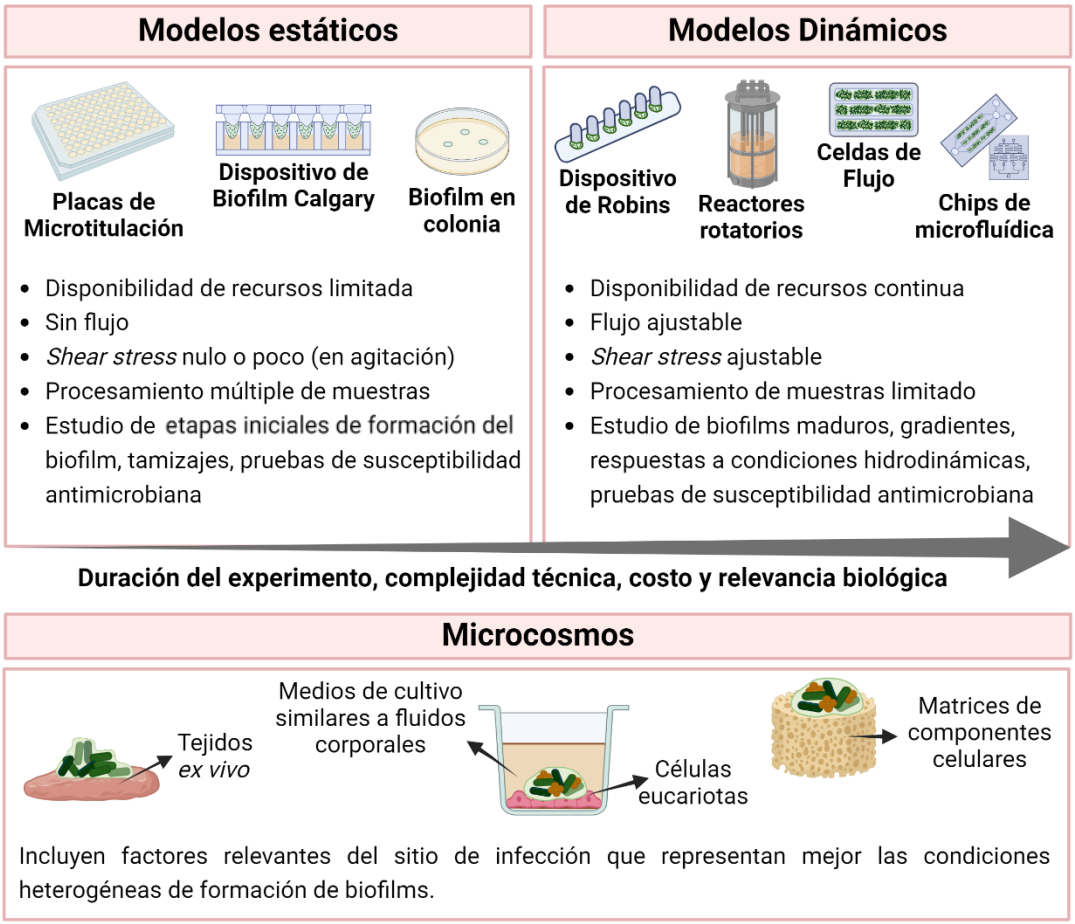

Figura 5. Principales modelos *in vitro* para el estudio de biofilms. Imagen creada en Biorender.

2.1.1 Estáticos

En estas plataformas la disponibilidad de nutrientes es finita y está limitada a las condiciones suministradas inicialmente [45, 46]. La formación y crecimiento de los biofilms se ve acompañado de la **depleción de nutrientes** y la **acumulación de productos de desecho**, lo que limita la duración de los experimentos [45, 46]. Sin embargo, el uso de estas plataformas es generalmente **sencillo** y **económico**, permitiendo la evaluación de **múltiples condiciones al mismo tiempo** (lo que en inglés se conoce como ***high-throughput screening***) [45-47]. Dentro de los modelos *in vitro* estáticos más comunes para el estudio de biofilms se encuentran:

- **Las placas de microtitulación**: Placas de poliestireno son inoculadas con cultivos microbianos e incubadas hasta obtener un biofilm en la superficie de los pozos. El crecimiento plantónico presente al final del experimento debe ser removido mediante lavados, lo que puede llevar a **desprendimiento del biofilm** y **subestimación de la biomasa** del mismo [45, 46].

- **El dispositivo de Biofilm Calgary:** Esta plataforma también hace uso de una placa de microtitulación para proveer el medio de cultivo. Sin embargo, el biofilm es formado en puntas que sobresalen de la tapa y se sumergen en el pozo cuando la placa se cierra [45, 46, 48]. Este sistema permite el cambio de la solución de crecimiento con **menor perturbación del biofilm** y **evita la sobreestimación de la biomasa** por células plantónicas sedimentadas [45].

- **El biofilm en colonia:** Este modelo los biofilms son crecidos como colonias en agar, lo que **permite la evaluación de cambios morfológicos** [45, 46]. Este método es relevante en el estudio de heridas crónicas [49].

Una limitación importante de estos modelos es que la **lectura es de punto final**, ya que las mediciones perturban al biofilm [45]. Nuevos modelos han incluido la monitorización en tiempo real, mejoras en reproducibilidad, aumento de la viabilidad del biofilm e inclusión de elementos particulares que mimetizan el microambiente de las infecciones clínicas [50]. La optimización ha sido posible mediante la inclusión de nuevas tecnologías, como el uso de plataformas bio-absorbentes como superficie de adhesión y la impresión 3D con biomateriales [50].

2.1.2 Dinámicos

Los modelos dinámicos proveen un **flujo constante de nutrientes** al biofilm, que a su vez **remueve el crecimiento plantónico y los productos de desecho** propios del crecimiento microbiano [45, 46, 51]. Estas condiciones **se asemejan más a las encontradas *in vivo*** (ej. cavidad oral y tracto urinario), lo que hace que los estudios de biofilm generen **resultados más confiables** [45]. Esto es de particular interés en el contexto clínico, donde la evaluación de susceptibilidad antimicrobiana debe predecir la eficacia del tratamiento y recuperación del paciente. Además, estos métodos permiten manipular parámetros, como la tensión cortante (*shear stress* en inglés) producida por la dinámica del fluido [46]. Sin embargo, estos modelos suelen ser **más complejos**, **costosos** y con **menos capacidad de procesamiento múltiple** [45, 51]. Dentro de los modelos *in vitro* dinámicos más comunes para el estudio de biofilms se encuentran:

- **El dispositivo de Robbins:** Este modelo permite la formación de biofilms en cupones a lo largo de un tubo con suministro constante de medio de cultivo [52]. Los cupones pueden ser de distintos materiales y el flujo puede alterarse a lo largo del experimento [45]. Aunque permite el **procesamiento de múltiple muestras**, la disposición en hilera con flujo unilateral hace que los biofilms no estén expuestos al mismo gradiente de nutrientes y desechos [51].

- **Los reactores rotatorios:** Estas plataformas incluyen el reactor anular rotatorio, el reactor de disco rotatorio y el reactor cilíndrico concéntrico [45]. Aunque cada dispositivo tiene su propio diseño, todas **permiten ajustar la tensión cortante** del biofilm de manera independiente al flujo del medio mediante la manipulación de la velocidad de rotación del sistema [45, 46].

- **Las celdas de flujo:** Esta plataforma consiste en una cámara de poliestireno cubierta con un cubreobjetos de vidrio, conectada mediante tubos a una bomba peristáltica que controla el flujo del medio de cultivo [45, 51]. Los principales problemas de este sistema son su **complejidad**, la formación de **burbujas de aire** que pueden perturbar el biofilm, la **obstrucción de los tubos** por crecimiento bacteriano, la alta demanda de **tiempo** y la **poca capacidad de procesamiento múltiple** de muestras [51]. Sin embargo, permite la **monitorización en tiempo real** del biofilm mediante **microscopía** y genera **condiciones hidrodinámicas relevantes** en el estudio de las infecciones [51].

- **Los dispositivos de microfluídica:** Estos dispositivos son modelos dinámicos miniaturizados que ofrecen **condiciones hidrodinámicas más controladas** y **menor requerimiento de reactivos** [45]. Al igual que las celdas de flujo, pueden permitir la **visualización** y **monitorización del biofilm en tiempo real** [51]. El **diseño de los chips es flexible**, lo que permite incorporar diferentes propiedades, como gradientes químicos, automatización, e incluso procesamiento múltiple de muestras [51]. Sin embargo, a pesar de las mejoras, estas plataformas siguen presentando problemas de **burbujas de aire** y **obstrucción de tubos**. Además, las condiciones controladas del flujo impiden el estudio de la estructura macroscópica del biofilm [45].

2.1.3 Microcosmos

Con el objetivo de ir más allá, innovaciones recientes han llevado al desarrollo de nuevos modelos *in vitro* denominados **microcosmos**. Estos sistemas pueden ser estáticos o dinámicos, pero se diferencian por el **uso de fuentes de nutrientes o superficies relevantes en los sitios de infección**. Para conseguir esto se puede hacer uso, por ejemplo, de tejidos *ex vivo*, medios de cultivo que simulan fluidos corporales (saliva, esputo, orina, etc.) o componentes tisulares (células eucariotas, colágeno, plasma, etc.) [46, 50, 51]. De esta manera, se crean escenarios más complejos que **representan mejor la heterogeneidad de las infecciones** [46].

2.2 Métodos de cuantificación

El estudio de los biofilms requiere de métodos de lectura que permitan su caracterización una vez formados. Un resumen de los principales métodos utilizados para cuantificar la biomasa y actividad metabólica de los biofilms se presenta en la Tabla 2.

En algunas ocasiones es deseable diseccionar el biofilm mediante el estudio individual de sus componentes. En este escenario, la especificidad de los **fluoróforos** los ha convertido en una de las herramientas claves más utilizadas [53]. Estas moléculas pueden tener **afinidad por determinadas estructuras celulares**, como los ácidos nucleicos (Syto 9 y DAPI), la membrana celular (FM-464) o la pared celular (Blanco de calcoflúor) [53]. Así mismo, algunos fluoróforos permiten el **marcaje exclusivo de componentes de la ECM**. Por ejemplo, proteínas (SYPRO Ruby), polisacáridos (Concanavalina A) y lípidos (Vybrant DiD) [49].

Los fluoróforos están disponibles comercialmente en una amplia variedad de colores de emisión, lo que permite su combinación y el **marcaje simultáneo de diferentes componentes en una misma muestra**. Además, la lectura puede realizarse mediante diferentes métodos, incluyendo la microscopía de fluorescencia, microscopia confocal, citometría de flujo y los lectores multimodo [53].

Tabla 2. Principales métodos para la cuantificación de biofilms.

		Método	Fundamento	Ventajas	Desventajas
Biomasa	**Conteo directo** [47, 53, 54]	Recuento de Unidades Formadoras de Colonia (CFUs, por sus siglas en inglés)	Las células del biofilm se remueven de las superficies mediante raspado y/o sonicación. Luego se realizan diluciones seriadas y se siembran en placas de Petri.	- Fácil - Disponible en todos los laboratorios	- Técnica laboriosa - No permite la cuantificación de microrganismos viables pero no cultivables
		Conteo automatizado de células: Contador Coulter y Citometría de flujo	Las células del biofilm son removidas y resuspendidas para posteriormente ser pasadas por dispositivos con aperturas pequeñas que detectan y cuantifican las células mientras fluyen.	- Fácil y rápido - Preciso - Puede proporcionar información adicional de las células	- Requiere equipo especializado - Cuenta células vivas y muertas
	Tinción [47, 53, 55]	Ensayo de Cristal Violeta (CV)	La biomasa total del biofilm (células y ECM) se tiñe con el colorante cristal violeta. Luego la tinción se eluye y la intensidad de la solución es medida por absorbancia.	- Versátil - Procesamiento múltiple - No requiere remover el biofilm - Fácil y rápido	- Poco sensible y reproducible - La biomasa del biofilm puede verse alterada en los pasos de lavado - No distingue entre células vivas o muertas
	Biología molecular [47, 55]	Reacción en Cadena de la Polimerasa (PCR, por sus siglas en inglés)	El número de células en el biofilm es medido indirectamente por la amplificación de un gen constitutivo y específico para la comunidad microbiana.	- Rápido - Permite la diferenciación de especies - Sensible	- Sobreestimación de la biomasa celular por presencia de ADNe - Costoso - No distingue entre células vivas o muertas

Biomasa	**Técnicas de microscopía** [47, 53-55]	Microscopía Confocal de Escaneo Láser (CLSM, por sus siglas en inglés)	Las células son teñidas con fluoróforos que permiten la adquisición de imágenes de las distintas capas del biofilm. Las imágenes son procesadas posteriormente con softwares especializados que permiten cuantificar diferentes parámetros.	- Monitorización en tiempo real - No destructivo - Imágenes 3D de gran resolución - Alta disponibilidad de fluoróforos - Permite diferenciación de especies	- Requiere equipo especializado y personal entrenado - Costoso - Pueden presentarse sesgos en la toma y selección de imágenes.
	Métodos físicos [47, 53, 55]	Peso	La biomasa total del biofilm (células y ECM) es calculada por diferencia de peso (seco o húmedo) con la superficie de adhesión sin inocular.	- Fácil y rápido - Disponible en todos los laboratorios	- Técnica laboriosa - Poco sensible
		Espectroscopía de Impedancia Eléctrica (EIS, por sus siglas en inglés)	La biomasa del biofilm se mide como el cambio de conducción de la corriente en un electrodo a medida que los microbios crecen.	- Monitorización en tiempo real - No destructivo	- Datos difíciles de interpretar
Actividad metabólica	**Sales de tetrazolio** [49, 53]	MTT, CTC, INT, TTC y XXT	Sales de tetratozolio son reducidas por las células metabólicamente activas de los biofilms generando formazán, un compuesto colorimétrico fluorescente.	- Fácil y rápido - Disponible en todos los laboratorios - Distintos métodos de lectura.	- Lectura de punto final - Requieren optimización según la especie
	Resazurina [47, 49]	Alamar Blue, PrestoBlue y Celltiter-Blue	Estos compuestos de resazurina son convertidos por las células del biofilm metabólicamente activas en resorufina, un compuesto rosado con fluorescencia.	- No tóxico para eucariotas ni procariotas - Fácil y rápido - Distintos métodos de lectura.	- Requieren optimización según la especie
	Fluoróforos [49]	FDA, FUN-1, calceína, etc.	Las células son teñidas con moléculas que una vez procesadas por las células emiten fluorescencia.	- Distintos métodos de lectura	- Requiere equipo especializado - Requieren optimización según la especie

3. Biofilms en el contexto clínico

En nuestro cuerpo existen comunidades microbianas con un papel protector y funcional, como es el caso de la microbiota intestinal. No obstante, según Los Institutos Nacionales de Salud (NIH, por sus siglas en inglés), **el 65% de las enfermedades microbianas y el 80% de las infecciones crónicas son causadas por la formación y persistencia de biofilms**, representando un problema mayor de salud pública a nivel mundial [56, 57].

3.1 Infecciones ocasionadas por la presencia de biofilms

Los biofilms pueden ocasionar **infecciones comunes**, como la placa dental, las infecciones del oído medio y las infecciones del tracto urinario. No obstante, su formación también desencadena **infecciones asociadas a morbilidad severa y mortalidad**, como la endocarditis, la osteomielitis y las enfermedades pulmonares crónicas [58]. Los mecanismos de protección inherentes del modo de vida sésil (Sección 1.4) hacen que una vez adquiridas, estas infecciones sean difíciles de erradicar, generando típicamente **enfermedades recurrentes y/o crónicas** [59].

La respuesta inmune frente a los biofilms lejos de conseguir su erradicación, resulta generalmente en daños colaterales en el tejido adyacente, siendo un aspecto importante de la patología de estas infecciones [60]. A esto se suma que la fase de dispersión del ciclo de vida de los biofilms (Sección 1.3) puede generar **infecciones locales secundarias y/o infecciones sistémicas**, aumentando el riesgo de sepsis en el paciente [32, 61, 62].

En este contexto, **las Infecciones Adquiridas en los Hospitales** (HAIs, por sus siglas en inglés), también denominadas nosocomiales, son de gran importancia, incluyendo aquellas **asociadas a dispositivos médicos** [57, 63, 64]. La prevalencia de las HAIs a nivel global es de 0.14% e incrementa un 0.06% cada año [65]. Dentro de ellas cabe mencionar la Neumonía Asociada a Ventiladores (VAP, por sus siglas en inglés), las Infecciones de Sitio Quirúrgico (SSIs, por sus siglas en inglés), las Infecciones del Tracto Urinario Asociadas a Catéteres (CA-UTIs, por sus siglas en inglés) y las Infecciones del Torrente Sanguíneo (BSIs, por sus siglas en inglés) [66].

La prolongación de las hospitalizaciones causada por las infecciones por biofilms genera una **carga económica** considerable para el sector público y privado en todo el mundo [59, 61]. Además de reducir la **calidad de vida de los pacientes** y aumentar el **riesgo de**

mortalidad [23]. Por ejemplo, se estima que el costo promedio de hospitalización por caso de SSIs, VAPs y Ca-UTIs en Estados Unidos es de alrededor de $25.000, $10.000 y $1.000, respectivamente [67]. Mientras que el costo global estimado de biofilms en pacientes con VAP es de $920 millones por año [68]. Por todas estas razones, y reconociendo su importancia en la salud humana, la Sociedad Europea de Microbiología Clínica y Enfermedades Infecciosas (ESCMID, por sus siglas en inglés) publicó en el año 2014 una guía para el diagnóstico y tratamiento de infecciones asociadas a biofilms [69].

3.1.1 Asociadas a dispositivos médicos

Los biofilms pueden formarse en las superficies abióticas de dispositivos de uso médico, constituyendo un **riesgo para el bienestar del paciente y comprometiendo el funcionamiento del dispositivo** [28]. La contaminación de los dispositivos se asocia generalmente con la transferencia de microorganismos desde la piel del mismo paciente o de las manos de los trabajadores de la salud, así como del agua, superficies contaminadas, e incluso el aire [28, 70]. Estas infecciones van de moderadas a severas, y pueden incluir queratitis y septicemia [32].

De los 2 millones de infecciones nosocomiales reportadas por el Centro de Control de Enfermedades (CDC, por sus siglas en inglés) de Estados Unidos, entre el 50-70% son atribuidas al implante de algún dispositivo médico [71]. Con una estimación de 500.000 tipos diferentes de dispositivos médicos disponibles a nivel mundial, cada tejido del cuerpo humano puede entrar en contacto con estos biomateriales, teniendo riesgo de desarrollar una infección por biofilms [71, 72] (Figura 6).

La causa más común es el **uso de catéteres** [32]. Cuando se usan por menos de diez días se asocian con biofilms en la superficie externa, mientras que cuando son usados por más de 30 días se relacionan con biofilms en el lumen [32]. Estas infecciones generalmente involucran microrganismos oportunistas de la piel, como especies de *Staphylococcus* y *Candida* [71], y especies que pueden crecer fácilmente en fluidos intravenosos, como *P. aeruginosa*, *Enterobacter* y *Klebsiella* [32]. Sin embargo, los catéteres más usados son los urinarios, siendo en este caso *Escherichia coli*, *Enterococcus faecalis* y *Proteus mirabilis* las bacterias más comunes en las Infecciones del Tracto Urinario (UTIs, por sus siglas en inglés) [32].

Por otra parte, las **infecciones asociadas a implantes** representan el 25.6% de todas las infecciones nosocomiales en Estados Unidos [64]. Los implantes con mayor tasa de infección son los dispositivos de asistencia ventricular (40%), las derivaciones ventriculares (10%), las válvulas cardíacas, los marcapasos y desfibriladores (4%), y las prótesis de cadera e implantes de pecho (2%) [56]. Por lo general, el dispositivo infectado debe removerse y reemplazarse para eliminar el biofilm [62, 64, 66]. Dicho procedimiento quirúrgico, denominado **cirugía de revisión**, conlleva riesgos inherentes. Además, no garantiza la eliminación completa de los microbios, especialmente cuando se trata de implantes complicados como válvulas cardíacas y prótesis [66]. Las cirugías de revisión conllevan un costo anual global de casi 8 millones de dólares [68].

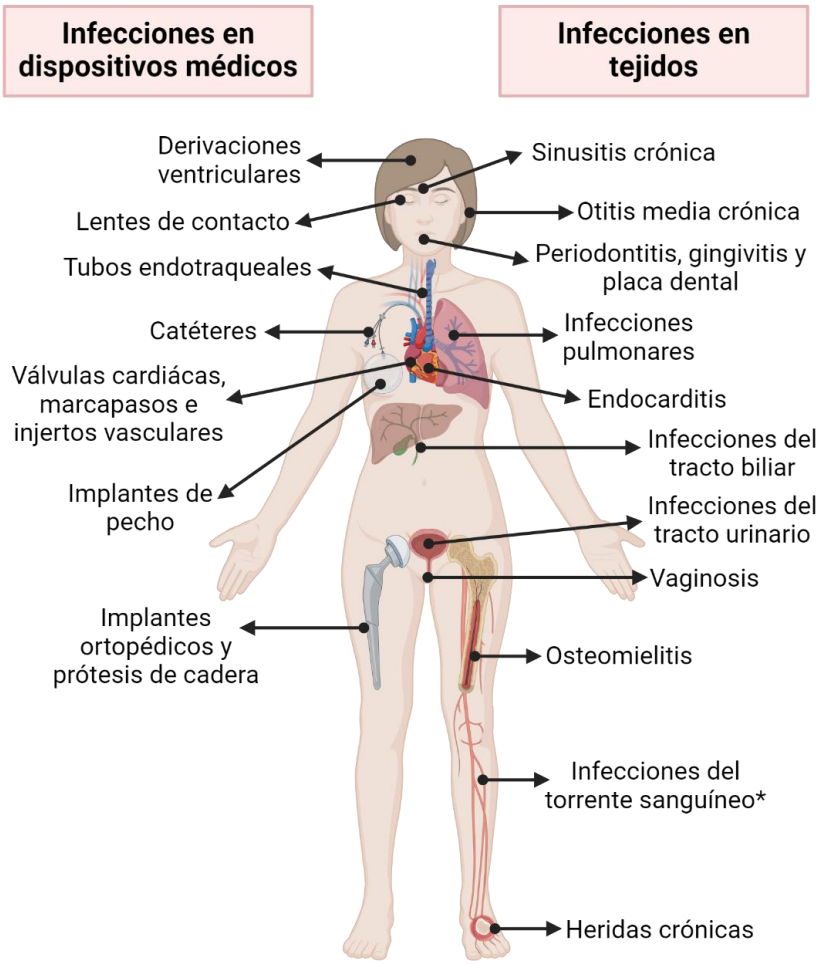

Figura 6. Infecciones asociadas a biofilms en el cuerpo humano. *Las infecciones del torrente sanguíneo son ocasionadas por las células de dispersión, y no por la presencia del biofilm *per se*. Imagen creada en Biorender.

3.1.2 No asociadas a dispositivos médicos

Las infecciones causadas por biofilms no asociadas a dispositivos médicos ocurren cuando nuestros tejidos proveen superficies bióticas para la adhesión de los microrganismos. Nuestras células y algunos de sus polímeros secretados pueden proveer una barrera adicional de protección en la penetración de los antimicrobianos, complicando su erradicación y de esta manera, prolongando la infección [32, 73]. Una gran variedad de infecciones asociadas a biofilms pueden presentarse en el cuerpo humano (Figura 6). A continuación, se presenta una breve descripción de cinco de ellas:

- **Infecciones de la cavidad oral:** alteraciones en el microbioma oral por parte de especies patógenas puede llevar al desarrollo de enfermedades infecciosas como la **periodontitis** y la **gingivitis** [56]. En estos casos, los biofilms desencadenan respuestas inflamatorias que dañan los tejidos suaves y huesos que soportan nuestros dientes [56, 70]. Además, las comunidades bacterianas también son las responsables de la **placa** y la **caries** [70].

- **Infecciones pulmonares:** la formación de biofilms en el tracto respiratorio está asociada a la reducción gradual de la diversidad de la microbiota natural [62]. En la **FQ,** los pacientes producen un moco viscoso ideal para la formación de biofilms [73, 74], siendo colonizados por *Staphylococcus aureus* y *Haemophilus influenzae* en las primeras etapas de vida [75]. Aunque los adultos pueden estar infectados por distintos microorganismos (*Achromobacter xylosoxidans, Stenotrophomonas maltophilia, Aspergillus fumigatus*, etc.), el 80% de los pacientes adquiere *P. aeruginosa* en la adolescencia tardía [73]. La presencia prolongada de *P. aeruginosa* genera inflamación crónica y daño tisular, que disminuye progresivamente la función pulmonar [75]. De manera similar, pacientes con **Enfermedad pulmonar obstructiva crónica** (EPOC) o **Bronquiectasia no asociada a fibrosis quística** (BQ) presentan infecciones persistentes y exacerbaciones relacionadas con biofilms de *H. influenzae, S. aureus* y *P. aeruginosa* [62, 74].

- **Heridas crónicas:** En algunas ocasiones el crecimiento de microorganismos interrumpe el proceso de curación y promueve inflamación, generando heridas crónicas [75]. Estas incluyen **úlceras de pie diabético, úlceras por presión y úlceras venosas**, y por lo general se asocian con biofilms de *S. aureus*, *Staphylococcus epidermidis* y *P. aeruginosa* [70, 75].

- **Endocarditis:** Heridas en el endotelio cardíaco pueden propiciar la formación de biofilms por parte de microrganismos oportunistas que causan **daño en las válvulas del corazón** [70]. Los biofilms además de dificultar el correcto funcionamiento de las válvulas cardíacas (naturales y prótesis), pueden desprender células que pueden actuar como **una fuente de infección continua del torrente sanguíneo** e incluso alcanzar **nuevos sitios de colonización** en el cerebro, riñones y extremidades [75]. Los microorganismos asociados a esta condición pertenecen a los géneros *Staphylococcus*, *Candida*, *Pneumococci*, *Streptococcus*, entre otras [70].

- **Osteomielitis:** Infecciones bacterianas en los huesos pueden provocar respuestas de células del sistema inmune que complican y permiten la propagación de la **infección en el tejido óseo** [70]. El microorganismo más aislado en esta rara condición en pacientes adultos es *S. aureus* (75% de los casos), pero otras especies recurrentes incluyen *Streptococci*, *Enterococci*, *Enterobacteria*, *Mycobacteria* y *P. aeruginosa* [62, 70, 73].

3.2 Estrategias para combatir biofilms

El impacto de los biofilms en la salud humana y su importancia a nivel global se debe en gran parte a los mecanismos de resistencia y tolerancia que poseen (Sección 1.4). Los **tratamientos convencionales fueron diseñados para células plantónicas, siendo, por lo general, inefectivos en la erradicación de los biofilms** [28, 33]. Por tal motivo, la comunidad científica trabaja constantemente en el desarrollo de alternativas terapéuticas que puedan sobrepasar los desafíos del tratamiento de estas comunidades, ya sea de manera independiente o como complemento a los antimicrobianos tradicionales [33].

3.2.1 Prevención

Las estrategias de prevención de biofilms se enfocan en encontrar agentes que interfieran en el proceso de formación, interrumpiendo el ciclo en las etapas iniciales para impedir el desarrollo de biofilm maduros. En este escenario, moléculas **inhibidoras del *quorum sensing*** y **bloqueadores de adhesinas y elementos de movilidad** (pilis y flagelos) interfieren en la adhesión de microorganismos a la superficie y la producción de la ECM [76-79].

Además, para prevenir la aparición de biofilms en dispositivos médicos, se han desarrollado estrategias de **recubrimiento de las superficies** con agentes antimicrobianos o anti-adhesivos. Así mismo, se han realizado **modificaciones de las superficies** e incluido **nuevos biomateriales** que dificultan la adhesión de los microorganismos [28, 80-82].

3.2.2 Erradicación

Diferentes estrategias para la eliminación de biofilms una vez establecidos han sido propuestas. De acuerdo con el mecanismo de acción, se encuentran (Figura 7):

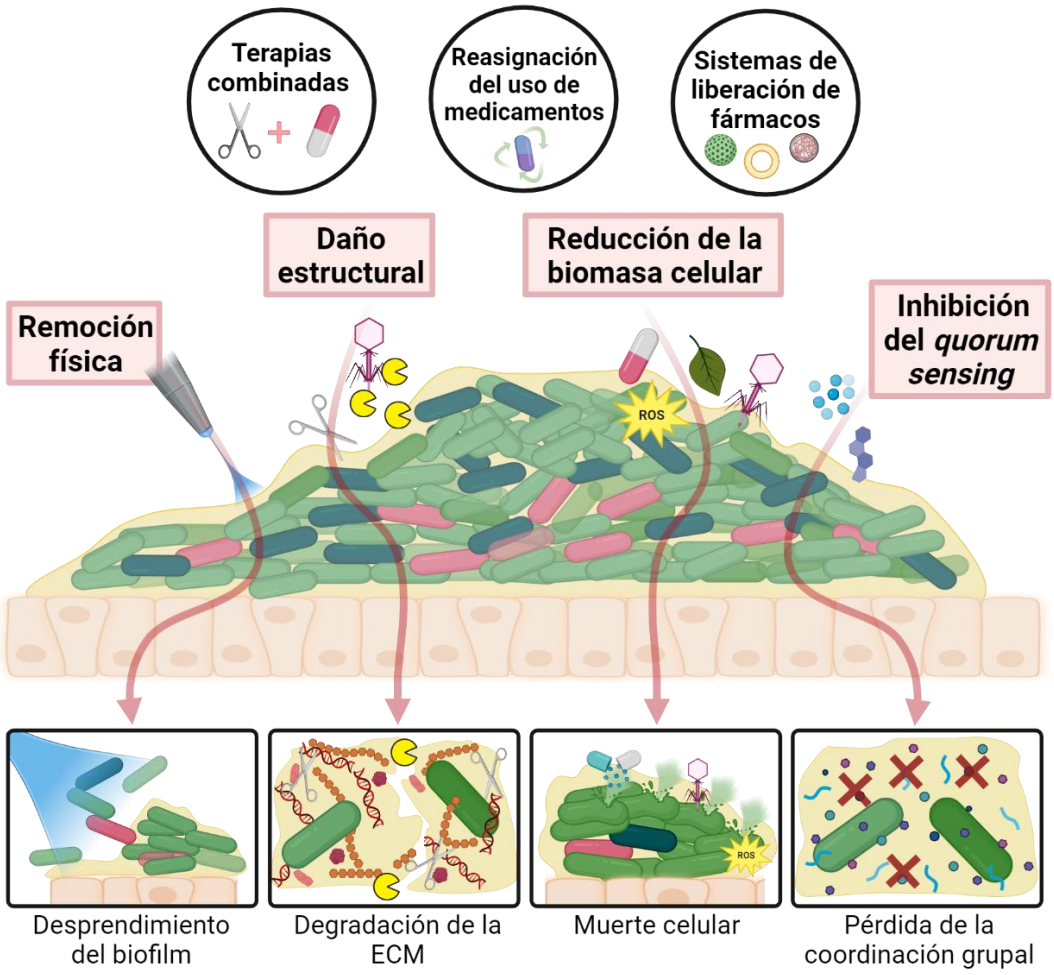

Figura 7. Principales estrategias para la erradicación de biofilms. Imagen modificada de Blanco-Cabra *et al*. (2024) [33] en Biorender.

- **Remoción física:** la eliminación física del biofilm mediante técnicas de **irrigación con chorros de agua** y **desbridamiento** son comunes en el manejo de heridas, infecciones orales e infecciones en las articulaciones [83]. Dentro de esta categoría también se incluye la **remoción de dispositivos médicos infectados** mediante las cirugías de revisión [84].

- **Daño estructural: Enzimas** capaces de degradar componentes de la ECM (Sección 1.2) afectan la integridad del biofilm (proteasas, DNasas, glucosidasas, **enzimas producidas por bacteriófagos**, etc.) [33, 82, 85]. Como consecuencia, los biofilms se desprenden de las superficies y la permeabilidad de los medicamentos aumenta, incrementando la sensibilidad de los microorganismos a los antimicrobianos. Debido a variaciones en la composición de la ECM propias de cada especie, **cócteles de enzimas combinados con antibióticos** han sido propuestos [84, 85].

- **Reducción de la biomasa celular:** Diferentes mecanismos de inducción de muerte celular tienen actividad antibiofilm. En primer lugar, los **agentes antimicrobianos** incluyen compuestos naturales (fitoquímicos, **péptidos antimicrobianos**, aceites esenciales, etc.), compuestos químicos (pequeñas moléculas, compuestos de plata, queladores, etc.) e incluso algunas moléculas identificadas mediante la **reasignación del uso de medicamentos** (***drug repurposing*** en inglés), como algunos quimioterápicos [33, 67, 86-88]. También podemos mencionar el uso de **estímulos externos locales** con efectos citotóxicos, como la terapia fotodinámica, el voltaje, el plasma no térmico, etc. [67, 82-84, 88, 89]. Y finalmente, el uso de **bacteriófagos** o **bacterias predadoras** que reconocen y lisan bacterias [67, 83, 85].

- **Inhibición del *quorum sensing*:** moléculas que bloquean y/o alteran las señales de comunicación microbiana pueden llevar a la disgregación y el desprendimiento del biofilm [82, 89].

De la mano de la identificación de nuevos tratamientos de erradicación, se han desarrollado **sistemas de liberación de medicamentos** (***Drug delivery systems*** en inglés) [84]. Los cuales aumentan la estabilidad, biodisponibilidad y seguridad de los compuestos, con la posibilidad de hacer liberación controlada de las moléculas en el sitio diana en algunos casos [84]. En este escenario, el uso de **nanosistemas** (nanopartículas, liposomas, micelas, dendrímeros, etc.) continúa siendo una aproximación prometedora para el manejo de infecciones ocasionados por biofilms [82, 90].

4. Microorganismos en las infecciones por biofilms

El modo de vida en forma de biofilm, tanto en tejidos como en dispositivos médicos, se ha convertido en un mecanismo clave de la virulencia de **patógenos oportunistas** [71]. Las infecciones por estos agentes se dan tras la **ruptura de las barreras cutáneas o mucosas** (traumas, heridas, cirugías, implantes de dispositivos médicos, etc.), la **disrupción de la microbiota protectora** (esquemas de antibióticos o medicamentos citostáticos) o **alteraciones en los mecanismos de defensa inmunológica** (inmunosupresión, diabetes mellitus, defectos de remoción de moco en pacientes con FQ, etc.) [91-95].

A continuación, se describe brevemente el impacto clínico, los factores de virulencia y las características de los biofilms de *P. aeruginosa*, *S. aureus*, *C. albicans* y *Candida parapsilosis*, microorganismos utilizados en los estudios realizados en esta tesis. Finalmente, se exponen las interacciones hongo-bacteria presentes en los biofilm inter-reino de *C. albicans* con *P. aeruginosa* y *S. aureus*.

4.1 *Pseudomonas aeruginosa*

P. aeruginosa es una de las bacterias Gram-negativas potencialmente más peligrosas para la salud humana. Causa infecciones en un amplio rango de sitios del cuerpo, que incluyen VAP, BSIs, SSIs, UTIs, queratitis, infecciones pulmonares crónicas, otitis media y heridas crónicas [91, 96-98]. Es el cuarto patógeno más frecuentemente aislado, siendo responsable de aproximadamente el 8% de las heridas crónicas y el 2-6% de las BSIs [99]. Recientemente, la Organización Mundial de la Salud (OMS) ha incluido a *P. aeruginosa* resistente a carbapenémicos como patógeno de prioridad alta para la investigación y desarrollo de nuevos antibióticos [100].

4.1.1 Factores de virulencia

El proceso de colonización de *P. aeruginosa* involucra factores de virulencia (Figura 8) que incluyen las **estructuras de movilidad**: el flagelo y el pili tipo IV [91, 93]. Estos apéndices, junto a las lectinas y las enzimas neuraminidasas intervienen en la **adhesión** a las superficies [91, 93, 101-104]. Posteriormente, un arsenal de **enzimas** y **toxinas** le permiten romper las barreras físicas de los tejidos y evadir la respuesta inmune, acciones necesarias en el proceso de invasión [91, 93, 103, 104]. En esta etapa de **infección aguda** distintas **proteasas extracelulares** (elastasas y proteasa alcalina), así como **moléculas citotóxicas** (Exotoxina A

y cianuro) y **hemolíticas** (Fosfolipasa C y ramnolípidos) son de suma importancia [91, 93, 102-104]. Incluyendo sideróforos y proteínas que permiten captar el hierro del ambiente (piochelina y piocianina) [91, 93]. En esta tarea, los **sistemas de secreción** permiten a la bacteria adaptarse, sobrevivir y explotar el microambiente del huésped, aumentando la severidad de las infecciones [93, 98, 103]. Por ejemplo, el Sistema de Secreción Tipo III (T3SS, por sus siglas en inglés) [93, 98] produce ExoS y ExoU. Moléculas responsables de inducir apoptosis, romper uniones célula-célula y presentar actividad citotóxica [105-109].

Por otra parte, la **capacidad de formar biofilms** es crucial en la patogénesis de *P. aeruginosa* [91, 93, 101, 103]. Las **infecciones crónicas** resultan de adaptaciones en el sistema *quorum sensing*, que disminuyen la producción de moléculas nocivas y priorizan la expresión de proteínas necesarias para el establecimiento y el mantenimiento de biofilms [93, 101, 102, 110-112].

Finalmente, los mecanismos de **resistencia antimicrobiana** de esta bacteria incluyen la producción de enzimas (β-lactamasas y enzimas modificadoras de aminoglucósidos), porinas de alta restricción y bombas de eflujo [91, 113, 114]. Por lo que es naturalmente resistente a antibióticos aminoglucósidos, β-lactámicos y quinolonas. Lo que no excluye la posibilidad de adquirir resistencia genotípica a otros fármacos (cefalosporinas, fluoroquinolonas y carbapenémicos) [113, 114]. La variedad de mecanismos hace posible la aparición de cepas resistentes a diferentes antibióticos simultáneamente [115, 116].

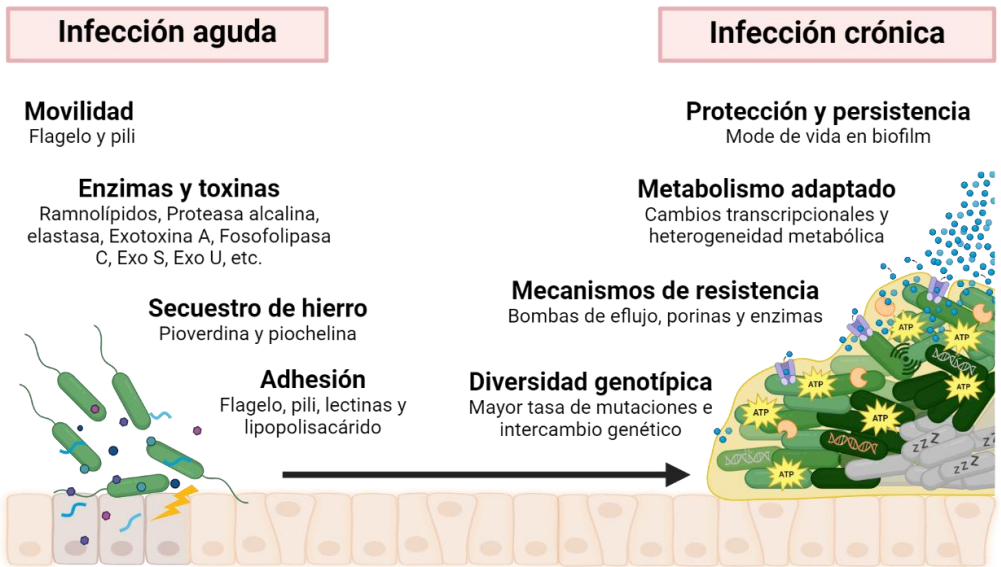

Figura 8. Principales factores de virulencia de *P. aeruginosa*. Imagen creada en Biorender.

4.1.2 Biofilms

La presencia de biofilms de *P. aeruginosa* está relacionada con el empeoramiento de la enfermedad y el pronóstico del paciente [117]. La ECM está compuesta por tres polisacáridos: **Psl**, **Pel** y **alginato** [101, 118]. Psl y Pel son importantes en la adhesión a la superficie y la integridad del biofilm, pues ambas moléculas confieren protección frente a antibióticos [101, 119-122]. Cuando el biofilm madura, Psl se localiza en la periferia de la estructura 3D, que en *P. aeruginosa* ha sido descrita como en forma de champiñón (*mushroom-like*) [96, 101]. La protección de Psl puede extenderse a células que no lo producen, incluyendo otras especies, actuando como "un bien común" [121]. El alginato, un polímero cargado negativamente, también desempeña un rol importante en la protección y maduración del biofilm [101]. Su producción está relacionada con el fenotipo mucoide, el cual influye en las propiedades viscoelásticas del biofilm y es muy importante en las infecciones pulmonares, ya que genera alta impermeabilidad a los antibióticos [101, 117, 123].

Otro componente fundamental de estos biofilms es el **ADNe**, que desempeña una gran variedad de funciones (Sección 1.2) [101]. Además, la interacción del ADNe con Pel aumenta la solidez de la estructura del biofilm [101]. De la misma manera, **proteínas extracelulares** como citoadesinas, lectinas, y apéndices (flagelos y fimbrias tipo IV) son importantes en la formación del biofilm [96].

4.2 *Staphylococcus aureus*

La bacteria Gram-positiva *S. aureus* es el primer agente causal de BSIs y endocarditis [94, 124]. No obstante, también causa infecciones osteoarticulares, neumonía, infecciones de la piel, infecciones asociadas a dispositivos médicos, entre otras, que pueden derivar en sepsis [94, 125].

4.2.1 Factores de virulencia

S. aureus posee una gran variedad de factores de virulencia que le permiten desarrollar infecciones (Figura 9), incluyendo mecanismos ingeniosos de **evasión del sistema inmune** [94]. Cuando las infecciones tienen lugar en la piel o los pulmones, la bacteria forma rápidamente **abscesos** [94]. Mientras que, cuando entra en la sangre, produce **toxinas citolíticas** (toxina α, leucotoxinas, hemolisina ϒ, modulinas solubles en fenol, etc) que

causan **inflamación**, atacan al sistema inmune, **alteran la coagulación** y comprometen la integridad vascular [94, 126-128]. Dentro del amplio repertorio de moléculas tóxicas, **la toxina α** es muy importante en la patogénesis de *S. aureus* [94, 129-132]. Forma poros en las células y rompe las uniones célula-célula, causando daño tisular [94, 126, 133].

Alternativamente, *S. aureus* puede aprovecharse del mecanismo de fagocitosis de las células del sistema inmune y usar neutrófilos y monocitos **para viajar desapercibido por el torrente sanguíneo** [94]. De esta manera, puede colonizar nuevos nichos de infección [94]. Su **supervivencia intracelular** es el resultado de moléculas y enzimas que combaten el daño por especies reactivas de oxígeno (ROS, por sus siglas en inglés), como la estafiloxantina, la superóxido dismutasa, la catalasa, la lactato deshidrogenasa, entre otras [94, 134-139].

Este microorganismo también produce **proteasas** que degradan péptidos antimicrobianos (AMPs, por sus siglas en inglés) [94, 140] y **DNasas** que le protegen de las trampas extracelulares de neutrófilos (NETs, por sus siglas en inglés) [94, 141]. Al igual que **proteínas que interfieren con la deposición de inmunoglobulinas** (SpA, Sbi y SSL10) e **inhiben el sistema del complemento** (SCIN, Efb, Ecb, SdrE, Cna, Eap y SSL7), dificultando el proceso de opsonización necesario para la fagocitosis [94, 126, 142-155]. Adicionalmente, produce **superantígenos** (SAgs), cuyo efecto a largo plazo altera la respuesta inmune. Esto puede ocasionar la proliferación de células T autorreactivas que resultan en el desarrollo o exacerbación de **enfermedades autoinmunes crónicas** [156]. La presencia de SAgs también se han asociado con infecciones del tracto respiratorio, como rinosinusitis crónica, asma y EPOC [157]. Otros mecanismos de evasión del sistema inmune incluyen la **formación de cápsulas**, producción de la Adesina Intercelular de Polisacáridos (**PIA**, por sus siglas en inglés) y la **formación de biofilms** [94, 128, 158-161]. Sin embargo, es importante mencionar que el modo de vida de biofilm implica cambios de expresión génica que disminuyen la virulencia bacteriana y propician la cronicidad de la infección [162].

La expresión de todos estos factores de virulencia depende de **reguladores transcripcionales globales** que responden a condiciones ambientales específicas [94, 163]. El sistema mejor estudiado es el **gen accesorio regulador (*agr*)**, que regula la expresión de factores de virulencia de acuerdo a la densidad celular [94, 163]. Este sistema es sensible a factores ambientales como el pH, ROS, y disponibilidad de ribosas [163-168]. La molécula efectora es el **RNAIII**, la cual a su vez codifica para la toxina δ e induce la sobre expresión de la **toxina α**, proteasas, hemolisinas y lipasas [163].

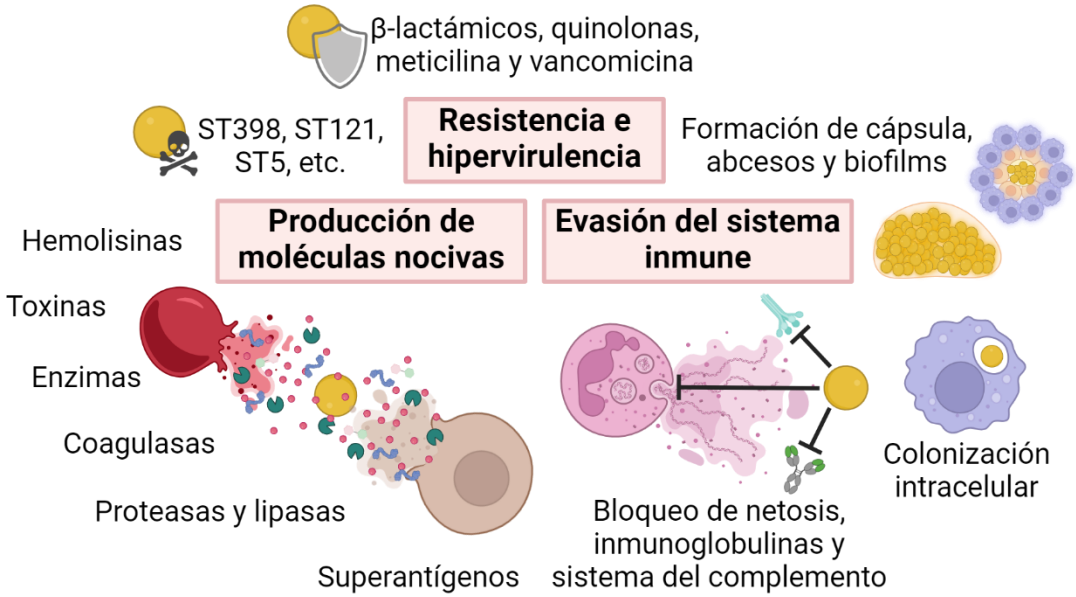

Figura 9. Principales factores de virulencia de *S. aureus*. Imagen creada en Biorender.

Por otra parte, *S. aureus* cuenta con **mecanismos de resistencia antibiótica** que contribuyen en su patogenicidad, aunque no son necesarios, pues existen cepas susceptibles con elevada virulencia. Por ejemplo, la Secuencia tipo 398, que causa infecciones fatales [169, 170]. Dentro de las cepas de esta bacteria la **resistencia a β-lactámicos y quinolonas** está ampliamente distribuida [171]. Las cepas de ***S. aureus* resistentes a meticilina** (**MRSA**, por sus siglas en inglés) son asociadas a mayor morbilidad, tiempos de hospitalización y mortalidad [171, 172]. Y aunque uno de los antibióticos de última línea es la **vancomicina**, cepas altamente resistentes o con resistencia intermedia han sido reportadas [171, 173, 174].

4.2.2 Biofilms

S. aureus lleva a cabo la adhesión a las superficies mediante componentes de superficie microbiana que reconocen moléculas de matriz adhesivas (MSCRAMM, por sus siglas en inglés), incluyendo la proteína FnBPA [94, 175]. Tanto la adhesión como la formación temprana de los biofilms son controlados por el regulador global **SarA** [162, 175]. La maduración del biofilm incluye la producción de una ECM compuesta principalmente por **ácidos teicoicos**, **proteínas** (microbianas y del huésped) y **ADNe**. Algunas células incluyen la producción de **PIA** [94, 128]. La estructura tridimensional es el resultado conjunto de la acción surfactante de las **modulinas solubles en fenol** y la actividad degradativa de

exoenzimas [94, 176]. Una vez los biofilm alcanzan el *quorum* poblacional, el **sistema *agr*** aumenta la expresión de enzimas y factores de virulencia que ayudan en el proceso de dispersión y equipan las células para combatir con el sistema inmune [128, 162, 177-180].

4.3 *Candida albicans*

Las especies de *Candida* son responsables de la mayoría de infecciones causadas por hongos [95]. *C. albicans* es el tercer agente causal de BSIs nosocomiales, con una tasa de mortalidad de hasta el 50% [39, 181]. La mayor fuente de candidemia es la traslocación por la barrera intestinal, ya que este microrganismo coloniza la mucosa del tracto digestivo [182, 183]. Además su presencia en la piel, mucosa oral y mucosa genital puede desencadenar infecciones locales como la onicomicosis, candidiasis orofaríngea, esofágica y vulvovaginal [95].

4.3.1 Factores de virulencia

La amplia distribución de *C. albicans* en los diferentes microambientes del cuerpo humano se debe a diferentes rasgos que le confieren **flexibilidad** y **adaptabilidad** (Figura 10). En primer lugar, la capacidad para alternar entre **diferentes morfotipos**: blastosporas, pseudohifas e hifas. Las hifas participan en la invasión de los tejidos, incluyendo el torrente sanguíneo, mediante la expresión de moléculas perjudiciales [95]. El repertorio involucra **proteasas** (Saps), **lipasas** (LIPs) y toxinas como la **hemolisina** y **candidalisina** que causan daño en los epitelios e inducen la respuesta inmune [95, 184, 185]. El proceso de filamentación puede ser activado por distintos estímulos ambientales como el pH, la temperatura y la falta de nutrientes [185, 186]. Así mismo, el peptidoglicano o N-acetilglucosamina (GlcNAc) de la pared bacteriana puede inducir el proceso de morfogénesis [185, 186].

Además de la forma, este hongo puede **adaptar su metabolismo** dependiendo de los nutrientes disponibles [95, 185, 187-195]. Fuentes de carbono alternativas en condiciones de escasez de glucosa incluyen ácidos carboxílicos, aminoácidos y GlcNAc [187]. *C. albicans* también puede **evadir la respuesta del sistema inmune** y **resistir a diferentes tipos de estrés** (oxidativo, nitrosativo, osmótico y térmico) [95, 185]. Por ejemplo, uno de los mecanismos de evasión consiste en enmascarar componentes de la pared celular o alterar su composición. A esto se le suma su **gran diversidad genética**, resultado del ciclo sexual de algunas cepas, cambios de ploidía y mutaciones [185].

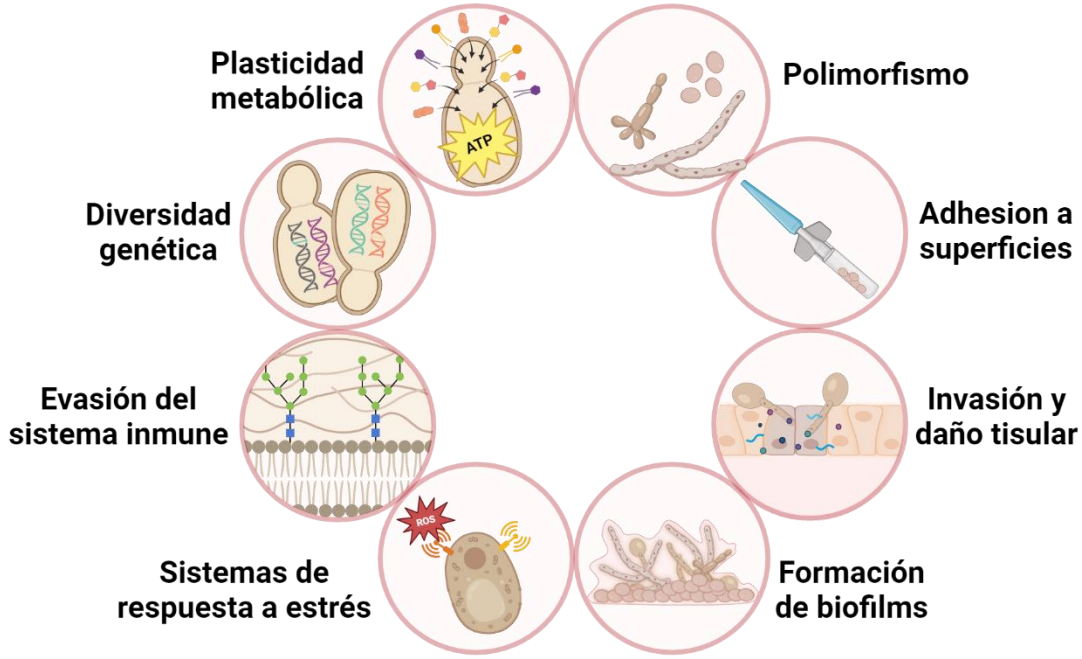

Figura 10. Principales factores de virulencia de *C. albicans*. Imagen creada en Biorender.

Por otra parte, *C. albicans* puede **adherirse a diferentes superficies** mediante adhesinas e invasinas (Als y Hwp1) [95]. Lo que está directamente relacionado con su **capacidad de formar biofilms estructuralmente complejos** [184, 196]. A su vez, el modo de vida de biofilm induce la expresión de bombas de eflujo que le confieren **resistencia** a azoles [197]. Así mismo, la ECM reduce la eficacia de los antifúngicos (azoles, equinocandinas y polienos) [19, 39, 197, 198], proceso en el cual las vesículas extracelulares son relevantes [199-201].

4.3.2 Biofilms

El impacto clínico de *C. albicans* se debe a la elevada virulencia y mayor mortalidad que ocasionan los biofilms [39]. **El ciclo de formación está estrechamente relacionado con el proceso de morfogénesis** [95, 202]. La **blastóspora** participa en el proceso de adhesión a las superficies, pero la inducción de la filamentación es clave para el crecimiento, maduración y estructura del biofilm. Las **hifas** sirven de soporte para otros tipos de células, incluyendo las pertenecientes a otras especies [39]. La ECM está compuesta por proteínas (55%), polisacáridos (25%), lípidos (15%) y ADNe (5%) [203]. Los principales polisacáridos son α-mananos, β-1,6-glucanos y β-1,3-glucanos [184]. Finalmente, las blastósporas vuelven a generarse en la etapa de dispersión, para colonizar nuevas superficies.

4.4 *Candida parapsilosis*

C. parapsilosis es responsable del 20-25% de las infecciones sistémicas en España [204]. Dentro de los grupos de riesgo más importantes se encuentran los neonatos con nutrición parenteral, los adultos en unidades de cuidado intensivo y los recipientes de trasplantes de órganos [205, 206]. Esta levadura es reconocida por su alta transmisión, siendo muy importante en el contexto intrahospitalario [206]. Dentro de las infecciones a las que ha sido asociada se encuentra peritonitis, endoftalmitis, endocarditis y artritis séptica [207].

4.4.1 Factores de virulencia

En general, la tasa de mortalidad asociada a *C. parapsilopsis* es baja, siendo considerada **menos virulenta que *C. albicans* y otras especies de *Candida*** [205, 206, 208, 209]. No obstante, el panorama podría cambiar en los próximos años debido al aumento en la **resistencia a antifúngicos** [206, 210-212]. *C. parapsilosis* posee intrínsicamente **menor susceptibilidad a las equinocandinas** que otras especies de *Candida* [197, 205]. Sin embargo, la **resistencia a los azoles** suele ser más frecuente, con una tendencia global al alza [205, 206, 210, 211, 213, 214].

Al igual que *C. albicans*, *C. parapsilosis* posee una gran variedad de factores de virulencia (Figura 11), incluyendo la **adhesión a distintas superficies**, y la subsecuente **formación de biofilms** [205, 206, 215, 216]. Estos factores son determinantes en la efectividad terapéutica, pues el modo de vida de biofilm puede conferirle a esta levadura **resistencia a los azoles y anfotericina B** [205]. El proceso de filamentación da origen a **pseudohifas**, pero no a hifas [205]. La morfogénesis es estimulada por factores ambientales, así como la presencia de ciertos aminoácidos [205, 217]. **Las pseudohifas son más resistentes que las blastósporas** frente a los ataques de los macrófagos e **inducen mayor daño celular *in vitro*** [218, 219].

La plasticidad metabólica de *C. parapsilosis* incluye el metabolismo de hidroxibencenos, hidroxibenzoatos y ftalatos, estos últimos presentes en materiales plásticos de uso médico [205]. Además, el arsenal de esta levadura incluye **compuestos inmunomoduladores** y **enzimas hidrolíticas**, como las aspartil proteasas (Saps) y lipasas (LIPs) [205, 215]. Sumado a **estrategias de evasión del sistema inmune**, como la capacidad de **sobrevivir intracelularmente** en fagocitos y células endoteliales [205].

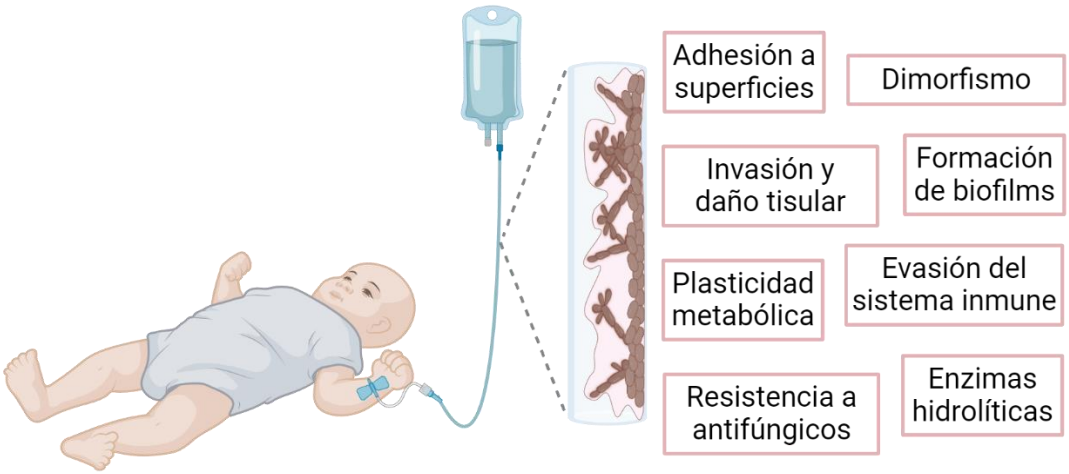

Figura 11. Principales factores de virulencia de *C. parapsilosis*. Imagen creada en Biorender.

4.4.2 Biofilms

C. parapsilosis forma biofilms rápidamente en presencia de **soluciones ricas en glucosa o lípidos** [220]. El ciclo de formación también **requiere del proceso de filamentación** [215]. Sin embargo, debido a la incapacidad de formar hifas, los biofilms de *C. parapsilosis* son descritos como **menos complejos y más delgados que los biofilms de *C. albicans*** [205]. Además, otra diferencia significativa es que la ECM está **compuesta principalmente por carbohidratos** y pocos niveles de proteína [215].

4.5 Biofilms inter-reino

La diversidad de la microbiota humana favorece las interacciones inter-especie y la formación de biofilms polimicrobianos (Sección 1.1) [207, 221]. A su vez, la complejidad de las interacciones inter-especie puede influenciar el comportamiento de los miembros de la comunidad, incluyendo su virulencia y susceptibilidad a agentes externos [44, 222-225]. Además, la respuesta inmune difiere entre biofilms mixtos y biofilm monomicrobianos [222]. Como resultado, **las infecciones derivadas de los consorcios multiespecie conllevan un reto terapéutico importante**, aumentando la incertidumbre de la respuesta del paciente y la progresión de la enfermedad [39, 207, 221-223, 225, 226].

Los hongos son una parte considerable de la biomasa de la microbiota humana, ya que aunque se encuentran en menor proporción, pueden ser 100 veces más grandes que las bacterias [227]. ***C. albicans* es el hongo patógeno aislado más frecuentemente en las infecciones hongo-bacteria**, incluyendo aquellas relacionadas con la formación de biofilms en la piel, los pulmones, la cavidad oral, el tracto gastrointestinal y la mucosa genital (Figura 12) [207, 221, 223]. El 27% de las BSIs nosocomiales causadas por *C. albicans* son polimicrobianas y suelen presentar mayor morbilidad y mortalidad [207, 223, 228].

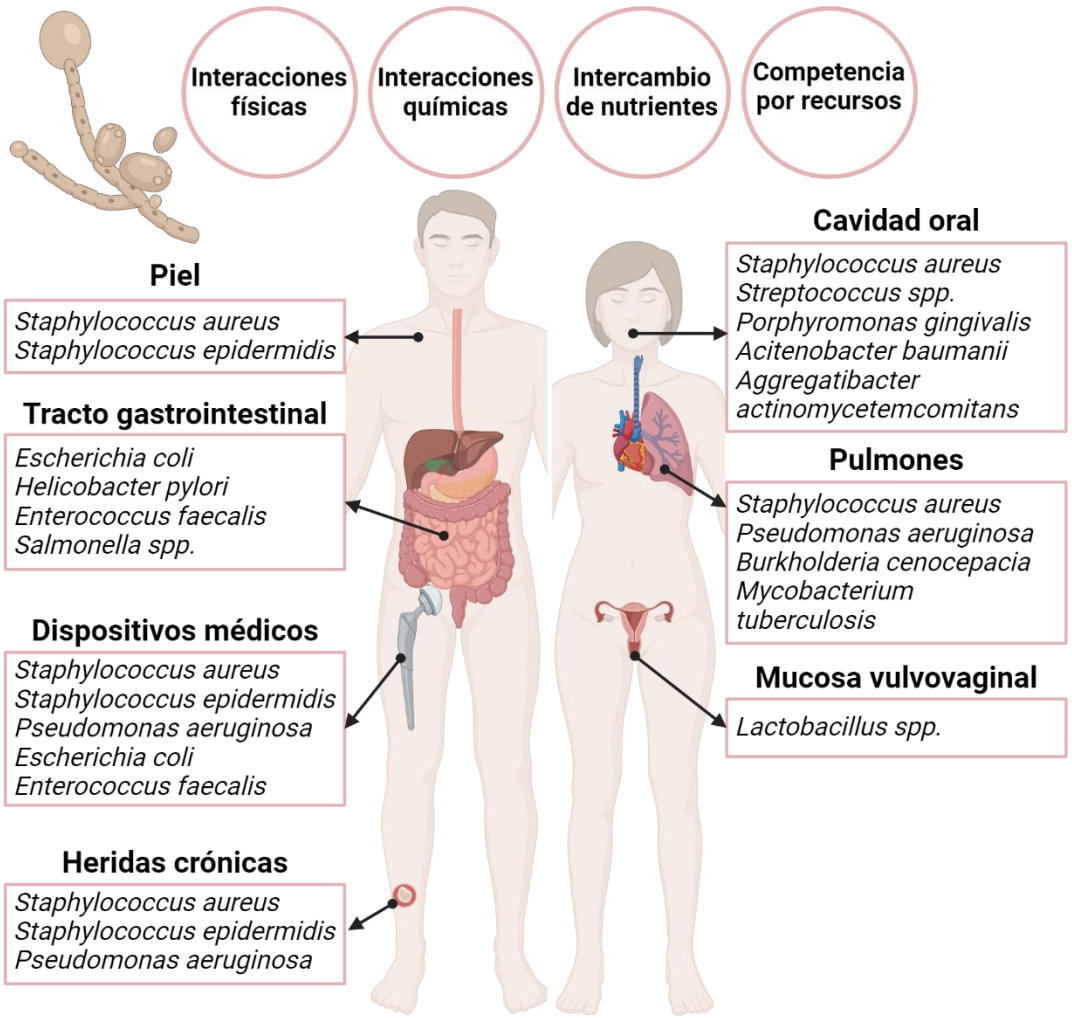

Figura 12. Principales especies bacterianas co-aisladas con *C. albicans* de acuerdo con el lugar de infección. Imagen creada en Biorender.

La presencia de *C. albicans* en los biofilms inter-reino ha sido asociada con distintos procesos que contribuyen al **mantenimiento de la homeostasis de la comunidad microbiana** [39]. Esto incluye proveer superficies de adhesión en las hifas, generar microambientes hipóxicos, aumentar la biomasa del biofilm y reducir la susceptibilidad a los antimicrobianos [13, 39, 221, 225, 229]. En diferentes infecciones orales, la presencia de *C. albicans* se describe como un potencial "cómplice activo"[229, 230]. Así mismo, su presencia en biofilms del tracto gastrointestinal se asocia con mayor mortalidad [207]. En otros escenarios, como las heridas o las infecciones pulmonares crónicas, el papel de los hongos generalmente se ignora, pues no se ha descifrado completamente [196, 226, 227]. La dificultad de discernir si la presencia de *C. albicans* en muestras clínicas significa contaminación, colonización o causa de infección aumenta la complejidad del tema.

Por estas razones es imprescindible el estudio de los consorcios hongo-bacteria implicados en las infecciones. **El entendimiento de las interacciones inter-especie ayudará en el desarrollo y mejoramiento de las estrategias terapéuticas** [39, 207, 221, 223, 224].

4.5.1 *Candida albicans – Pseudomonas aeruginosa*

Estos dos microorganismos son co-aislados frecuentemente de catéteres, heridas e infecciones pulmonares crónicas [39, 223]. Distintas interacciones han sido descritas entre ambas especies dentro de los biofilms polimicrobianos (Figura 13). En primer lugar, ***P. aeruginosa* se adhiere a las hifas de *C. albicans***, y tras la secreción de distintos factores de virulencia (Fosofolipasa C, ROS, C12AHL), **causa la muerte celular de los filamentos** [39, 223]. Por su parte, *C. albicans* secreta **farnesol**, lo que inhibe la producción de moléculas tóxicas de *P. aeruginosa* (Piocianina y PQS), favoreciendo su supervivencia y afectando la movilidad de la bacteria [39, 223].

Otros procesos antagónicos entre estas especies incluyen la **competencia por hierro**. *P. aeruginosa* produce agentes quelantes, mientras que *C. albicans* incrementa los procesos de internalización [39, 226]. Estudios en pez cebra y ratones han demostrado que las interacciones de competencia entre este dúo **aumentan la virulencia** de los biofilms mixtos, e induce la formación de células mutantes dentro de ellos [223, 231, 232].

No obstante, **algunas interacciones pueden ser beneficiosas para ambos microorganismos y perjudiciales para el huésped**. Por ejemplo, cuando los biofilms mixtos son formados en modelos *in vitro* dinámicos (Sección 2.1.2), hay un **mayor crecimiento de ambas especies** en comparación con sus contrapartes monomicrobianas [233]. La producción de fenazinas

por *P. aeruginosa* promueve la producción de etanol en *C. albicans*, que a su vez aumenta la producción de fenazinas, resultando en un incremento en la biomasa de *P. aeruginosa* [221]. El etanol además favorece la **supresión de la respuesta inmune** por parte de *P. aeruginosa* [234]. Adicionalmente, ambas especies pueden utilizar el ácido araquidónico para producir eicosanoides como la prostaglandina E2 [223]. Estas moléculas influencian la progresión de la infección, ya que modulan la respuesta inmune [235].

La asociación de estos dos microorganismos en biofilms también confiere **resistencia** a meropenem y fluconazol [223]. La protección de *P. aeruginosa* frente al antibiótico está dada por la **ECM** de *C. albicans* (mananos y glucanos). Mientras que la resistencia al antifúngico está dada por **adaptaciones metabólicas** inducidas por la secreción de 3-oxo-C12-HSL por parte de *P. aeruginosa*. Sin embargo, la presencia de *P. aeruginosa* puede aumentar la susceptibilidad de *C. albicans* a anfotericina B (AmB) y un nuevo tipo de AMPs denominados cerageninas [226].

4.5.2 *Candida albicans – Staphylococcus aureus*

Este dúo ha sido aislado de infecciones relacionadas con biofilms, como periodontitis, heridas crónicas, FQ, queratitis, endocarditis, infecciones asociadas a dispositivos médicos y BSIs [207, 228, 236]. Por lo general, la asociación de estas dos especies es catalogada como cooperativa e incluye distintos tipos de interacciones (Figura 13).

S. aureus se une a la adhesina Als3 de *C. albicans*, lo que puede favorecer la **diseminación de la bacteria** mediante dos mecanismos: 1) Las hifas atraen células fagocíticas que la bacteria usa como medio de transporte y/o 2) las hifas penetran en los tejidos profundos, llevando consigo células de *S. aureus*. Ambos mecanismos pueden desencadenar en una infección sistémica [207, 236]. Otros beneficios que *C. albicans* proporciona a *S. aureus* incluyen **estimulación en el crecimiento** y **protección frente a distintos antibióticos** (vancomicina, doxiciclina, nafcilina y oxacilina) [207, 221, 236]. Aunque concentraciones altas de farnesol reducen la viabilidad y formación de biofilms de *S. aureus*, dosis medias o bajas causan estrés oxidativo, activando bombas de eflujo y enzimas reductoras que confieren **resistencia a vancomicina y ROS** [223, 236, 237].

Por su parte, el peptidoglucano de la pared celular de *S. aureus* puede **inducir la formación de hifas** y potencialmente, la **formación de biofilms** de *C. albicans* [238, 239]. Así mismo, *S. aureus* puede producir lactato para **inhibir la filamentación** e inducir el

enmascaramiento de β-glucanos, dos estrategias que favorecen la **evasión del sistema inmune** [223, 238].

Finalmente, la presencia simultánea de *C. albicans* y *S. aureus* en infecciones intraabdominales (IAI, por sus siglas en inglés) ocasionan lo que se describe como "**sinergismo letal**" [236]. *C. albicans* **aumenta la virulencia** de *S. aureus* mediante la **activación del sistema *agr*** y la **producción de la toxina α**, lo que deriva en mayor **morbilidad y mortalidad** [133, 239-242]. Siendo importante también el aumento en la producción de citoquinas por parte del huésped [238].

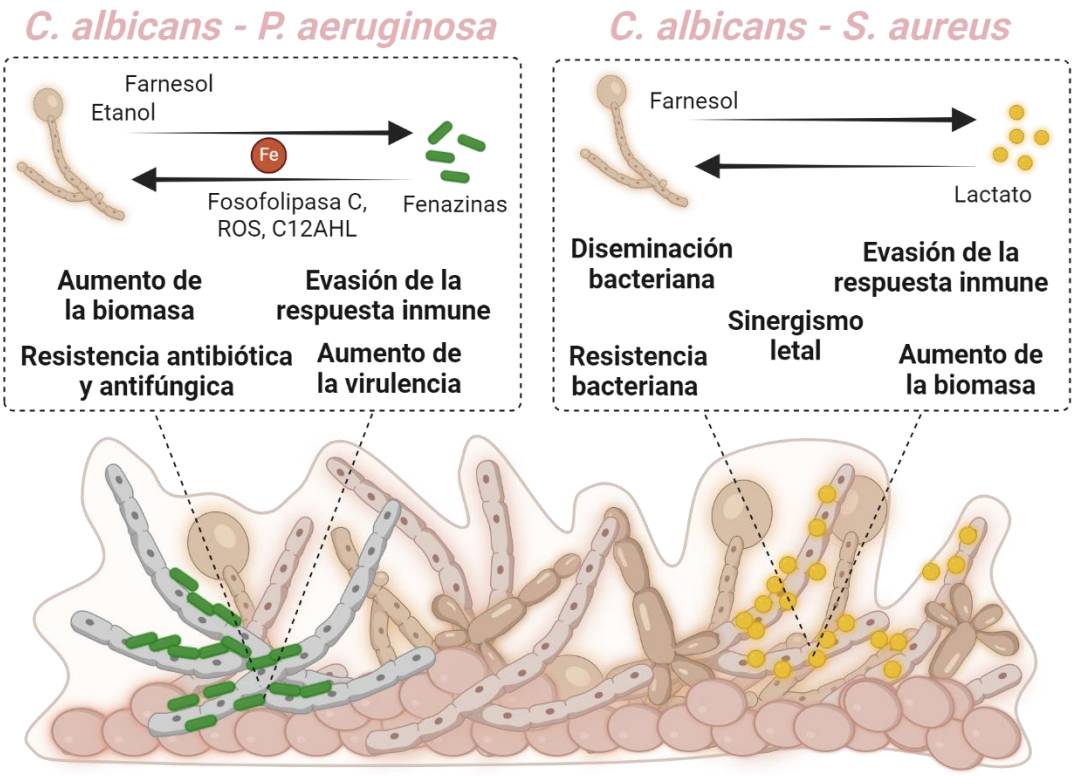

Figura 13. Principales interacciones de *C. albicans* con *P. aeruginosa* y *S. aureus*. Imagen creada en Biorender.

Objetivos

Este trabajo se enfoca en la comprensión de los biofilms como resultado de las interacciones entre especies y el medio ambiente, con el fin de identificar variables importantes para su estudio *in vitro* y entender variaciones en la virulencia. Los objetivos generales y específicos se enumeran a continuación:

1. Determinar la influencia de diferentes variables en las características de biofilms monomicrobianos y polimicrobianos.

- **1.1** Evaluar el impacto del medio de cultivo en la formación, susceptibilidad y virulencia de biofilms de *C. parapsilosis.*
- **1.2** Evaluar la importancia del primer colonizador en biofilms de *C. albicans* y *P. aeruginosa.*

2. Estudiar las interacciones microbianas de *C. albicans* con las bacterias patógenas *P. aeruginosa* y *S. aureus*.

3. Establecer métodos para evaluar la eficacia de terapias antibiofilm.

- **3.1** Evaluar tinciones de viabilidad y vitalidad en biofilms de *C. parapsilosis*.
- **3.2** Desarrollar una nueva tecnología para la evaluación de la susceptibilidad de biofilms.

Informes

Informe sobre el factor de impacto

Yo, el Dr. Eduard Torrents, en mi calidad de director y tutor de la presente tesis, declaro que el estado y factor de impacto de los artículos incluidos en la misma, a la fecha de su presentación, son los que se detallan a continuación. Además, resalto que todos los artículos ya publicados lo han sido en revistas científicas internacionales incluidas en el Journal Citation Reports y pertenecen al primer tercil de su área de conocimiento.

- El artículo 1 **"Culture media influences *Candida parapsilosis* growth, susceptibility, and virulence"** fue publicado en diciembre de 2023 en la revista *Frontiers in Cellular and Infection Microbiology*, con un factor de impacto de 4.6 (Q1) para el año 2023 en la categoría de microbiología.

- El artículo 2 **"Who arrived first? Priority effects on virulence and susceptibility of *Candida albicans* and *Pseudomonas aeruginosa* dual biofilms"** se presenta como manuscrito sometido en la revista *Communications Biology* (COMMSBIO-24-3873), con un factor de impacto 5.2 (Q1) para el año 2023 en la categoría de biología. Una versión *pre-print* (no sometida a revisión por pares) está disponible en el repositorio Research Square.

- El artículo 3 **"*Candida albicans* enhances *Staphylococcus aureus* virulence by progressive generation of new phenotypes"** se presenta como manuscrito sometido en la revista Current Research in Microbial Sciences (CRMICR-D-24-00290), con un factor de impacto de 4.8 (Q1) para el año 2023 en la categoría de microbiología. Una versión pre-print (no sometida a revisión por pares) está disponible en el repositorio bioRxiv.

- El artículo 4 **"Died or not dyed: Assessment of viability and vitality dyes on planktonic cells and biofilms from *Candida parapsilosis*"** fue publicado en marzo de 2024 en la revista *Journal of Fungi,* con un factor de impacto de 4.2 (Q1) para el año 2023 en la categoría de micología.

- El artículo 5 **"A new BiofilmChip for testing biofilm formation and antibiotic susceptibility"** fue publicado en agosto de 2021 en la revista *npj Biofilms and*

Microbiomes, con un factor de impacto de 8.5 (Q1) para el año 2021 en la categoría de microbiología.

Adicionalmente, se presenta en calidad de anexos dos artículos originales, un artículo de revisión y un capítulo de un libro, en los cuales la doctoranda ha participado durante el transcurso de su tesis. Aunque estos no se relacionan directamente con los objetivos presentados, pertenecen al campo de estudio de los biofilms, por lo que consideramos relevante su inclusión. Con respecto al artículo de revisión y al capítulo del libro, por motivos de espacio, la sección de anexos expone únicamente la información requerida para su consulta.

- El artículo 6 **"Antimicrobial and antibiofilm activity of human recombinant H1 histones against bacterial infections"** fue publicado en octubre de 2024 en la revista *mSystems* (mSystems00704-24), con un factor de impacto 5.0 (Q1) para el año 2023 en la categoría de microbiología.

- El artículo 7 **"Accessing the *In vivo* efficiency of clinically isolated phages against uropathogenic and invasive biofilm-forming *Escherichia coli* strains for phage therapy"** fue publicado en enero de 2023 en la revista *Cells,* con un factor de impacto de 5.1 (Q2) para el año 2023 en la categoría de biología celular.

- El artículo de revisión **"Nanomedicine against biofilm infections: A roadmap of challenges and limitations"** fue publicado en febrero de 2024 en la revista *Wiley Interdisciplinary Reviews: Nanomedicine and Nanobiotechnology*, con un factor de impacto de 6.9 (Q1) para el año 2023 en la categoría nanociencia y nanotecnología.

- El capítulo de libro **"Methods for studying biofilms: Microfluidics and translation in the clinical context"** fue publicado en mayo de 2023 en el volumen 53 Biofilms de la serie de libros de *Methods in Microbiology*.

Dr. Eduard Torrents Serra
Director y tutor de la tesis

Informe de participación en los artículos

Yo, el Dr. Eduard Torrents, declaro que la doctoranda Betsy Verónica Arévalo Jaimes ha participado en todos los artículos que forman parte de su tesis, tal como se detalla a continuación:

- En el artículo 1**, "Culture media influences *Candida parapsilosis* growth, susceptibility, and virulence"**, Verónica es la primera autora, ya que participó activamente en el diseño, ejecución y análisis de todos los experimentos. Adicionalmente, es la responsable de la escritura del manuscrito. La Dra. Núria Blanco-Cabra ayudó en la optimización de la formación de los biofilms y Joana Admella en el diseño y supervisión de los experimentos con el modelo animal *Galleria mellonella*. Por esta razón, este artículo podrá formar parte de la tesis de Joana Admella, en formato anexo.

- En el artículo 2**, "Who arrived first? Priority effects on virulence and susceptibility of *Candida albicans* and *Pseudomonas aeruginosa* dual biofilms"**, Verónica es la primera autora, ya que participó activamente en el diseño, ejecución y análisis de todos los experimentos. Adicionalmente, es la responsable de la escritura del manuscrito. No obstante, este artículo podrá formar parte de la tesis de Joana Admella, en formato de anexo, por su colaboración en los experimentos que involucraban el uso de la línea celular A549.

- En el artículo 3, **"*Candida albicans* enhances *Staphylococcus aureus* virulence by progressive generation of new phenotypes"**, Verónica es la primera autora, ya que participó activamente en el diseño, ejecución, análisis de todos los experimentos y adicionalmente, es la responsable de la escritura del manuscrito.

- En el artículo 4, **"Died or not dyed: Assessment of viability and vitality dyes on planktonic cells and biofilms from *Candida parapsilosis*"**, Verónica es la primera autora, ya que participó activamente en el diseño, ejecución, análisis de todos los experimentos y adicionalmente, es la responsable de la escritura del manuscrito.

- En el artículo 5, **"A new BiofilmChip for testing biofilm formation and antibiotic susceptibility"**, Verónica figura como segunda autora, ya que participó en el proceso de validación de la impedancia como medida de lectura del dispositivo y

su aplicación en muestras clínicas. Adicionalmente, participó en la revisión del manuscrito. La autoría principal del trabajo la comparten las Dras. Núria Blanco-Cabra y María José López quienes diseñaron el dispositivo, optimizaron la formación de biofilms y realizaron el análisis de datos y la escritura del manuscrito. Por tal razón, una versión previa no publicada de este artículo fue incluida como manuscrito en la tesis de Núria Blanco-Cabra en el 2020.

- En el artículo 6, **"Antimicrobial and antibiofilm activity of human recombinant H1 histones against bacterial infections"**, Verónica es la primera autora, ya que participó activamente en el diseño, ejecución y análisis de los experimentos de susceptibilidad antimicrobiana y antibiofilm de las histonas. Además, es la responsable de la escritura del manuscrito. El proceso de expresión, purificación y caracterización de las histonas fue realizado en el laboratorio de las Dras. Alicia Roque e Inmaculada Ponte. Mientras que los experimentos de Western-blot fueron realizados por Mónica Salinas-Pena en el laboratorio del Dr. Albert Jordan.

- En el artículo 7, **"Accessing the *In vivo* efficiency of clinically isolated phages against uropathogenic and invasive biofilm-forming *Escherichia coli* strains for phage therapy"**, Verónica figura como quinta autora, ya que solo participó en la evaluación de los bacteriófagos usando biofilms en continuo (Figura 5). Este artículo podrá formar parte de la tesis de Joana Admella como anexo, por su participación en los experimentos que involucraban el uso de *G. mellonella*.

- En el artículo de revisión, **"Nanomedicine against biofilm infections: A roadmap of challenges and limitations"**, Verónica figura como segunda co-autora ya que es la responsable de la escritura de la sección 2.4. Además, participó activamente en la revisión de la totalidad del manuscrito.

- En el capítulo de libro, **"Methods for studying biofilms: Microfluidics and translation in the clinical context"**, Verónica figura como primera co-autora ya que es la responsable de la escritura de la sección 4. Además, participó activamente en la revisión de la totalidad del manuscrito.

Dr. Eduard Torrents Serra

Director y tutor de tesis

Artículos

Artículo 1 (Publicación)

Culture media influences *Candida parapsilosis* growth, susceptibility, and virulence

Publicado en la revista *Frontiers in Cellular and Infection Microbiology*

DOI: 10.3389/fcimb.2023.1323619

13 de diciembre de 2023

Categoría Microbiología 2023: 1er tercil, 1er Cuartil, IF= 4.6

Betsy V. Arévalo-Jaimes[1,2], Joana Admella[1,2], Núria Blanco-Cabra[1,2] y Eduard Torrents[1,2]

[1]Grupo Infecciones Bacterianas y Terapias Antimicrobianas (BIAT), Instituto de Bioingeniería de Cataluña (IBEC), Barcelona, España.
[2]Sección de Microbiología, Departamento de Genética, Microbiología y Estadística, Facultad de Biología, Universitat de Barcelona, Barcelona, España.

Cita: Arévalo-Jaimes BV, Admella J, Blanco-Cabra N and Torrents E (2023) Culture media influences *Candida parapsilosis* growth, susceptibility, and virulence. *Front. Cell. Infect. Microbiol.* 13:1323619. DOI: 10.3389/fcimb.2023.1323619.

frontiers | Frontiers in Cellular and Infection Microbiology

TYPE Original Research
PUBLISHED 13 December 2023
DOI 10.3389/fcimb.2023.1323619

OPEN ACCESS

EDITED BY
Vânia Pobre,
Universidade Nova de Lisboa, Portugal

REVIEWED BY
Tahereh Navidifar,
Shoushtar Faculty of Medical Sciences, Shoushtar, Iran
Aize Pellón Rodríguez,
King's College London, United Kingdom

*CORRESPONDENCE
Eduard Torrents
etorrents@ibecbarcelona.eu;
eduard.torrents@ub.edu

RECEIVED 18 October 2023
ACCEPTED 27 November 2023
PUBLISHED 13 December 2023

CITATION
Arévalo-Jaimes BV, Admella J, Blanco-Cabra N and Torrents E (2023) Culture media influences *Candida parapsilosis* growth, susceptibility, and virulence. *Front. Cell. Infect. Microbiol.* 13:1323619. doi: 10.3389/fcimb.2023.1323619

Culture media influences *Candida parapsilosis* growth, susceptibility, and virulence

Betsy V. Arévalo-Jaimes[1,2], Joana Admella[1,2], Núria Blanco-Cabra[1,2] and Eduard Torrents[1,2*]

[1]Bacterial Infections and Antimicrobial Therapies Group (BIAT), Institute for Bioengineering of Catalonia (IBEC), The Barcelona Institute of Science and Technology (BIST), Barcelona, Spain, [2]Microbiology Section, Department of Genetics, Microbiology and Statistics, Faculty of Biology, University of Barcelona, Barcelona, Spain

Introduction: *Candida parapsilosis*, a pathogenic yeast associated with systemic infections, exhibits metabolic adaptability in response to nutrient availability.

Methods: We investigated the impact of RPMI glucose supplemented (RPMId), TSB, BHI and YPD media on *C. parapsilosis* growth, morphology, susceptibility (caspofungin and amphotericin B), and *in vivo* virulence (*Galleria mellonella*) in planktonic and biofilm states.

Results: High-glucose media favors growth but hinders metabolic activity and filamentation. Media promoting carbohydrate production reduces biofilm susceptibility. Virulence differences between planktonic cells and biofilm suspensions from the same media shows that biofilm-related factors influence infection outcome depending on nutrient availability. Pseudohyphal growth occurred in biofilms under low oxygen and shear stress, but its presence is not exclusively correlated with virulence.

Discussion: This study provides valuable insights into the intricate interplay between nutrient availability and *C. parapsilosis* pathogenicity. It emphasizes the importance of considering pathogen behavior in diverse conditions when designing research protocols and therapeutic strategies.

KEYWORDS

amphotericin B, caspofungin, antifungal, pseudohyphal growth, pathogenicity, *Galleria mellonella*, biofilm, *Candida*

Abbreviations: RPMId, RPMI with 0.2% glucose supplementation; CW, Calcofluor white; LWR, Length to wide ratio; AmB, Amphotericin B; CAS, Caspofungin diacetate.

10.3389/fcimb.2023.1323619

Introduction

Candida parapsilosis is an important pathogen in systemic infections, particularly prevalent in Latin America, parts of Asia, and Southern Europe. It is known for its ability to colonize medical devices and thrive in high-glucose environments, posing a threat to vulnerable patient groups including neonates, the elderly, and surgically treated individuals. Infections are often acquired from hands of healthcare workers or through prolonged use of total parenteral nutrition, central venous catheters, and other medically implanted devices (Tóth et al., 2019; Rupert and Rusche, 2022).

The formation of *C. parapsilosis* biofilms plays a critical role in patient outcomes, as these aggregates of blastospores and/or pseudohyphae, surrounded by an extracellular matrix (ECM) rich in carbohydrates, have been linked to increased morbidity, mortality, and resistance to conventional therapies (Tóth et al., 2019; Konečná et al., 2021). However, the role of pseudohyphal growth in *C. parapsilosis* pathogenicity remains relatively unexplored (Silva et al., 2009; Tóth et al., 2018; Banerjee et al., 2019). In contrast, the pathogenicity of *C. albicans* hyphae has been associated with the colonization and invasion process of epithelial barriers, major immune responses induction, and host cell damage via toxin secretion, among others (Silva et al., 2011; Lackey et al., 2013; Tóth et al., 2019).

In vitro biofilm studies of non-*albicans Candida* species should consider various culture variables, such as the inoculum concentration, temperature, levels of O_2 and CO_2, incubation period, growth media, and feeding conditions, as yeasts can adapt their metabolism based on nutrient availability, leading to changes in virulence factor expression, and stress-inducing environmental stimuli can influence morphology transition (Tan et al., 2016; Tóth et al., 2019; Konečná et al., 2021).

This study aims to investigate whether the effect of culture media on *C. parapsilosis* pathogenicity is attributed to metabolic or morphological adaptations, particularly pseudohyphal growth, induced by nutrient composition. We comprehensively assess the impact of nutrient availability on key biological traits of *C. parapsilosis*, utilizing four different culture media to evaluate growth, morphology, antifungal susceptibility, and *in vivo* virulence (using the *G. mellonella* model) of both planktonic and biofilm states. Our findings underscore the importance of establishing standardized culture conditions that mimic the natural infection environment to avoid cofounding alterations in biofilm properties. Overall, our study provides valuable insights into the intricate relationship between nutrient availability and *C. parapsilosis* pathogenicity.

Materials and methods

Bacterial strains and growth conditions

The fungaemia clinical isolate *Candida parapsilosis* 11103595 (Marcos-Zambrano et al., 2014) was stored at -80°C, and a loophole was recovered weekly to avoid genetic and epigenetic changes resulting from multiple passages. Incubation at 30°C for 24 h was performed on Yeast Peptone Dextrose (YPD) Agar: 1% Yeast Extract (Gibco, USA), 2% Meat Peptone (Scharlau, Spain), 2% D-glucose (Fisher Scientific S.L., USA), and 2% Bacteriological Agar (Scharlau, Spain).

Four different culture media commonly used in yeast biofilm studies (Lackey et al., 2013; Pereira et al., 2015; Tan et al., 2016; Tan et al., 2017; Leonhard et al., 2018; Gómez-Molero et al., 2021) were selected and ranked in terms of nutritional content, from highest to lowest: 1) YPD, a complex medium that supports yeast growth without selective conditions (Tan et al., 2016). It contains yeast extract and peptone that stimulate fungal replication. 2) Brain Heart Infusion (BHI) (Scharlau, Spain), a complex medium nutritionally rich but with lower glucose content than YPD. 3) Tryptic Soy Broth (TSB) (Scharlau, Spain), a complex medium with high peptone content and glucose levels similar to BHI. 4) RPMI-1640 with L-glutamine without sodium bicarbonate (Sigma-Aldrich, USA) supplemented with D-glucose at 0.2%, buffered at pH 7.0 and filter-sterilized, referred to as RPMId. A synthetic defined medium less nutritionally rich than the previous ones, but with the required amino acids and glucose content for yeast growth (Tan et al., 2016; Tan et al., 2017; Konečná et al., 2021).

Biofilm formation on silicone coupons

To obtain the inoculum for biofilm formation, yeast suspensions in each medium were prepared from YPD Overnight cultures (ON) (~16 h) at 200 rpm and 30°C. First, cells were recovered by a centrifugation at 4000, rpm for 5 min. Then, two washes with Phosphate Buffer Saline 1X (PBS) (Fisher Scientific S.L., USA) were performed. Finally, dilutions to an optical density of $\lambda = 550$ nm (OD_{550}) of 0.15 were made in each medium supplemented with 10% Fetal Bovine Serum (FBS) (Thermofisher, USA).

Silicone squares (area 1 cm^2, thickness 1.5 mm ± 0.3mm; Merefsa, Spain) were sterilized by autoclave and pre-treated with FBS at 37°C ON. A wash with PBS was performed before placing them in 24-wells cell culture plates (SPL Life Sciences, South Korea) filled with 600 µL/well of the previously prepared yeast suspensions. Biofilms were formed on a fed-batch condition by placing the silicone squares on a flat position at the bottom of the well. An exception was made at the morphological characterization experiment, where silicon squares were placed in a diagonal position inclined against the wall of the well, creating an Air Liquid Interphase (ALI) zone and a Bottom zone on the same surface.

Then, an adhesion step of 90 min was performed at 37°C and 60 rpm. Silicone squares were dipped in PBS to remove unattached cells and carefully passed to a new 24-well plate with the respective fresh media. Finally, incubation in the same conditions was carried out during 42-48 h with an intermediate step of media renewal at 24 h to create the fed-batch condition.

In addition, flow biofilms were formed using an in-house flow chamber for silicone disks (diameter 1.1 cm, thickness 1.5 mm ± 0.3mm; Merefsa, Spain) to explore morphological changes

associated with shear stress and continuous media replacement. The flow chamber was connected as previously described for a continuous-flow cell experiment (Cendra et al., 2019) with a constant flow rate of 70 mL/min of each medium tested for 24 h at 37 °C ± 3 °C. Silicone disks were pre-treated with FBS by injection into the system overnight, and a 2 h-adhesion step was performed after yeast suspension inoculation.

Morphological microscopic evaluation

Morphological characterization of planktonic cells and biofilms grown in the four media was performed. To this end, ON cultures were grown in the four culture media at 30°C, the standard temperature for yeast growth in laboratory settings, and at 37°C, the natural body temperature. Moreover, the effect of FBS 10% supplementation in planktonic cultures incubated at 37°C was also tested. Cells were recovered and washed twice with PBS (4000 rpm x 5 min). PBS-resuspended yeasts were imaged under a 100x magnification with a Nikon inverted fluorescent microscope ECLIPSE Ti–S/L100 (Nikon, Japan) coupled with a DS-Qi2 Nikon camera (Nikon, Japan) in Bright Field.

On the other hand, *C. parapsilosis* biofilms formed on the fed-batch condition (ALI and Bottom zone) and the continuous flow system were visualized via chitin staining with 10 µM Calcofluor white (CW) (Biotium, USA) under a Zeiss LSM 800 confocal scanning laser microscope (CSLM). Images were processed and measured using ImageJ Fiji software. Briefly, the area and the Length-to-Width Ratio (LWR, denoted as aspect ratio in ImageJ) were calculated from randomly chosen cells (n=30) from planktonic and biofilm conditions. Pseudohyphae were defined as forming chains of cells with box-shaped ends and LWR greater than three, and blastospores as cells oval-shaped with a lower LWR (Rupert and Rusche, 2022).

Growth, metabolic activity, and susceptibility assays

The growth of planktonic cells at 37°C and 150 rpm in the different media was recorded on 96-well polystyrene plates with a flat bottom (Corning, USA) for 15 h in a SPARK Multimode Microplate Reader (Tecan, Switzerland). Absorbance readings at 550 nm were taken every 15 min.

The minimum inhibitory concentration of 50% (MIC_{50}) for caspofungin diacetate (CAS) (Merck Life Science, Spain) and amphotericin B (AmB) (Gibco, USA) is defined as the concentration of the antifungal that inhibited growth by 50%, and it was previously determined for the employed *C. parapsilosis* isolate in our laboratory as 2 mg/mL and 0.125 mg/mL, respectively. To evaluate susceptibility variations due to media composition, planktonic cultures were grown on 96-well polystyrene plates with a flat bottom, with each media supplemented with 4 and 2 mg/mL of CAS and 0.5, 0.25 and 0.125 mg/mL of AmB. Controls were treated with culture media without antifungals. Absorbance readings at 550 nm were taken every 15 min for 10 h on a SPARK Multimode Microplate Reader and MIC_{50} of each media was determined.

As the metabolic activity of *C. parapsilosis* biofilms could be reduced by echinocandins, but resistance against azoles and standard formulations of AmB has been reported (Tóth et al., 2019), we treated 42 h mature biofilms formed on each medium with concentrations of CAS MIC_{50} x 5 (10 mg/mL) and AmB MIC_{50} x 10 (1.25 mg/mL). Control squares were treated with culture media without antifungals. 6 h after treatment, Crystal Violet (CV) (Merck Life Science, Spain) assay or PrestoBlue Cell Viability assay (Thermo Fisher Scientific, USA) were performed to quantify biomass and metabolic activity, respectively. Briefly, biofilm biomass quantification was assessed by CV 0.1% (w/v) staining for 5 min followed by a distaining step with acetic acid glacial (Scharlau, Spain) at 33% (v/v). Typical washing and fixation steps were omitted due to easy biofilm detachment from the silicone surface. OD_{570} was measured in a Microplate spectrophotometer Benchmark Plus (Bio-Rad, USA). Moreover, a CV assay was performed on biofilms after the adhesion step to evaluate differences in *C. parapsilosis* adhesion ability according to growth media (t= 0 h).

To assess biofilm metabolic activity, silicone squares were placed in tubes containing 1 mL of PBS, and biofilms were resuspended by vortex for 1 min thrice, followed by 5 min submersion in an Ultrasonic cleaner Branson2000, (Branson Ultrasonics, Netherlands). A solution 1:10 of the resazurin-based reagent PrestoBlue in RPMId media was added to each biofilm suspension. After 30 min at 37°C in the dark, fluorescence (λ_{Exc}= 535 nm and l_{em}=615 nm) was measured in a SPARK Multimode microplate reader. In addition, to corroborate the metabolic activity evaluation, biofilms were stained with FUN-1 (Thermo Fisher Scientific, USA), a green intracellular dye that converts to orange-red fluorescent cylindrical intravacuolar structures (CIVS) when cells with intact membranes have metabolic activity (Millard et al., 1997). FUN-1 at 20 mM and CW at 10 mM were added, and biofilms were incubated for 30 min at 30°C and 60 rpm after 15 h of treatment. CLSM images at 63x were processed by ImageJ software.

Finally, biofilm carbohydrate content from non-treated samples was broadly estimated from 48 h biofilms formed on each media by staining α-mannopyranosyl and α-glucopyranosyl residues from polysaccharides present in the extracellular matrix (ECM) and the fungal cell wall with 25 mg/mL Concanavalin A-Alexa Fluor 647 (ConA-A647) (Invitrogen, USA) (Shopova et al., 2013) plus CW 10 mM. CLSM images at 40X were processed by Fiji-ImageJ software. Quantification was performed with COMSTAT2 plugin from Image J software.

Galleria mellonella maintenance and *in vivo* virulence testing

G. mellonella larvae were fed with an artificial diet (15% corn flour, 15% wheat flour, 15% infant cereal, 11% powdered milk, 6% brewer's yeast, 25% honey, and 13% glycerol) and reared at 34 °C in darkness (Moya-Andérico et al., 2021).

Yeast suspensions from ON planktonic cultures in each medium were diluted in PBS, and 10 mL of three different

concentrations ($1x10^7$, $5x10^7$ and $1x10^8$ CFUs/mL) were injected into the hemocoel of eight 200 mg larvae per group, through the second left proleg using a 26-gauge microsyringe (Hamilton, Reno, NV, USA). CFUs were counted by serial plating on YPD agar and incubated for 24 h at 30°C. A control group was injected with 10 mL of PBS. All larvae were incubated at 37 °C, and mortality was monitored during 16-48 h post-injection with observations done at 16, 20, 24, 38, 42, 46 and 48 h. The same procedure was performed to determine the *in-vivo* virulence of biofilm suspensions from 24 h biofilms grown on each media in the fed-batch system. Briefly, silicon squares were placed in tubes containing 1 mL of PBS. Biofilms were resuspended by vortex during 1 min thrice, followed by 5 min on the Ultrasonic cleaner Branson2000. Biofilm suspensions were subjected to an additional vortex immediately before each larvae inoculation.

Statistical analysis

All presented data were obtained from n = 3 independent samples and *in vivo* assays were performed using n = 8 larvae. Data were analyzed by GraphPad Prism 9.00 and are presented as mean ± standard deviation. A two-way ANOVA analysis with a Tukey's multiple comparisons test was performed to compare biofilm biomass from each media at two different time points (Figure 1B). Ordinary one-way ANOVA with Šidák's multiple comparison test was conducted to compare LWR and area of cells from cultures and biofilms grown on different media within each evaluated condition (Figures 2B, C). An additional comparison of the area of cells grown in RPMId in each evaluated condition was performed (Figure 2C). Biofilm biomass and metabolic activity from control and treated biofilm samples (Figures 3A, B) were compared with a two-way ANOVA analysis with Šidák's multiple comparison. Finally, Long-rank tests were conducted between Kaplan Meyer curves to evaluate virulence differences (Figures 5B–D). A defined p-value <0.05 was considered statistically significant in all cases. Moreover, when required, a Shapiro-Wilk and Kolmogorov-Smirnov test were used to evaluate normality, and the p-value was automatically adjusted for multiplicity.

Use of generative AI and AI-assisted technologies in the writing process

ChatGPT version GPT-3.5 from OpenAI was used during the preparation of this work to improve readability and language. After using this tool, the authors reviewed and edited the content as needed.

Results

Culture media impact *C. parapsilosis* growth and morphology

First, we assessed the impact of four commonly used media on the growth of *C. parapsilosis* planktonic cultures and biofilms formed under fed-batch conditions. YPD supported the highest planktonic growth, as evident from the absorbance curve

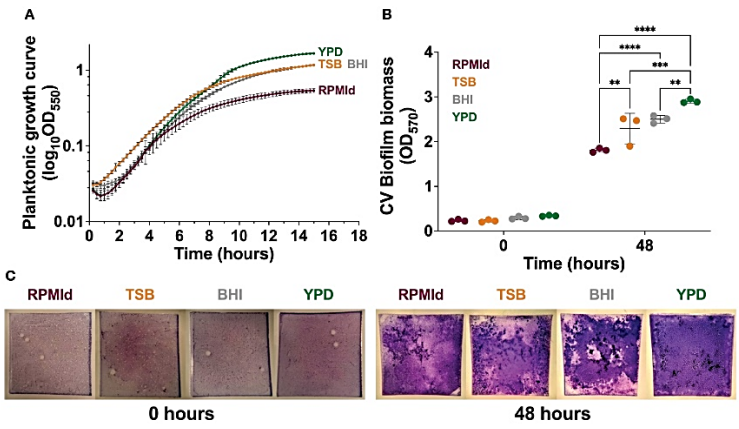

FIGURE 1
Influence of culture media on *C. parapsilosis* growth. **(A)** Planktonic growth curves on different culture media by absorbance measurements taken every 15 min for 15 h. The absorbance of each respective media was subtracted from each curve, and mean lines and standard deviation bars from 3 different experiments (4 wells per media) are presented. **(B)** Biofilm biomass quantification on each media by Crystal violet (CV) assay after the adhesion step (0 h) and biofilm maturation process (48 h). The plotted values represent 3 different biological experiments, with each value corresponding to the mean derived from 3-6 technical replicates. Error bars display mean and standard deviation across the biological replicates. Data was compared by a two-way ANOVA analysis with a Tukey's multiple tests (**p-value <0.01; ***p-value <0.001; ****p-value <0.0001). **(C)** Representative macroscopic images of silicone squares dyed with CV after the adhesion step (0 h) and biofilm maturation process (48 h) on each media.

10.3389/fcimb.2023.1323619

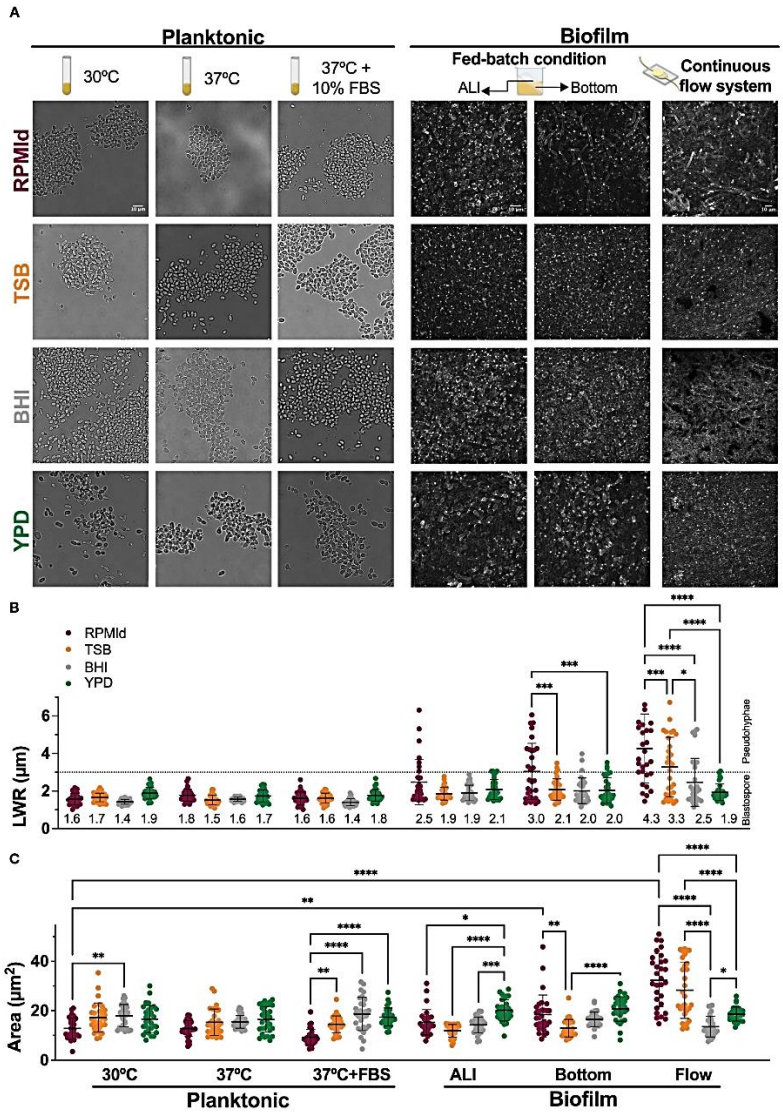

FIGURE 2
C. parapsilosis morphology under different media and growth conditions. **(A)** From left to right: bright-field microscopy images of overnight cultures grown in four different media at 30°C and 37°C without and with 10% of Fetal Bovine serum (FBS) supplementation; 48h biofilms grown on silicone squares placed in an inclined position in 24-wells plates to obtain an Air Liquid Interphase (ALI) and a Bottom zone; Biofilms formed on silicone coupons under continuous flow inside a custom-made device at 70 µL/min for 24h. Confocal images of biofilms were taken using Calcofluor White dye and processed with Image-J to create Z-stacks of top layers. The scale bar of 10 mm is the same for each growth condition. **(B)** Length-to-wide ratio (LWR) and **(C)** area of randomly selected cells (n=30) from each media and condition measured with Image J Horizontal dashed line represents the LWR limit for morphology classification: dots below the dashed line correspond to cells considered blastospores, and dots above the line are considered pseudohyphae cells. Numbers in LWR graph correspond to mean value. Error bars display mean and standard deviation. Data was compared by a one-way ANOVA analysis with Šidák's multiple comparison test (∗*p*-value <0.05; ∗∗*p*-value <0.01; ∗∗∗*p*-value <0.001; ∗∗∗∗*p*-value <0.0001).

10.3389/fcimb.2023.1323619

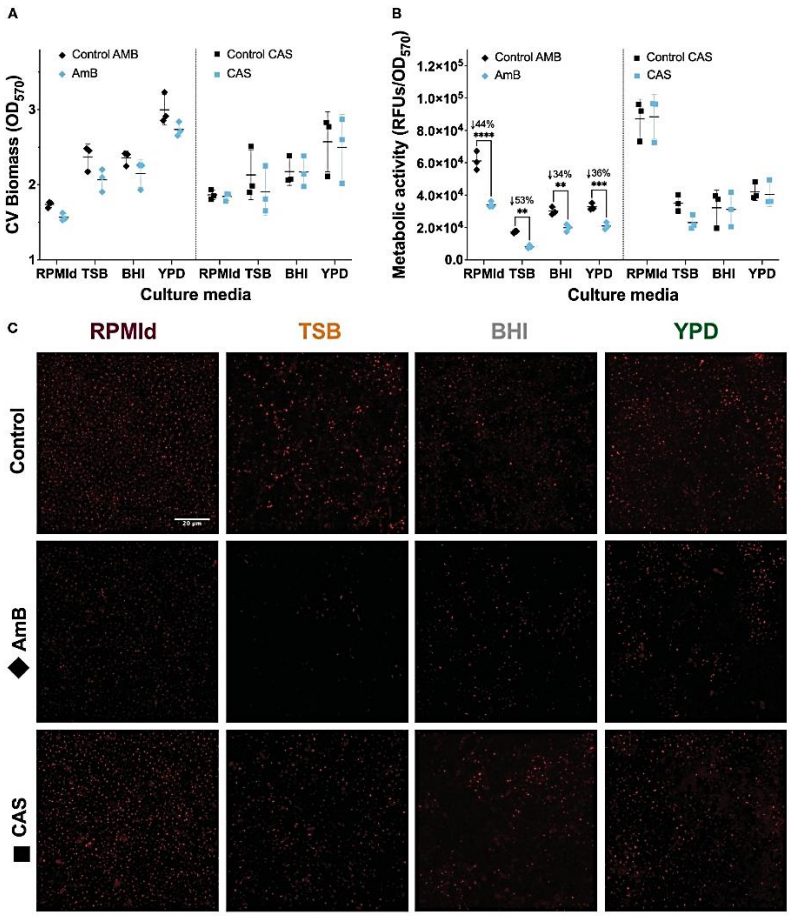

FIGURE 3
C. parapsilosis biofilm susceptibility to AmB and CAS at different culture media. 42 h biofilms grown in all media and treated for 6 h with 1.25 mg/mL of AmB and 10 mg/mL of CAS were analyzed by **(A)** Biomass quantification with Crystal Violet (CV) assay, and metabolic activity evaluation by **(B)** PrestoBlue assay, and **(C)** FUN-1 vitality staining. Biofilm experiments were conducted in triplicate. The plotted values represent 3 different biological experiments, with each value corresponding to the mean derived from 3-6 technical replicates. Error bars display mean and standard deviation. Asterisks indicate statistically significant differences versus control in an Ordinary two-way ANOVA with Šidák's multiple comparison test (∗∗*p*-value <0.01; ∗∗∗*p*-value <0.001; ∗∗∗∗*p*-value <0.0001). The percentage of reduction concerning control is indicated with the symbol ↓ on top of the asterisks. RFUs, Relative Fluorescence Units. Z-stacks of red fluorescence channel display intravacuolar structures as an indicator of metabolically active cells. All images were processed with Image-J. The scale bar (20 mm) is the same for all images.

(Figure 1A), followed by TSB and BHI, while RPMId showed the lowest growth. The trend was consistent in fed-batch biofilms, as seen through Crystal violet (CV) staining (Figures 1B, C 48 h). To ensure that media properties did not influence biofilm biomass (Figures 1B, C 48 h) by attachment variations, a CV assay after the adhesion step was performed (Figures 1B, C 0 h), showing no significant differences among media.

Next, we investigated how culture media influenced *C. parapsilosis* morphology using microscopic analysis (Figure 2). According to the Length-to-Wide Ratio (LWR), planktonic cultures predominantly exhibited blastopores (~1.5 µm) regardless of the culture media used (Figures 2A, B). RPMId-grown cells showed a significant reduction in cell size at 30°C and 37°C + FBS conditions (Figure 2C. Planktonic. Fuchsia dots).

More relevant morphological differences were observed in biofilms formed under three different conditions (see methods section). 1) At the Air Liquid Interface (ALI) of fed-batch biofilms, RPMId and YPD showed pseudohyphae, with a proportion of 23% and 3%, respectively (Figures 2A, B. Biofilm-ALI. Fuchsia and green dots). RPMId induces pseudohyphae cells

10.3389/fcimb.2023.1323619

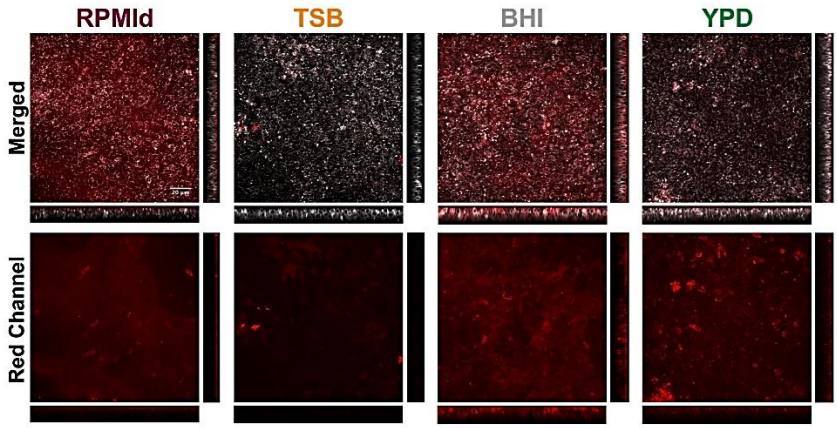

FIGURE 4
Visualization of the carbohydrate content of *C. parapsilosis* biofilms formed on different media by ConA-A647 staining. 48h biofilms grown on silicone squares with different media were stained with Calcofluor White (grey) to visualize cell walls and ConA-A647 (red) to visualize α-mannopyranosyl and α-glucopyranosyl residues from polysaccharides present in the extracellular matrix and the fungal cell wall. Images were processed with Image-J to create Z-stacks. Orthogonal views from cuts at the center of the X and Y axis are displayed. The XZ orthogonal displays deeper to superficial stacks from bottom to top, while YZ orthogonal display them from right to left. The scale bar (20 μm) is the same for all images.

with greater length (1.5-6.3 μm) (Figure 2B. Biofilm-ALI. Fuchsia dots), and YPD produced significatively larger cells (30%) compared to the other media (~20 μm^2 vs ~14 μm^2) (Figure 2C. Biofilm-ALI. Green dots).

2) In the Bottom zone of fed-batch biofilms, where oxygen availability was lower, pseudohyphal growth was evident in all media, but more pronounced in RPMId (Figure 2B. Biofilm-Bottom. Fuchsia dots), with 50% pseudohyphae compared to 3% in TSB, BHI and YPD. YPD and RPMId produced biofilms with the largest cells (20.7 μm^2 and 18.5 μm^2, respectively) (Figure 2C. Biofilm-Bottom. Green and fuchsia dots).

Finally, 3) in continuous flow biofilms with shear stress, RPMId showed a significant higher proportion of pseudohyphae (~70%), followed by TSB (~50%), while BHI had 30% and YPD had almost none (3%) (Figures 2A, B Biofilm-Flow). RPMId and TSB produced significant the largest cells (32.3 μm^2 and 28.3 μm^2, respectively) (Figure 2C. Biofilm-Flow. Fuchsia and orange dots).

Notably, RPMId-grown cells were longer in the continuous flow system (4.3 μm) compared to the bottom (3 μm) and ALI zone (2.5 μm) of fed-batch biofilms and planktonic cultures (~1.8 μm) (Figure 2C. Fuchsia dots). This difference is significative when comparing planktonic cultures at 30°C with biofilms formed at the bottom of the fed-batch systems and biofilms formed under flow condition. These results highlight the role of culture media in shaping *C. parapsilosis* growth and morphology in various conditions.

Culture media influences *C. parapsilosis* antifungal susceptibility

Then, we assessed the impact of culture media on antifungal susceptibility of *C. parapsilosis* planktonic cultures and fed-batch biofilms. The Minimum Inhibitory Concentration 50% (MIC_{50}) of planktonic cultures to caspofungin (CAS) was ≤ 2 mg/mL for all media, while for amphotericin B (AmB), it was higher in YPD (0.25 mg/mL) compared to the other media (0.125 mg/mL).

In biofilms, which can impede antifungal treatment through compound sequestering (Tóth et al., 2019), we observed distinct results compared to planktonic cultures (Figure 3). No effect on biomass or metabolic activity was observed in biofilms following treatment with CAS at 10 mg/mL (Figure 3A, B. blue squares). In contrast, AmB at 1.25 mg/mL effectively reduced the metabolic activity of biofilms from all media tested (Figure 3A, B blue diamonds). FUN-1 staining confirmed the metabolic activity after antifungal treatment (Figure 3C), showing a reduction in red fluorescent cylindrical intravacuolar structures (CIVS) in AmB-treated biofilms from all media (Figure 3C).

To understand whether the variations in biofilm susceptibility were related to differences in the ECM, we estimated the biofilm carbohydrate content using ConA-A647 staining and COMSTAT2 quantification (Figure 4). The analysis revealed notable differences in carbohydrates on the cell wall and ECM, depending on the culture media used. BHI biofilms had the highest carbohydrate content (20.25 + 3.18 mm^3/mm^2), followed by RPMId (10.83 + 2.82 mm^3/mm^2), YPD (8.66 + 3.02 mm^3/mm^2), and TSB (2.64 + 1.93 mm^3/mm^2). Additionally, there was an association between biofilm carbohydrate content (Figure 4) and the decrease in metabolic activity after AmB treatment (Figure 3B). Notably, variation in the quantity of carbohydrates on the cell wall also played an important role. BHI biofilms, with a higher level of carbohydrate in both ECM and cell wall (Figure 4), showed a lower reduction in metabolic activity after AmB treatment (34%) (Figure 3B), while TSB-formed biofilms, with little carbohydrate content in the cell wall (Figure 4), presented the highest decline in metabolic activity (53%) (Figure 3B).

10.3389/fcimb.2023.1323619

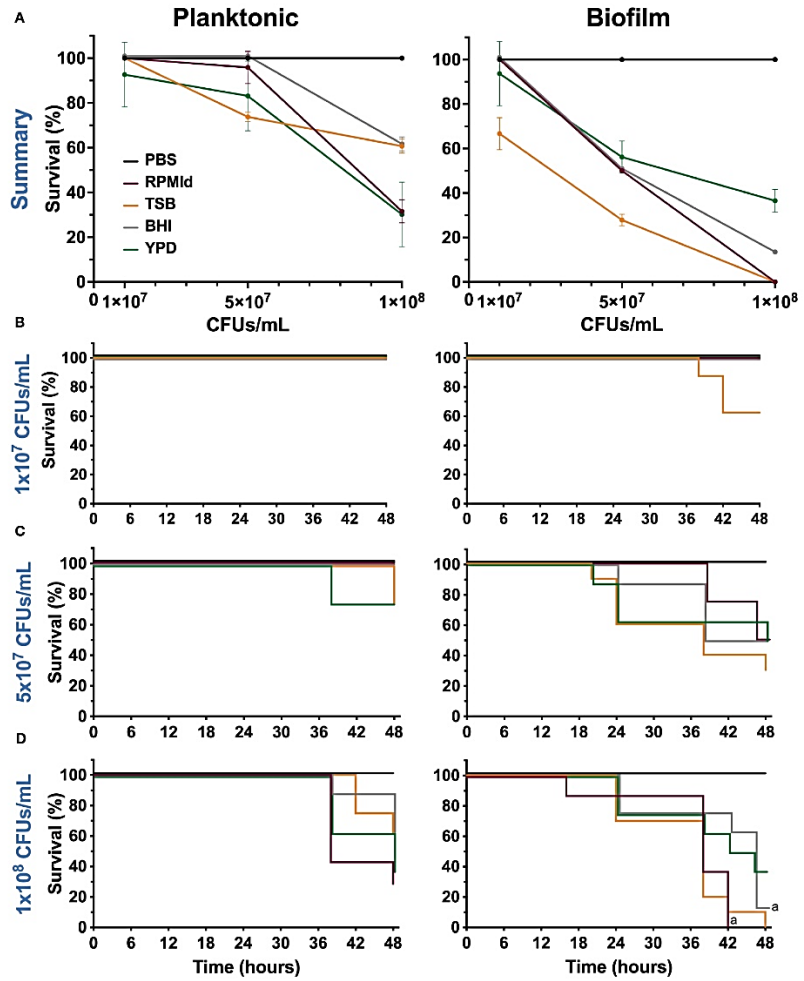

FIGURE 5
Virulence of *C. parapsilosis* cells from planktonic cultures and biofilm suspensions grown in different media on *G. mellonella* larvae. **(A)** Survival percentage of *G. mellonella* larvae at 48 h after inoculation of three different concentrations. Error bars display mean and standard deviation. Kaplan-Meier survival curves of (*G. mellonella* larvae injected with *C. parapsilosis* cells from planktonic cultures and biofilm suspensions formed on various media at concentrations of **(B)** $1x10^7$ CFUs/mL, **(C)** $5x10^7$ CFUs/mL and **(D)** $1x10^8$ CFUs/mL. Control larvae were injected with PBS. Larval mortality was monitored for 16-48 h post-injection with observations done at 16, 20, 24, 38, 42, 46 and 48 h. Significant differences among media used were evaluated by a long-rank test (a: *p*-value <0.05 between specified lines). The results presented in this figure are representative of the same experiment repeated three times with similar outcomes, each condition having 8 larvae.

Culture media affects *C. parapsilosis* virulence

Our final aim was to evaluate variations in *C. parapsilosis* virulence according to the growth media and growth mode. To achieve this, we injected three different concentrations of planktonic cultures and PBS-resuspended fed-batch biofilms of *C. parapsilosis* grown from each medium into *G. mellonella* larvae and evaluated the survival percentage until 48 h post-infection (Figure 5).

In the planktonic state, we observed virulence differences depending on the culture media used when injected $5x10^7$ CFUs/mL and $1x10^8$ CFUs/mL (Figure 5A). There was an important decrease in survival percentage when cells from BHI, RPMId and YPD reached the highest concentration, although this decline was less pronounced in BHI. In contrast, we observed a progressive decline in the survival percentage in relation to the concentration when injecting cells from TSB.

As expected, the slope of survival curves was more pronounced when injected with biofilm suspensions than planktonic cells

(Figure 5B). In this case, the decline in survival percentage was progressive in all media according to the inoculated concentration, but clearly, the most virulent cells came from TSB.

The Kaplan-Meier survival curves of the different concentrations of both states showed significant difference only between biofilm suspensions from RPMId and BHI at a concentration of $1x10^8$ CFUs/mL (Figures 5B–D).

Discussion

The increasing incidence of *Candida*-systemic infections in the last two decades (Sharma and Chakrabarti, 2023) has boosted yeast research. However, a significant concern in yeast studies is the inconsistency in selecting culture media for growth, biofilm formation, and antifungal susceptibility testing (Konečná et al., 2021). In this study, we thoroughly evaluated the impact of four commonly used culture media in *C. parapsilosis*' main pathogenic features, both in planktonic and different biofilm growth modes. Our results clearly demonstrate specific pathogenic advantages depending on the culture media employed (Table 1).

The biomass quantification (Figure 1) showed that *C. parapsilosis* growth in planktonic and biofilm states is directly proportional to the richness of the culture medium, specifically to the high-glucose content. This finding aligns with the prevalence of *C. parapsilosis* in systemic infections of patients receiving parenteral nutrition (Nosek et al., 2009; Pereira et al., 2015; Tan et al., 2016; Herek et al., 2019; Tóth et al., 2019; Santos et al., 2020; Konečná et al., 2021). Moreover, media containing abundant nutrients and glucose inhibit pseudohyphal growth, suggesting that the transition to pseudohyphae in *C. parapsilosis* may be an evolutionarily conserved response to starvation (Lackey et al., 2013; Rupert and Rusche, 2022). Consistent with this observation, our morphological evaluation did not reveal filamentation in *C. parapsilosis* planktonic cultures (Figure 2. Planktonic) as we assessed only completed media. Additionally, a negligible proportion of pseudohyphae were present in biofilms formed in YPD medium, which had the highest glucose availability (Figure 2B. Biofilm. Green dots).

Furthermore, as reported for *C. albicans* (Thein et al., 2007; Paramonova et al., 2009), we observed that *C. parapsilosis* filamentation is promoted by low oxygen and shear conditions (Figures 2A, B. Biofilm-Bottom and Flow). This phenomenon is further enhanced when yeast is grown under the filament inducing medium RPMI (fuchsia dots). Moreover, in the continuous flow model, which is highly relevant considering the nature of *C. parapsilosis* infection, the degree of biofilm filamentation is inversely proportional to the richness of the media employed (Figures 2A, B Biofilm-Flow). This shows that the morphology of *C. parapsilosis* cells, and consequently, the composition of biofilms, is the result of multiple interacting factors. Besides, pseudohyphal growth in this *Candida* specie allows it to survive under limited and harsh conditions, such as low nutrient availability, low oxygen levels, and shear stress forces.

Little is known about the influence of *C. parapsilosis* morphology on antifungal susceptibility. A recent study showed that cellular processes involved in pseudohyphal growth and CAS susceptibility are related when *C. parapsilosis* is grown on glycerol at 37°C but not when grown on glucose (Rupert and Rusche, 2022). Thus, although correlations between pseudohyphal growth and susceptibility to antifungals could exist in *C. parapsilosis*, they

TABLE 1 Summary of culture media influence on *C. parapsilosis* main characteristics.

	RPMId	TSB	BHI	YPD
Main Characteristics				
Overall nutrients	++	+++	+++	++++
Glucose content	4 g/L (0,4%)	2,5 g/L (0,25%)	2 g/L (0,2%)	20 g/L (2%)
Nitrogen content	Amino Acids »1 g/L (0.1%)	Casein and Soya peptone 20 g/L (2%)	Animal tissue peptone and Brain-Heart Infusion 27 g/L (2,7%)	Yeast extract and Meat peptone 30 g/L (3%)
Planktonic				
Growth	+	+++	+++	++++
Resistance	+	++	+	+++
Virulence	++	++	+	+++
Biofilm				
Growth	+	+++	+++	++++
Metabolic activity	++++	++	++	++
Filamentation	++++	+++	++	+
Carbohydrate content	++	+	++++	++
Resistance	+++	++	++++	++++
Virulence	+++	++++	+++	++

+ low, ++ medium, +++ high, ++++ superhigh.

may be restricted to particular scenarios. In this study, we evaluated *C. parapsilosis* susceptibility to CAS, the recommended first-line empirical treatment of patients with systemic candidiasis (Tóth et al., 2019), and complemented the results by exploring the polyene AmB. However, under the evaluated conditions, our results do not provide evidence of the mentioned association.

On the other hand, previous studies had described variations in biofilm drug susceptibility according to glucose levels (Santos et al., 2020; Gómez-Molero et al., 2021). For instance, reducing the metabolic activity of *C. parapsilosis* biofilms by 70% requires a concentration of 0.5 μg/mL and 16 μg/mL of AmB when formed on RPMI and YPD medium, respectively (Gómez-Molero et al., 2021). This could be directly related to the fact that increasing glucose concentrations produces *C. parapsilosis* biofilms with higher amounts of carbohydrates in the ECM (Pereira et al., 2015). To test this hypothesis, we broadly estimate the carbohydrate content of biofilms formed on each medium by COMSTAT2 quantification of ConA-A647 stained biomass (Figure 4). We noticed that a greater carbohydrate content in both the cell wall and ECM (Figure 4) correlates with a lower decrease in biofilm metabolic activity after AmB treatment (Figures 3B, C). This is consistent with previous reports of antifungal tolerance correlating with the presence of glucans and mannans on *Candida* biofilm ECM, which decreased the drug's capacity to penetrate and reach cells (Dominguez et al., 2018; Nett and Andes, 2020). Moreover, we hypothesize that some media could favor an increase in carbohydrate content of the cell wall as rescue mechanism against AmB fungal membrane damage.

Nonetheless, it is important to mention that we used ConA-A647 staining as a first exploratory method for biofilm carbohydrate quantification (a dye specific for α-mannopyranosyl and α-glucopyranosyl residues from polysaccharides), but more accurate techniques must be performed to validate our data. Likewise, it is relevant to assess the influence of culture media on other cell wall and ECM components (chitin, β-1,3 glucan, protein, eDNA, etc.) and evaluate their impact on biofilm susceptibility. By doing so, new combinations of antifungals and specific ECM-disrupting compounds will be identified as a strategic treatment for *C. parapsilosis* biofilm infections.

Finally, we evaluated whether the *in vivo* virulence of *C. parapsilosis* varies according to nutrient availability (Figure 5). To that end, we used *G. mellonella*, an alternative animal model suitable for studying *C. parapsilosis* infections (Gago et al., 2014; Jacobsen, 2014; Souza et al., 2015; Binder et al., 2020; Rupert and Rusche, 2022). It was previously reported that the virulence of *C. parapsilosis* cultures on *G. mellonella* is not associated with the metabolic activity and biomass of biofilms formed by the same strains (Marcos-Zambrano et al., 2020). Thus, we injected suspensions from planktonic cultures and biofilms. As far as we know, this is the first report of inoculation of biofilm suspensions into *G. mellonella*. Although we realize this does not represent a chronic infection model, we wanted to determine if metabolic and morphologic adaptations to biofilm state and/or the presence of ECM components exerted variation in virulence depending on the culture media used. Indeed, differences in virulence between planktonic cultures and biofilm suspensions from the same media showed that, depending on nutrient availability, some biofilm factors could favor *C. parapsilosis* pathogenicity (Figure 4). For instance, the host immune response: *C. parapsilosis* biofilms are more resistant to neutrophil killing than planktonic cells, probably due to extracellular mannan-glucan (Camarillo-Márquez et al., 2018; Nett and Andes, 2020). Besides, yeast β - (1,3) glucan alters hemocyte subpopulations in *G. mellonella* and enhance their ability to kill (Sheehan and Kavanagh, 2018).

On the other hand, the biofilm state implies metabolic adaptations that can have a role in pathogenicity (Tóth et al., 2019). For example, the hydrolytic lipases are enzymes required for biofilm formation but also host tissue damage and modulation of the immune system (Tóth et al., 2019; Zoppo et al., 2021). Moreover, Rupert & Rusche (2022) found that *G. mellonella* survival was different if *C. parapsilosis* cells were pre-grown on a medium containing glucose or glycerol (Rupert and Rusche, 2022). Thus, *C. parapsilosis* virulence is affected by the carbon source available before infection, suggesting a critical effect of yeast metabolic adaptations on host mortality. Notably, they did not observe any correlation between pseudohyphal growth and virulence outcomes (Rupert and Rusche, 2022).

Filamentation in *C. albicans* is important for tissue invasion; however, a blastospore-locked mutant had shown virulence advantages in a mouse model of systemic infection (Dunker et al., 2021). Similarly, a mutant with hyphal formation defects have shown that filamentation alone is insufficient to kill *G. mellonella* (Fuchs et al., 2010), indicating that blastospores themselves are not less virulent than filamentation forms (Dunker et al., 2021). In fact, most pathogenic dimorphic fungi do not grow as hyphae in the body, like *Histoplasma* spp., *Blastomyces* spp., *Candida auris* and *Candida glabrata* (Sudbery et al., 2004; Galocha et al., 2019; Dunker et al., 2021). In the case of *C. parapsilosis*, pseudohyphae has not been associated with invasion or cell damage (Kim et al., 2006; Silva et al., 2009; Tóth et al., 2018). A hyperfilamentous mutant had shown a downregulation of genes important for pathogenicity and less organ fungal burden on mice (Banerjee et al., 2019). Similarly, a mutated strain with extremely long and aggregating pseudohyphae had increased survival to killing by J774.1 macrophage-like cells but was avirulent on *G. mellonella* and had reduced fungal burden on mice (Tóth et al., 2018).

Our virulence results agree with the previously exposed information (Figure 5). Nutrient availability of different culture media influences *G. mellonella* survival after *C. parapsilosis* infection with cells from planktonic cultures or biofilms. As expected, we observed that biofilm suspensions had a more pronounced effect on larvae survival. However, we cannot explain virulence solely by correlating it with one of the studied factors (biomass, metabolic activity, filamentation, carbohydrate content). Instead, we believed that different biological traits contribute to *C. parapsilosis* virulence, with metabolic adaptations being a critical focus for further research. Future work on variations in the expression of specific virulence factors (lipases, proteinases, adhesins, etc.) according to nutrient availability could help narrow the landscape. Notably, TSB media produces biofilms that are more virulent but more susceptible to the evaluated antifungals, suggesting a trade-off in *C. parapsilosis* performance.

Our experiments were performed using a single clinical isolate of *C. parapsilosis*, but we expect the overall findings to be useful and applicable. A detailed outline of culture media influence on *C. parapsilosis* main characteristics are summarized in Table 1. This

study reaffirms the importance of understanding how pathogenic microorganisms behave under different conditions to establish research protocols that better resemble the infection site. Only in this way we will find appropriate therapeutic strategies. Considering the impact of glucose on *C. parapsilosis* biofilms, it could be recommendable that candidemia studies be performed considering two different scenarios: catheter-associated infections with low glucose concentrations (0.06-0.1% bloodstream) (Dunker et al., 2021) or infections associated with parenteral nutrition with high glucose concentrations (10-30%) (Herek et al., 2019).

Data availability statement

The raw data supporting the conclusions of this article will be made available by the authors, without undue reservation.

Author contributions

BA-J: Conceptualization, Data curation, Formal Analysis, Investigation, Methodology, Software, Validation, Visualization, Writing – original draft, Writing – review & editing. JA: Data curation, Formal Analysis, Investigation, Methodology, Writing – review & editing. NB-C: Data curation, Investigation, Methodology, Supervision, Writing – review & editing. ET: Conceptualization, Formal Analysis, Funding acquisition, Investigation, Project administration, Resources, Supervision, Validation, Visualization, Writing – review & editing.

Funding

The author(s) declare financial support was received for the research, authorship, and/or publication of this article. This study was partially supported by grants PID2021-125801OB-100, PLEC2022-009356 and PDC2022-133577-I00 funded by MCIN/AEI/10.13039/501100011033 and "ERDF A way of making Europe", the CERCA program and AGAUR-Generalitat de Catalunya (2021SGR01545), the European Regional Development Fund (FEDER) and Catalan Cystic Fibrosis association. The project that gave rise to these results received the support of a fellowship from "la Caixa" Foundation (ID1000, 10434). The fellowship code is "LCF/BQ/DI20/11780040" and was granted to BA-J. JA thanks Generalitat de Catalunya for its financial support through the FI program (2021FI_B00118). NB-C acknowledges Ministerio de Universidades, Spain, for the Margarita Salas grant funded by the European Union-Next Generation EU.

Acknowledgments

We thank Dr Jesus Guinea Ortega from the Department of Clinical Microbiology and Infectious Diseases, Hospital General Universitario Gregorio Marañón, Madrid, Spain, for the generous gift of the *Candida parapsilosis*1110, 3595 used in this study. We also thank ChatGPT version GPT-3.5 from OpenAI for the service of language proofreading during the preparation of this work.

Conflict of interest

The authors declare that the research was conducted in the absence of any commercial or financial relationships that could be construed as a potential conflict of interest.

Publisher's note

All claims expressed in this article are solely those of the authors and do not necessarily represent those of their affiliated organizations, or those of the publisher, the editors and the reviewers. Any product that may be evaluated in this article, or claim that may be made by its manufacturer, is not guaranteed or endorsed by the publisher.

References

Banerjee, M., Lazzell Anna, L., Romo Jesus, A., Lopez-Ribot Jose, L., and Kadosh, D. (2019). Filamentation is associated with reduced pathogenicity of multiple non-*albicans Candida* species. *mSphere* 4, e00656–e00619. doi: 10.1128/mSphere.00656-19

Binder, U., Arastehfar, A., Schnegg, L., Hörtnagl, C., Hilmioğlu-Polat, S., Perlin, D. S., et al. (2020). Efficacy of LAMB against emerging azole- and Multidrug-Resistant Candida parapsilosis isolates in the *Galleria mellonella* model. *J. Fungi* 6, 377. doi: 10.3390/jof6040377

Camarillo-Márquez, O., Córdova-Alcántara, I. M., Hernández-Rodríguez, C. H., García-Pérez, B. E., Martínez-Rivera, M. A., and Rodríguez-Tovar, A. V. (2018). Antagonistic interaction of *Staphylococcus aureus* toward *Candida glabrata* during in *vitro* biofilm formation Is caused by an apoptotic mechanism. *Front. Microbiol.* 9.

Cendra, M. D. M., Blanco-Cabra, N., Pedraz, L., and Torrents, E. (2019). Optimal environmental and culture conditions allow the in *vitro* coexistence of *Pseudomonas aeruginosa* and *Staphylococcus aureus* in stable biofilms. *Sci. Rep.* 9, 16284. doi: 10.1038/s41598-019-52726-0

Dominguez, E., Zarnowski, R., Sanchez, H., Covelli Antonio, S., Westler William, M., Azadi, P., et al. (2018). Conservation and divergence in the *Candida* Species biofilm matrix mannan-glucan complex structure, function, and genetic control. *mBio* 9, e00451–e00418. doi: 10.1128/mBio.00451-18

Dunker, C., Polke, M., Schulze-Richter, B., Schubert, K., Rudolphi, S., Gressler, A. E., et al. (2021). Rapid proliferation due to better metabolic adaptation results in full virulence of a filament-deficient *Candida albicans* strain. *Nat. Commun.* 12, 3899. doi: 10.1038/s41467-021-24095-8

Fuchs, B. B., Eby, J., Nobile, C. J., El Khoury, J. B., Mitchell, A. P., and Mylonakis, E. (2010). Role of filamentation in *Galleria mellonella* killing by *Candida albicans*. *Microbes Infection* 12, 488–496. doi: 10.1016/j.micinf.2010.03.001

Gago, S., García-Rodas, R., Cuesta, I., Mellado, E., and Alastruey-Izquierdo, A. (2014). *Candida parapsilosis, Candida orthopsilosis,* and *Candida metapsilosis* virulence in the non-conventional host *Galleria mellonella*. *Virulence* 5, 278–285. doi: 10.4161/viru.26973

Galocha, M., Pais, P., Cavalheiro, M., Pereira, D., Viana, R., and Teixeira, M. C. (2019). Divergent approaches to virulence in *C. albicans* and *C. glabrata*: Two sides of the same coin. *Int. J. Mol. Sci.* 20, 2345. doi: 10.3390/ijms20092345

Gómez-Molero, E., De-La-Pinta, I., Fernández-Pereira, J., Groß, U., Weig, M., Quindós, G., et al. (2021). *Candida parapsilosis* colony morphotype forecasts biofilm formation of clinical isolates. *J. Fungi* 7, 33. doi: 10.3390/jof7010033

Herek, T. C., Menegazzo, V. R., Ogaki, M. B., Perini, H. F., Maia, L. F., and Furlaneto, M. C. (2019). Biofilm formation by blood isolates of *Candida parapsilosis* sensu stricto in the presence of a hyperglycidic solution at comparable concentrations of total

parenteral nutrition. *Rev. da Sociedade Bras. Medicina Trop.* 52, e-20180182. doi: 10.1590/0037-8682-0182-2018

Jacobsen, I. D. (2014). *Galleria mellonella* as a model host to study virulence of *Candida*. *Virulence* 5, 237–239. doi: 10.4161/viru.27434

Kim, S.-K., Bissati, K. E., and Mamoun, C. B. (2006). Amino acids mediate colony and cell differentiation in the fungal pathogen *Candida parapsilosis*. *Microbiology* 152, 2885–2894. doi: 10.1099/mic.0.29180-0

Konečná, K., Němečková, I., Diepoltová, A., Vejsová, M., and Janďourek, O. (2021). The impact of cultivation media on the in *vitro* biofilm biomass production of. *Candida Curr. Microbiol.* spp 78, 2104–2111. doi: 10.1007/s00284-021-02452-6

Lackey, E., Vipulanandan, G., Childers Delma, S., and Kadosh, D. (2013). Comparative evolution of morphological regulatory functions in *Candida* Species. *Eukaryotic Cell* 12, 1356–1368. doi: 10.1128/EC.00164-13

Leonhard, M., Zatorska, B., Moser, D., Tan, Y., and Schneider-Stickler, B. (2018). Evaluation of combined growth media for in *vitro* cultivation of oropharyngeal biofilms on prosthetic silicone. *J. Materials Science: Materials Med.* 29, 45. doi: 10.1007/s10856-018-6051-7

Marcos-Zambrano, L. J., Bordallo-Cardona, M.Á., Borghi, E., Falleni, M., Tosi, D., Muñoz, P., et al. (2020). *Candida* isolates causing candidemia show different degrees of virulence in *Galleria mellonella*. *Med. Mycology* 58, 83–92. doi: 10.1093/mmy/myz027

Marcos-Zambrano, L. J., Escribano, P., Bouza, E., and Guinea, J. (2014). Production of biofilm by *Candida* and non-*Candida* spp. isolates causing fungemia: Comparison of biomass production and metabolic activity and development of cut-off points. *Int. J. Med. Microbiol.* 304, 1192–1198. doi: 10.1016/j.ijmm.2014.08.012

Millard, P. J., Roth, B. L., Thi, H. P., Yue, S. T., and Haugland, R. P. (1997). Development of the FUN-1 family of fluorescent probes for vacuole labeling and viability testing of yeasts. *Appl. Environ. Microbiol.* 63, 2897–2905. doi: 10.1128/aem.63.7.2897-2905.1997

Moya-Andérico, L., Vukomanovic, M., Cendra, M. D. M., Segura-Feliu, M., Gil, V., Del Río, J. A., et al. (2021). Utility of *Galleria mellonella* larvae for evaluating nanoparticle toxicology. *Chemosphere* 266, 129235. doi: 10.1016/j.chemosphere.2020.129235

Nett, J. E., and Andes, D. R. (2020). Contributions of the biofilm matrix to *Candida* pathogenesis. *J. Fungi (Basel)* 6, 21. doi: 10.3390/jof6010021

Nosek, J., Holesova, Z., Kosa, P., Gacser, A., and Tomaska, L. (2009). Biology and genetics of the pathogenic yeast *Candida parapsilosis*. *Curr. Genet.* 55, 497–509. doi: 10.1007/s00294-009-0268-4

Paramonova, E., Krom, B. P., van der Mei, H. C., Busscher, H. J., and Sharma, P. K. (2009). Hyphal content determines the compression strength of *Candida albicans* biofilms. *Microbiology* 155, 1997–2003. doi: 10.1099/mic.0.021568-0

Pereira, L., Silva, S., Ribeiro, B., Henriques, M., and Azeredo, J. (2015). Influence of glucose concentration on the structure and quantity of biofilms formed by *Candida parapsilosis*. *FEMS Yeast Res.* 15, fov043. doi: 10.1093/femsyr/fov043

Rupert, C. B., and Rusche, L. N. (2022). The pathogenic yeast *Candida parapsilosis* forms pseudohyphae through different signaling pathways depending on the available carbon source. *mSphere* 7, e00029–e00022. doi: 10.1128/msphere.00029-22

Santos, F., Leite-Andrade, M. C., Brandão, I. D. S., Alves, A. I. D. S., Buonafina, M. D. S., Nunes, M., et al. (2020). Anti-biofilm effect by the combined action of fluconazole and acetylsalicylic acid against species of Candida parapsilosis complex. *Infection Genet. Evol.* 84, 104378. doi: 10.1016/j.meegid.2020.104378

Sharma, M., and Chakrabarti, A. (2023). Candidiasis and other emerging yeasts. *Curr. Fungal Infection Rep.* 17, 15–24. doi: 10.1007/s12281-023-00455-3

Sheehan, G., and Kavanagh, K. (2018). Analysis of the early cellular and humoral responses of *Galleria mellonella* larvae to infection by *Candida albicans*. *Virulence* 9, 163–172. doi: 10.1080/21505594.2017.1370174

Shopova, I., Bruns, S., Thywissen, A., Kniemeyer, O., Brakhage, A. A., and Hillmann, F. (2013). Extrinsic extracellular DNA leads to biofilm formation and colocalizes with matrix polysaccharides in the human pathogenic fungus *Aspergillus fumigatus*. *Front. Microbiol.* 4, 141. doi: 10.3389/fmicb.2013.00141

Silva, S., Henriques, M., Oliveira, R., Azeredo, J., Malic, S., Hooper, S. J., et al. (2009).). Characterization of *Candida parapsilosis* infection of an in *vitro* reconstituted human oral epithelium. *Eur. J. Oral. Sci.* 117, 669–675. doi: 10.1111/j.1600-0722.2009.00677.x

Silva, S., Negri, M., Henriques, M., Oliveira, R., Williams, D. W., and Azeredo, J. (2011). Adherence and biofilm formation of non-*Candida albicans Candida* species. *Trends Microbiol.* 19, 241–247. doi: 10.1016/j.tim.2011.02.003

Souza, A. C. R., Fuchs Beth, B., Pinhati Henrique, M. S., Siqueira Ricardo, A., Hagen, F., Meis Jacques, F., et al. (2015). *Candida parapsilosis* resistance to fluconazole: molecular mechanisms and in *vivo* impact in infected *Galleria mellonella* larvae. *Antimicrobial Agents Chemotherapy* 59, 6581–6587. doi: 10.1128/AAC.01177-15

Sudbery, P., Gow, N., and Berman, J. (2004). The distinct morphogenic states of *Candida albicans*. *Trends Microbiol.* 12, 317–324. doi: 10.1016/j.tim.2004.05.008

Tan, Y., Leonhard, M., Ma, S., and Schneider-Stickler, B. (2016). Influence of culture conditions for clinically isolated non-*albicans Candida* biofilm formation. *J. Microbiological Methods* 130, 123–128. doi: 10.1016/j.mimet.2016.09.011

Tan, Y., Leonhard, M., and Schneider-Stickler, B. (2017). Evaluation of culture conditions for mixed biofilm formation with clinically isolated non-*albicans Candida* species and *Staphylococcus epidermidis* on silicone. *Microbial Pathogenesis* 112, 215–220. doi: 10.1016/j.micpath.2017.10.002

Thein, Z. M., Samaranayake, Y. H., and Samaranayake, L. P. (2007). *In vitro* biofilm formation of *Candida albicans* and non-*albicans Candida* species under dynamic and anaerobic conditions. *Arch. Oral. Biol.* 52, 761–767. doi: 10.1016/j.archoralbio.2007.01.009

Tóth, R., Cabral, V., Thuer, E., Bohner, F., Németh, T., Papp, C., et al. (2018). Investigation of *Candida parapsilosis* virulence regulatory factors during host-pathogen interaction. *Sci. Rep.* 8, 1346. doi: 10.1038/s41598-018-19453-4

Tóth, R., Nosek, J., Mora-Montes Héctor, M., Gabaldon, T., Bliss Joseph, M., Nosanchuk Joshua, D., et al. (2019). *Candida parapsilosis*: from genes to the bedside. *Clin. Microbiol. Rev.* 32, e00111–e00118. doi: 10.1128/CMR.00111-18

Zoppo, M., Poma, N., Di Luca, M., Bottai, D., and Tavanti, A. (2021). Genetic manipulation as a tool to unravel Candida parapsilosis species complex virulence and drug resistance: State of the art. *J. Fungi* 7, 459. doi: 10.3390/jof7060459

Artículo 2 (Manuscrito)

Who arrived first? Priority effects on virulence and susceptibility of *Candida albicans* and *Pseudomonas aeruginosa* dual biofilms

Sometido en la revista *Communications Biology* (COMMSBIO-24-3873)

Categoría Biología 2023: 1er tercil, 1er Cuartil, IF= 5.2

Betsy V. Arévalo-Jaimes[1,2], Joana Admella[1,2] y Eduard Torrents[1,2]

[1]Grupo Infecciones Bacterianas y Terapias Antimicrobianas (BIAT), Instituto de Bioingeniería de Cataluña (IBEC), Barcelona, España.

[2]Sección de Microbiología, Departamento de Genética, Microbiología y Estadística, Facultad de Biología, Universitat de Barcelona, Barcelona, España.

Cita versión *pre-print*: Arevalo, B. V., Admella, J & Torrents, E. (2024). Who arrived first? Priority effects on *Candida albicans* and *Pseudomonas aeruginosa* dual biofilms. *Research Square*, 2024-09. DOI: 10.21203/rs.3.rs-4672806/v1.

Who arrived first? Priority effects on *Candida albicans* and *Pseudomonas aeruginosa* dual biofilms

Betsy V. Arévalo-Jaimes[1,2], Joana Admella[1,2] & Eduard Torrents[1,2*]

[1]Bacterial infections and antimicrobial therapies group, Institute for Bioengineering of Catalonia (IBEC), The Barcelona Institute of Science and Technology, Barcelona, Spain.

[2]Microbiology Section, Department of Genetics, Microbiology and Statistics, Faculty of Biology, University of Barcelona, Barcelona, Spain.

*Corresponding author:

Dr. Eduard Torrents: etorrents@ibecbarcelona.eu

Abstract

Historical processes in community assembly, such as the arrival order of species, strongly influence their interactions causing priority effects. *Candida albicans* and *Pseudomonas aeruginosa* are frequently co-isolated from biofilm-based infections of the skin, lungs, and medical devices. Their relationship, predominantly antagonistic, involves physical and chemical interactions. However, the presence and implications of priority effects among these microorganisms remain largely unexplored. Here, we developed dual biofilms with differing inoculation times for each species and assessed the resulting microbial communities' *in vitro* virulence and susceptibility. Our findings showed that the inoculation order impacts biofilm composition, structure, virulence, and antimicrobial susceptibility. The first colonizer had an advantage for surface colonization. Consecutive colonization increased biofilm virulence and negated *C. albicans*' protective effect on *P. aeruginosa* PAET1 against meropenem treatment. Finally, we propose N-acetylcysteine as an adjuvant for treating *C. albicans* and *P. aeruginosa* interkingdom infections, working independently of priority effects.

Keywords: polymicrobial interactions, first colonizer, co-infections, antifungal treatment, N-acetylcysteine, interkingdom biofilms, fungi-bacteria.

Introduction

Fungi and bacteria colonization of various body microenvironments leads to interkingdom polymicrobial infections, which are common in the oral cavity, gastrointestinal system, skin, respiratory tract, and urinary tract [1,2]. The most prevalent fungal pathogen in constant interaction with a diverse array of bacteria is *Candida albicans* [2]. Moreover, most human infectious diseases are caused by biofilm-forming pathogens, which can colonize biotic surfaces and medical devices [1]. *C. albicans* is particularly known for its propensity to form biofilms independently or in conjunction with other microorganisms [3].

C. albicans and *Pseudomonas aeruginosa* are frequently co-isolated from biofilm-based infections of the skin, lungs, and medical devices [4]. The relationship between these microorganisms involves physical and chemical interactions and is predominantly classified as antagonistic [1]. However, their polymicrobial biofilms have reported virulence and susceptibility advantages [1], highlighting that interactions within microbial communities are complex and dynamic [5]. In pulmonary co-infections of *C. albicans* and *P. aeruginosa,* the clinical impact of the fungal species remains incompletely understood [6]. Experimental and clinical observations suggest that the presence of *Candida* may contribute to respiratory diseases, albeit indirectly [7]. However, there is currently insufficient clinical data to support antifungal treatment following *Candida* identification [7].

Mixed-species biofilms pose a significant clinical challenge due to their difficulty in diagnosis and treatment [3]. Interspecies interactions within polymicrobial biofilms are relevant for host-response, drug resistance, and disease progression [3]. For example, in polymicrobial biofilms, *Candida* acts as a physical scaffold for bacteria attachment and growth, creates hypoxic microenvironments that protect anaerobic bacteria, and produces an extracellular matrix that shields bacteria from antibiotics [1,8,9]. However, most biofilm studies focus on single species.

Studies in microbial ecology have revealed that historical processes in community assembly, such as the order and time of species arrival to a habitat, strongly influence species interaction [10,11]. These interactions, termed priority effects, have been observed in mammalian gut and skin microbiomes, as well as in fungal-bacterial biofilms [5,11]. *In vitro* and *ex-vivo* biofilm experiments with *C. albicans* and bacteria found in chronic wound infections have shown that priority effects increase the relative abundance of early colonizers at the

expense of late colonizers [5]. However, the presence of priority effects on dual biofilms of *C. albicans* and *P. aeruginosa* and their implications remain largely unexplored.

Therefore, this study aimed to evaluate whether priority effects influence the virulence of *C. albicans* and *P. aeruginosa* polymicrobial biofilms and explore therapeutic strategies for their treatment. We developed dual biofilms with differing inoculation times for each species and studied the resulting microbial communities. We found that priority effects influence biofilm structure and composition. In addition, successive colonization increased biofilm virulence and negated *C. albicans*' protective effect on *P. aeruginosa* PAET1 against meropenem treatment. Our findings shows that priority effects impact significantly the virulence and susceptibility of resulting biofilms, underscoring the importance of *C. albicans* presence in interkingdom biofilms.

Results

Composition and structure of *C. albicans* and *P. aeruginosa* biofilms with different inoculation times

We devised a protocol to obtain polymicrobial biofilms of *C. albicans* and *P. aeruginosa* PAET1 with different inoculation orders (Fig. 1a). The CFUs count revealed differences in polymicrobial communities composition. *P. aeruginosa* PAET1 biomass (CFUs per mL) is significantly higher when it is the early colonizer (1Pa2Ca) compared to the other polymicrobial conditions (1Ca2Pa and CaPa) and the monomicrobial control (Pa) (Fig. 1a and Supplementary Table 1). This translates into a higher relative abundance (97.75%) of *P. aeruginosa* PAET1 in the 1Pa2Ca condition, compared to the 86-89% reported in 1Ca2Pa and CaPa conditions (Fig. 1b). Notably, no significant differences in the total number of CFUs per mL (sum of both *P. aeruginosa* PAET1 and *C. albicans* CFUs per mL) were observed within the different polymicrobial biofilms (Fig. 1b and Suplemmentary Table 1).

However, it is important to consider that *C. albicans* cells are larger than bacteria cells, resulting in biofilms where fungal growth accounts for a significant portion of biofilm structure (Fig. 2). Notably, *C. albicans* was primarily found in blastospore morphology under all conditions. The differences in biomass composition reported by CFUs counting were also observed in the microscopy images, with more bacteria cells present in the 1Pa2Ca condition (Fig. 2a). Overall, bacteria size allowed *P. aeruginosa* PAET1 to be located within *Candida* cells, reaching the surface regardless of the inoculation order (Fig. 2b). Notably, variations in bacteria distribution along biofilm layers were observed among conditions.

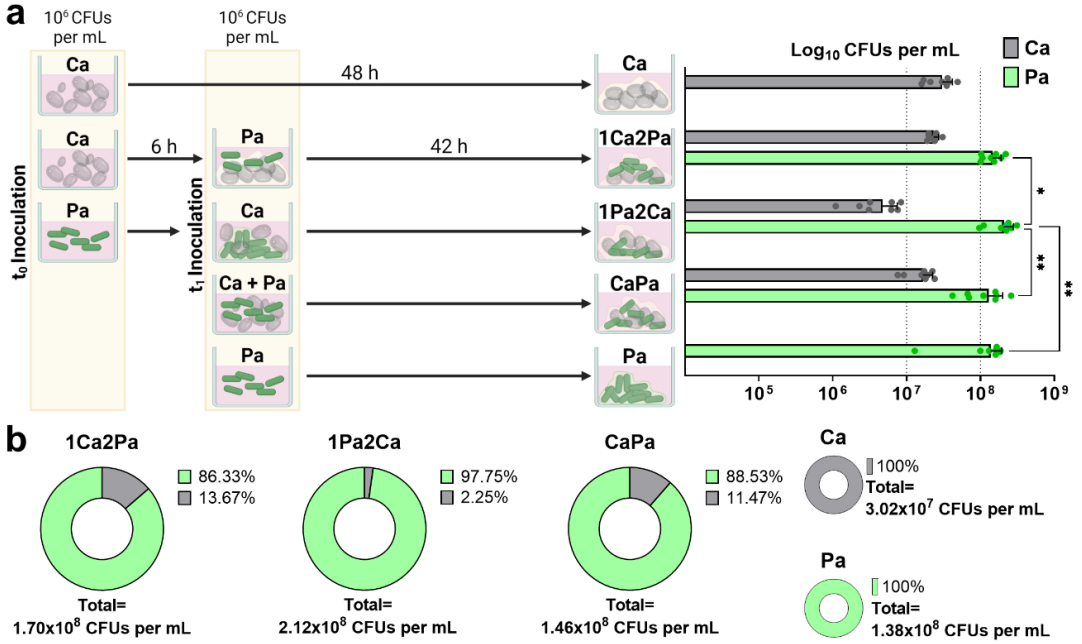

Fig. 1 Composition of dual biofilms of *C. albicans* (Ca, grey) and *P. aeruginosa* PAET1 (Pa, green) according to the inoculation time of each species. a Protocol of the biofilm development process of each polymicrobial biofilm condition and the monomicrobial controls with their respective biomass cell quantification (Log CFUs per mL). Initial inoculum size was 10^6 CFUs per mL for both t_0 and t_1. Asterisks indicate statistically significant differences among all conditions in an Ordinary two-way ANOVA with Tukey's multiple comparison test (∗*p*-value <0.05 and ∗∗*p*-value <0.01). **b** Relative abundance of each species and total number of CFUs per mL (mean) in the polymicrobial and monomicrobial biofilms. The experiments were conducted 8 times. Data are represented as mean ± standard deviation.

When *P. aeruginosa* PAET1 was added earlier (1Pa2Ca), bacterial cells formed a thick bottom layer (Fig. 2b), covering almost all the abiotic surface and reducing the space for *C. albicans* attachment (Fig. 2c). In contrast, in the condition where *C. albicans* was added earlier (1Ca2Pa), the bacteria had less abiotic surface available to attach, resulting in a bottom layer that was less thick and dense (Fig. 2b). This caused that *P. aeruginosa* PAET1 to use *C. albicans* as a biotic surface for attachment, leading to a more pornounced cell-to-cell interaction between the interkingdom species (Fig. 2c) and a greater distribution of the bacteria along all biofilm layers (Fig. 2b). Conversely, when both microorganisms were inoculated simultaneously (CaPa), the species competed for atachment to the abiotic surface, favoring intra-species aggregation, observed as clusters of cells, over inter-species interaction (Fig. 2c). This resulted in an overlap of *C. albicans* and *P. aeruginosa* PAET1 throughout biofilm layers (Fig. 2b). Moreover, the higher competitive behaviour among the

microorganisms in this polymicrobial condition (CaPa)represented a higher mortality for *C. albicans* compared to its monomicrobial biofilm (Ca) (Supplementary Fig. 1), resulting in polymicrobial biofilms that were less thick than the others (Fig. 2b).

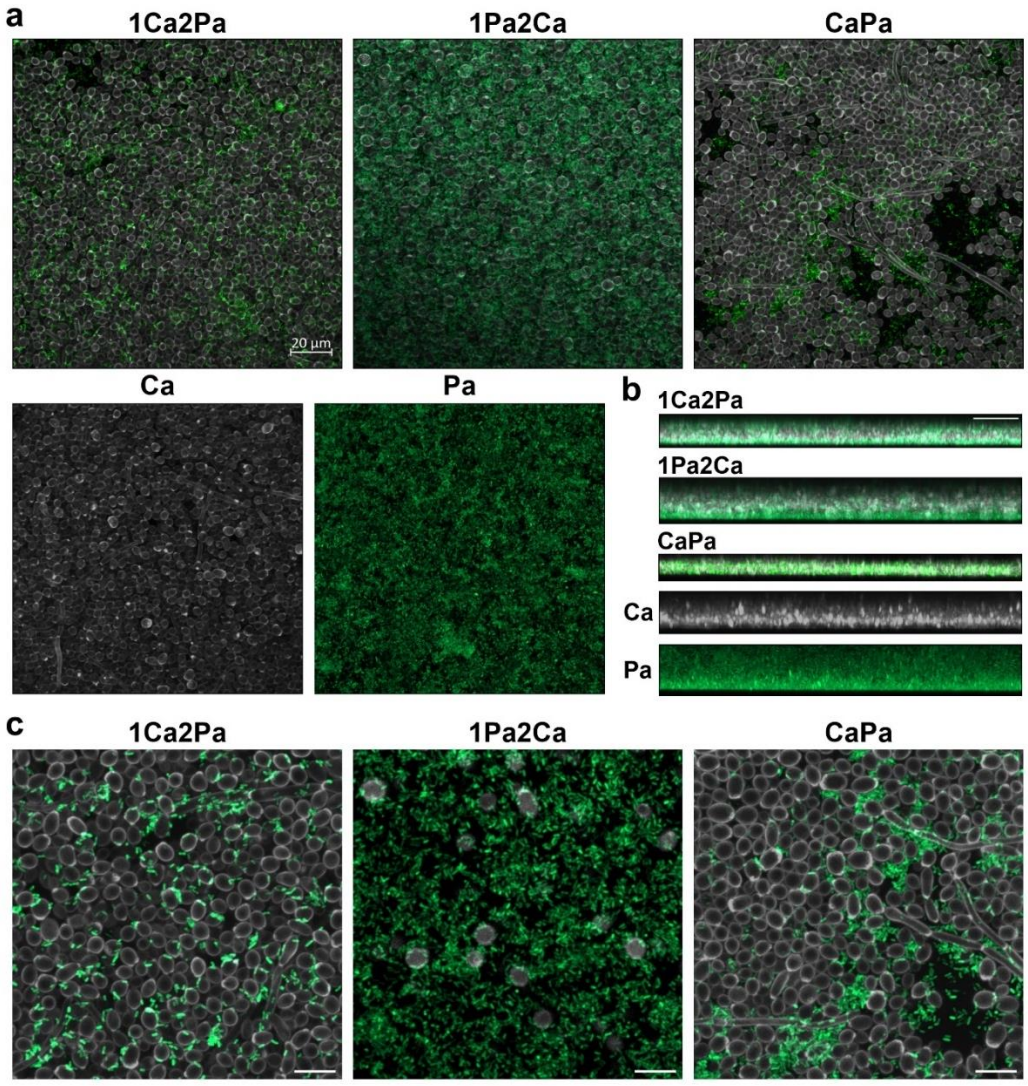

Fig. 2 Dual biofilms of *C. albicans* (Ca, grey) and *P. aeruginosa* PAET1 (Pa, green) according to the inoculation time of each species. a Z-stacks, **b** orthogonal views and **c** zoomed snapshots of confocal laser images for each biofilm condition. Microorganisms were visualized using the *P. aeruginosa* PAET-GFP strain and the dye Calcofluor white. Images were processed using the Zeiss software. The scale bar represents 20 µm in panel a and b, and 10 µm in panel c. 1Ca2Pa= Biofilm formed with an initial inoculum of *C. albicans* followed by addition of *P. aeruginosa* PAET1 6 h later. 1Pa2Ca= Biofilm formed with an initial inoculum of *P. aeruginosa* PAET1 followed by *C. albicans* addition 6 h later. CaPa= biofilm formed with an initial inoculum with both species. Ca= monomicrobial biofilm of *C. albicans.* Pa= monomicrobial biofilm of *P. aeruginosa*.

Virulence assessment of *C. albicans* and *P. aeruginosa* biofilms with different inoculation times

To evaluate whether the resulting priority effects induce virulence variations of the polymicrobial biofilms, early staged biofilms (20-24 h) were formed on top of A549 alveolar cells (Fig. 3). In these experiments, polymicrobial biofilms were generated from an inoculum of ~10^5 CFUs per mL, while the monomicrobial controls were formed from inoculum of ~10^5 CFUs per mL (Ca 1x and Pa 1x) and ~10^6 CFUs per mL (Ca 2x and Pa 2x). In this way, we could evaluate the impact of inoculum size on the final biomass of each microorganism by comparing the monomicrobial biofilms 1x to 2x (Fig. 3a). We found that halving the inoculum size did not affect the obtained number of CFUs per mL from *P. aeruginosa* PAET1 biofilms (Supplementary Table 1). However, the reduction of the inoculum had a statistically significant effect on *C. albicans* biofilms, causing a decrease of ~1 Log_{10} CFUs per mL in Ca 1x compared to Ca 2x (Supplementary Table 1).

Next, we assessed whether the inclusion of eukaryotic cells in the *in vitro* model induced alterations in the biomass of each species. We compared the biomass of Ca and Pa monomicrobial biofilms from Fig. 1a protocol to Ca 2x and Pa 2x monomicrobial biofilms from the Fig. 3a protocol. No statistically significant differences were observed in the final number of CFUs per mL for either microorganism under both conditions (Supplementary Table 1). These protocols used the same inoculum size for bacteria and fungi; however, the experiments that included eukaryotic cells (Fig. 3) were incubated for half the time compared to those that did not (Fig. 1) (24 h vs 48 h for *C. albicans* and 20 h vs 42 h for *P. aeruginosa* PAET1). This indicates that the inclusion of eukaryotic cells stimulates microorganism growth in monomicrobial biofilms of *C. albicans* and *P. aeruginosa* PAET1.

Fig. 3 showed that the 1Pa2Ca condition formed in the presence of eukaryotic cells retained a significantly higher biomass of *P. aeruginosa* PAET1 compared to the other polymicrobial biofilms (Fig. 3a and Supplementary Table 1). In terms of total CFUs per mL, no statistically significant differences were reported among the three polymicrobial biofilms (Fig. 3b and Supplementary Table 1). However, the composition of the polymicrobial communities was different when eukaryotic cells were included in the experiment. The relative abundance of *P. aeruginosa* PAET1 in the 1Ca2Pa condition decreases to 75% but reaches almost 100% in CaPa and 1Pa2Ca, compared to biofilms formed directly on the plate (Fig. 3b vs Fig 1b).

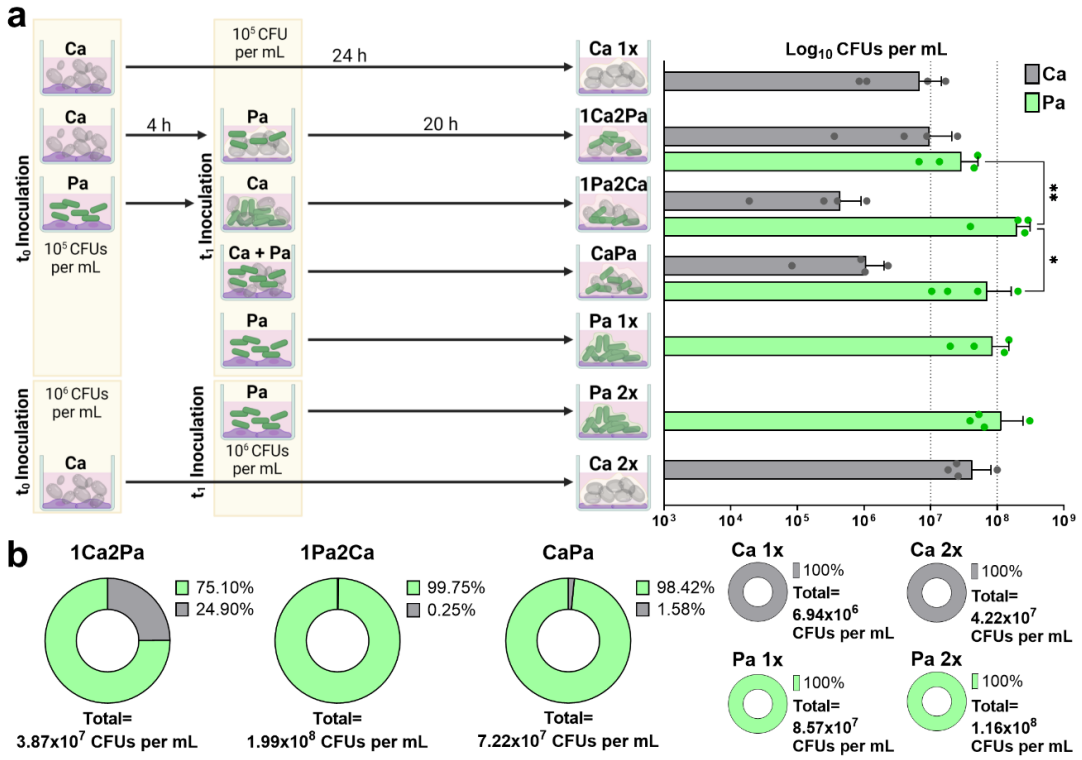

Fig. 3 Composition of early-stage biofilms of *C. albicans* (Ca, gray) and *P. aeruginosa* PAET1 (Pa, green) on top of A549 cells according to the inoculation time of each specie. a Protocol of the biofilm formation process for each polymicrobial biofilm condition and the monomicrobial controls, with their respective biomass quantification (Log CFUs per mL). Inoculum size was specified for each condition without variation among t_0 and t_1. Asterisks indicate statistically significant differences among conditions in an Ordinary two-way ANOVA with Tukey's multiple comparison tests (∗*p*-value <0.05 and ∗∗*p*-value <0.01). **b** Relative abundance of each species and total number of CFUs per mL (Mean) in the polymicrobial and monomicrobial biofilms. The experiments were conducted 4 times. Data are represented as mean ± standard deviation. 1Pa2Ca= Biofilm formed with an initial inoculum of *P. aeruginosa* PAET1 followed by *C. albicans* addition 6 h later. CaPa= biofilm formed with an initial inoculum with both species. Ca 1x= monomicrobial biofilm of *C. albicans.* Pa 1x= monomicrobial biofilm of *P. aeruginosa*. Ca 2x = monomicrobial biofilm of *C. albicans* from inoculum at double concentration of Ca 1x. Pa 2x= monomicrobial biofilm of *P. aeruginosa* from inoculum at double concentration of Pa 1x.

After biofilm characterization, we focused on the viability evaluation of the A549 cells (Fig. 4). Observing the morphologies of the infected eukaryotic cells compared to the control, we noticed different alterations that led to cell death in some cases (dark cells in Fig. 4a). In general, infected cells appeared to be expanded, particularly in the conditions Pa 1x, Pa 2x, and 1Pa2Ca. The quantification of the viability of A549 cells by trypan blue (Fig. 4b) showed that all monomicrobial biofilms decreased cell viability in ~0.1-0.4 log_{10}, with

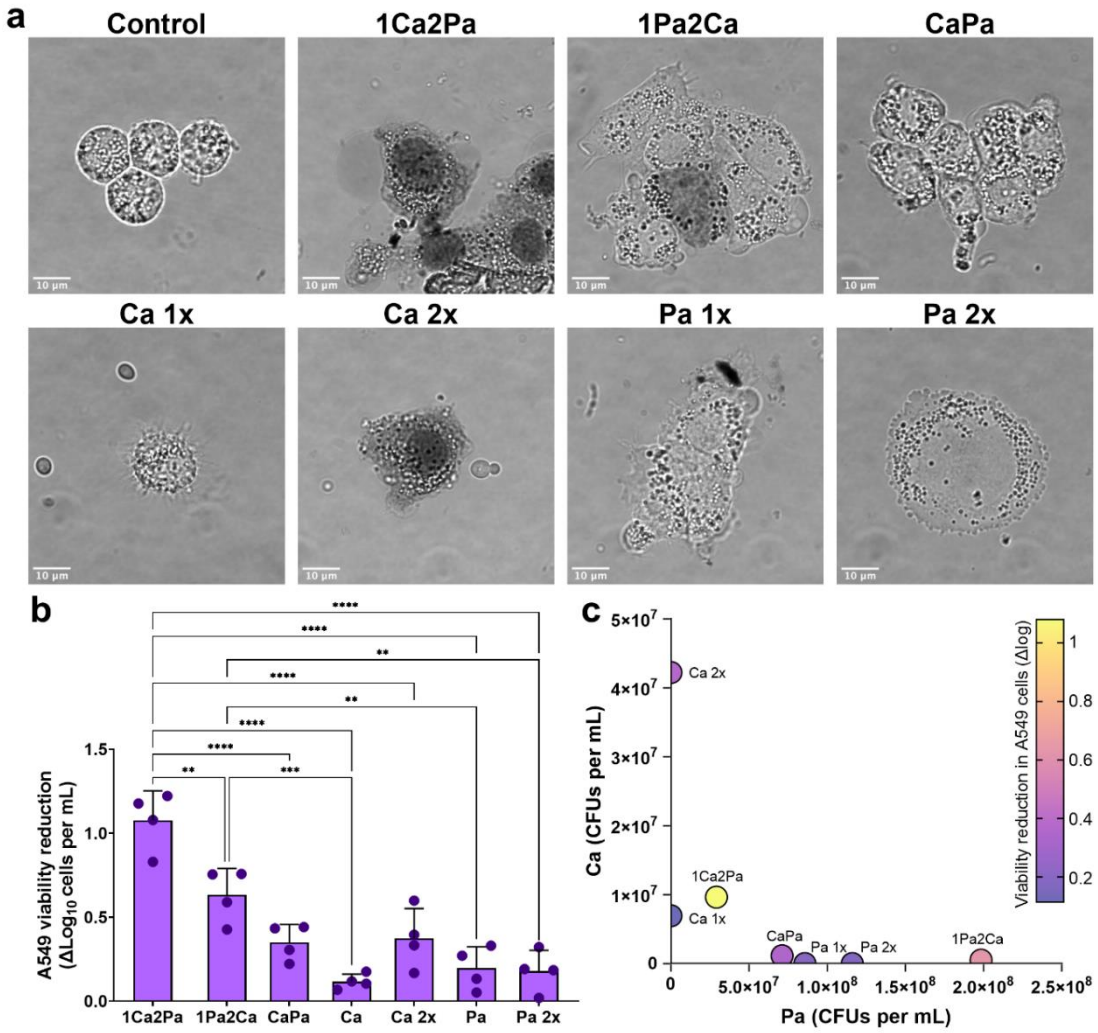

Fig. 4 Viability assessment of A549 cells with early-stage dual biofilms of *C. albicans* (Ca) and *P. aeruginosa* PAET1 (Pa) according to the inoculation time of each species. a Images of A549 cells detached and stained with trypan blue at the end of the experiment. Dark cells indicate cell death. Scale bar of 10 µm. **b** Quantifying the viability reduction of A549 cells (ΔLog_{10} cells per mL) after the biofilm formation process compared to uninfected cells. Asterisks indicate statistically significant differences among conditions in an Ordinary one-way ANOVA with Tukey's multiple comparison test (∗∗*p*-value <0.01; ∗∗∗*p*-value < 0.001; ∗∗∗∗*p*-value < 0.0001). **c** Graphical representation of the multiple linear regression model of viability reduction. The experiments were conducted 4 times. Data are represented as mean ± standard deviation. 1Pa2Ca= Biofilm formed with an initial inoculum of *P. aeruginosa* PAET1 followed by *C. albicans* addition 6 h later. CaPa= biofilm formed with an initial inoculum with both species. Ca 1x= monomicrobial biofilm of *C. albicans.* Pa 1x= monomicrobial biofilm of *P. aeruginosa*. Ca 2x = monomicrobial biofilm of *C. albicans* from inoculum at double concentration of Ca 1x. Pa 2x= monomicrobial biofilm of *P. aeruginosa* from inoculum at double concentration of Pa 1x.

the highest values reported for Ca 2x but without statistical significance (Supplementary Table 1). Regarding the polymicrobial biofilms, those formed by simultaneous colonization (CaPa) showed a viability reduction similar to the monomicrobial controls (0.35 log_{10} cells per mL). However, the scenario changes when biofilms were formed by successive colonization. When *P. aeruginosa* was added first (1Pa2Ca), the log_{10} reduction in cell viability reached 0.63, indicating that these biofilms are statistically significantly more virulent than the monomicrobial biofilms (Supplementary Table 1). But, when *C. albicans* was the early colonizer (1Ca2Pa), the reduction in cell viability increases to 1.07 log_{10} cells per mL, making this condition the most virulent compared to all the others (Supplementary Table 1).

Finally, we created a multiple linear regression model to establish if viability differences were associated with the quantity of fungal cells per bacteria cells present in the polymicrobial community. We found a high goodness of fit of the model (r^2=0.9918), in which each parameter was statistically significant: CFUs per mL of *P. aeruginosa* PAET1 (*p*-value= 0.0281), CFUs per mL of *C. albicans* (*p*-value= 0.0127), and the interaction of CFUs per mL of both microorganisms (p-value= 0.0003). This can be clearly seen in Fig. 4c, where an increase in the number of CFUs per mL in both Ca (y-axis) and Pa (x-axis) led to higher mortality of A549 cells (higher viability reduction). Likewise, in polymicrobial biofilms, the interaction of the quantity of both microorganism also accounts for higher virulence of the interkingdom communities than the monomicrobial counterparts.

Treatment response of *C. albicans* and *P. aeruginosa* biofilms with different inoculation times

Considering that priority effects of *C. albicans* and *P. aeruginosa* dual biofilms involved virulence differences, we decided to explore the response of the polymicrobial biofilms against a 15 h treatment with conventional antimicrobials (Fig. 5a). Each biofilm condition, monomicrobial and polymicrobial, had an untreated control that allowed us to calculate the change in the Log_{10} CFUs per mL of the treated samples. Thus, a higher change represents a more significant reduction in the Log_{10} CFUs per mL and, therefore, higher susceptibility of the evaluated microorganism to the treatment.

We found that meropenem (MER) at 5 µg per mL has the same effect on *P. aeruginosa* PAET1 when grown in the polymicrobial biofilms 1Ca2Pa and 1Pa2Ca, compared to Pa monomicrobial control (Fig. 5b and Supplementary Table 1). However, a decrease in

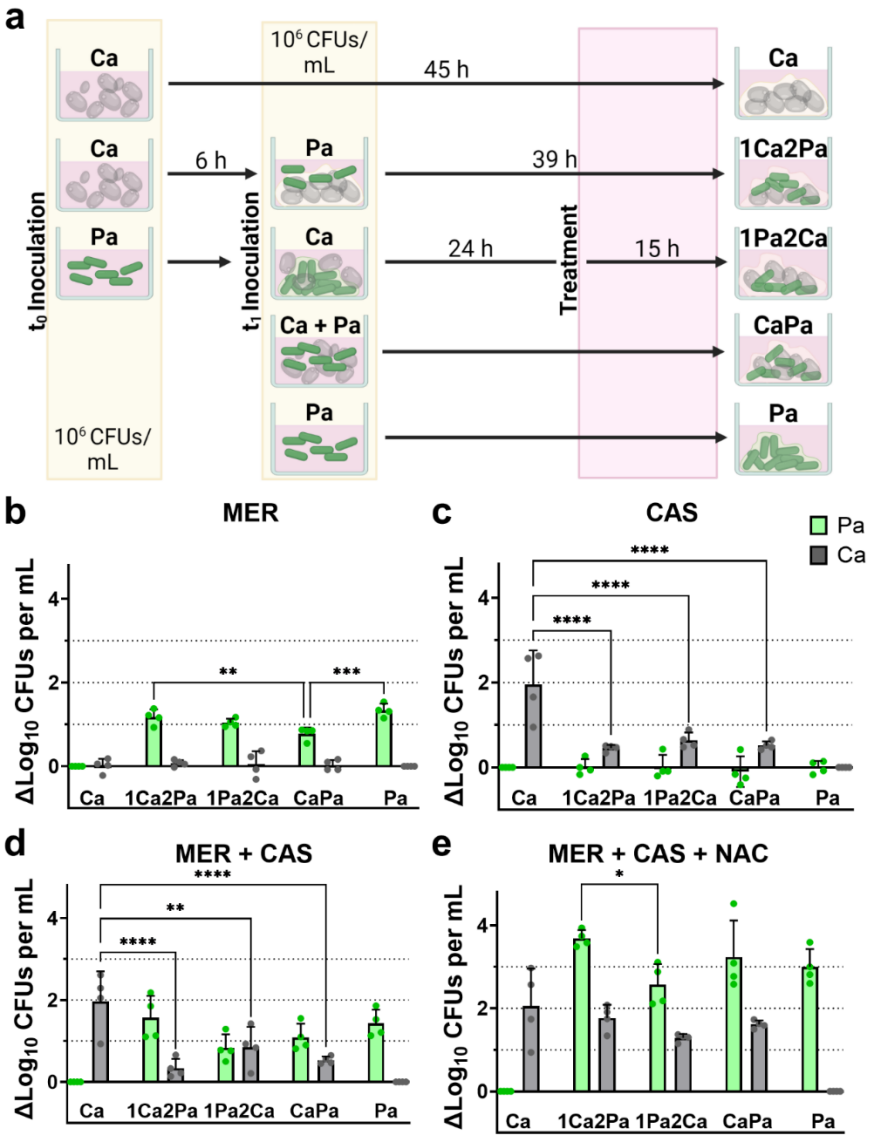

Fig. 5 Susceptibility assessment of *C. albicans* (Ca, grey) and *P. aeruginosa* PAET1 (Pa, green) in dual biofilms according to the inoculation time of each species. a Protocol of biofilm formation process and treatment of each polymicrobial biofilm condition and their monomicrobial controls. Inoculum size was 10^6 CFUs per mL for both t_0 and t_1. Quantification of the biomass reduction of each microorganism (ΔLog CFUs per mL) after treatment with **b** Meropenem (MER) at 5 µg per mL, **c** Caspofungin (CAS) at 5 µg per mL, **d** Meropenem and caspofungin (MER + CAS) and **e** Meropenem, caspofungin and N-acetylcysteine at 1 mg per mL (MER + CAS + NAC). Asterisks indicate statistically significant differences among conditions in an Ordinary two-way ANOVA with Tukey's multiple comparison test (∗*p*-value <0.05; ∗∗*p*-value <0.01; ∗∗∗*p*-value < 0.001 and ∗∗∗∗*p*-value < 0.0001). The experiments were conducted 4 times. Data are represented as mean ± standard deviation. 1Pa2Ca= Biofilm formed with an initial inoculum of *P. aeruginosa* PAET1 followed by *C. albicans*

addition 6 h later. CaPa= biofilm formed with an initial inoculum with both species. Ca= monomicrobial biofilm of *C. albicans.* Pa= monomicrobial biofilm of *P. aeruginosa*.

susceptibility to this antibiotic was found in the condition CaPa. On the other hand, *C. albicans* susceptibility to caspofungin (CAS) at 5 µg per mL was reduced in all polymicrobial biofilms in comparison to Ca (Fig. 5c and Supplementary Table 1). When both antimicrobial agents were given simultaneously (Fig. 5d), we observed that the variation in susceptibility to MER found in *P. aeruginosa* PAET1 in the CaPa biofilm was lost, but the decreased response to CAS in *C. albicans* polymicrobial biofilms remained (Fig. 5d and Supplementary Table 1).

We went further and added the mucolytic agent N-acetylcysteine (NAC) at 1 mg per mL to the previous combined treatment (Fig. 5e). As a result, no differences in susceptibility of *P. aeruginosa* PAET1 and *C. albicans* were longer observed between the polymicrobial biofilms and their monomicrobial counterparts (Supplementary Table 1). In the case of *P. aeruginosa* PAET1, NAC acted as a potent antimicrobial by itself (Supplementary Fig. 2a) or as an adjuvant on the antibiotic treatment (Supplementary Fig. 2b) of monomicrobial and polymicrobial biofilms. On the contrary, the concentration used of NAC did not have a relevant antifungal activity by itself (Supplementary Fig. 2a and Supplementary Table 1). Moreover, the adjuvant effect of NAC observed in the combined therapies MER + CAS + NAC (Fig. 5d) and NAC + CAS (Supplementary Fig. 2c) was restricted to the polymicrobial biofilms (Supplementary Table 1). This suggests that the decrease in susceptibility to CAS is associated with the protection that the *P. aeruginosa* matrix confers to *C. albicans*. As can be observed in the Supplementary Fig. 3, most ECM polysaccharides in the polymicrobial biofilms appear to be secreted by *P. aeruginosa PAET1*.

Discussion

The coexistence of multiple pathogenic species in the same host can lead to higher virulence, increasing disease risk and severity, compared to monomicrobial infections [12,13]. The order in which microorganisms infect the host strongly influences their interactions [12]. Depending on the system, the first or second arriver could have advantages that favor survival [12]. However, the priority effects of pathogen coexistence have been little explored.

In this study, we studied polymicrobial biofilms of *C. albicans* and *P. aeruginosa* PAET1 with different inoculation times. CFUs counts and microscopy images showed that being the first colonizer confers an advantage for surface adhesion and further biofilm

development in polymicrobial biofilms. This is clearly observed in the 1Pa2Ca condition, where *P. aeruginosa* PAET1 arrival reduces the potential adhesion sites for *C. albicans*, resulting in the domination of the community composition by the bacteria (Fig. 1-3). This exclusion effect occurs naturally in the gastrointestinal and vaginal tracts, where local microbiota restricts *C. albicans* colonization [14]. It has also been reported *in vitro* with bacteria from burn wounds [5].

When fungi arrive first (1Ca2Pa), the percentage of *C. albicans* in the community composition increased in comparison with the other polymicrobial biofilms (Fig. 1, and more markedly in Fig. 3), but *P. aeruginosa* PAET1 continued dominating in number. We explain this bacterial dampening of the priority effects by their small size and ability to colonize fungal structures [5,15], allowing them to attach between and on top of *C. albicans* cells (Fig. 2). This reaffirms the scaffold role of *C. albicans* in polymicrobial biofilms by increasing the attachment surface, and the importance of including fungi in the study of microbial communities associated with disease [5].

Lastly, in the situation of the synchronous arrival of bacteria and yeast (CaPa), both species compete for attachment to the underlying substrate, as previously reported for other *C. albicans*-bacteria interactions [5,16]. This competition led to a patchy distribution of both microorganisms on the surface, with intra-species clumps (Fig. 2). Interestingly, in the CaPa condition, higher *C. albicans* death was observed, followed by 1Ca2Pa (Supplementary Fig. 1). This could indicate that *P. aeruginosa* PAET1 utilizes mechanisms that compromise fungal integrity to gain access to colonization space, supported by the antagonistic relationship described elsewhere among this duo [17-27].

However, the clinical consequences of the association of *C. albicans* and *P. aeruginosa* remain unclear. Contradictory conclusions from *in vivo* studies range from reduction of virulence to synergy and enhanced mortality of co-infections compared to mono-infections [6]. *P. aeruginosa* and *C. albicans* are frequently co-isolated from tracheobronchial samples, being more common in patients with cystic fibrosis (CF) and ventilator-associated pneumonia (VAP) [6,27-29]. In both conditions, co-infection with this pair leads to reduced lung function, prolonged hospital stays, and higher intensive care unit mortality [27]. For those reasons, we decided to include pulmonary epithelial cells in the model and evaluate virulence variations of the polymicrobial biofilms associated with priority effects.

The simultaneous inoculation of bacteria and fungi (CaPa) showed an increase in virulence compared to Ca or Pa biofilms (Fig. 4b), but it was not statistically significant. This disagrees with previous *in vivo* studies in pulmonary models that found higher biofilm biomass, virulence, and inflammation in polymicrobial biofilms of *C. albicans* and *P. aeruginosa* compared to their monomicrobial infections [30-34]. We believe the discrepancy is due to the short duration of the experiment (20 h of inter-species interaction); prolonged exposure of the epithelial cells to biofilm growth would likely increase the magnitude of virulence differences. However, it is interesting to note that CaPa was the condition with more inter-species competition (Supplementary Fig. 1) but less virulence (Fig. 4b).

On the other hand, biofilms formed by sequential inclusion of microorganisms produced a significant reduction in epithelial cell viability compared to the monomicrobial control, being 1Ca2Pa the most virulent group (Fig. 4b). This result is highly significant because co-infections in the real context are unlikely to be simultaneous [35]. Previous work showed that mouse mortality is higher when preformed *P. aeruginosa* biofilms are inoculated with *C. albicans* than when they are not [32,36]. Moreover, the addition of *C. albicans* to preformed biofilms of *P. aeruginosa* induces the expression of the bacterial genes *mucA* and *psl*, and higher inflammatory responses than mixed biofilms formed by simultaneous inoculation [32]. In contrast, the effect of *P. aeruginosa* after *C. albicans* colonization is not that clear. Previous instillation of *C. albicans* protected mice against *P. aeruginosa* virulence (bacterial burden and lung injury), presumably by a priming effect [28,37,38]. Conversely, Roux et al. reported that previous instillation of *C. albicans* increases *P. aeruginosa* colonization, pneumonia development, and cytokine production in rats [39,40]. In patients, *C. albicans* colonization of the respiratory tract was identified as a risk factor for *Pseudomonas* VAP [41,42].

Our model showed that not only does the individual burden of each specie account for the virulence of polymicrobial biofilms, but also the community composition (interaction of both microorganisms' biomass) (Fig. 4c). However, we do not know which type of priority effects are responsible for the increase in *P. aeruginosa* PAET1 virulence in the epithelial pulmonary cells after *C. albicans* colonization (1Ca2Pa) compared to its monomicrobial infection (Pa) (Fig. 4b). Described interactions between both microorganisms could play a role, such as *C. albicans* stimulation of *P. aeruginosa* expression of virulence factors (pyoverdine, phenazines and rhamnolipids) and biofilm formation [27,33,34,43].

Our results support the hypothesis of *C. albicans* as a co-conspirator in pulmonary infections, agreeing with previous studies that associate its presence in the respiratory tract with higher morbidity or mortality [44,45]. However, the co-isolation of *C. albicans* and *P. aeruginosa* from respiratory samples does not consider antifungal administration unless there is histological evidence of fungal infection [27,28,46]. Mainly due to the lack of agreement on the significance of *C. albicans* presence and inconclusive evidence on the implementation of antifungal treatment in humans [6,28,33,44,46,47]. Therefore, *C. albicans* detection is usually assumed as colonization [46]. Hoping to contribute to elucidating these questions, we tested whether priority effects influence microbial response to antibiotic and antifungal treatment, alone and in combination.

We found that *P. aeruginosa* PAET1 susceptibility to MER decreases when its biofilm is formed concomitantly with *C. albicans* (CaPa) compared to when it is formed alone (Pa) (Fig. 5b). This effect has been reported before and was associated with the mannan and glucan polysaccharides of the extracellular matrix (ECM) [48]. However, we found that the protective effect was abolished after the mixed antibiotic and antifungal treatment MER + CAS (Fig. 5b), suggesting some contribution of fungal activity. Surprisingly, this synergistic effect was not present in polymicrobial biofilms formed from the sequential addition of colonizers (1Ca2Pa and 1Pa2Ca) (Fig. 5b), showing that community priority effects can impact microbial antibiotic susceptibility.

We also saw that in polymicrobial biofilms, *P. aeruginosa* PAET1 protects *C. albicans* from CAS treatment, regardless of the arrival time of colonizers (Fig. 5c). Combined antibiotic and antifungal treatment MER + CAS did not alter this effect (Fig. 5d), but the inclusion of NAC did (Fig. 5e), suggesting involvement of *P. aeruginosa* PAET1 ECM rather than bacterial activity (Supplementary Fig. 3). More studies need to confirm these findings, but susceptibility changes derived from polymicrobial interactions are frequently associated with the extended protection of one species' ECM for another [48-50].

Nevertheless, as the history of colonization events can be patient-specific, treatments not affected by priority effects should be preferred in the management of polymicrobial biofilms. For these reasons, we reaffirm the inclusion of N-acetylcysteine as an exciting option in the treatment of *C. albicans* and *P. aeruginosa* co-infections, as previously reported [32]. We believe that the inclusion of biofilm disrupting agents could help elucidate whether antifungals are required to eradicate interkingdom biofilms. Our study showed that MER + CAS combination did not significantly improve the reduction of both

microorganisms in any polymicrobial condition compared to MER treatment alone (Fig. 5b vs Fig. 5d). However, the comparison of MER treatment with NAC + MER and MER + CAS + NAC resulted in an increased reduction of at least 1 Log_{10} of CFUs per mL of *P. aeruginosa*, and *C. albicans* and *P. aeruginosa*, respectively, in all polymicrobial conditions (Fig. 5b vs Fig. 5e and Supplementary Fig. 2b). Whether the reduction in *C. albicans* biomass has clinical relevance in disease outcomes remains a question that needs to be answered.

Our study confirms that priority effects modify community structure and function [51,52], making it necessary to consider them in modeling *in vitro* systems. We recognize that the protocol used to assess biofilm virulence can be tested to extend the duration of biofilm growth and to evaluate the treatment effectiveness. But it allowed us to identify that sequential colonization favors microbial interactions that enhance virulence against alveolar epithelial cells, being more marked in the 1Ca2Pa condition. Contrary, the successive addition of species abolishes the protective effect of *C. albicans* to *P. aeruginosa* against MER. Finally, N-acetylcysteine could enhance the treatment efficacy of *C. albicans* and *P. aeruginosa* interkingdom infections, independently of the priority effects.

Materials and methods

Bacterial strains and growing conditions

This study used two clinical isolates: *Candida albicans* 10045727 obtained from a patient with fungaemia [53] and *Pseudomonas aeruginosa* PAET1 from a cystic fibrosis patient with persistent infection [54]. Additionally, *P. aeruginosa* PAET1 expressing the GFP plasmid pETS-PA was employed in imaging experiments [55]. Bacteria were cultured at 37 ºC in Luria Bertani (LB) medium (Scharlab S.L.), while fungi were grown at 30 ºC in Yeast Petone Dextrose (YPD) medium consisting of 1% Yeast Extract (Gibco), 2% Meat Peptone (Scharlab S.L.), 2% D-glucose (Fisher Scientific S.L.).

Biofilm formation

Overnight cultures (16 h at 200 rpm) of *C. albicans* (30 ºC) and *P. aeruginosa* PAET1 (37 ºC) were centrifuged at 4000 rpm (Labnet Spectrafuge™ 6C) for 5 min and washed twice with Phosphate Buffer Saline 1X (PBS) (Fisher Scientific S.L.). Suspensions with a final optical density of λ = 550 nm (OD_{550}) of 0.1 for yeast and 0.005 for bacteria, which corresponds to ~10^6 Colony Forming Units per mL (CFUs per mL) of both microorganisms, were prepared in RPMI-1640 with L-glutamine without sodium bicarbonate (Sigma-Aldrich) supplemented

with 0.2% D-glucose (referred to as RPMId). Then, suspensions were added to 96-well polystyrene plates with a flat bottom (Corning, USA).

Three different protocols for polymicrobial biofilm formation were established based on the colonization order: 1) Initial inoculum of *C. albicans* followed by addition of *P. aeruginosa* PAET1 6 h later, referred to as 1Ca2Pa. 2) Initial inoculum of *P. aeruginosa* PAET1 followed by *C. albicans* addition 6 h later, referred to as 1Pa2Ca. 3) Initial inoculum with both species, referred to as CaPa. Monomicrobial biofilms of *C. albicans* and *P. aeruginosa* were included as controls and denoted as Ca and Pa, respectively (Figure 1A). To enhance adhesion to the surface, RPMId used for the initial inoculation (t_0) was supplemented with 10% Fetal Bovine Serum (FBS) (Gibco). A PBS wash was performed before the second inoculation (t_1). Biofilms were incubated at 37 ºC for a total time of 48 h, with an intermediate step of media renewal at 24 h.

To quantify the resulting biomass from each biofilm protocol, wells underwent a PBS wash before the removal of biofilms using a pipette tip. The biofilm suspensions were then subjected to sonication in an ultrasonic bath (Branson 200 ultrasonic cleaner) for 5 min, followed by 30 s vortexing to aid cell disaggregation. Serial dilutions were plated on LB and YPD agar for *P. aeruginosa* and *C. albicans* growth, respectively. CFUs were counted after 24 h.

Microscopic characterization

To observe the microscopic structure of biofilms, *P. aeruginosa* PAET1-GFP and *C. albicans* biofilms were formed on 8-well cell culture slides (SPL Life Sciences) following the protocol described above. The cell culture slides underwent an overnight pretreatment with FBS at 37 °C to enhance microorganism adhesion to the surface. The wells were washed with PBS before t_0 to remove the excess of FBS.

The cell culture slides were then incubated, and matured biofilms were visualized using a LSM 800 confocal scanning laser microscope (Zeiss). *P. aeruginosa* PAET1 was visualized by the GFP plasmid, while *C. albicans* was stained with the chitin dye Calcofluor White (CW) (Thermo Fisher Scientific) at 10 μM. Propidium Iodide from the LIVE/DEAD BacLight Bacterial Viability Kit (Thermo Scientific) was used to stain dead cells (compromised membranes) and Concanavalin A-Alexa Fluor 647 (Invitrogen) to stain polysaccharides of the extracellular matrix (ECM), according to manufacturer's instructions. Images were processed using Zeiss software.

Virulence assessment

Differences in the virulence of early staged biofilms of *C. albicans* and *P. aeruginosa* PAET1 with distinct inoculation times were evaluated *in vitro* using the adenocarcinomic alveolar A549 cell line (ATCC CCL-185). Cells were cultured in T-75 tissue culture flasks (Thermo Fisher Scientific) and grown in Dulbecco's Modified Eagle Medium: Nutrient mixture F12 (DMEM/F12; Thermo Fisher Scientific), supplemented with 10% (v/v) FBS (Thermo Fisher Scientific), 100 Units per mL of penicillin/streptomycin (Thermo Fisher Scientific) and 2.5 µg per mL of amphotericin B (Thermo Fisher Scientific). Cells were passaged and maintained in a humidified incubator at 37 ºC and 5% CO_2 (ICOmed, Memmert).

For viability experiments, $2x10^5$ cells per well were seeded in a 24-well plate (SPL Life Sciences) in Dulbecco's Modified Eagle Medium and incubated at 37 ºC and 5% CO_2 for 24 h. On day 2, the media was changed to antibiotic and antifungal-free DMEM/F12 (only with 10% FBS) to avoid any possible interferences with infection. On day 3, before cell infection, the media was replaced with DMEM/F12 supplemented with 10% FBS and 5% bovine serum albumin (BSA; Panreac Química S.L.U.). Cells were then infected with ~10^5 CFUs per mL of each microorganism from an overnight culture previously washed with PBS to obtain the three different polymicrobial biofilms based on the inoculation time (Figure 3A). Uninfected cells and cells infected with *P. aeruginosa* PAET1 (Pa 1x) and *C. albicans* (Ca 1x) alone served as controls. Additional controls of monomicrobial biofilms (Ca 2x and Pa 2x), where the concentration of the inoculum was doubled (~10^6 CFUs per mL), were included to discard mortality associated with higher infection load in polymicrobial biofilms. After 4 hours of t_0, wells were washed with PBS, and t_1 was performed. Biofilms were allowed to grow for a total of 24 h since t_0.

Subsequently, wells were washed once with PBS, and cells were detached by the addition of 0.2 ml of trypsin-EDTA at 0.25% (Thermo Fisher Scientific) for 10 minutes at 37 ºC and 5% CO_2. Following trypsin inactivation with 0.2 ml of antibiotic and antifungal-free media, 10 µl of cell suspensions was mixed 1:1 with trypan blue and counted in a Neubauer chamber. Cell viability was calculated by averaging the count of live cells in 5 squares of the chamber, multiplied by 2 (dilution factor of the dye) and by 10^4 to obtain the number of cells per mL. The reduction in cell viability after infection was calculated by subtracting the base ten logarithms of viable cells per mL in infected wells from the control well (ΔLog_{10} Viable cells per mL = Log_{10} Viable cells per $mL_{Control}$ - Log_{10} Viable cells per $mL_{infected}$). The

same detached and stained eukaryotic cells were visualized in differential interference contrast (DIC) to see morphological changes after infection, using a Nikon inverted fluorescent microscope ECLIPSE Ti–SperL100 (Nikon, Japan) coupled with a DS-Qi2 Nikon camera (Nikon, Japan). Images were processed with Image J Fiji software.

In parallel, wells were processed to recover bacteria and fungi attached to cells. This involved washing wells thrice with PBS, before trypsin addition and inactivation. The suspensions were sonicated in an ultrasonic bath for 5 min and vortexed for 30 s. Serial dilutions were plated onto LB and YPD agar for colony counting of *P. aeruginosa* PAET1 and *C. albicans*, respectively.

Susceptibility Evaluation

The antimicrobial susceptibility of polymicrobial biofilms according to the inoculation time of each species was assessed using the antibiotic meropenem (MER) at 5 µg per mL (Sharlab, S.L.), the antifungal caspofungin (CAS) at 5 µg per mL (Merck Life Science), and the mucolytic N-acetylcysteine (NAC) at 1 mg per mL (Sigma-Aldrich), as well as their combinations (MER + CAS, NAC + MER, NAC + CAS, MER + CAS + NAC). Each biofilm condition included control wells treated with RPMId.

Biofilms were treated 24 h after t_1 inoculation (Figure 5A). 15 h post-treatment, biofilms were washed and prepared for CFUs quantification as described in the "biofilm formation" section. The reduction in biomass after treatment was calculated by subtracting the base ten logarithms of CFUs per mL of treated samples from their respective control sample (ΔLog_{10} CFUs per mL = Log_{10} CFUs per $mL_{Control}$ - Log_{10} CFUs per $mL_{Treated}$).

Statistics and Reproducibility

Graphics and comparisons were conducted using GraphPad Prism v10. Statistical differences among the mean of conditions were evaluated by Unpaired t-test, One-way ANOVA or two-way ANOVA as appropriate and stated in each figure and Supplementary table 1. Correction for multiple comparisons was also included when required. In addition, a multiple linear regression model to explain variations in the viability reduction of the infected eukaryotic cells was created: A549 viability reduction (Δlog cells per mL) ~ Intercept + *P. aeruginosa* (CFUs per mL) + *C. albicans* (CFUs per mL) + *P. aeruginosa* (CFUs per mL): *C. albicans* (CFUs per mL). A significant level of $p < 0.05$ was established for all tests.

Acknowledgements

We thank Dr Jesus Guinea Ortega from the Department of Clinical Microbiology and Infectious Diseases, Hospital General Universitario Gregorio Marañón, Madrid, Spain, for the generous gift of the *Candida albicans* 10045727 used in this study. Likewise, A549 cells were a generous gift of Dr. Esther Julián from the Autonomous University of Barcelona, Bellaterra, Spain.

This study was partially supported by grants PID2021-125801OB-100, PLEC2022-009356 and PDC2022-133577-I00 funded by MCIN/AEI/10.13039/501100011033 and "ERDF A way of making Europe", the CERCA programme and *AGAUR-Generalitat de Catalunya* (2021SGR01545), the European Regional Development Fund (FEDER) and Catalan Cystic Fibrosis association. The project that gave rise to these results received the support of a fellowship from the "La Caixa" Foundation (ID 100010434). The fellowship code is "LCF/BQ/DI20/11780040".

Funding sources were not involved in the research conduction or article preparation.

Author contributions

B.V.A.-J. contributed to the study design, performed the experiments, analyzed the data and wrote the manuscript. J.A. collaborated in the design and execution of experiments that involved eukaryotic cells and reviewed the manuscript. E. T. contributed to the design and supervision of the study and the revision of the manuscript. All authors read and approved the final version of the manuscript.

Conflict of Interest

All authors declare no conflict of interest.

Data availability

The datasets generated during and/or analyzed during the current study are available from the corresponding author upon reasonable request.

References

1 Khan, F. *et al.* Mixed biofilms of pathogenic *Candida*-bacteria: regulation mechanisms and treatment strategies. *Crit. Rev. Microbiol.* **47**, 699-727 (2021). https://doi.org/10.1080/1040841X.2021.1921696

2 Dhamgaye, S., Qu, Y. & Peleg, A. Y. Polymicrobial infections involving clinically relevant Gram-negative bacteria and fungi. *Cell. Microbiol.* **18**, 1716-1722 (2016). https://doi.org/10.1111/cmi.12674

3 Rodrigues, M. E., Gomes, F. & Rodrigues, C. F. *Candida spp.*/Bacteria Mixed Biofilms. *J. Fungi* **6**, 5 (2020). https://doi.org/10.3390/jof6010005

4 Grainha, T., Jorge, P., Alves, D., Lopes, S. P. & Pereira, M. O. Unraveling *Pseudomonas aeruginosa* and *Candida albicans* communication in coinfection scenarios: Insights through network analysis. *Frontiers in cellular and infection microbiology* **10**, 550505-550505 (2020). https://doi.org/10.3389/fcimb.2020.550505

5 Cheong, J. Z. A. *et al.* Priority effects dictate community structure and alter virulence of fungal-bacterial biofilms. *ISME J.* **15**, 2012-2027 (2021). https://doi.org/10.1038/s41396-021-00901-5

6 Fourie, R. & Pohl, C. H. Beyond Aantagonism: The interaction between *Candida* species and *Pseudomonas aeruginosa*. *J. Fungi* **5**, 34 (2019). https://doi.org/10.3390/jof5020034

7 Pendleton, K. M., Huffnagle, G. B. & Dickson, R. P. The significance of *Candida* in the human respiratory tract: our evolving understanding. *Pathogens and Disease* **75** (2017). https://doi.org/10.1093/femspd/ftx029

8 Ponde, N. O., Lortal, L., Ramage, G., Naglik, J. R. & Richardson, J. P. *Candida albicans* biofilms and polymicrobial interactions. *Crit. Rev. Microbiol.* **47**, 91-111 (2021). https://doi.org/10.1080/1040841X.2020.1843400

9 Pohl, C. H. Recent advances and opportunities in the study of *Candida albicans* polymicrobial biofilms. *Front. Cell. Infect. Microbiol.* **12** (2022).

10 Olsen, N. M. C. *et al.* Priority of early colonizers but no effect on cohabitants in a synergistic biofilm community. *Frontiers in Microbiology* **10** (2019). https://doi.org/10.3389/fmicb.2019.01949

11 Debray, R. *et al.* Priority effects in microbiome assembly. *Nat. Rev. Microbiol.* **20**, 109-121 (2022). https://doi.org/10.1038/s41579-021-00604-w

12 Clay, P. A., Dhir, K., Rudolf, V. H. W. & Duffy, M. A. Within-Host priority effects systematically alter pathogen coexistence. *Am. Nat.* **193**, 187-199 (2018). https://doi.org/10.1086/701126

13 Clay, P. A., Duffy, M. A. & Rudolf, V. H. W. Within-host priority effects and epidemic timing determine outbreak severity in co-infected populations. *Proc. of R. Soc. B* **287**, 20200046 (2020). https://doi.org/10.1098/rspb.2020.0046

14 Eichelberger, K. R., Paul, S., Peters, B. M. & Cassat, J. E. *Candida*–bacterial cross-kingdom interactions. *Trends in Microbiology* **31**, 1287-1299 (2023). https://doi.org/10.1016/j.tim.2023.08.003

15 El-Azizi, M. A., Starks, S. E. & Khardori, N. Interactions of *Candida albicans* with other *Candida* spp. and bacteria in the biofilms. *Journal of Applied Microbiology* **96**, 1067-1073 (2004). https://doi.org/10.1111/j.1365-2672.2004.02213.x

16 Shirtliff, M. E., Peters, B. M. & Jabra-Rizk, M. A. Cross-kingdom interactions: *Candida albicans* and bacteria. *FEMS Microbiol. Lett.* **299**, 1-8 (2009). https://doi.org/10.1111/j.1574-6968.2009.01668.x

17 Peleg, A. Y., Hogan, D. A. & Mylonakis, E. Medically important bacterial–fungal interactions. *Nat. Rev. Microbiol.* **8**, 340-349 (2010). https://doi.org/10.1038/nrmicro2313

18 Hogan, D. A. & Kolter, R. *Pseudomonas-Candida* interactions: An ecological role for virulence factors. *Science* **296**, 2229-2232 (2002). https://doi.org/10.1126/science.1070784

19 Hogan, D. A., Vik, A. & Kolter, R. A *Pseudomonas aeruginosa* quorum-sensing molecule influences *Candida albicans* morphology. *Mol. Microbiol.* **54**, 1212-1223 (2004). https://doi.org/10.1111/j.1365-2958.2004.04349.x

20 Méar, J. B. *et al. Candida albicans* and *Pseudomonas aeruginosa* interactions: More than an opportunistic criminal association? *Med. Mal. Infect.* **43**, 146-151 (2013). https://doi.org/10.1016/j.medmal.2013.02.005

21 Salvatori, O. *et al.* Bacteria modify *Candida albicans* hypha formation, microcolony properties, and survival within macrophages. *mSphere* **5**, 10.1128/msphere.00689-00620 (2020). https://doi.org/10.1128/msphere.00689-20

22 McAlester, G., apos, Gara, F. & Morrissey, J. P. Signal-mediated interactions between *Pseudomonas aeruginosa* and *Candida albicans*. *J. Med. Microbiol.* **57**, 563-569 (2008). https://doi.org/10.1099/jmm.0.47705-0

23 Bandara, H., Yau, J. Y. Y., Watt, R. M., Jin, L. J. & Samaranayake, L. P. *Pseudomonas aeruginosa* inhibits *in-vitro Candida* biofilm development. *BMC Microbiol.* **10**, 125 (2010). https://doi.org/10.1186/1471-2180-10-125

24 Morales Diana, K. *et al.* Control of *Candida albicans* metabolism and biofilm formation by *Pseudomonas aeruginosa* phenazines. *mBio* **4**, 10.1128/mbio.00526-00512 (2013). https://doi.org/10.1128/mbio.00526-12

25 Gibson, J., Sood, A. & Hogan, D. A. *Pseudomonas aeruginosa-Candida albicans* interactions: localization and fungal toxicity of a phenazine derivative. *Appl. Environ. Microbiol.* **75**, 504-513 (2009). https://doi.org/10.1128/AEM.01037-08

26 Lopez-Medina, E. *et al. Candida albicans* inhibits *Pseudomonas aeruginosa* virulence through suppression of pyochelin and pyoverdine biosynthesis. *PLoS Pathog.* **11**, e1005129 (2015). https://doi.org/10.1371/journal.ppat.1005129

27 Kahl, L. J. *et al.* Interkingdom interactions between *Pseudomonas aeruginosa* and *Candida albicans* affect clinical outcomes and antimicrobial responses. *Curr. Opin. Microbiol.* **75**, 102368 (2023). https://doi.org/https://doi.org/10.1016/j.mib.2023.102368

28 Faure, E., Bortolotti, P., Kipnis, E., Faure, K. & Guery, B. Studying microbial communities *in vivo*: A model of host-mediated interaction between *Candida albicans* and *Pseudomonas aeruginosa* in the airways. *JoVE*, e53218 (2016). https://doi.org/doi:10.3791/53218

29 Haiko, J., Saeedi, B., Bagger, G., Karpati, F. & Özenci, V. Coexistence of *Candida* species and bacteria in patients with cystic fibrosis. *Eur. J. Clin. Microbiol. Infect. Dis.* **38**, 1071-1077 (2019). https://doi.org/10.1007/s10096-019-03493-3

30 Bergeron Audrey, C. *et al. Candida albicans* and *Pseudomonas aeruginosa* interact to enhance virulence of mucosal infection in transparent zebrafish. *Infect. Immun.* **85**, e00475-00417 (2017). https://doi.org/10.1128/iai.00475-17

31 Phuengmaung, P. *et al.* Rapid synergistic biofilm production of *Pseudomonas* and *Candida* on the pulmonary cell surface and in mice, a possible cause of chronic mixed organismal lung lesions. *Int. J. Mol. Sci.* **23** (2022).

32 Phuengmaung, P. *et al.* Coexistence of *Pseudomonas aeruginosa* With *Candida albicans* enhances biofilm thickness through alginate-related extracellular matrix but is attenuated by N-acetyl-l-cysteine. *Front. Cell. Infect. Microbiol.* **10**, 594336-594336 (2020). https://doi.org/10.3389/fcimb.2020.594336

33 O'Brien, S. & Fothergill, J. L. The role of multispecies social interactions in shaping *Pseudomonas aeruginosa* pathogenicity in the cystic fibrosis lung. *FEMS Microbiol. Lett.* **364**, fnx128 (2017). https://doi.org/10.1093/femsle/fnx128

34 Trejo-Hernández, A., Andrade-Domínguez, A., Hernández, M. & Encarnación, S. Interspecies competition triggers virulence and mutability in *Candida albicans–Pseudomonas aeruginosa* mixed biofilms. *ISME J.* **8**, 1974-1988 (2014). https://doi.org/10.1038/ismej.2014.53

35 Ramsay, C. & Rohr, J. R. The application of community ecology theory to co-infections in wildlife hosts. *Ecol.* **102**, e03253 (2021). https://doi.org/https://doi.org/10.1002/ecy.3253

36 Neely, A. N., Law, E. J. & Holder, I. A. Increased susceptibility to lethal *Candida* infections in burned mice preinfected with *Pseudomonas aeruginosa* or pretreated with proteolytic enzymes. *Infect. Immun.* **52**, 200-204 (1986). https://doi.org/10.1128/iai.52.1.200-204.1986

37 Ader, F. *et al.* Short term *Candida albicans* colonization reduces *Pseudomonas aeruginosa*-related lung injury and bacterial burden in a murine model. *Crit. Care* **15**, R150 (2011). https://doi.org/10.1186/cc10276

38 Mear, J. B. *et al. Candida albicans* airway exposure primes the lung innate immune response against *Pseudomonas aeruginosa* infection through innate lymphoid cell recruitment and Interleukin-22-associated mucosal response. *Infection and Immunity* **82**, 306-315 (2014). https://doi.org/10.1128/iai.01085-13

39 Roux, D. *et al. Candida albicans* impairs macrophage function and facilitates *Pseudomonas aeruginosa* pneumonia in rat. *Critical Care Medicine* **37** (2009).

40 Roux, D. *et al.* Airway fungal colonization compromises the immune system allowing bacterial pneumonia to prevail. *Crit. Care Med.* **41**, e191-199 (2013). https://doi.org/10.1097/CCM.0b013e31828a25d6

41 Azoulay, E. *et al.* Candida Colonization of the Respiratory Tract and Subsequent *Pseudomonas* Ventilator-Associated Pneumonia. *Chest* **129**, 110-117 (2006). https://doi.org/10.1378/chest.129.1.110

42 Hamet, M. *et al. Candida* spp. airway colonization could promote antibiotic-resistant bacteria selection in patients with suspected ventilator-associated pneumonia. *Intensive Care Med.* **38**, 1272-1279 (2012). https://doi.org/10.1007/s00134-012-2584-2

43 Purschke, F. G., Hiller, E., Trick, I. & Rupp, S. Flexible survival strategies of *Pseudomonas aeruginosa* in biofilms result in increased fitness compared with *Candida albicans*. *Molecular & Cellular Proteomics* **11**, 1652-1669 (2012). https://doi.org/10.1074/mcp.M112.017673

44 Pendleton, K. M., Huffnagle, G. B. & Dickson, R. P. The significance of *Candida* in the human respiratory tract: our evolving understanding. *Pathog. Dis.* **75** (2017). https://doi.org/10.1093/femspd/ftx029

45 Huang, D., Qi, M., Hu, Y., Yu, M. & Liang, Z. The impact of *Candida spp* airway colonization on clinical outcomes in patients with ventilator-associated pneumonia: A systematic review and meta-analysis. *Am. J. Infect. Control* **48**, 695-701 (2020). https://doi.org/https://doi.org/10.1016/j.ajic.2019.11.002

46 Liu, J., Yu, Y.-T., Xu, C.-H. & Chen, D.-C. *Candida* colonization in the respiratory tract: What is the significance? *Front. Med.* **7**, 598037-598037 (2021). https://doi.org/10.3389/fmed.2020.598037

47 Meena, D. S. & Kumar, D. *Candida* pneumonia: An innocent bystander or a silent killer? *Med. Princ. Pract.* **31**, 98-102 (2021). https://doi.org/10.1159/000520111

48 Alam, F., Catlow, D., Di Maio, A., Blair, J. M. A. & Hall, R. A. *Candida albicans* enhances meropenem tolerance of *Pseudomonas aeruginosa* in a dual-species biofilm. *J. Antimicrob. Chemother.* **75**, 925-935 (2020). https://doi.org/10.1093/jac/dkz514

49 Kong, E. F. *et al.* Commensal protection of *Staphylococcus aureus* against antimicrobials by *Candida albicans* biofilm matrix. *mBio* **7**, 10.1128/mbio.01365-01316 (2016). https://doi.org/10.1128/mbio.01365-16

50 Lohse, M. B., Gulati, M., Johnson, A. D. & Nobile, C. J. Development and regulation of single- and multi-species *Candida albicans* biofilms. *Nature Reviews Microbiology* **16**, 19-31 (2018). https://doi.org/10.1038/nrmicro.2017.107

51 Fukami, T. Historical contingency in community assembly: Integrating niches, species pools, and priority effects. *Annu. Rev. Ecol. Evol. Syst.* **46**, 1-23 (2015). https://doi.org/10.1146/annurev-ecolsys-110411-160340

52 Stroud, J. T. *et al.* Priority effects transcend scales and disciplines in biology. *Trends in Ecology & Evolution* (2024). https://doi.org/10.1016/j.tree.2024.02.004

53 Marcos-Zambrano, L. J., Escribano, P., Bouza, E. & Guinea, J. Production of biofilm by *Candida* and non-*Candida spp*. isolates causing fungemia: Comparison of biomass production and metabolic activity and development of cut-off points. *Int. J. Med. Microbiol.* **304**, 1192-1198 (2014). https://doi.org/https://doi.org/10.1016/j.ijmm.2014.08.012

54 Crespo, A., Gavaldà, J., Julián, E. & Torrents, E. A single point mutation in class III ribonucleotide reductase promoter renders *Pseudomonas aeruginosa* PAO1 inefficient for anaerobic growth and infection. *Sci. Rep.* **7**, 13350 (2017). https://doi.org/10.1038/s41598-017-14051-2

55 Rubio-Canalejas, A., Admella, J., Pedraz, L. & Torrents, E. *Pseudomonas aeruginosa* nonphosphorylated AlgR induces ribonucleotide reductase expression under oxidative stress infectious conditions. *mSystems* **8**, e01005-01022 (2023). https://doi.org/10.1128/msystems.01005-22

Material Suplementario

Supplementary Table 1. Detailed results of statistical comparisons.

Comparison of interest	Statistical test	Variable	Conditions compared	Adjusted *p*-value	Summary
Fig. 1a Number of CFUs per mL of each microorganism in the different biofilms (n=8)	Two-way ANOVA with Tukey's multiple comparisons test	CFUs per mL of *P. aureginosa* PAET1	Pa vs 1Pa2Ca	0.0067	**
			Pa vs CaPa	0.9933	Ns
			Pa vs 1Ca2Pa	0.9891	Ns
			1Pa2Ca vs CaPa	0.0017	**
			1Pa2Ca vs 1Ca2Pa	0.0266	*
			CaPa vs 1Ca2Pa	0.8965	Ns
		CFUs per mL of *C. albicans*	Ca vs 1Pa2Ca	0.7047	Ns
			Ca vs CaPa	0.9606	Ns
			Ca vs 1Ca2Pa	0.9968	Ns
			1Pa2Ca vs CaPa	0.9744	Ns
			1Pa2Ca vs 1Ca2Pa	0.8841	Ns
			CaPa vs 1Ca2Pa	0.9974	Ns
Fig. 1b Total number of CFUs per mL in the different biofilms (n=8)	One-way ANOVA with Tukey's multiple comparisons test	Sum of CFUs per mL of *P. aeruginosa* PAET1 and *C. albicans*	Pa vs 1Pa2Ca	0.0830	Ns
			Pa vs CaPa	0.9982	Ns
			Pa vs 1Ca2Pa	0.7725	Ns
			1Pa2Ca vs CaPa	0.1528	Ns
			1Pa2Ca vs 1Ca2Pa	0.5773	Ns
			CaPa vs 1Ca2Pa	0.9076	Ns
			Ca vs 1Pa2Ca	<0.0001	****
			Ca vs CaPa	0.0020	**
			Ca vs 1Ca2Pa	0.0002	***
			Ca vs Pa	0.0047	**
Fig. 3a Experiments with eukaryotic cells Number of CFUs per mL of each microorganism in monomicrobial controls with different	Unpaired *t*-test Two-tailed *p*-value	Number of CFUs per mL of *P. aureginosa*	Pa 1x vs Pa 2x	0.7524	Ns
		Number of CFUs per mL of *C. albicans*	Ca 1x vs Ca 2x	0.0359	*

inoculum size (n=4)					
Fig. 1a and Fig. 3a Number of CFUs per mL of each microorganism in monomicrobial controls with and without eukaryotic cells (n=4 and n=8)	Mann-Whitney test Two-tailed *p*-value	Number of CFUs per mL of *P. aureginosa*	Pa from Fig. 1a vs Pa 2x from Fig. 3a	0.4606	Ns
	Unpaired *t*-test Two-tailed *p*-value	Number of CFUs per mL of *C. albicans*	Ca from Fig. 1a vs Ca 2x from Fig. 3a	0.6501	Ns
Fig. 3a Number of CFUs per mL of each microorganism in the different biofilms (n=4)	Two-way ANOVA with Tukey's multiple comparisons test	CFUs per mL of *P. aureginosa* PAET1	Pa 1x vs 1Pa2Ca	0.0862	Ns
			Pa 1x vs CaPa	0.9998	Ns
			Pa 1x vs 1Ca2Pa	0.7781	Ns
			Pa 2x vs 1Pa2Ca	0.3756	Ns
			Pa 2x vs CaPa	0.9112	Ns
			Pa 2x vs 1Ca2Pa	0.3123	Ns
			1Pa2Ca vs CaPa	0.0354	*
			1Pa2Ca vs 1Ca2Pa	0.0018	**
			CaPa vs 1Ca2Pa	0.9340	Ns
		CFUs per mL of *C. albicans*	Ca 1x vs 1Pa2Ca	>0.9999	Ns
			Ca 1x vs CaPa	>0.9999	Ns
			Ca 1x vs 1Ca2Pa	>0.9999	Ns
			Ca 2x vs 1Pa2Ca	0.9357	Ns
			Ca 2x vs CaPa	0.9400	Ns
			Ca 2x vs 1Ca2Pa	0.9806	Ns
			1Pa2Ca vs CaPa	>0.9999	Ns
			1Pa2Ca vs 1Ca2Pa	>0.9999	Ns
			CaPa vs 1Ca2Pa	>0.9999	Ns
Fig. 3b Total number of CFUs per mL in the polymicrobial biofilms (n=4)	One-way ANOVA with Tukey's multiple comparisons test	Sum of CFUs per mL of *P. aeruginosa* PAET1 and *C. albicans*	1Pa2Ca vs CaPa	0.4281	Ns
			1Pa2Ca vs 1Ca2Pa	0.1865	Ns
			CaPa vs 1Ca2Pa	0.8398	Ns

Fig. 4b Cell viability according to biofilm infection (n=4)	One-way ANOVA with Tukey's multiple comparisons test	Reduction in cell viability	Pa 1x vs 1Pa2Ca	0.0033	**
			Pa 1x vs CaPa	0.6931	Ns
			Pa 1x vs 1Ca2Pa	<0.0001	****
			Pa 2x vs 1Pa2Ca	0.0022	**
			Pa 2x vs CaPa	0.5861	Ns
			Pa 2x vs 1Ca2Pa	<0.0001	****
			Ca 1x vs 1Pa2Ca	0.0005	***
			Ca 1x vs CaPa	0.2430	Ns
			Ca 1x vs 1Ca2Pa	<0.0001	****
			Ca 2x vs 1Pa2Ca	0.1581	Ns
			Ca 2x vs CaPa	>0.9999	Ns
			Ca 2x vs 1Ca2Pa	<0.0001	****
			1Pa2Ca vs CaPa	0.1009	Ns
			1Pa2Ca vs 1Ca2Pa	0.0026	**
			CaPa vs 1Ca2Pa	<0.0001	****
Fig. 5b Biofilms susceptibility to MER	Two-way ANOVA with Tukey's multiple comparisons test	Changes in CFUs per mL of *P. aureginosa* PAET1	Pa vs 1Pa2Ca	0.0750	Ns
			Pa vs CaPa	0.0001	****
			Pa vs 1Ca2Pa	0.5727	Ns
			1Pa2Ca vs CaPa	0.1383	Ns
			1Pa2Ca vs 1Ca2Pa	0.7399	Ns
			CaPa vs 1Ca2Pa	0.0084	**
		Changes in CFUs per mL of *C. albicans*	Ca vs 1Pa2Ca	0.9936	Ns
			Ca vs CaPa	0.9999	Ns
			Ca vs 1Ca2Pa	0.9774	Ns
			1Pa2Ca vs CaPa	0.9989	Ns
			1Pa2Ca vs 1Ca2Pa	0.9998	Ns
			CaPa vs 1Ca2Pa	0.9926	Ns
Fig. 5c Biofilms susceptibility to CAS	Two-way ANOVA with Tukey's multiple comparisons test	Changes in CFUs per mL of *P. aureginosa* PAET1	Pa vs 1Pa2Ca	>0.9999	Ns
			Pa vs CaPa	0.9901	Ns
			Pa vs 1Ca2Pa	>0.9999	Ns
			1Pa2Ca vs CaPa	0.9852	Ns
			1Pa2Ca vs 1Ca2Pa	>0.9999	Ns
			CaPa vs 1Ca2Pa	0.9863	Ns
		Changes in CFUs per mL of *C. albicans*	Ca vs 1Pa2Ca	<0.0001	****
			Ca vs CaPa	<0.0001	****
			Ca vs 1Ca2Pa	<0.0001	****
			1Pa2Ca vs CaPa	0.9807	Ns
			1Pa2Ca vs 1Ca2Pa	0.9250	Ns
			CaPa vs 1Ca2Pa	0.9984	Ns

Fig. 5d Biofilms susceptibility to MER + CAS	Two-way ANOVA with Tukey's multiple comparisons test	Changes in CFUs per mL of *P. aureginosa* PAET1	Pa vs 1Pa2Ca	0.1992	Ns
			Pa vs CaPa	0.7134	Ns
			Pa vs 1Ca2Pa	0.9875	Ns
			1Pa2Ca vs CaPa	0.8722	Ns
			1Pa2Ca vs 1Ca2Pa	0.0753	Ns
			CaPa vs 1Ca2Pa	0.4158	Ns
		Changes in CFUs per mL of *C. albicans*	Ca vs 1Pa2Ca	0.0022	**
			Ca vs CaPa	<0.0001	****
			Ca vs 1Ca2Pa	<0.0001	****
			1Pa2Ca vs CaPa	0.7670	Ns
			1Pa2Ca vs 1Ca2Pa	0.3400	Ns
			CaPa vs 1Ca2Pa	0.9486	Ns
Fig. 5e Biofilms susceptibility to MER + CAS +NAC	Two-way ANOVA with Tukey's multiple comparisons test	Changes in CFUs per mL of *P. aureginosa* PAET1	Pa vs 1Pa2Ca	0.6883	Ns
			Pa vs CaPa	0.9495	Ns
			Pa vs 1Ca2Pa	0.2565	Ns
			1Pa2Ca vs CaPa	0.2763	Ns
			1Pa2Ca vs 1Ca2Pa	0.0159	*
			CaPa vs 1Ca2Pa	0.6610	Ns
		Changes in CFUs per mL of *C. albicans*	Ca vs 1Pa2Ca	0.1635	Ns
			Ca vs CaPa	0.6683	Ns
			Ca vs 1Ca2Pa	0.9077	Ns
			1Pa2Ca vs CaPa	0.8583	Ns
			1Pa2Ca vs 1Ca2Pa	0.5915	Ns
			CaPa vs 1Ca2Pa	0.9889	Ns
Supplementary Fig. 2a Biofilms susceptibility to NAC	Two-way ANOVA with Tukey's multiple comparisons test	Changes in CFUs per mL of *P. aureginosa* PAET1	Pa vs 1Pa2Ca	0.9796	Ns
			Pa vs CaPa	0.7007	Ns
			Pa vs 1Ca2Pa	0.6287	Ns
			1Pa2Ca vs CaPa	0.9488	Ns
			1Pa2Ca vs 1Ca2Pa	0.3057	Ns
			CaPa vs 1Ca2Pa	0.0788	Ns
		Changes in CFUs per mL of *C. albicans*	Ca vs 1Pa2Ca	0.5387	Ns
			Ca vs CaPa	0.8906	Ns
			Ca vs 1Ca2Pa	0.3977	Ns
			1Pa2Ca vs CaPa	0.9671	Ns
			1Pa2Ca vs 1Ca2Pa	0.9992	Ns
			CaPa vs 1Ca2Pa	0.9022	Ns
Supplementary Fig. 2b	Two-way ANOVA with Tukey's multiple	Changes in CFUs per mL of *P. aureginosa* PAET1	Pa vs 1Pa2Ca	0.0033	**
			Pa vs CaPa	0.7128	Ns
			Pa vs 1Ca2Pa	0.4997	Ns

Biofilms susceptibility to NAC + MER	comparisons test		1Pa2Ca vs CaPa	0.0733	Ns
			1Pa2Ca vs 1Ca2Pa	0.1491	Ns
			CaPa vs 1Ca2Pa	0.9967	Ns
		Changes in CFUs per mL of *C. albicans*	Ca vs 1Pa2Ca	0.5054	Ns
			Ca vs CaPa	0.9878	Ns
			Ca vs 1Ca2Pa	0.9966	Ns
			1Pa2Ca vs CaPa	0.7963	Ns
			1Pa2Ca vs 1Ca2Pa	0.3119	Ns
			CaPa vs 1Ca2Pa	0.9167	Ns
Supplementary Fig. 2c Biofilms susceptibility to NAC + CAS	Two-way ANOVA with Tukey's multiple comparisons test	Changes in CFUs per mL of *P. aureginosa* PAET1	Pa vs 1Pa2Ca	0.2889	Ns
			Pa vs CaPa	0.7565	Ns
			Pa vs 1Ca2Pa	0.7103	Ns
			1Pa2Ca vs CaPa	0.0253	*
			1Pa2Ca vs 1Ca2Pa	0.0208	*
			CaPa vs 1Ca2Pa	>0.9999	Ns
		Changes in CFUs per mL of *C. albicans*	Ca vs 1Pa2Ca	0.7197	Ns
			Ca vs CaPa	0.9995	Ns
			Ca vs 1Ca2Pa	0.5181	Ns
			1Pa2Ca vs CaPa	0.5876	Ns
			1Pa2Ca vs 1Ca2Pa	0.9973	Ns
			CaPa vs 1Ca2Pa	0.3911	Ns

n= Number, CFUs= Colony Forming Units, 1Pa2Ca= Biofilm formed with an initial inoculum of *P. aeruginosa* PAET1 followed by *C. albicans* addition 6 h later, CaPa= biofilm formed with an initial inoculum with both species, Ca= monomicrobial biofilm of *C. albicans,* Pa= monomicrobial biofilm of *P. aeruginosa*, Ca 1x = monomicrobial biofilm of *C. albicans* from experiments with eukaryotic cells, Pa 1x= monomicrobial biofilm of *P. aeruginosa* experiments with eukaryotic cells, Ca 2x = monomicrobial biofilm of *C. albicans* from experiments with eukaryotic cells with inoculum at double concentration of Ca 1x , Pa 2x= monomicrobial biofilm of *P. aeruginosa* from experiments with eukaryotic cells with inoculum at double concentration of Pa 1x. MER= Meropenem, CAS= Caspofungin, NAC= N-acetylcysteine

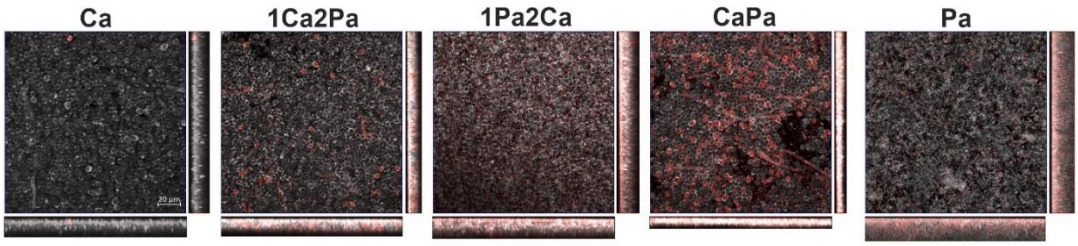

Suplementary Fig. 1 Dead cells (red) in biofilms of *C. albicans* (Ca, grey) and *P. aeruginosa* PAET1 (Pa, white) according to the inoculation time of each species. Z-stacks and orthogonal views of confocal laser images for each biofilm condition are displayed. Microorganisms were visualized using the *P. aeruginosa* PAET1-GFP strain and the dye Calcofluor white. Dead cells were stained with Propidium iodide. Images were processed using the Zeiss software. The scale bar of 20 µm is consistent for all cases. 1Ca2Pa= Biofilm formed with an initial inoculum of *C. albicans* followed by the addition of *P. aeruginosa* PAET1 6 h later. 1Pa2Ca= Biofilm formed with an initial inoculum of *P. aeruginosa* PAET1 followed by *C. albicans* addition 6 h later. CaPa= biofilm formed with an initial inoculum with both species. Ca= monomicrobial biofilms of *C. albicans.* Pa= monomicrobial biofilm of *P. aeruginosa*.

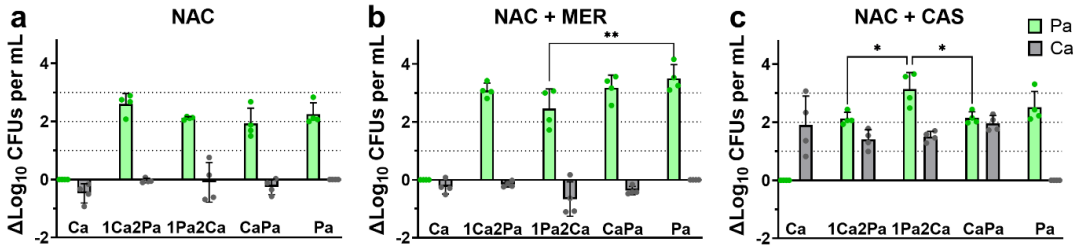

Supplementary Fig. 2 Quantification of the biomass reduction of each microorganism (ΔLog CFUs per mL) after treatment with **a** N-acetylcysteine (NAC) at 1 mg per mL, **b** N-acetylcysteine and meropenem at 5 µg per mL (NAC + MER) and **c** N-acetylcysteine and caspofungin (CAS) at 5 µg per mL (NAC + CAS). Asterisks indicate statistically significant differences among conditions in an Ordinary two-way ANOVA with Tukey's multiple comparison test (∗*p*-value <0.05; ∗∗*p*-value <0.01. The experiments were conducted 4 times. Data are represented as mean ± standard deviation.

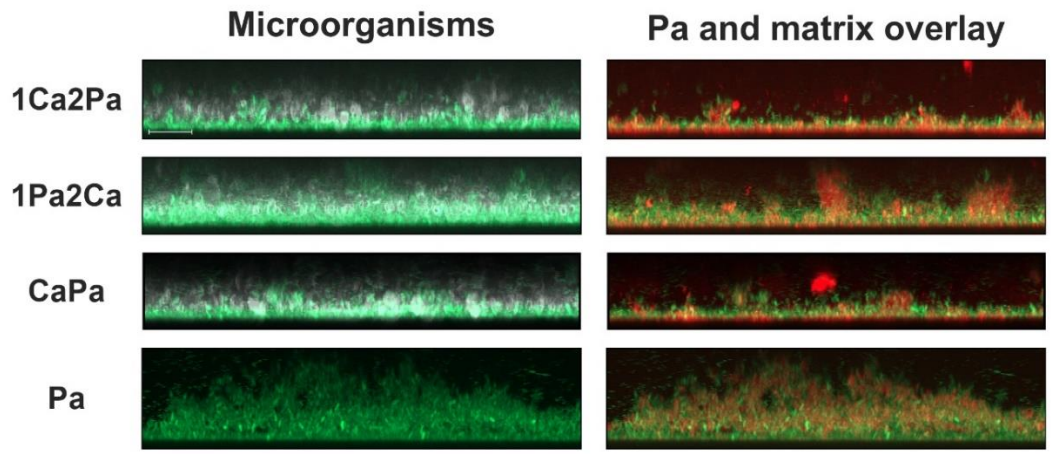

Supplementary Fig. 3 Matrix content (extracellular polysaccharides) in *C. albicans* and *P. aeruginosa* biofilms. Orthogonal views (xz) of confocal laser images for each biofilm condition visualized using the *P. aeruginosa* PAET-GFP strain (green) and the dyes Calcofluor white (grey) and Concanavalin A-Alexa fluor 647 (red) to stain *C. albicans* and ECM carbohydrates, respectively. Images were processed using the Zeiss software. The scale bar of 10 µm is consistent for all cases. 1Ca2Pa= Biofilm formed with an initial inoculum of *C. albicans* followed by addition of *P. aeruginosa* PAET1 6 h later. 1Pa2Ca= Biofilm formed with an initial inoculum of *P. aeruginosa* PAET1 followed by *C. albicans* addition 6 h later. CaPa= biofilm formed with an initial inoculum with both species. Ca= monomicrobial biofilm of *C. albicans.* Pa= monomicrobial biofilm of *P. aeruginosa*.

Artículo 3 (Manuscrito)

Candida albicans enhances *Staphylococcus aureus* virulence by progressive generation of new phenotypes

Sometido en la revista *Current Research in Microbial Sciences*

(CRMICR-D-24-00290)

Categoría Microbiología 2023: 1er tercil, 1er Cuartil, IF= 4.8

Betsy V. Arévalo-Jaimes[1,2] y Eduard Torrents[1,2]

[1]Grupo Infecciones Bacterianas y Terapias Antimicrobianas (BIAT), Instituto de Bioingeniería de Cataluña (IBEC), Barcelona, España.

[2]Sección de Microbiología, Departamento de Genética, Microbiología y Estadística, Facultad de Biología, Universitat de Barcelona, Barcelona, España.

Cita versión *pre-print*: Arevalo, B. V., & Torrents, E. (2024). *Candida albicans* enhance *Staphylococcus aureus* virulence by progressive generation of new phenotypes. *bioRxiv*, 2024-06. DOI: 10.1101/2024.06.26.600854.

Candida albicans enhance *Staphylococcus aureus* virulence by progressive generation of new phenotypes

Betsy Verónica Arévalo-Jaimes[a,b] and Eduard Torrents[a,b#]

[a]Bacterial infections and antimicrobial therapies group, Institute for Bioengineering of Catalonia (IBEC), The Barcelona Institute of Science and Technology, Barcelona, Spain.

[b]Microbiology Section, Department of Genetics, Microbiology and Statistics, Faculty of Biology, University of Barcelona, Barcelona, Spain.

Running Head: *C. albicans* induces *S. aureus* virulent variants

#Addres correspondence to Dr. Eduard Torrents, etorrents@ibecbarcelona.eu

Abstract word count: 162 abstract section + 113 importance section

Main text word count: 4167

Abstract

Candida albicans and *Staphylococcus aureus* have been co-isolated from several biofilm-associated diseases, including those related to medical devices. This association confers advantages to both microorganisms, resulting in detrimental effects on the host. To elucidate this phenomenon, the present study investigated colony changes derived from non-physical interactions between *C. albicans* and *S. aureus*. We performed proximity assays by confronting colonies of the yeast and the bacteria on agar plates at six different distances for 9 days. We found that colony variants of *S. aureus* originated progressively after prolonged exposure to *C. albicans* proximity, specifically in response to pH neutralization of the media by the fungi. The new phenotypes of *S. aureus* were more virulent in a *Galleria mellonella* larvae model compared to colonies grown without *C. albicans* influence. This event was associated with an upregulation of *RNAIII* and *AgrA* expression, suggesting a role for α-toxin. Our findings indicate that *C. albicans* enhances *S. aureus* virulence by inducing the formation of more aggressive colonies.

Importance

For decades, it has been known that *C. albicans* increase *S. aureus* virulence, resulting in a "lethal synergism". However, it was only recently identified that this outcome is driven by the sustained activation of the staphylococcal *agr* system in response to *C. albicans* environmental modifications. Our experimental design allowed us to observe individual changes over time caused by the proximity of both microorganisms. As a result, we report for first time that *C. albicans* exposure induces the generation and favors the growth of *S. aureus* colony variants with increased expression of virulence factors. Our findings highlight the importance to understanding the intricate connection between environmental responses, virulence and fitness in *S. aureus* pathogenesis.

Keywords: *Galleria mellonella*, polymicrobial interactions, interkingdom interactions, synergistic effects, proximity assay, *agr* system, mortality, pathogenicity

Introduction

In the past, Koch's postulates helped identify the etiological causes of several monomicrobial infections (1). Then, high-throughput genome sequencing techniques significantly expanded the notion of microbial biodiversity harbored within the body, revealing, for instance, more than 1000 species residing in the gut (1). Currently, it is recognized that the coexistence of multiple microorganisms in the same host niche fosters interactions among them that can drive disease onset and outcome (1). Furthermore, these complex communities can adopt the biofilm mode of life, secreting an extracellular matrix that surrounds and protects them from environmental attacks, including antimicrobial agents (1, 2)

Among the polymicrobial infections, those involving the presence of fungi and bacteria are particularly significant in the clinical context (2). The yeast *Candida albicans* and the Gram-positive bacterium *Staphylococcus aureus* are among the most prevalent nosocomial pathogens responsible for severe morbidity and mortality (3). This duo is frequently present in intra-abdominal infections that can disseminate and produce systemic infections that are very difficult to treat (1, 2). Moreover, *C. albicans* and *S. aureus* have been co-isolated from several biofilm-associated diseases, including chronic wound infections, cystic fibrosis, urinary tract infections, and medical-device-related infections (1, 2). Being part of these polymicrobial biofilms confers several advantages to both members, such as enhanced tolerance to vancomycin in *S. aureus* (4) and to miconazole in *C. albicans* (5). Likewise, the addition of conditioned medium from *S. aureus* dramatically increases *C. albicans* biofilm growth (6).

The cooperative relationship of these microorganisms involves both physical interactions and interspecies communication (2, 7). The chemical interactions between *C. albicans* and *S. aureus* include secreted molecules from the quorum sensing (QS) system (1, 2). In *S. aureus*, the best-characterized QS system is the accessory regulatory (*agr*) system, consisting of the promoter P2 and P3 that drive the expression of the transcripts ARNII and ARNIII, respectively (1). RNAII is encoded for four genes *agrA*, *agrB*, *agrC* and *agrD*. AgrB is a membrane protein that modifies and secretes the pre-signal peptide AgrD into its mature form, the autoinducing peptide 2 (AIP-2). AIP-2 is recognized by the membrane-bound protein kinase AgrC, which phosphorylates AgrA, activating P2 and P3. RNAIII is the effector molecule of the *agr* system and is responsible for toxin production, including α-toxin, a fundamental tool in *S. aureus*' pathogenicity (1).

Polymicrobial infections are often associated with poor patient prognosis (7, 8). In the case of *C. albicans* and *S. aureus*, it has long been known that their intraperitoneal coinfection has a synergistic effect on mouse mortality (9). Increased virulence of *C. albicans* and *S. aureus* co-infection has also been reported in zebrafish embryos, *Galleria mellonella* larvae, and patients with systemic infections (10, 11). However, it was only recently that the major lethality driver and its mechanism of activation were identified. *C. albicans* ribose catabolism and alkalinization of the extracellular pH led to sustained activation of the staphylococcal *agr* system and the production of the effector molecule α-toxin (3, 12, 13). α-toxin can cause membrane damage, lysis, eicosanoid stimulation, disruption of tight junctions, activation of platelet aggregation, and dysregulation of the hemostatic system, leading to organ failure (1).

Further studies elucidating the details of the "lethal synergism" among this interkingdom association will aid in the development of new therapeutic targets. As the understanding of microbial interactions makes it clearer that the successful treatment of polymicrobial infections will arise from targeting the community as a whole (6). For this reason, the present study aimed to investigate colony changes resulting from non-physical but close interactions in a long-term *C. albicans* and *S. aureus* co-culture. To that end, proximity assays confronting the yeast and bacteria at six different distances for 9 days were developed. We found that *S. aureus* virulence enhancement results from progressive phenotypical diversification of the original colonies.

Results

***C. albicans* proximity promotes the generation of *S. aureus* colony variants**

We observed non-physical interactions between the well-known opportunistic pathogens *S. aureus* (Sa) and *C. albicans* (Ca) through a proximity assay spanning six different distances over 9 days (Fig. 1). Inoculum drops deposited on the agar allowed for the development of well-defined colonies of both microorganisms, which were visible from day 1. In the case of *C. albicans*, colonies expanded progressively over the days. However, in the control (Ca – Ca), the size of the colonies decreased with increasing proximity, while in the proximity assay (Ca – Sa), the size remained constant across positions (Fig. S1).

In contrast, the size of *S. aureus* colonies in the proximity assay (Ca – Sa) remained constant (Fig. 1). However, between day 5 and 7, small points of additional growth of *S. aureus* were observed within the original colony (see Fig. 1 small white arrows). The

quantity and size of the growth spots increased over time, leading to fusion, and covering the original colony entirely. By days 7-9, the expansion of new *S. aureus* colonies continued and extended beyond the edges of the original colonies (see Fig. 1 small white arrows). Interestingly, the emergence of new phenotypes was linked to the proximity to *C. albicans*, where the process of generating new variants was faster at the closest position (P1= 1 cm). Consequently, the effect gradually decreased over subsequent positions, being minimal in the last ones (P5= 4 cm and P6= 5 cm) and absent in the control plate (Sa – Sa).

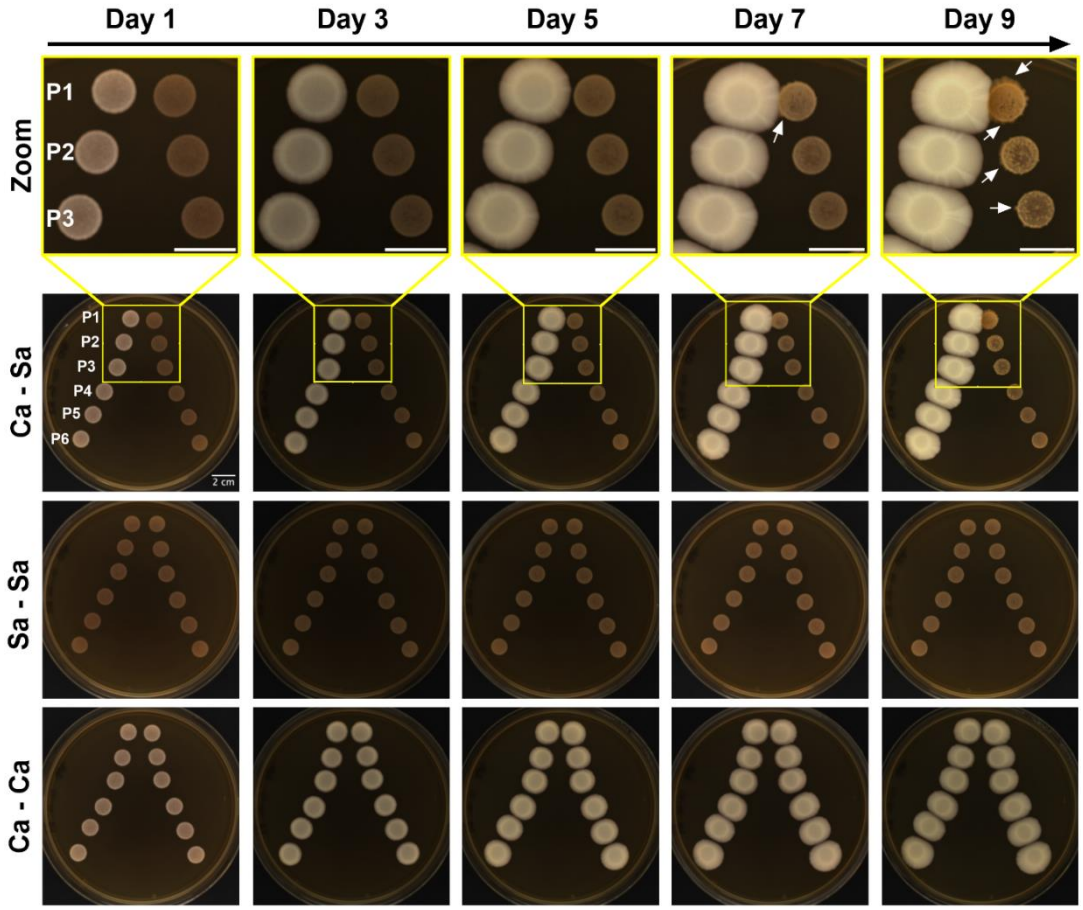

FIG 1 Proximity assay timeline of *C. albicans* (Ca) and *S. aureus* (Sa). Ca – Sa depicts zoomed (top) and original images (bottom) of *C. albicans* colonies (left) developed at six different distances (P1= 1 cm, P2= 1.5 cm, P3= 2 cm, P4= 3 cm, P5= 4 cm and P6= 5 cm) from *S. aureus* colonies (right) monitored over 9 days with a 1-day interval. White arrows indicate evident growth of new phenotypes within *S. aureus* original colonies. Sa – Sa represents the control condition in which *S. aureus* inoculum was used in both columns, while Ca – Ca is the control condition where *C. albicans* inoculum was used in both columns. The displayed images are representative of three different experiments and were processed with ImageJ software. The scale bar of 2 cm applies to all cases.

The described production of new *S. aureus* colonies was absent in proximity assays with other bacteria but were present with *Candida parapsilosis* (Fig. 2), indicating that the colony generation effect could be a specific interaction of *S. aureus* with the genus *Candida*.

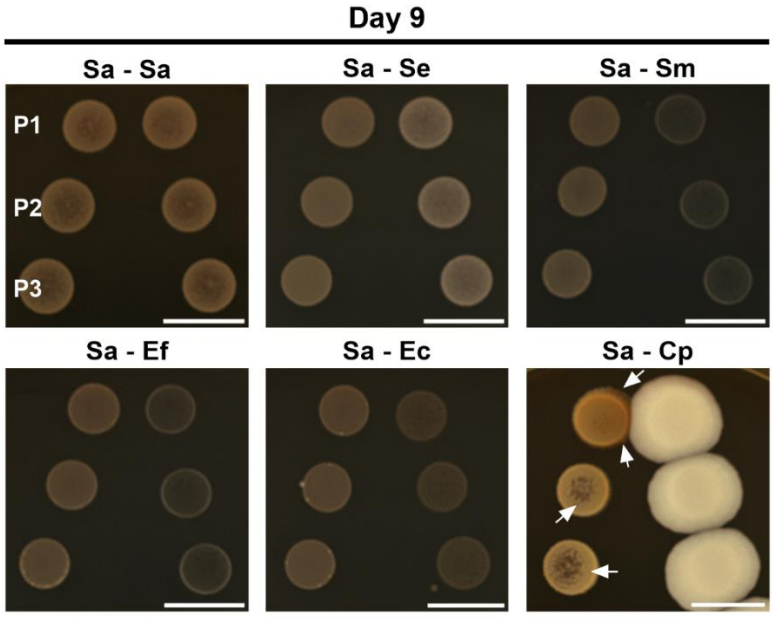

FIG 2 Proximity assay of *S. aureus* (Sa) with other microorganisms. Zoomed images of *S. aureus* colonies (left) with itself (Sa – Sa), *S. epidermidis* (Sa – Se), *S. mutans* (Sa – Sm), *E. faecalis* (Sa – Ef), *E. coli* (Sa – Ec) and *C. parapsilosis* (Sa – Cp) (right) at day 9. Displayed images are representative of three different experiments and were processed with ImageJ software. The scale bar corresponds to 2 cm and applies to all cases. The shown distances correspond to P1= 1 cm, P2= 1.5 cm and P3= 2 cm.

Generation of *S. aureus* colony variants depend on pH and initial glucose levels

Considering the ability of *C. albicans* to alkalinize the media and the influence of pH on *S. aureus* virulence (13-16), we evaluated whether the appearance of *S. aureus* colony variants induced by *C. albicans* were related to pH changes. To this end, we performed the proximity assay by adding the pH indicator Bromocresol purple to the YPD agar medium (Fig. 3). The Sa – Sa control revealed that *S. aureus* growth from day 1 was accompanied by a pH decrease, which persisted throughout the experiment. In contrast, Ca – Ca control demonstrated that *C. albicans* growth led to a progressive increase in pH. These individual behaviors were maintained when both microorganisms were grown together (Ca – Sa). However, we observed that after day 5, *C. albicans* proximity to *S. aureus* nullified bacterial acidification. This alkalinization resulted in a predominance of a neutral pH in the positions

with closer proximity between the species (P1-P3) by day 9. Though, the most meaningful finding, was the perfect overlap between *C. albicans* pH modulation and the origination of *S. aureus* colony variants (Fig. 3). Thus, we tested if *C. albicans* induced the formation of colony variants in other bacterial species, finding positive results with *S. epidermidis* and *E. coli* (Fig. S2).

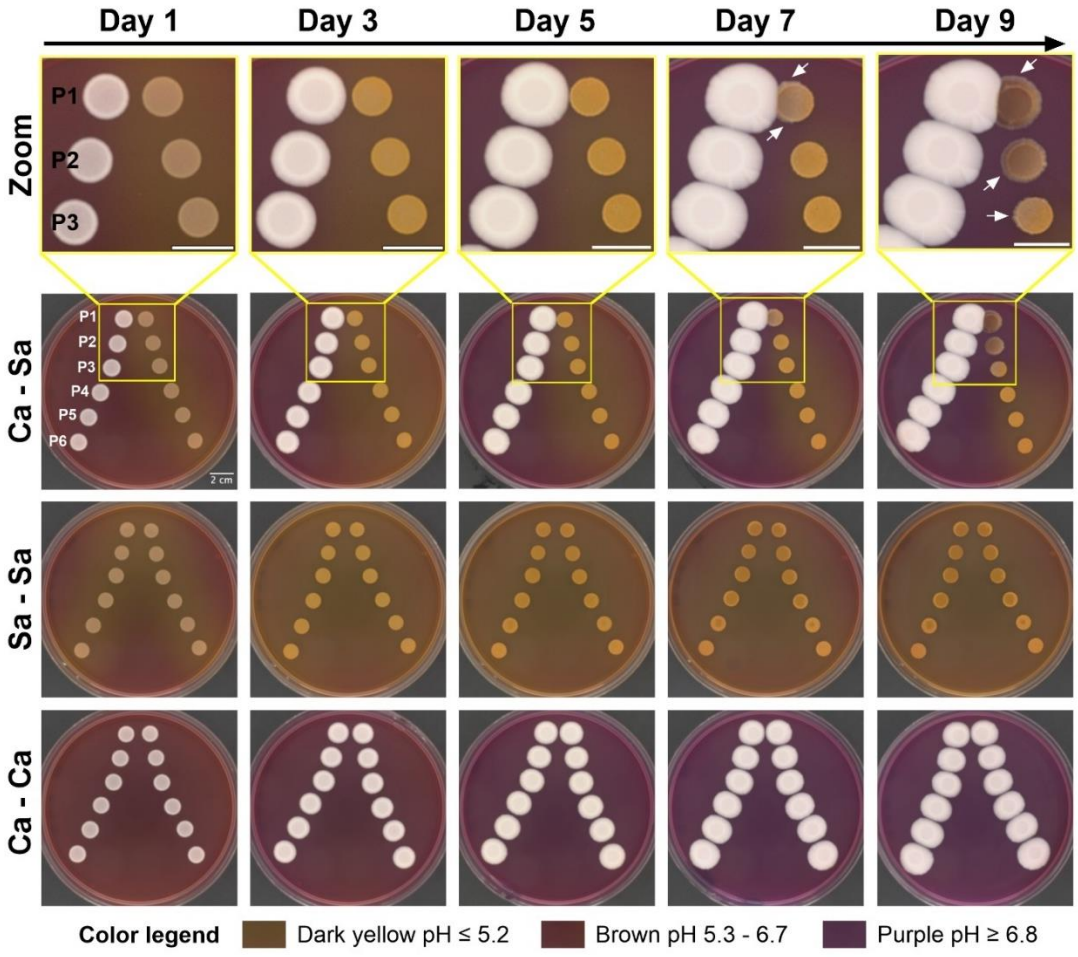

FIG 3 Timeline of pH changes in a proximity assay of *C. albicans* (Ca) and *S. aureus* (Sa). Ca – Sa depicts zoomed (top) and original images (bottom) of *C. albicans* colonies (left) developed at six different distances from *S. aureus* colonies (right) in YPD agar with bromocresol purple. Plates were monitored over 9 days with a 1-day interval. White arrows indicate evident growth of new phenotypes within *S. aureus* original colonies. Sa – Sa represents the control condition in which *S. aureus* inoculum was used in both columns, while Ca – Ca is the control condition where *C. albicans* inoculum was used in both columns. The displayed images are representative of three different experiments and were processed with ImageJ software. The scale bar of 2 cm applies to all cases. The shown distances correspond to P1= 1 cm, P2= 1.5 cm, P3= 2 cm, P4= 3 cm, P5= 4 cm, and P6= 5 cm.

Next, we assessed if the sole action of pH alkalinization was sufficient to induce the generation of *S. aureus* colony variants. Thus, we exposed *S. aureus* colonies grown in a proximity assay configuration to increasing quantities of NaOH 2M for 7 days (Fig. 4A). Again, we observed the appearance of *S. aureus* colony variants in positions (P1-P3) with greater exposure to pH changes. As expected, the PBS control did not induce either pH changes or generation of *S. aureus* variant colonies. This finding showed that the presence of *C. albicans* is not necessary to obtain the phenotypic variants of *S. aureus* even though in the case of proximity assays is the responsible of this pH change.

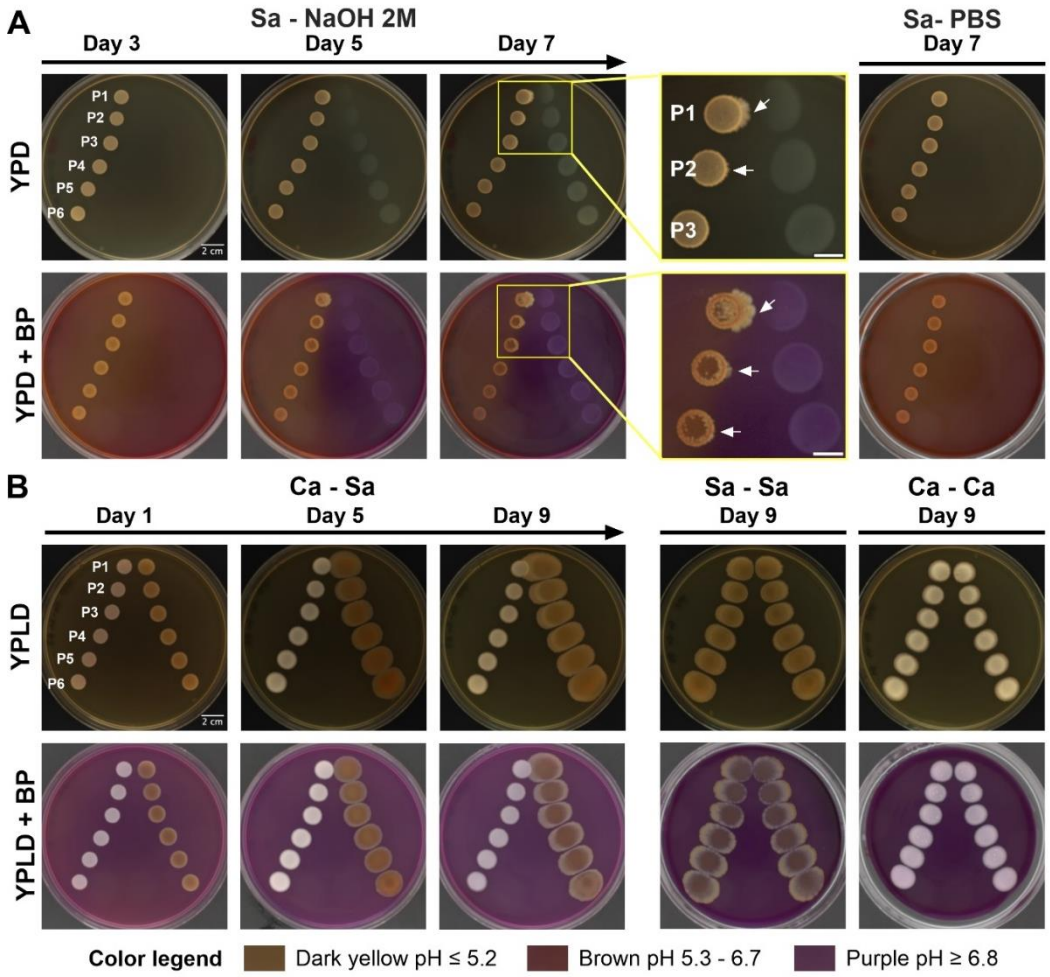

FIG 4 pH and glucose dependence in the generation of *S. aureus* colony variants. (A) Timeline of the effect of *S. aureus* colonies' exposure to NaOH 2M (Sa – NaOH 2M) in both YPD and YPD with bromocresol purple (YPD + BP). Zoomed images from day 7 are displayed. White arrows indicate evident growth of new phenotypes within *S. aureus* original colonies. Sa – PBS represents the control condition. (B) Timeline of glucose effect on *S. aureus* variant colonies' generation in a proximity assay

of *S. aureus* with *C. albicans* (Ca – Sa) in both YPLD (YPD with glucose at 0.2 %) and YPLD with bromocresol purple (YPLD + BP). Sa – Sa is the control condition in which *S. aureus* inoculum was used in both columns, while Ca – Ca is the control condition where *C. albicans* inoculum was used in both columns. Displayed images are representative of three different experiments and were processed with ImageJ software. The scale bar of 2 cm applies to all cases. The shown distances correspond to P1= 1 cm, P2= 1.5 cm, P3= 2 cm, P4= 3 cm, P5= 4 cm, and P6= 5 cm.

Furthermore, we decided to test the role of glucose in the development of *S. aureus* colony variants, considering that glucose availability was reported to influence the Staphylococcal *agr* system (15) (Fig. 4B). A proximity assay between *S. aureus* and *C. albicans* in YPD with low glucose (YPLD) showed substantial variations in the growth of both microorganisms. Firstly, *C. albicans* growth decreased compared to YPD colonies, reflected in a smaller colony size at the end of the experiment in the control (Ca – Ca) and, more markedly, in the interaction with *S. aureus* (Ca – Sa). In contrast, *S. aureus* colonies growing in YPLD expanded overtime, reaching a colony size considerably higher than when they grew in YPD, regardless of the presence of *C. albicans*. Additionally, *S. aureus* growth was not accompanied by the acidification of the media, resulting in the total dominance of *C. albicans* alkalinization and the pH neutralization of the complete plate. These changes did not promote the generation of *S. aureus* colony variants.

S. aureus colony variants exhibit increased virulence

To assess virulence differences of *S. aureus* colony variants, we conducted a proximity assay for 10 days. Each *S. aureus* colony was designated with a number, including controls (Fig. 5A). Colonies 1 to 4 corresponded to the new variants gradually generated at P1-P3 positions, where colony 4 represent the phenotype developed after initial exposure to basic pH, and colony 1 represented the phenotype obtained after sustained exposure. Colony 5 and 6 corresponded to the border and center of *S. aureus* growth at positions P4-P6, where no meaningful pH change was present. Controls were taken from a Sa – Sa plate incubated for 10 days (colony 7) and 1 day (colony 8).

Infection of *G. mellonella* with *S. aureus* colonies showed significant differences in larval survival (Fig. 5B). Larvae infected with colonies 5, 6 and 7 did not show mortality. Meanwhile, the median survival of larvae infected with colonies 1, 2, 3, 4 and 8 was 15 h, 19 h, 21 h, 40 h and 40 h, respectively. According to the Log rank test, colonies 1 and 2 exhibited enhanced virulence compared to control colony 8. These variations cannot be attributed to differences in metabolic activity, as no statistically significant deviation was observed in the PrestoBlue results between colonies 1-5 and the control colony 8 (Fig. 5C).

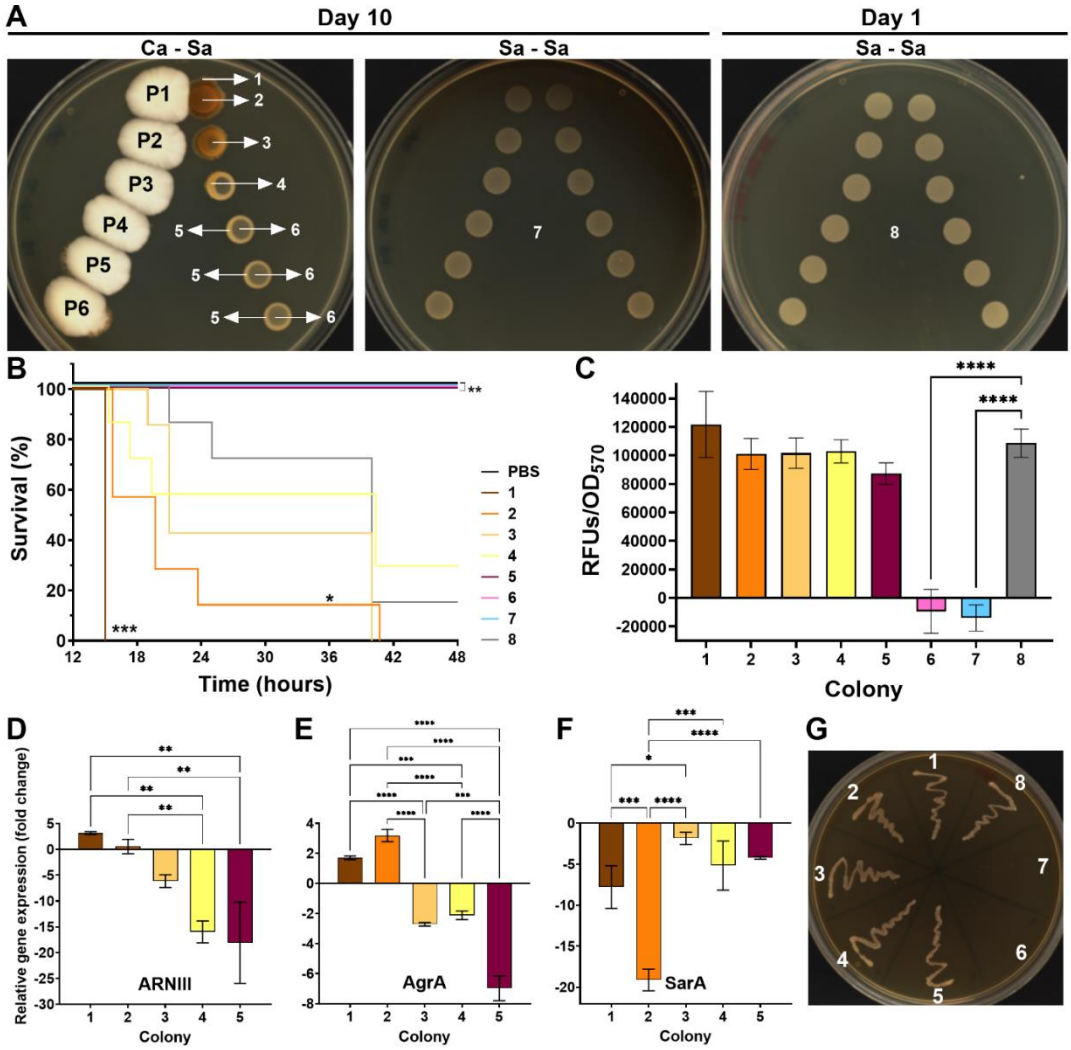

FIG 5 Virulence assessment of *S. aureus* colony variants. (A) Colonies of *S. aureus* obtained after a proximity assay with *C. albicans* (Ca – Sa) for 10 days were numbered. Colonies obtained from *S. aureus* controls (Sa – Sa) at day 10 and day 1 were also included. The shown distances correspond to P1= 1 cm, P2= 1.5 cm and P3= 2 cm, P4= 3 cm, P5= 4 cm, and P6= 5 cm. (B) Kaplan-Meier survival curves of *G. mellonella* larvae after inoculation with all different *S. aureus* colonies, with each condition involving 8 larvae. Asterisks indicate statistically significant differences in virulence in comparison to control colony 8 by a long-rank test. (C) Evaluation of the metabolic activity of *S. aureus* colonies by PrestoBlue assay. Asterisks indicate statistically significant differences versus control colony 8 in an Ordinary one-way ANOVA with Šidák's multiple comparison test. RFUs= Relative Fluorescence Units. Fold change of (D) ARNIII, (E) AgrA, and (F) SarA gene expression of *S. aureus* colonies 1-5 in comparison to control colony 8. Asterisks indicate statistically significant differences among colonies in an Ordinary one-way ANOVA with Šidák's multiple comparison test. (G) Reversion test of *S. aureus* colonies. The results presented in this figure are representative of the same experiment repeated three times. Images were processed with ImageJ software and error bars display mean and standard deviation. ∗*p*-value <0.05, ∗∗*p*-value <0.01, ∗∗∗*p*-value <0.001, and ∗∗∗∗*p*-value <0.0001

However, the complete survival of larva infected with colonies 6 and 7 was justified by their lack of metabolic activity.

Thus, the expression of three important virulence genes of *S. aureus* was evaluated in colonies 1-5 compared to the control colony 8 (Fig. 5D-F). We found that colony 1, the most virulent, exhibited increased expression of *ARNIII* and *agrA* but decreased expression of *sarA*. This induction of *agrA* and reduction of *sarA* expression were more pronounced in colony 2, although no change in RNAIII was observed in this case. Colonies 3-5 showed decreased expression of all genes; however, repression of the *agrA* gene was higher in colony 5 compared to colonies 3 and 4. Therefore, *S. aureus* variant colonies (colonies 1-4) originating in response to external pH changes exhibited increased virulence, associated to expression changes, compared to the original colonies (colonies 5-6) and the colonies formed under control conditions (Sa – Sa) for 10 days (colony 7) and 1 day (colony 8).

Finally, the re-plating of the colonies showed no differences among their growth (Fig. 5G), indicating that the colony variant phenotype is reversible.

Discussion

The ability of both *C. albicans* and *S. aureus* to colonize a wide variety of human body sites increases the likelihood of shared host niches and the development of mixed infections (7). Survival in different microenvironments requires metabolic flexibility controlled by time- and space-specific regulatory networks (17, 18). This implies that environmental factors can influence disease outcomes (13). Moreover, in the context of polymicrobial infections, the environmental response of one microorganism can affect the behavior of other species (13).

In the case of *S. aureus*, the regulatory network controlling virulence responds to various environmental cues that drive the bacterium throughout the infection process (17). For instance, the *agr* system, responsible for ARNIII expression and α-toxin secretion, is sensitive to acidic or alkaline conditions, with a maximum activity near neutral pH (1, 14, 15). Furthermore, *S. aureus* virulence is enhanced by *C. albicans,* resulting in what is described as lethal synergism (9). Recent studies have shown that this effect is associated with an increase in *S. aureus* α-toxin production via *agr* activation, in response to extracellular ribose depletion and media neutralization caused by *C. albicans* (3, 12, 13). However, questions regarding this cooperative microbial interaction mediated by environmental crosstalk remain.

In this study, we performed a proximity assay that allowed us to monitor colony changes resulting from non-physical interactions between *S. aureus* and *C. albicans.* In contrast to previous studies that used liquid conditions for co-culture, our experiment permitted the simultaneous evaluation of six different distances between species growth. Long-term plate incubation (over 9-10 days) compensated for the higher diffusion times and loss of volatile compounds present in solid agar, allowing events to be recorded sequentially. As a result, our investigation reports that *C. albicans* enhances *S. aureus* virulence by inducing the generation of successive new colony variants (Fig. 1 and Fig. 5). The origin of the colony variants coincided with the pH change induced by *C. albicans*-mediated media alkalinization (Fig. 3), although *C. albicans* is not strictly required for their generation, as their appearance under other artificial pH modulators (NaOH) was also confirmed (Fig. 4).

Importantly, *G. mellonella* larvae survival (Fig. 5B) decreased in relation to the generation time of the colony variant. Colonies generated after prolonged exposure to *C. albicans* proximity (colonies 1-2) caused significantly higher mortality compared to those exposed for a shorter time (colonies 3-4) or not exposed at all (colonies 5 and 8) (Fig. 5A-B). This agrees with the lethal synergism observed from *in vivo* experiments of systemic and local infections after co-inoculation of both microorganisms (3, 9-11, 19, 20). Our results showed that *G. mellonella* larvae survival at 24 h decreased from 71.4% when infected with colony 8 to 0-14% when infected with colonies 1 and 2, respectively. These values are consistent with the previous study by Sheehan *et al.* (2020) using this animal model, where larvae infected with *S. aureus* alone and in combination with *C. albicans* showed a survival of 80% vs 30% at 24 h (10).

Moreover, our experimental setting allowed us to recreate the interaction between both species, but to evaluate the virulence of *S. aureus* colonies by themselves. The isolation of the different *S. aureus* colonies from the proximity assay before larvae inoculation demonstrated that, although *C. albicans* is the responsible for the increase of *S. aureus* virulence, it is not required for the lethal effect. In addition, the qRT-PCR results showed that the increase in *S. aureus* virulence is related to an up-regulation of *ARNIII* and *agrA*, two important genes controlled by the *agr* system (Fig. 5D-E). Therefore, we believe the high pathogenicity of *S. aureus* colony variants originated after *C. albicans* exposure is related to an increase in α-toxin expression, as previously reported (3), although we did not perform a direct detection of this molecule.

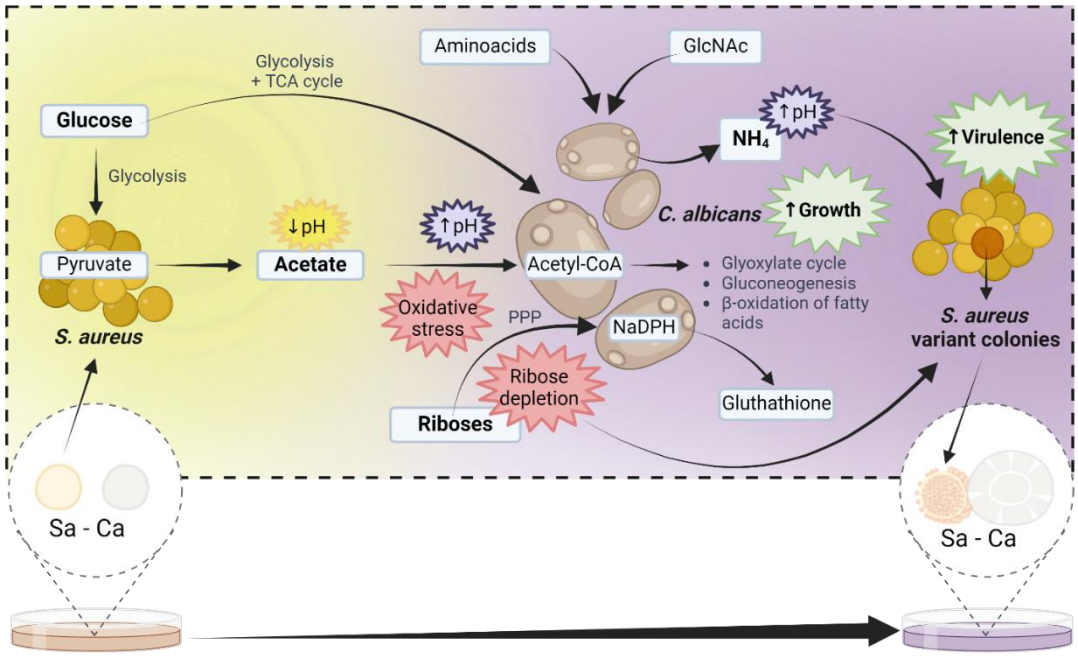

FIG 6 Working model of *S. aureus* and *C. albicans* metabolic interactions and their associated environmental changes influencing *S. aureus* virulence. *S. aureus* catabolism of glucose produces the excretion of acetate into the media, which decreases the pH. The acetate molecule serves as a precursor of Acetyl-coA, positively impacting the growth of *C. albicans*. Acetate consumption through different metabolic routes helps neutralize the pH of the media, in conjunction with ammonia (NH_4) production derived from amino acids and/or N-acetylglucosamine (GlcNAc) metabolism. Additionally, extracellular acetate can induce oxidative stress in *C. albicans* cells, leading to ribose metabolism in the Pentose Phosphate Pathway (PPP) to produce the required NADPH for glutathione synthesis. pH neutralization and ribose depletion of the media by *C. albicans* activate the Staphylococcal *agr* system, increasing *S. aureus* virulence. TCA= Tricarboxylic Acids. Image created with Biorender.com.

Considering our recent discoveries and those of others, we propose a comprehensive model of *C. albicans-S. aureus* metabolic interactions and microenvironmental changes that could result in the enhancement of *S. aureus* virulence through new variants generation (Fig. 6). First, the aerobic growth of *C. albicans* under high glucose couples the glycolysis pathway with the TCA cycle (21). Although glucose is its preferred carbon source, this yeast can simultaneously metabolize alternative sources through enzymes from the gluconeogenic and glyoxylate cycle (22-25). Meanwhile, *S. aureus* aerobic growth in glucose rich-media causes repression of the tricarboxylic acid (TCA) cycle by CcpA. Thus, pyruvate obtained from glycolysis is converted to acetate and excreted into the media, causing pH decrease and downregulating the staphylococcal *agr* system (15, 18).

Acetate may serve as source of acetyl-coA, the central intermediate in carbon metabolism (26). It is naturally present in blood and within macrophages and neutrophils (26). Once glucose is depleted, *C. albicans* can utilize acetate as a carbon source, entering the glyoxylate cycle, passing through the TCA cycle, and ultimately producing glucose in the gluconeogenic pathway (21). Additionally, acetate at physiological relevant concentrations up-regulates enzymes related to fatty acid metabolism (26). Therefore, this could be an explanation of the *S. aureus* positive impact on *C. albicans* growth (as observed in Fig. S1).

Furthermore, we believe that the consumption of acetate by *C. albicans* has an alkalinizing effect on the media, as reported with the metabolism of other carboxylic acids (α-ketoglutarate, pyruvate, and lactate) (27). However, the environmental changes in pH exerted by *C. albicans* may also involve two alternative mechanisms that this yeast has evolved to counteract acidic environments (27). The capacity to manipulate extracellular pH is related to survival inside phagocytic cells of the immune system and hyphal morphogenesis, being essential for fungal fitness *in vitro* and *in vivo* (16, 27). Both metabolism of amino acids and N-acetylglucosamine results in ammonia externalization, leading to a pH increase in the media (7, 16, 28, 29). This pH neutralization offers optimal conditions for the staphylococcal *agr* system, inducing α-toxin production (7).

Recently, the work of the field experts Peters and colleagues discovered a fundamental role of *C. albicans* ribose catabolism in activating the *agr* system of *S. aureus* (12). Although our experiments do not evaluate this new factor, as were performed before the publication of this finding, we propose that *C. albicans* ribose catabolism may be related to the production of NADPH by the Pentose Phosphate Pathway as a response to counteract the oxidative damage induced by acetate. Physiological relevant concentrations of acetate have been shown to induce oxidative stress in *C. albicans* cells, leading to glutathione secretion into the media, and NADPH is an important molecule in the glutathione redox cycle (26, 30, 31).

Bringing all these points together suggests that the lethal synergism observed in *C. albicans* and *S. aureus* co-infection results from a series of metabolic interactions that include environmental changes to which both species react. This is supported by the phenotype reversion of the colony variants after replating (Fig. 5G) once the corresponding stimuli were removed. However, we do not yet understand the evolutionary advantage that allows *S. aureus* cells that progressively adapt the transcription of virulence genes (*agr* system) in response to environmental stimuli (pH and ribose depletion) to have greater

fitness, generating the appearance of colony variants. Nevertheless, evidence of *S. aureus* interconnection between metabolism and virulence is increasing daily, with more metabolic transcriptional regulators influencing the expression of virulence factors described each time (18).

Finally, we highlight the utility of the proximity assay as a simple, inexpensive, and easy- to-implement technique for studying visible colony changes resulting from non-physical interactions among microorganisms. Moreover, its use as a screening technique allowed us to identify similar interactions between *C. albicans* and two other bacterial pathogens, *S. epidermidis* and *E. coli*, suggesting potential avenues for future experiments. Additionally, we found that the *C. parapsilosis* clinical isolate used in this study can alkalinize the pH (data not shown) and therefore induce the generation of *S. aureus* colony variants.

Materials and methods

Bacterial strains and growing conditions

The fungaemia clinical isolates *Candida albicans* 10045727 and *Candida parapsilosis* 11103595 (32), and the bacterial strains *Staphylococcus aureus* ATCC 12600 (CECT 86), *Staphylococcus epidermidis* ATCC 1798 (CECT 231), *Streptococcus mutans* ATCC 25175 (CECT 479), *Enterococcus faecalis* ATCC 19433 (CECT 481) and *Escherichia coli* CFT073 (ATCC 700928) were used in this study. Each microorganism was recovered from a -80 stock. Bacteria were cultured at 37 ºC in Tryptic Soy Agar (TSA) (Scharlab S.L.) or Luria Bertani (LB) agar (Scharlab S.L.), while fungi were grown at 30 ºC in Yeast Petone Dextrose (YPD) medium consisting of 1% Yeast Extract (Gibco), 2% Meat Peptone (Scharlab S.L.), 2% D-glucose (Fisher Scientific S.L.), and, when required, 2% Bacteriological Agar (Scharlab S.L.). Similarly, overnight cultures were obtained after 16 h of incubation at 200 rpm and 30 ºC in YPD for *Candida* and 37 ºC in Tryptic Soy Broth (TSB) (Scharlab S.L.) or LB broth for bacterial strains.

Proximity assays

Overnight cultures of *C. albicans* and *S. aureus* were centrifuged at 4000 rpm (Labnet Spectrafuge™ 6C) for 5 min and washed twice with Phosphate Buffer Saline 1X (PBS) (Fisher Scientific S.L.). Suspensions with a final optical density of λ = 550 nm (OD_{550}) of 0.1 for yeast and 0.005 for bacteria (~$1x10^6$ CFUs/mL of both microorganisms) were prepared in PBS. Then, a 5 µl drop of each suspension was deposited in two parallel columns on YPD

agar in a manner where the distance between both microorganisms drops increased progressively (Ca – Sa). In total, six different distances were tested: P1= 1 cm, P2= 1.5 cm, P3= 2 cm, P4= 3 cm, P5= 4 cm, and P6= 5 cm. Petri dishes were incubated at 37 °C for 9 days, and colony growth were recorded by imaging with the colony counter ProtoCOL 3 (Synbiosis). All images were processed with ImageJ software. Controls were created by facing drops from the same microorganism (Sa – Sa and Ca – Ca). Experiments were conducted thrice with 3 technical replicates each time. The same procedure was followed using YPD agar with Bromocresol purple at 0.08 mg/ml, denoted as YPD + BP, and YPD agar prepared with low D-glucose content (0.2 %), referred as YPLD.

Finally, we used a slightly modified proximity assay to confirm the pH influence on *S. aureus* colonies. First, a 5 µl drop from an *S. aureus* suspension was deposited on the agar in each corresponding position, leaving the facing positions empty. From day 1 to day 3, a 10 µl drop of a solution of NaOH 2M was applied in the morning and afternoon to the facing positions. On day 4, the quantity of the drop was increased to 15 µl, and on day 6, to 20 µl. *S. aureus* responses were monitored until day 7. Control plates followed the same procedure but with addition of PBS.

To confirm the specificity of the observed interactions between *C. albicans* and *S. aureus*, additional proximity assays were conducted using both microorganisms against different species (*S. epidermidis*, *S. mutans*, *E. coli*, *E. faecalis* and *C. parapsilosis*). Required controls were also included.

Virulence assessment of *S. aureus* colony variants

Differences in the virulence of the obtained colonies of *S. aureus* growing in the different positions of the proximity assay with *C. albicans* were evaluated using the animal model *G. mellonella.* Maintenance and injection of *G. mellonella* larvae were carried out as previously reported by our laboratory (33).

Six different colonies of *S. aureus* from the proximity assays with *C. albicans* (Ca – Sa) were obtained after 10 days of incubation. Control colonies were obtained from control plates of *S. aureus* – *S. aureus* (Sa – Sa) after 10 days and 1 day of incubation. Cells were recovered with a pipette tip, resuspended in PBS until an OD_{550}= 1.8, and injected into the hemocoel of eight larvae using a 26-gauge microsyringe (Hamilton). PBS-treated larvae were included as control. The experiment was conducted three times, and larvae were

monitored for a total of 48 h post-injection with intervals of 2h from 15 h-25 h and 40-48 h.

At the same time, 100 µl of *S. aureus* cells suspensions were centrifugated (4000 rpm x 1 min) and resuspended in a solution 1:10 of the resazurin-based reagent PrestoBlue in TSB media. After 30 min at 37°C in the dark, the metabolic activity of the colonies was measured by fluorescence (λExc= 535 nm and λem=635 nm) and OD_{570} in a SPARK Multimode microplate reader. The remaining volume of cells suspensions was mixed with 500 mL of the stabilization solution RNAlater (Invitrogen) and frozen at -20 °C until further processing.

Characterization of gene expression of *S. aureus* colony variants

Cells suspensions of *S. aureus* colonies 1-5 obtained in a proximity assay with *C. albicans* (Ca – Sa) were used for RNA extraction using the GeneJET RNA Purfication Kit (Thermo Fisher Scientific). RNA obtained was treated with 10x TURBO DNase (Life technologies). DNA contamination was discarded by PCR amplification of the 16S rRNA housekeeping gene. RNA quantification was performed on a NanoDrop 1000 Spectrophotometer (Thermo Fisher Scientific). Reverse transcription of RNA was performed by mixing the Maxima Reverse Transcriptase (Thermo Fisher Scientific) with Random Hexamer primers (Thermo Fisher Scientific) according to the manufacturer's instructions. The obtained cDNA was stored at -20 °C until use.

Quantitative real-time PCR (qRT-PCR) was performed with the PowerUp SYBR Green Master Mix (Applied Biosystems) in a StepOnePlus™ Real-Time PCR System (Applied Biosystems) according to the manufacturer's protocol. The sequences of primers used for gene amplification can be consulted at Vaudaux et al., 2002 (34). Relative expression of *RNAIII*, *agrA* and *sarA* genes were calculated using the values from control colony 8.

Reversion test of *S. aureus* colony variants

A small inoculum of each colony of *S. aureus* were taken at the end of a proximity assay (Ca – Sa) with a pipette tip and plated on a new YPD plate. Same procedure was performed with control colonies (Sa – Sa). After 24 h of incubation, the growth of the colonies was evaluated.

Statistical analysis

All data were statistically analyzed using GraphPad Prism version 10.00 (GraphPad Software, USA). Comparison of means among groups was performed by One-way ANOVA tests with a Šídák's multiple comparisons test. Comparison of Kaplan-Meier survival curves were made by Log-rank tests. A *p*-value <0.05 was considered statistically significant.

Acknowledgments

We thank Dr Jesus Guinea Ortega from the Department of Clinical Microbiology and Infectious Diseases, Hospital General Universitario Gregorio Marañón, Madrid, Spain, for the generous gift of the *Candida albicans* 10045727 and *Candida parapsilosis* 11103595 isolates used in this study.

This study was partially supported by grants PID2021-125801OB-100, PLEC2022-009356 and PDC2022-133577-I00 funded by MCIN/AEI/ 10.13039/501100011033 and "ERDF A way of making Europe", the CERCA programme and *AGAUR-Generalitat de Catalunya* (2021SGR01545), the European Regional Development Fund (FEDER) and Catalan Cystic Fibrosis association. The project that gave rise to these results received the support of a fellowship from "la Caixa" Foundation (ID 100010434). The fellowship code is "LCF/BQ/DI20/11780040".

Funding sources were not involved in the research conduction or article preparation.

Declarations

Conflict of Interest: All authors declare that they have no conflict of interest.

Data availability: The datasets generated during and/or analysed during the current study are available from the corresponding author on reasonable request.

References

1. Todd OA, Peters BM. 2019. *Candida albicans* and *Staphylococcus aureus* pathogenicity and polymicrobial interactions: Lessons beyond Koch's postulates. *J Fungi* 5:81.
2. Carolus H, Van Dyck K, Van Dijck P. 2019. *Candida albicans* and *Staphylococcus* Species: A threatening twosome. *Front Microbiol* 10:2162.
3. Todd OA, Fidel PL, Jr., Harro JM, Hilliard JJ, Tkaczyk C, Sellman BR, Noverr MC, Peters BM. 2019. *Candida albicans* augments *Staphylococcus aureus* virulence by engaging the Staphylococcal *agr* quorum sensing system. *mBio* 10:e00910-19.
4. Kong EF, Tsui C, Kucharíková S, Andes D, Van Dijck P, Jabra-Rizk MA. 2016. Commensal protection of *Staphylococcus aureus* against antimicrobials by *Candida albicans* biofilm matrix. *mBio* 7:e01365-16.
5. Kean R, Rajendran R, Haggarty J, Townsend EM, Short B, Burgess KE, Lang S, Millington O, Mackay WG, Williams C, Ramage G. 2017. *Candida albicans* mycofilms support *Staphylococcus aureus* colonization and enhances miconazole resistance in dual-species interactions. *Front Microbiol* 8:244638.
6. Lin YJ, Alsad L, Vogel F, Koppar S, Nevarez L, Auguste F, Seymour J, Syed A, Christoph K, Loomis JS. 2013. Interactions between *Candida albicans* and *Staphylococcus aureus* within mixed species biofilms. *BIOS* 84:30-39.
7. Eichelberger KR, Cassat JE. 2021. Metabolic adaptations during *Staphylococcus aureus* and *Candida albicans* co-infection. *Front Immunol* 12:797550.
8. Peters BM, Jabra-Rizk MA, O'May GA, Costerton JW, Shirtliff ME. 2012. Polymicrobial interactions: impact on pathogenesis and human disease. *Clin Microbiol Rev* 25:193-213.
9. Carlson E. 1982. Synergistic effect of *Candida albicans* and *Staphylococcus aureus* on mouse mortality. *Infect Immun* 38:921-924.
10. Sheehan G, Tully L, Kavanagh KA. 2020. *Candida albicans* increases the pathogenicity of *Staphylococcus aureus* during polymicrobial infection of *Galleria mellonella* larvae. *Microbiol* 166:375-385.
11. Wu Y-M, Huang P-Y, Cheng Y-C, Lee C-H, Hsu M-C, Lu J-J, Wang S-H. 2021. Enhanced virulence of *Candida albicans* by *Staphylococcus aureus*: Evidence in clinical bloodstream infections and infected zebrafish embryos. *J Fungi* 7:1099.
12. Saikat P, Olivia AT, Kara RE, Christine T, Bret RS, Mairi CN, James EC, Paul L Fidel, Jr., Brian MP. 2024. A fungal metabolic regulator underlies infectious synergism during *Candida albicans-Staphyloccocus aureus* intra-abdominal co-infection. *bioRxiv* 2024.02:15.580531.
13. Todd OA, Noverr MC, Peters BM. 2019. *Candida albicans I*mpacts *Staphylococcus aureus* alpha-toxin production via extracellular alkalinization. *mSphere* 4:10.1128.
14. Regassa LB, Betley MJ. 1992. Alkaline pH decreases expression of the accessory gene regulator (*agr*) in *Staphylococcus aureus*. *J Bacteriol* 174:5095-5100.
15. Regassa LB, Novick RP, Betley MJ. 1992. Glucose and nonmaintained pH decrease expression of the accessory gene regulator (*agr*) in *Staphylococcus aureus*. *Infect Immun* 60:3381-3388.
16. Vylkova S, Lorenz MC. 2014. Modulation of phagosomal pH by *Candida albicans* promotes hyphal morphogenesis and requires Stp2p, a regulator of amino acid transport. *PLOS Pathog* 10:e1003995.
17. Jenul C, Horswill AR. 2019. Regulation of *Staphylococcus aureus* Virulence. *Microbiol Spectr* 7:10.1128.
18. Richardson AR. 2019. Virulence and Metabolism. *Microbiol Spectr* 7:10.1128.
19. Hu Y, Niu Y, Ye X, Zhu C, Tong T, Zhou Y, Zhou X, Cheng L, Ren B. 2021. *Staphylococcus aureus* synergized with *Candida albicans* to increase the pathogenesis and drug resistance in cutaneous abscess and peritonitis murine models. *Pathogens* 10:1036.
20. Vila T, Kong EF, Montelongo-Jauregui D, Van Dijck P, Shetty AC, McCracken C, Bruno VM, Jabra-Rizk MA. 2021. Therapeutic implications of *C. albicans-S. aureus* mixed biofilm in a murine subcutaneous catheter model of polymicrobial infection. *Virulence* 12:835-851.
21. Wijnants S, Vreys J, Van Dijck P. 2022. Interesting antifungal drug targets in the central metabolism of *Candida albicans*. *Trends Pharmacol Sci* 43:69-79.
22. Miramón P, Lorenz MC. 2017. A feast for *Candida*: Metabolic plasticity confers an edge for virulence. *PLOS Pathog* 13:e1006144.

23. Sandai D, Yin Z, Selway L, Stead D, Walker J, Leach Michelle D, Bohovych I, Ene Iuliana V, Kastora S, Budge S, Munro Carol A, Odds Frank C, Gow Neil AR, Brown Alistair JP. 2012. The Evolutionary rewiring of ubiquitination targets has reprogrammed the regulation of carbon assimilation in the pathogenic yeast *Candida albicans*. *mBio* 3:10.1128.
24. Lorenz MC. 2013. Carbon catabolite control in *Candida albicans*: New wrinkles in metabolism. *mBio* 4:10.1128.
25. Williams RB, Lorenz MC. 2020. Multiple alternative carbon pathways combine to promote *Candida albicans* stress resistance, immune interactions, and virulence. *mBio* 11:10.1128.
26. Bayot J, Martin C, Chevreux G, Camadro J-M, Auchère F. 2023. The adaptive response to alternative carbon sources in the pathogen *Candida albicans* involves a remodeling of thiol- and glutathione-dependent redox status. *Biochem J* 480:197-217.
27. Danhof Heather A, Vylkova S, Vesely Elisa M, Ford Amy E, Gonzalez-Garay M, Lorenz Michael C. 2016. Robust extracellular pH modulation by *Candida albicans* during growth in carboxylic acids. *mBio* 7:10.1128.
28. Naseem S, Min K, Spitzer D, Gardin J, Konopka JB. 2017. Regulation of Hyphal Growth and N-Acetylglucosamine Catabolism by Two Transcription Factors in *Candida albicans*. *Genet* 206:299.
29. Vesely EM, Williams RB, Konopka JB, Lorenz MC. 2017. N-Acetylglucosamine metabolism promotes survival of *Candida albicans* in the phagosome. *mSphere* 2:10.1128.
30. Komalapriya C, Kaloriti D, Tillmann AT, Yin Z, Herrero-de-Dios C, Jacobsen MD, Belmonte RC, Cameron G, Haynes K, Grebogi C, de Moura APS, Gow NAR, Thiel M, Quinn J, Brown AJP, Romano MC. 2015. Integrative model of oxidative stress adaptation in the fungal pathogen *Candida albicans*. *PLOS ONE* 10:e0137750.
31. Wang Y, Cao Y-Y, Jia X-M, Cao Y-B, Gao P-H, Fu X-P, Ying K, Chen W-S, Jiang Y-Y. 2006. Cap1p is involved in multiple pathways of oxidative stress response in *Candida albicans. Free Radic Biol Med* 40:1201-1209.
32. Marcos-Zambrano LJ, Escribano P, Bouza E, Guinea J. 2014. Production of biofilm by *Candida* and non-*Candida spp.* isolates causing fungemia: Comparison of biomass production and metabolic activity and development of cut-off points. *Int J Med Microbiol* 304:1192-1198.
33. Moya-Andérico L, Admella J, Torrents E. 2021. A clearing protocol for *Galleria mellonella* larvae: Visualization of internalized fluorescent nanoparticles. *New Biotechnol* 60:20-26.
34. Vaudaux P, Francois P, Bisognano C, Kelley William L, Lew Daniel P, Schrenzel J, Proctor Richard A, McNamara Peter J, Peters G, Von Eiff C. 2002. Increased expression of clumping factor and fibronectin-binding proteins by hemB mutants of *Staphylococcus aureus* expressing small colony variant phenotypes. *Infect Immun* 70:5428-5437.

Material Suplementario

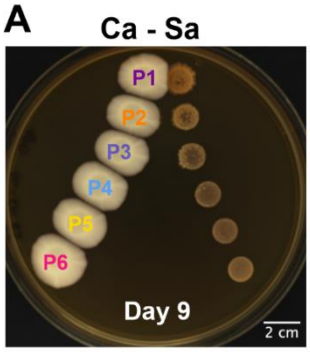

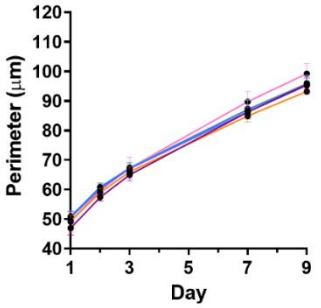

Position	Starting Population (Y0)	Maximum population (YM)
P1	40.28	103.1
P2	42.72	99.65
P3*	44.3	103.5
P4*	44.65	104.2
P5*	44.15	103.7
P6*	42.27	107.9

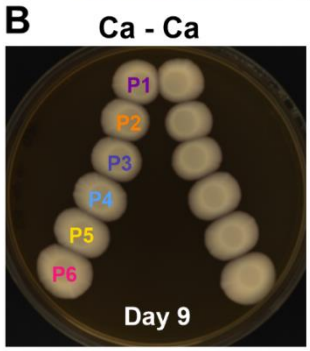

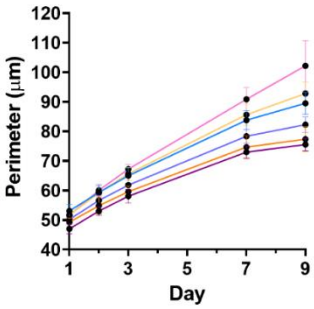

Position	Starting Population (Y0)	Maximum population (YM)
P1	40.49	79.80
P2	43.04	82.61
P3*	43.83	88.49
P4*	44.81	100.3
P5*	45.35	103.7
P6*	45.81	124.6

FIG S1 Colony size of *C. albicans* when growing near to A) *S. aureus* or B) itself (control). Growth was monitored at six different distances between colonies (P1= 1 cm, P2= 1.5 cm, P3= 2 cm, P4= 3 cm, P5= 4 cm and P6= 5 cm) over 9 days with measurements taken on days 1, 2, 3, 5 and 9. Parameters Y0 and YM were calculated from a logistic growth fit of the data, followed by calculation of statistically differences among curves compared with P1 (*=*p*-value<0.05). Image processing and perimeter measurements were performed with ImageJ. Data are representative of three experiments, and error bars represent standard deviation.

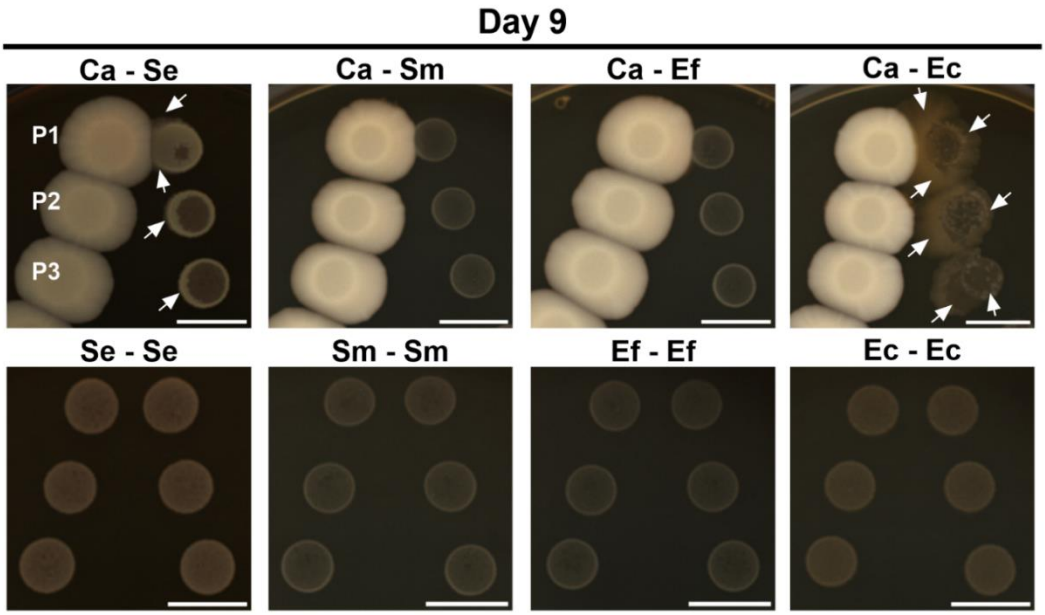

FIG S2 Proximity assay of *C. albicans* (Ca) with other bacteria. Zoomed images of *C. albicans* colonies (left) with *S. epidermidis* (Ca – Se), *S. mutans* (Ca – Sm), *E. faecalis* (Ca – Ef) and *E. coli* (Ca – Ec) (left) at day 9 are depicted. Controls of the growth of each bacteria growing near to itself are also shown: *S. epidermidis* (Se – Se), *S. mutans* (Sm – Sm), *E. faecalis* (Ef – Ef) and *E. coli* (Ec – Ec). Displayed images are representative of three different experiments and were processed with ImageJ software. The scale bar corresponds to 2 cm and applies to all cases. The shown distances correspond to P1= 1 cm, P2= 1.5 cm, and P3= 2 cm.

Artículo 4 (Publicación)

Died or not dyed: Assessment of viability and vitality dyes on planktonic cells and biofilms from *Candida parapsilosis*

Publicado en la revista *Journal of Fungi*

DOI: 10.3390/jof10030209

11 de marzo de 2024

Categoría Micología 2023: 1er tercil, 1er Cuartil, IF= 4.2

Betsy V. Arévalo-Jaimes[1,2] y Eduard Torrents[1,2]

[1]Grupo Infecciones Bacterianas y Terapias Antimicrobianas (BIAT), Instituto de Bioingeniería de Cataluña (IBEC), Barcelona, España.
[2]Sección de Microbiología, Departamento de Genética, Microbiología y Estadística, Facultad de Biología, Universitat de Barcelona, Barcelona, España.

Cita: Arévalo-Jaimes, B. V., & Torrents, E. (2024). Died or Not Dyed: Assessment of Viability and Vitality Dyes on Planktonic Cells and Biofilms from *Candida parapsilosis*. *J. Fungi*, 10(3), 209. DOI: 10.3390/jof10030209.

Journal of *Fungi*

MDPI

Article

Died or Not Dyed: Assessment of Viability and Vitality Dyes on Planktonic Cells and Biofilms from *Candida parapsilosis*

Betsy Verónica Arévalo-Jaimes [1,2] and Eduard Torrents [1,2,*]

[1] Bacterial Infections and Antimicrobial Therapies Group, Institute for Bioengineering of Catalonia (IBEC), 08028 Barcelona, Spain; varevalo@ibecbarcelona.eu
[2] Microbiology Section, Department of Genetics, Microbiology and Statistics, Faculty of Biology, University of Barcelona, 08028 Barcelona, Spain
* Correspondence: etorrents@ibecbarcelona.eu; Tel.: +34-934-034-756

Abstract: Viability and vitality assays play a crucial role in assessing the effectiveness of novel therapeutic approaches, with stain-based methods providing speed and objectivity. However, their application in yeast research lacks consensus. This study aimed to assess the performance of four common dyes on *C. parapsilosis* planktonic cells as well as sessile cells that form well-structured biofilms (treated and not treated with amphotericin B). Viability assessment employed Syto-9 (S9), thiazole orange (TO), and propidium iodide (PI). Metabolic activity was determined using fluorescein diacetate (FDA) and FUN-1. Calcofluor white (CW) served as the cell visualization control. Viability/vitality percentage of treated samples were calculated for each dye from confocal images and compared to crystal violet and PrestoBlue results. Heterogeneity in fluorescence intensity and permeability issues were observed with S9, TO, and FDA in planktonic cells and biofilms. This variability, influenced by cell morphology, resulted in dye-dependent viability/vitality percentages. Notably, PI and FUN-1 exhibited robust *C. parapsilosis* staining, with FUN-1 vitality results comparable to PrestoBlue. Our finding emphasizes the importance of evaluating dye permeability in yeast species beforehand, incorporating cell visualization controls. An improper dye selection may lead to misinterpreting treatment efficacy.

Keywords: biofilms; microscopy; imaging; amphotericin B; stain-based methods; yeast staining; fluorescence; live and dead

Citation: Arévalo-Jaimes, B.V.; Torrents, E. Died or Not Dyed: Assessment of Viability and Vitality Dyes on Planktonic Cells and Biofilms from *Candida parapsilosis*. *J. Fungi* **2024**, *10*, 209. https://doi.org/10.3390/jof10030209

Academic Editors: Célia F. Rodrigues and Lucia Černáková

Received: 8 February 2024
Revised: 7 March 2024
Accepted: 8 March 2024
Published: 11 March 2024

1. Introduction

Fungal diseases caused by yeasts present a significant threat in the field of medicine [1]. The genera *Trichosporon*, *Rhodotorula*, and *Malassezia* are among the several yeasts responsible for superficial and invasive human infections [1]. *Candida* spp. are responsible for the greatest number of fungal infections caused by fungal pathogens [1,2]. *Candida parapsilosis*, in particular, has been identified as the causative agent in approximately 25% of invasive *Candida* infections in several European countries [3]. Its increasing prevalence, coupled with the emergence of antifungal resistance and its ability to form biofilms, highlights the need for developing novel treatment strategies.

In this context, cell viability assays play a crucial role in evaluating treatment efficacy. Determining the percentage of live cells within a population can be achieved using various techniques, with stain-based methods offering speed and objectivity by relying on the dye's permeability into the cell membrane. These methods also help overcome the challenge of viable but non-culturable cells [4]. However, in certain scenarios, the impact of a treatment cannot be solely assessed by the proportion of live/dead cells. In such cases, the use of dyes that evaluate physiological/metabolic capabilities, known as cell vitality dyes, becomes essential [4].

Currently, there are numerous stain-based methods available; however, there is no consensus or established guidelines for their applications in yeast research, particularly

J. Fungi **2024**, *10*, 209

concerning *Candida* spp. Therefore, the aim of this study was to evaluate the performance and utility of four commonly used viability and vitality dyes on *C. parapsilosis* planktonic cells and biofilms treated with Amphotericin B (AmB). Significantly different cell staining was observed in *C. parapsilosis* 11103595 depending on the dye used, emphasizing the importance of carefully selecting and using stain-based methods for yeast studies, particularly when evaluating treatment efficacy.

2. Results

2.1. Viability and Vitality Staining of C. parapsilosis 11103595 Overnight Cultures

In this study, we employed the well-established stain calcofluor white (CW) as a general dye for yeast cell imaging, which in some cases allowed us to identify permeability issues for yeast staining. First, cells from overnight cultures of *C. parapsilosis* 11103595 were stained with the combinations Syto 9 (S9) + propidium iodide (PI) and thiazole orange (TO) + propidium iodide for the viability assessment, and fluorescein diacetate (FDA) and FUN-1 for the vitality assessment (Figure 1), as described in Section 4.4.

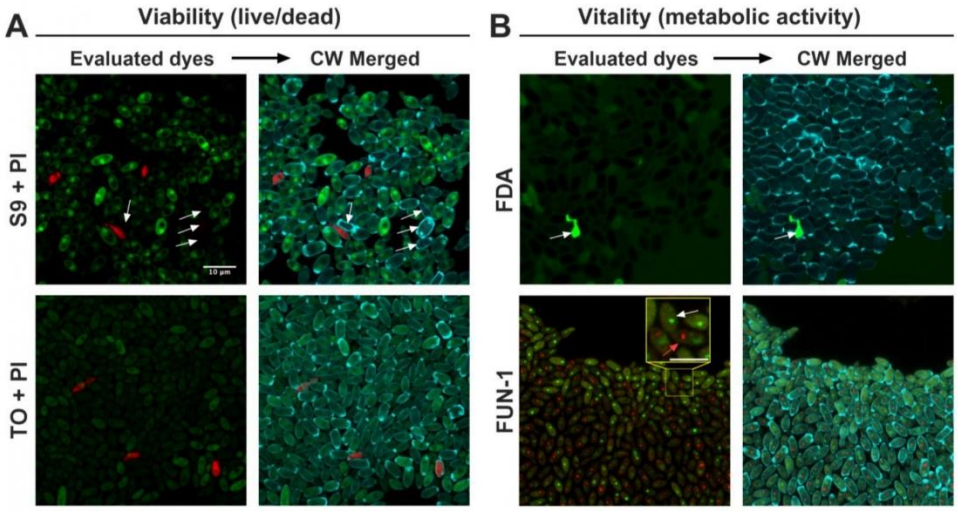

Figure 1. Viability and vitality staining of *C. parapsilosis* 11103595 overnight cultures. (**A**) Viability assessment of *C. parapsilosis* 11103595 planktonic cells using S9 (green) + PI (red) and TO (green) + PI (red) staining. Dyes were compared with CW (blue) merged image for cell visualization control. White arrows in the S9 + PI row highlight some of the cells that were not stained with S9 but were visible with CW. (**B**) Vitality evaluation using FDA (green) and FUN-1 (green and red) staining. CW (blue) merged image was used as a cell visualization control. White arrows in the FDA row indicate high intensity only in a dead cell. White arrow in the zoomed in image of the FUN-1 row shows a green non-metabolically active cell, while the red arrow shows a cell with red cylindrical intravacuolar structures (CIVSs), indicating metabolic activity. Confocal images were processed using ImageJ v1.54f. The scale bar of 10 µm is consistent for all cases, except in the FUN-1 zoomed-in image where it represents a 5 µm length. Images were taken at 100×. S9 = Syto9, PI = propidium iodide, TO = thiazole orange, CW = calcofluor white, FDA = fluorescein diacetate.

Observations from the viability assessment revealed that the S9 dye was unevenly incorporated into the yeasts, with some cells exhibiting bright staining, while others remained unstained (Figure 1. S9 + PI. See white arrows). Similarly, the TO dye demonstrated irregular staining, with most cells displaying only faint green dye, indicating poor permeability of this dye. The use of PI as an indicator of dead cells (cells with a damaged

membrane) yielded consistent results across both dye combinations, with good staining intensity in all cases.

Regarding the metabolic assessment (vitality), FDA staining showed a high background signal, faint staining in the dyed cells, and intense fluorescence within a dead cell (Figure 1. FDA. See white arrow), suggesting minimal metabolic activity. In contrast, FUN-1 staining revealed red cylindrical intravacuolar structures (CIVSs) in most cells, indicating the presence of metabolic activity (Figure 1. FUN-1). Moreover, FUN-1 displayed good permeability inside the cells, with each cell containing green fluorescence (see white arrow pointing to a metabolically inactive cell in Figure 1. FUN-1) or green/red fluorescence (see red arrow pointing to a metabolically active cell with CIVSs in Figure 1. FUN-1).

Control staining with CW allowed for cell visualization regardless of their respective viability and vitality states. Moreover, since this dye is specific for cell wall chitin, alterations in cell morphology after treatments could also be evaluated [5,6].

2.2. Total Biomass and Metabolic Activity of *C. parapsilosis* 11103595 Biofilms Treated with AmB

C. parapsilosis 11103595 biofilms formed on silicon coupons for 24 h were treated with AmB at 2.5 µg/mL (MIC_{50} × 10) for 20 h, following the procedure outlined in Section 4.3. Crystal violet assay and PrestoBlue were used, respectively, for total biomass (cell biomass and extracellular matrix) and metabolic activity quantification (Figure 2) to obtain a reference value of treatment effect on biofilms using conventional techniques [7,8]. Our results demonstrate a significant reduction in both total biomass (Figure 2A) and metabolic activity (Figure 2B) by ~23% and ~39%, respectively, compared to the control after a single dose of AmB treatment.

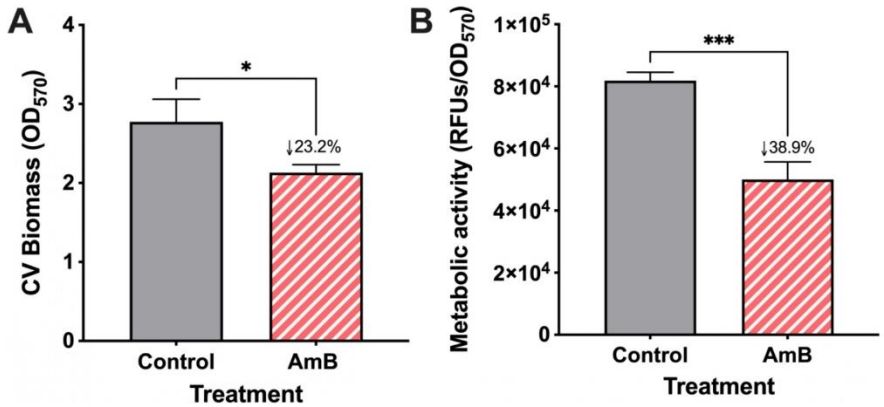

Figure 2. Total biomass and metabolic activity of *C. parapsilosis* 11103595 biofilms treated with amphotericin B (AmB). (**A**) Total biomass quantification (cell biomass and extracellular matrix) with crystal violet (CV) assay and (**B**) metabolic activity evaluation by PrestoBlue assay after 20 h treatment with 2.5 µg/mL of AmB. Biofilm results experiments were conducted in triplicate. Numbers after the symbol ↓ indicate the percentage of decrease in the mean value with respect to the control. Data are represented as mean ± standard deviation. Asterisks indicate statistically significant differences versus control in an unpaired *t*-test (*: p-value < 0.05, ***: p-value < 0.001). RFUs = relative fluorescence units.

2.3. Viability and Vitality Staining of *C. parapsilosis* 11103595 Biofilms Treated with AmB

Then, we evaluated the efficacy of AmB treatment on *C. parapsilosis* 11103595 biofilms using stain-based methods under the conditions described (see Section 4.4). For each staining condition, we quantified the cell biomass from the confocal images using COMSTAT 2 and compared the mean values of the treated and control biofilms (Figures 3 and 4). Then,

J. Fungi **2024**, *10*, 209

to assess the performance of the viability and vitality dyes, we used the data derived from the CW dye, our cell visualization control, and calculated the corrected biomass.

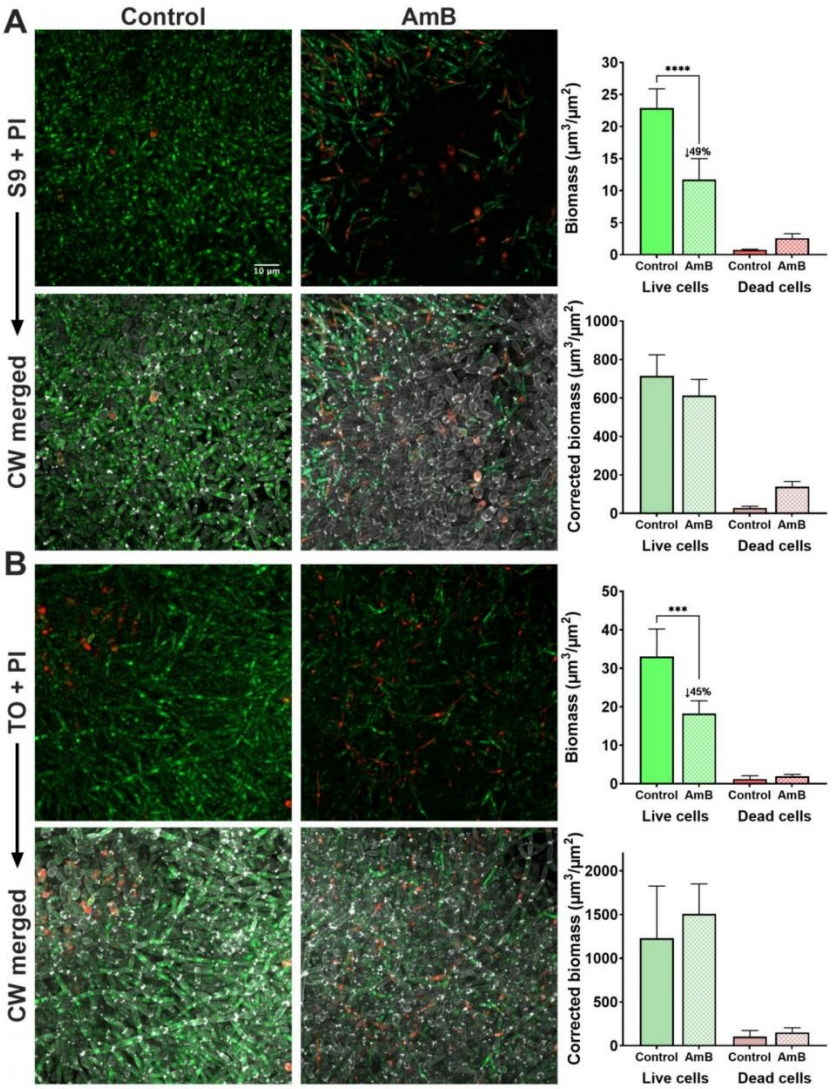

Figure 3. Viability staining of *C. parapsilosis* 11103595 biofilms treated with amphotericin B (AmB). (**A**) Viability assessment using S9 (green live cells) + PI (red dead cells) dye with the respective biomass quantification. (**B**) Viability assessment using TO (green live cells) + PI (red dead cells) dyes with the respective biomass quantification. Each dye combination was compared with the CW (gray) merged image and the respective biomass correction. Biomass quantifications were performed from images at a 10× magnification with the plugin COMSTA2 from ImageJ software v1.54f. Data are represented as mean ± standard deviation from $n \geq 3$ replicates. Asterisks indicate statistically significant differences versus control (***: p-value < 0.001; ****: p-value < 0.0001). Numbers after the

J. Fungi **2024**, *10*, 209

symbol ↓ indicate the percentage of decrease in the mean value with respect to the control. Z-stack of biofilm top layers from confocal images at a 63× magnification were created using ImageJ v1.54f. The scale bar of 10 µm is consistent for all cases. S9 = Syto9, PI = propidium iodide, TO = thiazole orange, CW = calcofluor white.

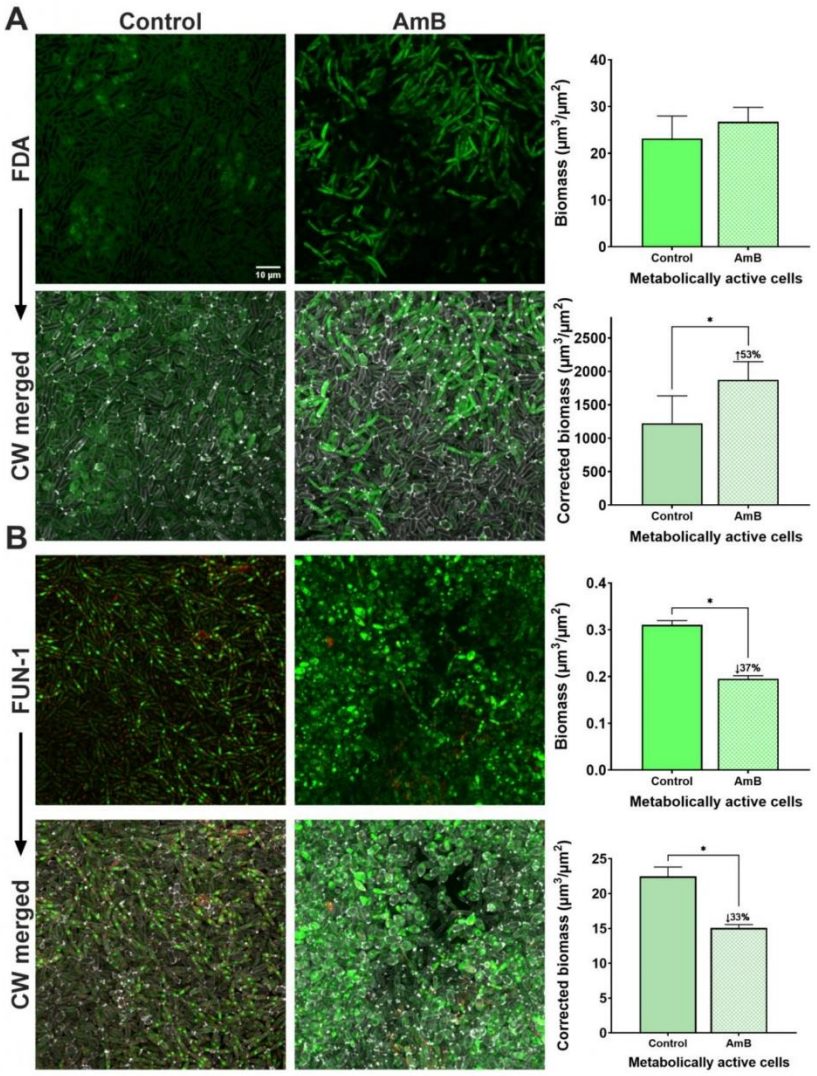

Figure 4. Vitality staining of *C. parapsilosis* 11103595 biofilms treated with amphotericin B (AmB). (**A**) Vitality assessment using FDA (green metabolically active cells) dye with the respective biomass quantification. (**B**) Vitality assessment using FUN-1 (green metabolically unactive cells and green/red metabolically active cells) with the respective biomass quantification. Each dye was compared with the CW (gray) merged image and the respective biomass correction. Biomass quantifications were performed from images at a 10× magnification with the plugin COMSTA2 from ImageJ software v1.54f.

Data are represented as mean ± standard deviation from n ≥ 3 replicates. Asterisks indicate statistically significant differences versus control (*: p-value < 0.05). Numbers after the symbol ↑ indicate the percentage of increase in the mean value with respect to the control, while numbers after the symbol ↓ indicate the percentage of decrease in the mean value with respect to the control. Z-stack of biofilm top layers from confocal images at a 63× magnification were created using ImageJ v1.54f. The scale bar of 10 µm is consistent for all cases. CW = calcofluor white, FDA = fluorescein diacetate.

Regarding the viability dyes (Figure 3), we can see that S9 has a poor performance to assess treatment efficacy in *C. parapsilosis* 11103595 biofilms. The S9 + PI row of Figure 3A shows a very significant (p-value < 0.0001) reduction (49%) in the live cells biomass in treated samples compared to the control. Notably, most of the stained cells in treated samples had a pseudohyphae morphology. However, once the images are contrasted with the CW staining, we can see these results are not real because unstained cells become visible in the AmB-treated image. Consequently, when biomass is corrected with the values of CW staining, we did not obtain a statistically significant difference in the live cells of treated samples compared to the control.

Similar results were obtained from the TO dye (Figure 3B). The TO + PI row indicates a reduction of 45% in the biomass of live cells (p-value < 0.001) from treated samples compared to the control. However, no difference is observed when the live biomass is corrected using the quantification of the CW dye. On the other hand, PI exhibited bright fluorescence and good permeability in both the control and treated samples, regardless of the viability dye used in combination. Additionally, an increase in the biomass of dead cells was observed in the treated samples compared to the control samples (3.4-fold in the S9 + PI condition and 1.6-fold in the TO + PI condition), as expected after the antifungal action. Although not statistically significant, this increase remained after the correction in biomass with the CW dye values (5-fold in the S9 + PI condition and 1.5-fold in the TO + PI condition).

Despite the unsatisfactory performance of the evaluated viability dyes to assess treatment efficacy in *C. parapsilosis* 11103595 biofilms, we calculated the viability percentage of treated and non-treated biofilms using the uncorrected biomass data from S9 + PI and TO + PI conditions. Then, we calculated the change in the viability percentage obtained after treatment, aiming to see the erroneous conclusions that would be derived from the data. As it can be seen in Table 1, S9 reports a reduction of 15% in the viability percentage of *C. parapsilosis* 11103595 biofilms treated with 2.5 µg/mL of AmB, while TO indicates a change 2.5-fold lower (6%).

Table 1. Viability and vitality evaluations of *C. parapsilosis* 11103595 biofilms by COMSTAT 2 quantification.

Evaluated Dye	Non-Treated Biofilms	AmB-Treated Biofilms	Change (%)
%Viability (live cells biomass/(live cells biomass + dead biomass))			
S9–PI	96.6 ± 0.3	81.9 ± 2.9	−15.2 ± 2.8
TO–PI	94.9 ± 3.7	89.1 ± 1.4	−6 ± 2.6
Metabolically active biomass ($\mu m^3/\mu m^2$)			
FDA	23.1 ± 4.8	26.8 ± 3.1	+17.1 ± 10.5
FUN-1 [1]	31.1 ± 0.9	19.5 ± 0.6	−37.1 ± 1.1

[1] Red/green ratio. Data corresponds to mean ± standard deviation from 3 replicates; AmB = amphotericin B; % = percentage; S9 = Syto9; TO = thiazole orange; PI = propidium iodide; FDA = fluorescein diacetate; CW = calcofluor white.

Next, we evaluated changes in the biomass of metabolically active cells in *C. parapsilosis* 11103595 biofilms treated with AmB using vitality dyes (Figure 4). We found that control samples stained with FDA exhibited a high background signal and only a few stained cells (Figure 4A). This noise led to an erroneous elevated biomass value of metabolically active cells (23 ± 5 $\mu m^3/\mu m^2$). In AmB-treated samples, cells (mostly elongated pseudohyphae) displayed good intensity of staining. The obtained biomass of metabolically active cells in the treated sample was 27 ± 3 $\mu m^3/\mu m^2$; however, no comparison could be made

due to the lack of a good control. Moreover, the high background staining of the control also influenced the outcome of the biomass correction using the CW data. Therefore, the obtention of reliable data regarding the change in metabolic activity in *C. parapsilosis* 11103595 biofilms treated with AmB using FDA dye was impossible in our study.

In the case of FUN-1, we found red CIVSs in most cells of the control sample, accounting for a biomass of 15.8 ± 2 $\mu m^3/\mu m^2$ (Figure 4B). This value was reduced to 10 ± 0.4 $\mu m^3/\mu m^2$ in samples treated with AmB. Once we calculated the biomass of cells metabolically active in each condition (cell biomass from red channel/cell biomass from green channel), we saw a reduction of 37% in treated samples compared to the control. Moreover, when the data were corrected using CW quantification data, this difference was maintained (33%).

Finally, we also calculated the vitality percentages of treated and non-treated biofilms using the uncorrected biomass data from FDA and FUN-1 dyes to obtain the change in vitality percentages after treatment (Table 1). In this way, we could see how FDA data lead to the erroneous conclusion of a 17% increase in the metabolic activity of cells from *C. parapsilosis* 11103595 biofilms after treatment with 2.5 µg/mL of AmB. In contrast, FUN-1 data presented a 37% reduction in the metabolic activity of the biofilm cells, a value very similar to the result obtained by the PrestoBlue assay (Figure 2B).

Notably, the presence of filamentation in cells growing in biofilms allowed us to observe differences in dye penetration based on cell morphology that were not appreciable in the planktonic cultures. Overall, when S9 and TO were employed, cytoplasmic staining was more associated with long pseudohyphae. Instead, localized staining, presumably of nucleic acids, observed as multiple points, was associated with short pseudohyphae and blastospores (Figure 3).

3. Discussion

Dyes used for assessing viability rely on permeability differences between live and dead cells, which are indicative of membrane integrity [4]. However, before implementing a dye, it is crucial to evaluate and standardize its performance in the microorganism of interest to avoid the misinterpretation of treatment efficacy in a real-world context. In this study, permeability differences not associated with cell viability/vitality were observed when using S9, TO, and FDA dyes for *C. parapsilosis* 11103595 staining.

We decided to further test the dyes' performances in cells growing in biofilms. *C. parapsilosis* is known for its ability to adhere and form biofilms on medical-related devices [9]. Biofilms formed by *C. parapsilosis* are aggregates of blastospores and/or pseudohyphae embedded in an extracellular matrix that protect the cells from external aggressions [9]. Thus, biofilm formation is associated with a higher resistance to antifungals. Considering the threat that *C. parapsilosis* represents for human health, especially for neonates [9], it becomes important to develop new therapeutic approaches. However, this progress need to be accompanied by established methods that allow testing treatment efficacy.

Most studies that evaluate the efficacy of novel potential antibiofilm agents use standard techniques (crystal violet assay, CFU plate counting, tetrazolium salts, or resazurin-based methods) accompanied by a visualization method for the confirmation and complementation of results. Direct imaging of biofilms allows the assessment of structural changes after treatment, while fluorescence staining permits selective labeling, providing additional information regarding biofilm composition and the viability/vitality of the microorganisms [10]. However, the fast and accurate visualization of these methods provide them with the potential to be used on their own as alternatives of conventional methods. This is the case for the whole slide imaging technique, a promising tool for the diagnosis and antifungal susceptibility evaluation of *Candida* spp. both in planktonic and biofilm states [11–13].

Regarding the results obtained in this study, it is important to mention that the performance of the evaluated dyes was similar in planktonic and biofilm cells. This suggest that the extracellular matrix present in the biofilm does not have a significant influence on

dye permeability inside the cells. Although, this means that the problems observed with S9, TO, and FDA in the overnight cultures were also present in biofilms. However, S9 and FDA are commonly used in studies of antimicrobial efficacy on the planktonic and biofilm cells of *Candida* spp. without the use of cell visualization controls [14–19]. Moreover, TO is used in cell viability analysis by flow cytometry [20,21], where it is easier to miss the presence of permeability issues. Unstained cells after S9 and TO staining become evident after AmB treatment of biofilms. This interference with dye permeability could be the result of yeast adaptations to antimicrobial treatments as reported previously [22–24]. For instance, the modulation of sterol composition has been proposed as a mechanism of resistance against AmB in *Candida* spp. [9].

On the contrary, PI showed good staining intensity on planktonic and biofilm cells. Thus, we believed that using PI as an indicator of cell death (compromised membrane integrity) in combination with a total cell visualization marker, such as bright field, or a membrane/cell wall dye, could be a good alternative to evaluate antifungal activity in *C. parapsilosis*. This strategy has been successfully implemented previously by several authors on different *Candida* spp. [25–27].

In our study, the identification of permeability issues was possible thanks to the incorporation of CW as a control of cell visualization. This agrees with studies that have proven the usefulness of CW for the rapid identification of *Candida* spp. even in clinical samples [28,29]. However, it is important to carefully select the cell visualization control depending on the treatment under evaluation. For instance, CW may not be the best option when the evaluated treatment affects the cell wall or alters its composition. As an example, take the case of N-acetylcysteine that acts on the polysaccharides of the fungal cell wall or caspofungin that can stimulate the chitin synthesis of *Candida* spp., inducing changes in the cell wall structure and paradoxical growth [24,30].

On the other hand, the ability of yeasts to switch between morphologies adds another level of complexity. Variations in dye distribution inside the cell (cytoplasmatic or associated with nucleic acid binding) were observed, with a tendency of uniform staining more present in pseudohyphae than blastospores. We hypothesize that this variation can be associated with differences in the cell wall structure. Although we did not find a study that compares the cell wall composition of blastopore and pseudohyphae in *C. parapsilosis*, cell length has been associated with increasing adhesion, hydrophobicity, and high expression of mannose-rich glycoconjugates in this species [31].

Quantification using stain-based methods relies on the fact that the fluorescence intensity correlates with the amount of fluorophore present, which in turn represents the number of cell structures or cells in a sample [32]. This principle is applicated in standardized methods that evaluate treatment efficacy in a rapid manner using viability/vitality dyes and fluorescence readers. The same fundament is also employed in the bioinformatic quantification of fluorescence intensity from microscopy images. In our study, we used the latter approach to calculate cell biomass (Figures 3 and 4) and the percentages of viability or vitality of the biofilms treated with AmB for each dye (Table 1). In addition, we used the cell biomass measure obtained from the CW dye and corrected the biomass of the evaluated dyes (Figures 3 and 4).

In the case of viability dyes, both showed a reduction in the viability percentage after treatment, which was discredited once the cell biomass values were corrected by the CW measure (Figure 3). Overall, PI dye exhibited a good staining intensity in the control and treated samples, although no statistical difference was observed among them (Figure 3). The reference crystal violet technique showed a decrease of 23% in total biomass (p-value < 0.05) after the treatment of *C. parapsilosis* 11103595 biofilms with 2.5 µg/mL of AmB. However, it is important to consider that this reduction not only considers cell biomass but also extracellular matrix biomass.

On the other hand, the results obtained by the PrestoBlue assay show that the concentration of AmB used in the study has a greater impact on the metabolic activity of biofilms than on their biomass (Figure 2). However, the high background signal of FDA dye in

the control samples prevented the reliable measurement of metabolically active biomass (Figure 4A) and vitality percentage change (Table 1). The fact that cells in the treated biofilm samples exhibited good staining intensity without background noise suggest that FDA's poor performance can be associated with permeability issues. AmB is a widely used antifungal drug that affects the plasma membrane by creating pores and sequestering ergosterol, leading to increased cell permeability [33]. Therefore, we hypothesize that AmB treatment favors FDA staining by increasing cell dye uptake.

Conversely, the FUN-1 dye showed a good performance in cell staining with a vitality percentage change similar to that obtained with the PrestoBlue assay (Figures 2B and 4B). The biomass correction with the CW measure showed a reduction in metabolic activity very close to the original (33%), indicating a good reliability of the dye on its own. Our results are in agreement with the study of Cho et al. (2023), in which a good performance of FUN-1 combined with CW for the viability assessment of *C. parapsilosis* cells after treatment with tacrolimus was observed [34]. Similarly, Miranda-Cadena et al. (2021) used a commercial alternative (LIVE/DEAD yeast viability kit) composed of FUN-1 and CW to assess the fungicidal and antibiofilm activities of three phytocompounds against *Candida* spp. [35].

Different challenges are observed in the assessment of biofilm susceptibility. Although conventional methods are high throughput, these in vitro models poorly represent the in vivo situation, leading to susceptibility data that may disagree with clinical output [36]. Dynamic models allows media flow above the biofilm surface, mimicking better in vivo conditions and providing more reliable outcomes when evaluating antimicrobial compounds [37]. Several of these devices, including microfluidic platforms, are closed and depend on microscopic readings, usually performed with confocal scanning laser microscopy and fluorescent dyes [37]. In these cases, the correct dye selection becomes very important to standardize the techniques before the susceptibility testing of biofilms, because an adequate choice can help in the assessment of new antifungal/antibiofilm agents and in the development of new methods for assessing biofilm susceptibility, both being important requirements to address in the clinical setting.

In conclusion, our results highlight the importance of evaluating dye permeability in the specific species and growth mode of interest, especially when it comes to yeasts with dimorphism. The differences in fluorescence intensity observed among yeast morphologies present in biofilms suggest variations in permeability. Therefore, before utilizing stain-based methods for quantification purposes, we recommend conducting a microscopic evaluation using bright-field images or membrane/cell wall dyes as controls for cell visualization. This approach can reveal a completely different picture of the situation, as demonstrated in the case of AmB-treated biofilms stained with S9 (Figure 3A). Furthermore, we confirm the good performance of PI and FUN-1 dyes for *C. parapsilosis* 11103595 studies.

Although the findings of this article were derived from a single clinical isolate of *C. parapsilosis*, and therefore, these results may not universally apply to other yeasts, they reinforce the central message of the study: the significance of evaluating dye performance in the specific microorganism of interest before practical implementation.

4. Materials and Methods

4.1. Bacterial Strains and Growing Conditions

This study was conducted using the fungaemia clinical isolate *Candida parapsilosis* 11103595 [38]. To prevent genetic and/or epigenetic changes due to multiple passages, a fresh loopful of the strain was retrieved from a −80 °C stock each week. The recovery process was produced in Yeast Petone Dextrose (YPD) medium, which consisted of 1% yeast extract (Gibco, Carlsbad, CA, USA), 2% meat peptone (Scharlau, Sentmenat, Spain), 2% D-glucose (Fisher Scientific S.L., Madrid, Spain), and 2% of bacteriological agar (Scharlau, Sentmenat, Spain) for solidification when required. Incubation at 30 °C for 24 h was performed.

4.2. Biofilm Formation on Silicon Coupons

Overnight cultures of ~16 h at 200 rpm and 30 °C were centrifugated at 4000 rpm for 5 min and washed twice with Phosphate Buffer Saline 1× (PBS) (Fisher Scientific S.L., Madrid, Spain). The yeast suspensions were adjusted to a final optical density (λ = 550 nm (OD_{550})) of 0.15 in RPMI-1640 with L-glutamine without sodium bicarbonate (Merck Sigma-Aldrich, Madrid, Spain), supplemented with 0.2% D-glucose (referred to as RPMId) and 10% Fetal Bovine Serum (FBS) (Gibco, Carlsbad, CA, USA).

Autoclaved silicon squares (area of 1 cm^2, thickness: 1.5 mm ± 0.3 mm) (Merefsa, Sant Boi de Llobregat, Spain) were pre-treated with FBS at 37 °C overnight and washed with PBS. The silicon squares were then placed in 24-well cell culture plates (Labclinics, Barcelona, Spain) with 600 µL of the yeast suspension. Adhesion was allowed to occur for 90 min at 37 °C and 60 rpm. Unattached cells were removed by washing with PBS before transferring the silicon to a new 24-well plate containing fresh RPMId medium. The plate was then incubated under the same conditions for a total of 44 h, including growth and treatment periods.

4.3. Biofilm Total Biomass and Metabolic Activity

Biofilms formed over 24 h were treated with 2.5 µg/mL of AmB (Gibco, Carlsbad, CA, USA), which corresponds to approximately ten times the MIC_{50} value of the evaluated strain as previously determined in our laboratory (MIC_{50} = 0.25 µg/mL). After an additional 20 h of treatment, total biomass and metabolic activity were measured as described below. Biofilms treated with media alone (RPMId) were used as controls.

Biofilm total biomass was firstly quantified by staining the silicon square with 0.1% (*v*/*v*) crystal violet (Merck Life Science, Darmstadt, Germany) for 5 min, followed by distaining with 33% (*v*/*v*) acetic acid (Gibco, Carlsbad, CA, USA). The different washes and the fixation step were avoided to prevent biofilm detachment. Then, the crystal violet solution was measured by optical density at 570 nm (OD_{570}) using a Microplate Spectrophotometer Benchmark Plus (Biorad, Barcelona, Spain).

To assess metabolic activity, the total biomass from the silicon squares was resuspended in 1 mL of PBS. Each sample underwent a cycle of vortexing for 1 min, followed by ultrasonic bath treatment in a Branson 200 ultrasonic cleaner (Branson Ultrasonics, Brookfield, WI, USA) for 10 min, and another round of vortexing for 1 min. Cells were then harvested and resuspended in a solution of PrestoBlue Cell Viability Reagent (Invitrogen, Carlsbad, CA, USA) in RPMId media at a 1:10 ratio. The suspension was incubated for 3 h at 37ºC in the dark. Fluorescence (λ_{Exc} = 535 nm and λ_{em} = 615 nm) and OD_{570} were measured using a SPARK Multimode microplate reader (Tecan, Männedorf, Switzerland).

4.4. Dyes Evaluation

Four different dyes commonly used for yeast staining [16,17,20,34,39–45], two for cell viability and two for cell vitality, were selected. Additionally, the chitin dye CW (Thermo Fisher Scientific, Carlsbad, CA, USA) at 10 µM was used as the control for cell visualization.

For the viability assessment, the dyes used were S9 (Live/Dead BacLight Bacterial Viability Kit) (Thermo Fisher Scientific, Carlsbad, CA, USA) at 30 µM and TO (Yeast Live-or-Dye Fixable Live/Dead Staining Kit) (Biotium, Fremont, CA, USA) at 10 µM. These green-fluorescent dyes are membrane-permeable and can stain both live and dead cells. They were tested in combination with PI (Live/Dead BacLight Bacterial Viability Kit) (Thermo Fisher Scientific, Carlsbad, CA, USA) at a concentration of 5 µM as a dead cell indicator.

Vitality was assessed using FDA (Merck Sigma-Aldrich, Madrid, Spain) at 10 µg/mL and the yeast-specific FUN-1 dye (Thermo Fisher Scientific, Carlsbad, CA, USA) at 20 µM. FDA becomes fluorescent green in metabolically active cells with intact membranes, as it is hydrolyzed by intracellular esterases. On the other hand, the FUN-1 dye becomes fluorescent green after binding to protein and nucleic acids [46]. Moreover, endogenous

biochemical reactions lead to the formation of red CIVSs, allowing the identification of yeast cells with intact membranes and metabolic capacity [46].

The performance evaluation of the dyes was first performed on planktonic cells from overnight cultures. Cells were harvested with a centrifugation step at 4000 rpm for 5 min and washed twice with PBS before staining. Images at a 100× magnification were obtained using an LSM 800 confocal scanning laser microscope (Zeiss, Oberkochen, Germany) and processed using Fiji – Image J software v1.54f [47].

Then, 24 h-formed biofilms were treated with 2.5 μg/mL of AmB or RPMId for 20 h and subsequently stained for analysis. Images at a 60× magnification were obtained and processed in the same way as with planktonic cultures. Biomass quantification of cells was performed using the ImageJ plugin COMSTAT2 [48–50]. Corrected biomass of viability dyes was obtained by multiplying the biomass measure of each channel (green live cells and dead live cells) with the biomass measure from the CW channel. Similarly, the corrected biomass of FDA dye was obtained by multiplying the measure of biomass from the green channel (metabolically active cells) with the biomass measure from the CW channel. In the case of FUN-1, the corrected biomass of metabolically active cells was obtained by multiplying the biomass measure of each channel (green and red) with the biomass measure from the CW channel and then calculating the red channel/green channel ratio, following the manufacturer's instructions [46].

The percentage of viability was calculated according to the following formula: ((Live Cells/(Live Cells + Dead Cells) × 100, where "Live cells" correspond to the biomass measurement ($\mu m^3/\mu m^2$) obtained from S9 or TO staining, and "Dead cells" are determined based on the biomass measurement from PI staining. Similarly, the vitality percentage for FDA was derived from the quantified biomass of stained cells, while the vitality percentage for FUN-1 was calculated as the ratio of red biomass to green biomass.

4.5. Quantification and Statistical Analysis

Graphics and comparisons between treated and untreated biofilms were conducted using GraphPad Prism v9. Statistical differences were evaluated by an unpaired *t*-test with a significant level of $p < 0.05$.

Author Contributions: B.V.A.-J.: conceptualization; data curation; formal analysis; investigation; methodology; validation; visualization; writing—original draft preparation and review and editing. E.T.: conceptualization; funding acquisition; methodology; project administration; resources; supervision; writing—review and editing. All authors have read and agreed to the published version of the manuscript.

Funding: This study was partially supported by grants PID2021-125801OB-100, PLEC2022-009356, and PDC2022-133577-I00 funded by MCIN/AEI/10.13039/501100011033 and "ERDF A way of making Europe", the CERCA programme and AGAUR-Generalitat de Catalunya (2021SGR01545), the European Regional Development Fund (FEDER), and Catalan Cystic Fibrosis Association. The project that gave rise to these results was supported by a fellowship received from "La Caixa" Foundation (ID 100010434). The fellowship code is "LCF/BQ/DI20/11780040".

Institutional Review Board Statement: Not applicable.

Informed Consent Statement: Not applicable.

Data Availability Statement: Dataset available on request from the authors.

Acknowledgments: We thank Jesus Guinea Ortega from the Department of Clinical Microbiology and Infectious Diseases, Hospital General Universitario Gregorio Marañón, Madrid, Spain, for the generous gift of the *Candida parapsilosis* 11103595 used in this study.

Conflicts of Interest: The authors declare no conflicts of interest. The funders had no role in the design of the study; in the collection, analyses, or interpretation of data; in the writing of the manuscript; or in the decision to publish the results.

References

1. Sharma, M.; Chakrabarti, A. Candidiasis and other emerging yeasts. *Curr. Fungal Infect. Rep.* **2023**, *17*, 15–24. [CrossRef] [PubMed]
2. Pendleton, K.M.; Huffnagle, G.B.; Dickson, R.P. The significance of *Candida* in the human respiratory tract: Our evolving understanding. *Pathog. Dis.* **2017**, *75*, ftx029. [CrossRef]
3. Tóth, R.; Nosek, J.; Mora-Montes Héctor, M.; Gabaldon, T.; Bliss Joseph, M.; Nosanchuk Joshua, D.; Turner Siobhán, A.; Butler, G.; Vágvölgyi, C.; Gácser, A. *Candida parapsilosis*: From genes to the bedside. *Clin. Microbiol. Rev.* **2019**, *32*, e00111-18. [CrossRef] [PubMed]
4. Kwolek-Mirek, M.; Zadrag-Tecza, R. Comparison of methods used for assessing the viability and vitality of yeast cells. *FEMS Yeast Res.* **2014**, *14*, 1068–1079. [CrossRef] [PubMed]
5. Bettauer, V.; Costa Anna Carolina Borges, P.; Omran Raha, P.; Massahi, S.; Kirbizakis, E.; Simpson, S.; Dumeaux, V.; Law, C.; Whiteway, M.; Hallett Michael, T. A Deep Learning Approach to Capture the Essence of *Candida albicans* Morphologies. *Microbiol. Spectr.* **2022**, *10*, e01472-22. [CrossRef] [PubMed]
6. Gil, C.; Pomés, R.; Nombela, C. Isolation and characterization of *Candida albicans* morphological mutants derepressed for the formation of filamentous hypha-type structures. *J. Bacteriol.* **1990**, *172*, 2384–2391. [CrossRef] [PubMed]
7. Bahamondez-Canas, T.F.; Heersema, L.A.; Smyth, H.D.C. Current Status of In Vitro Models and Assays for Susceptibility Testing for Wound Biofilm Infections. *Biomedicines* **2019**, *7*, 34. [CrossRef]
8. Wilson, C.; Lukowicz, R.; Merchant, S.; Valquier-Flynn, H.; Caballero, J.; Sandoval, J.; Okuom, M.; Huber, C.; Brooks, T.D.; Wilson, E.; et al. Quantitative and Qualitative Assessment Methods for Biofilm Growth: A Mini-review. *Res. Rev. J. Eng. Technol.* **2017**, *6*, 1–25. Available online: http://www.rroij.com/open-access/quantitative-and-qualitative-assessment-methods-for-biofilm-growth-a-minireview-.pdf (accessed on 20 February 2024).
9. Branco, J.; Miranda, I.M.; Rodrigues, A.G. *Candida parapsilosis* Virulence and Antifungal Resistance Mechanisms: A Comprehensive Review of Key Determinants. *J. Fungi* **2023**, *9*, 80. [CrossRef]
10. Mountcastle, S.E.; Vyas, N.; Villapun, V.M.; Cox, S.C.; Jabbari, S.; Sammons, R.L.; Shelton, R.M.; Walmsley, A.D.; Kuehne, S.A. Biofilm viability checker: An open-source tool for automated biofilm viability analysis from confocal microscopy images. *NPJ Biofilms Microbiomes* **2021**, *7*, 44. [CrossRef]
11. Raas, M.W.D.; Silva, T.P.; Freitas, J.C.O.; Campos, L.M.; Fabri, R.L.; Melo, R.C.N. Whole slide imaging is a high-throughput method to assess Candida biofilm formation. *Microbiol. Res.* **2021**, *250*, 126806. [CrossRef] [PubMed]
12. Cai, J.; Xiong, H.; Cao, M.; Liu, L.; Zhang, L.; Wang, Q. Progressive Attention Guidance for Whole Slide Vulvovaginal Candidiasis Screening. In Proceedings of the Medical Image Computing and Computer Assisted Intervention—MICCAI 2023, Cham, Switzerland, 8–12 October 2023; pp. 233–242.
13. Song, D.; Liu, H.; Huang, Y.; Dongari-Bagtzoglou, A.; Lei, Y. High-Throughput Monitoring of Pathogenic Fungal Growth Using Whole Slide Imaging for Rapid Antifungal Susceptibility Assessment. *Anal. Lett.* **2023**, 1–14. [CrossRef]
14. Tsutsumi-Arai, C.; Terada-Ito, C.; Tatehara, S.; Imamura, T.; Takebe, Y.; Ide, S.; Satomura, K. Fungicidal activity of grapefruit seed extract against the pathogenic *Candida* species causing oral candidiasis. *J. Oral Maxillofac. Surg. Med. Pathol.* **2021**, *33*, 626–632. [CrossRef]
15. Reddy, G.K.K.; Kumar, P.H.; Padmavathi, A.R.; Kutala, V.K.; Sandur, S.K.; Nancharaiah, Y.V. Antifungal and antibiofilm action of triphenylphosphonium-conjugated curcumin on *Candida albicans*: Efficacy and activity mechanisms. *Int. Biodeterior. Biodegrad.* **2024**, *189*, 105751. [CrossRef]
16. Zhang, Q.; Zhang, J.; Zhang, Y.; Sui, Y.; Du, Y.; Yang, L.; Yin, Y. Antifungal and anti-biofilm activities of patchouli alcohol against *Candida albicans*. *Int. J. Med. Microbiol.* **2024**, *314*, 151596. [CrossRef] [PubMed]
17. Powell, L.C.; Adams, J.Y.M.; Quoraishi, S.; Py, C.; Oger, A.; Gazze, S.A.; Francis, L.W.; von Ruhland, C.; Owens, D.; Rye, P.D.; et al. Alginate oligosaccharides enhance the antifungal activity of nystatin against candidal biofilms. *Front. Cell. Infect. Microbiol.* **2023**, *13*, 1122340. [CrossRef] [PubMed]
18. Cacaci, M.; Squitieri, D.; Palmieri, V.; Torelli, R.; Perini, G.; Campolo, M.; Di Vito, M.; Papi, M.; Posteraro, B.; Sanguinetti, M.; et al. Curcumin-Functionalized Graphene Oxide Strongly Prevents *Candida parapsilosis* Adhesion and Biofilm Formation. *Pharmaceuticals* **2023**, *16*, 275. [CrossRef]
19. Zhu, B.; Li, Z.; Yin, H.; Hu, J.; Xue, Y.; Zhang, G.; Zheng, X.; Chen, W.; Hu, X. Synergistic Antibiofilm Effects of Pseudolaric Acid A Combined with Fluconazole against Candida albicans via Inhibition of Adhesion and Yeast-To-Hypha Transition. *Microbiol. Spectr.* **2022**, *10*, e01478-21. [CrossRef]
20. Cheng, R.; Xu, Q.; Hu, F.; Li, H.; Yang, B.; Duan, Z.; Zhang, K.; Wu, J.; Li, W.; Luo, Z. Antifungal activity of MAF-1A peptide against *Candida albicans*. *Int. Microbiol.* **2021**, *24*, 233–242. [CrossRef]
21. Ferreira, G.R.S.; Brito, J.d.S.; Procópio, T.F.; Santos, N.D.d.L.; de Lima, B.J.R.C.; Coelho, L.C.B.B.; Navarro, D.M.d.A.F.; Paiva, P.M.G.; Soares, T.; de Moura, M.C.; et al. Antimicrobial potential of Alpinia purpurata lectin (ApuL): Growth inhibitory action, synergistic effects in combination with antibiotics, and antibiofilm activity. *Microb. Pathog.* **2018**, *124*, 152–162. [CrossRef]
22. Hifney, A.F.; Soliman, Z.; Ali, E.F.; Hussein, N.A. Microbial and microscopic investigations to assess the susceptibility of *Candida parapsilosis* and *Prototheca ciferrii* to phyco-synthesized titanium dioxide nanoparticles and antimicrobial drugs. *S. Afr. J. Bot.* **2022**, *151*, 791–799. [CrossRef]
23. Lotfali, E.; Ghasemi, R.; Fattahi, A.; Keymaram, M.; Shafiei, M.; Norouzi, M.; Ayatollahi, A. Activities of Nanoparticles Against Fluconazole-Resistant *Candida parapsilosis* in Clinical Isolates. *ASSAY Drug Dev. Technol.* **2021**, *19*, 501–507. [CrossRef] [PubMed]

24. Bizerra Fernando, C.; Melo Analy, S.A.; Katchburian, E.; Freymüller, E.; Straus Anita, H.; Takahashi Hélio, K.; Colombo Arnaldo, L. Changes in Cell Wall Synthesis and Ultrastructure during Paradoxical Growth Effect of Caspofungin on Four Different *Candida* Species. *Antimicrob. Agents Chemother.* **2011**, *55*, 302–310. [CrossRef] [PubMed]
25. Dias, L.P.; Santos, A.L.E.; Araújo, N.M.S.; Silva, R.R.S.; Santos, M.H.C.; Roma, R.R.; Rocha, B.A.M.; Oliveira, J.T.A.; Teixeira, C.S. Machaerium acutifolium lectin alters membrane structure and induces ROS production in *Candida parapsilosis*. *International J. Biol. Macromol.* **2020**, *163*, 19–25. [CrossRef] [PubMed]
26. Malveira, E.A.; Souza, P.F.N.; Neto, N.A.S.; Aguiar, T.K.B.; Rodrigues, N.S.; Henrique, C.W.B.; Silva, A.F.B.; Lima, L.B.; Albuquerque, C.C.; Freitas, C.D.T. Essential Oil from *Croton blanchetianus* Leaves: Anticandidal Potential and Mechanisms of Action. *J. Fungi* **2022**, *8*, 1147. [CrossRef] [PubMed]
27. Li, Z.; Zhu, B.; Chen, W.; Hu, J.; Xue, Y.; Yin, H.; Hu, X.; Liu, W. Pseudolaric Acid A: A Promising Antifungal Agent Against Prevalent Non-albicans *Candida* Species. *Infect. Drug Resist.* **2023**, *16*, 5953–5964. [CrossRef] [PubMed]
28. Hu, L.; Zhou, P.; Zhao, W.; Hua, H.; Yan, Z. Fluorescence staining vs. routine KOH smear for rapid diagnosis of oral candidiasis—A diagnostic test. *Oral Dis.* **2020**, *26*, 941–947. [CrossRef]
29. Jahanshahi, G.; Shirani, S. Detection of *Candida albicans* in oral squamous cell carcinoma by fluorescence staining technique. *Dent. Res. J.* **2015**, *12*, 115.
30. Nunes, T.S.; Rosa, L.M.; Vega-Chacón, Y.; Mima, E.G. Fungistatic Action of N-Acetylcysteine on Candida albicans Biofilms and Its Interaction with Antifungal Agents. *Microorganisms* **2020**, *8*, 980. [CrossRef]
31. Abi-Chacra, É.A.; Souza, L.O.P.; Cruz, L.P.; Braga-Silva, L.A.; Gonçalves, D.S.; Sodré, C.L.; Ribeiro, M.D.; Seabra, S.H.; Figueiredo-Carvalho, M.H.G.; Barbedo, L.S.; et al. Phenotypical properties associated with virulence from clinical isolates belonging to the Candida parapsilosis complex. *FEMS Yeast Res.* **2013**, *13*, 831–848. [CrossRef]
32. McGoverin, C.; Robertson, J.; Jonmohamadi, Y.; Swift, S.; Vanholsbeeck, F. Species dependence of SYTO 9 staining of bacteria. *Front. Microbiol.* **2020**, *11*, 545419. [CrossRef] [PubMed]
33. Mesa-Arango, A.C.; Rueda, C.; Román, E.; Quintin, J.; Terrón María, C.; Luque, D.; Netea Mihai, G.; Pla, J.; Zaragoza, O. Cell wall changes in Amphotericin B-resistant strains from *Candida tropicalis* and relationship with the immune responses elicited by the host. *Antimicrob. Agents Chemother.* **2016**, *60*, 2326–2335. [CrossRef]
34. Cho, O.; Takada, S.; Odaka, T.; Futamura, S.; Kurakado, S.; Sugita, T. Tacrolimus (FK506) Exhibits Fungicidal Effects against *Candida parapsilosis* Sensu Stricto via Inducing Apoptosis. *J. Fungi* **2023**, *9*, 778. [CrossRef] [PubMed]
35. Miranda-Cadena, K.; Marcos-Arias, C.; Mateo, E.; Aguirre-Urizar, J.M.; Quindós, G.; Eraso, E. In vitro activities of carvacrol, cinnamaldehyde and thymol against *Candida* biofilms. *Biomed. Pharmacother.* **2021**, *143*, 112218. [CrossRef] [PubMed]
36. Coenye, T. Biofilm antimicrobial susceptibility testing: Where are we and where could we be going? *Clin. Microbiol. Rev.* **2023**, *36*, e00024-23. [CrossRef] [PubMed]
37. Alcàcer-Almansa, J.; Arévalo-Jaimes, B.V.; Blanco-Cabra, N.; Torrents, E. Methods for studying biofilms: Microfluidics and translation in the clinical context. In *Methods in Microbiology*; Academic Press: Cambridge, MA, USA, 2023.
38. Marcos-Zambrano, L.J.; Escribano, P.; Bouza, E.; Guinea, J. Production of biofilm by *Candida* and non-*Candida* spp. isolates causing fungemia: Comparison of biomass production and metabolic activity and development of cut-off points. *Int. J. Med. Microbiol.* **2014**, *304*, 1192–1198. [CrossRef]
39. Madeira, P.L.B.; Carvalho, L.T.; Paschoal, M.A.B.; de Sousa, E.M.; Moffa, E.B.; da Silva, M.A.d.S.; Tavarez, R.d.J.R.; Gonçalves, L.M. In vitro effects of lemongrass extract on *Candida albicans* biofilms, human cells viability, and denture surface. *Front. Cell Infect. Microbiol.* **2016**, *6*, 71. [CrossRef] [PubMed]
40. Maione, A.; Bellavita, R.; de Alteriis, E.; Galdiero, S.; Albarano, L.; La Pietra, A.; Guida, M.; Parrilli, E.; D'Angelo, C.; Galdiero, E.; et al. WMR peptide as antifungal and antibiofilm against *albicans* and Non-*albicans Candida* species: Shreds of evidence on the mechanism of action. *Int. J. Mol. Sci.* **2022**, *23*, 2151. [CrossRef]
41. Seneviratne, C.J.; Silva, W.J.; Jin, L.J.; Samaranayake, Y.H.; Samaranayake, L.P. Architectural analysis, viability assessment and growth kinetics of *Candida albicans* and *Candida glabrata* biofilms. *Arch. Oral Biol.* **2009**, *54*, 1052–1060. [CrossRef]
42. Honraet, K.; Goetghebeur, E.; Nelis, H.J. Comparison of three assays for the quantification of *Candida* biomass in suspension and CDC reactor grown biofilms. *J. Microbiol. Methods* **2005**, *63*, 287–295. [CrossRef]
43. Köhler, G.A.; Assefa, S.; Reid, G. Probiotic interference of *Lactobacillus rhamnosus* GR-1 and *Lactobacillus reuteri* RC-14 with the opportunistic fungal pathogen *Candida albicans*. *Infect. Dis. Obstet. Gynecol.* **2012**, *2012*, 636474. [CrossRef] [PubMed]
44. Mishra, N.N.; Ali, S.; Shukla, P.K. Arachidonic acid affects biofilm formation and PGE2 level in *Candida albicans* and non-*albicans* species in presence of subinhibitory concentration of fluconazole and terbinafine. *Braz. J. Infect. Dis.* **2014**, *18*, 287–293. [CrossRef] [PubMed]
45. Al-Dhaheri, R.S.; Douglas, L.J. Apoptosis in *Candida* biofilms exposed to amphotericin B. *J. Med. Microbiol.* **2010**, *59*, 149–157. [CrossRef]
46. Millard, P.J.; Roth, B.L.; Thi, H.P.; Yue, S.T.; Haugland, R.P. Development of the FUN-1 family of fluorescent probes for vacuole labeling and viability testing of yeasts. *Appl. Environ. Microbiol.* **1997**, *63*, 2897–2905. [CrossRef] [PubMed]
47. Schindelin, J.; Arganda-Carreras, I.; Frise, E.; Kaynig, V.; Longair, M.; Pietzsch, T.; Preibisch, S.; Rueden, C.; Saalfeld, S.; Schmid, B. Fiji: An open-source platform for biological-image analysis. *Nat. Methods* **2012**, *9*, 676–682. [CrossRef] [PubMed]
48. Schneider, C.A.; Rasband, W.S.; Eliceiri, K.W. NIH Image to ImageJ: 25 years of image analysis. *Nat. Methods* **2012**, *9*, 671–675. [CrossRef] [PubMed]

49. Heydorn, A.; Nielsen, A.T.; Hentzer, M.; Sternberg, C.; Givskov, M.; Ersboll, B.K.; Molin, S. Quantification of biofilm structures by the novel computer program COMSTAT. *Microbiology* **2000**, *146*, 2395–2407. [CrossRef]
50. Vorregaard, M. *Comstat2—A Modern 3D Image Analysis Environment for Biofilms*; Technical University of Denmark: Lyngby, Denmark, 2008.

Artículo 5 (Publicación)

A new BiofilmChip for testing biofilm formation and antibiotic susceptibility

Publicado en la revista *npj Biofilms and Microbiomes*

DOI: 10.1038/s41522-021-00236-1

3 de agosto de 2021

Categoría Microbiología 2021: 1er tercil, 1er Cuartil, IF= 8.5

Núria Blanco-Cabra[1,7], María José López-Martínez[2,3,4,7], Betsy V. Arévalo-Jaimes[1], María Teresa Martin-Gómez[5], Josep Samitier[2,3,4] y Eduard Torrents[1,6]

[1]Grupo Infecciones Bacterianas y Terapias Antimicrobianas (BIAT), Instituto de Bioingeniería de Cataluña (IBEC), Barcelona, España.

[2]Grupo Nanobioingeniería, Instituto de Bioingeniería de Cataluña (IBEC), Barcelona, España.

[3]Centro de investigación Biomédica en Red. Bioingeniería, Biomateriales y Nanomedicina (CIBER-BBN), Madrid, España.

[4]Departamento de Electrónica e Ingeniería Biomédica, Universitat de Barcelona, Barcelona, España.

[5]Departamento de Microbiología, Hospital Universitario Vall d'Hebron, Bacrelona, España.

[6]Sección de Microbiología, Departamento de Genética, Microbiología y Estadística, Facultad de Biología, Universitat de Barcelona, Barcelona, España.

[7]Estos autores contribuyeron equitativamente en el trabajo.

Cita: Blanco-Cabra, N., López-Martínez, M. J., Arévalo-Jaimes, B. V., Martin-Gómez, M. T., Samitier, J., & Torrents, E. (2021). A new BiofilmChip device for testing biofilm formation and antibiotic susceptibility. *npj Biofilms Microbiomes*, 7(1), 62. DOI: 10.1038/s41522-021-00236-1.

npj | Biofilms and Microbiomes

www.nature.com/npjbiofilms

ARTICLE OPEN

Check for updates

A new BiofilmChip device for testing biofilm formation and antibiotic susceptibility

Núria Blanco-Cabra[1,7], Maria José López-Martínez[2,3,4,7], Betsy Verónica Arévalo-Jaimes[1], María Teresa Martin-Gómez[5], Josep Samitier[2,3,4] and Eduard Torrents[1,6]✉

Currently, three major circumstances threaten the management of bacterial infections: increasing antimicrobial resistance, expansion of chronic biofilm-associated infections, and lack of an appropriate approach to treat them. To date, the development of accelerated drug susceptibility testing of biofilms and of new antibiofouling systems has not been achieved despite the availability of different methodologies. There is a need for easy-to-use methods of testing the antibiotic susceptibility of bacteria that form biofilms and for screening new possible antibiofilm strategies. Herein, we present a microfluidic platform with an integrated interdigitated sensor (BiofilmChip). This new device allows an irreversible and homogeneous attachment of bacterial cells of clinical origin, even directly from clinical specimens, and the biofilms grown can be monitored by confocal microscopy or electrical impedance spectroscopy. The device proved to be suitable to study polymicrobial communities, as well as to measure the effect of antimicrobials on biofilms without introducing disturbances due to manipulation, thus better mimicking real-life clinical situations. Our results demonstrate that BiofilmChip is a straightforward tool for antimicrobial biofilm susceptibility testing that could be easily implemented in routine clinical laboratories.

npj Biofilms and Microbiomes (2021)7:62 ; https://doi.org/10.1038/s41522-021-00236-1

INTRODUCTION

Biofilms are communities of microorganisms that form on and attach to living and nonliving surfaces. These communities are ubiquitous, as they are found in natural, industrial and medical environments. Biofilms can be beneficial under some conditions, for example, for biodegradation in wastewater treatment, but they are often undesired because of their ability to cause infections, contamination, biofouling, and biocorrosion[1].

The attached microorganisms form microcolonies on a surface, where the bacteria are embedded in the extracellular polymeric substances (EPS) that form the biofilm matrix[2]. The matrix protects the microorganisms and makes biofilms very difficult to eradicate because it increases their resistance to biological, mechanical, physical, and chemical treatments[3]. Taking into account that approximately 80% of chronic infections in animals and humans are estimated to be biofilm-related[4], their formation presents a severe threat in the battle against antimicrobial recalcitrance, and related treatments require several billions of US dollars each year worldwide[5,6]. Moreover, to date, no antibiotic that can successfully eradicate biofilms has been found, so there is a great need for new strategies to combat biofilms[7] while awaiting for the development of effective antibiofilm molecules.

Model systems of in vitro biofilms are essential in research laboratories for testing new antibiofilm compounds, as well as in clinical laboratories for determining the optimal treatment of biofilm-related infections. There is a wide selection of different monitoring techniques for biofilm growth and characterization, varying in the analysis scale, handling time, sensitivity and final detection technique employed[8]. Standard methods mostly rely on colorimetric measurements and are commercially available, i.e., the microtiter plate method[9,10], the MBEC Assay®[11,12], the Biofilm Ring Test[13,14] and the Lubbock system[15]. These techniques allow the screening of different antimicrobials in a high-throughput way, but they are generally destructive endpoint diagnostic tools and require removal of the formed biofilm from the growth substrate used. For this reason, these systems cannot be exploited for online monitoring characterization.

Moreover, the majority of these high-throughput screening techniques involve the use of static devices with limited nutrients, which form biofilms that do not resemble all the biofilms' characteristics found during natural infections. On the other hand, dynamic devices allow bacteria to grow under flow conditions that eliminate the planktonic growth[16]. Examples of these devices are the Robbins device[17], the Drip-Flow reactor[18] or the Rotary biofilm reactor[19]. Although having some limitations (e.g., the prior knowledge of the device flow dynamics, the heterogeneity of the biofilm development, or the low-throughput of these dynamic devices), they can better mimic real in vivo infective conditions[20]. One of the recurrent problems with such flow conditions is the need for large volumes of media and tubing, which prevent high-throughput screening.

Furthermore, most of the available techniques require advanced microscopy systems to monitor biofilm growth[21–24]. Recently, Acea Bioscience (San Diego, USA) released xCELLigence based on electrical impedance spectroscopy (EIS) measured on the basis of a defined Cell Index (CI) parameter[25]. This technique is based on the detection of changes in the diffusion coefficient of a redox solute, which is recorded as an electrochemical reaction on

[1]Bacterial Infections and Antimicrobial Therapies Group, Institute for Bioengineering of Catalonia (IBEC), The Barcelona Institute of Science and Technology (BIST), Barcelona, Spain. [2]Nanobioengineering Group, Institute for Bioengineering of Catalonia (IBEC), The Barcelona Institute of Science and Technology (BIST), Barcelona, Spain. [3]Networking Biomedical Research Center in Bioengineering, Biomaterials and Nanomedicine (CIBER-BBN) Monforte de Lemos 3-5, Madrid, Spain. [4]Department of Electronics and Biomedical Engineering, University of Barcelona, Barcelona, Spain. [5]Microbiology Department, Hospital Universitari Vall d'Hebron, Barcelona, Spain. [6]Microbiology Section, Department of Genetics, Microbiology and Statistics, Faculty of Biology, University of Barcelona, Barcelona, Spain. [7]These authors contributed equally: Núria Blanco-Cabra, Maria José López-Martínez. ✉email: etorrents@ibecbarcelona.eu

Published in partnership with Nanyang Technological University

npj nature partner journals

the electrode; thus, this technique provides an excellent nondestructive method for real-time and in situ measurements independent of confocal microscopy. Indeed, EIS was shown to be suitable for online monitoring of biofilm formation, although all the experiments were performed under static conditions and did not resemble all features of natural infections[26,27].

Microfluidics represents the next generation of fluidic platforms for biomedical research[28]. The Bioflux[29] and other microfluidic devices[30,31] provide dynamic systems with significant control over the flow rate settings, potential for real-time analysis and, particularly for biofilms, greater similarity to the in vivo infective environments by creating the physical conditions encountered in natural environments[32].

Even though antibiotics that affect planktonic growth typically become useless when the bacteria form a biofilm, none of the abovementioned techniques have been used in clinical laboratories to find appropriate treatments for a chronic biofilm infection, as they are too complex and require costly and intricate equipment operated by experienced personnel. Instead, antibiotic efficacy and susceptibilities are determined using planktonic bacteria. Furthermore, real biofilm-forming infections are known to be polymicrobial, which modify their antibiotic susceptibility[33], but conventional antimicrobial susceptibility test is performed on single isolates obtained from complex samples, thereby missing other important species and their interactions in clinical samples[34].

In this work, we developed a microfluidic system to grow and analyze biofilms using samples from different sources (in vitro bacteria cultures, clinical samples, etc.) to be used in clinical or industrial settings. This device can be used to determine a personalized treatment for a patient suffering a chronic infection, even though more studies are necessary to validate this. We proposed an innovative rapid method for studying new anti-biofouling strategies, including drug susceptibility testing of different bacterial species using EIS. This microfluidic platform allows homogeneous biofilm growth that can be easily monitored without using a confocal microscope and enables the development and co-culture of polymicrobial biofilms that resemble the real biofilm infections found in complex matrixes such as sputum samples (e.g., cystic fibrosis infections).

RESULTS

Chip fabrication and characterization

A microfluidic platform with an integrated interdigitated sensor (BiofilmChip) was designed to monitor the growth and treatment of a biofilm in a controlled manner (Fig. 1a, b). The chip was

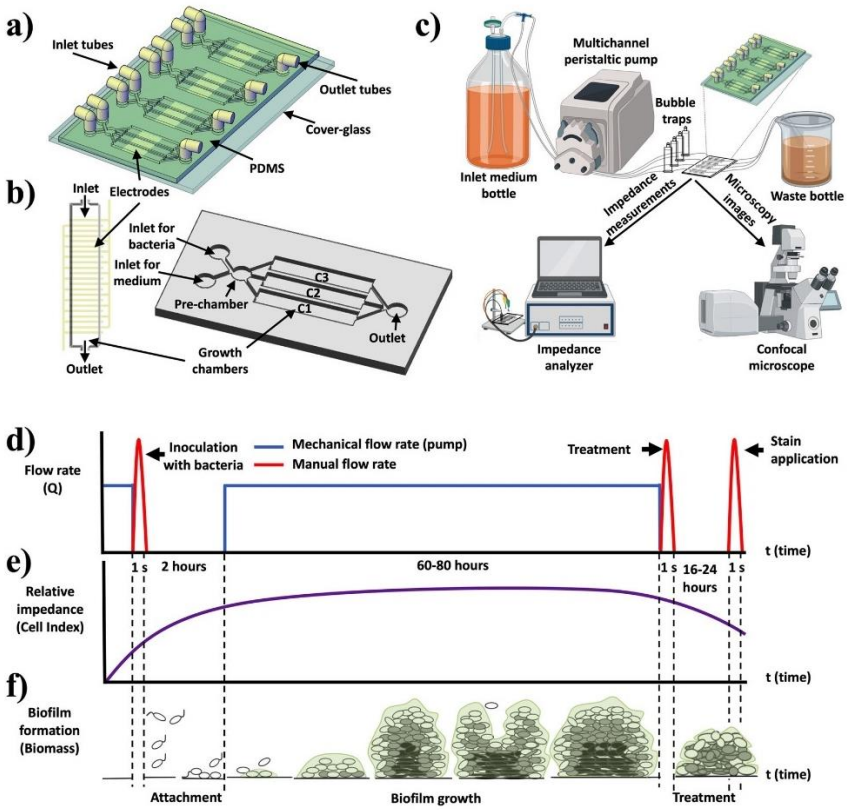

Fig. 1 Biofilm chip design. **a** BiofilmChip 3D view, **b** 3D view of one chamber with the electrodes and one set of 3 chambers, **c** experimental setup, **d** changes in the mechanical flow rate (in blue) and the manual flow rate (in red, only during the inoculation with bacteria and applications of treatment or stain), **e** expected relative impedance and **f** biofilm formation over time. Figure created in part with www.biorender.com.

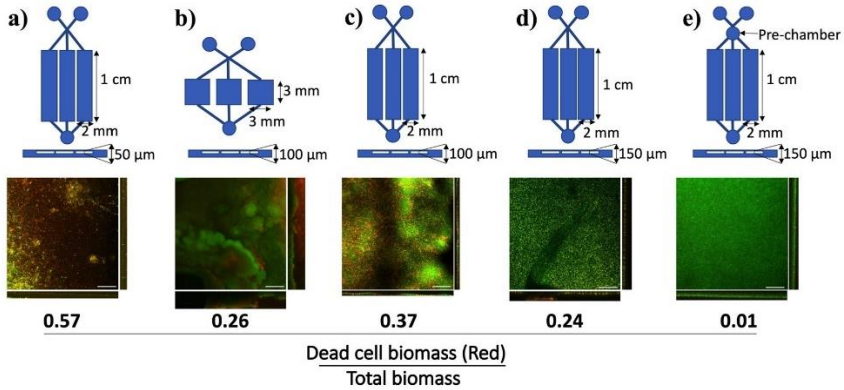

Fig. 2 BiofilmChip dimensions, geometry and functional characterization. schematic representations of the different manufactured chip geometries. The *P. aeruginosa* PAO1 biofilm structure formed in each chip is shown in the confocal microscopy images (sum and orthogonal views). In all cases, the biofilm was grown for 72 h and stained with the LIVE/DEAD BacLight Bacterial Viability Kit. At the bottom of the images, average proportion of dead cells (stained in red) in the total biofilm biomass from three different experiments is shown. Scale bar represents 50 µm.

prepared by a combination of standard photolithography and soft lithography techniques. The final system setup is shown in Fig. 1c. Briefly, the medium bottle was connected through tubing to the microfluidic device. Medium was pumped through the system via a high-precision peristaltic pump (see the Material and Methods for details).

Following the experimental scheme shown in Fig. 1d, f, a biofilm formed and grew inside the chambers via irreversible attachment of bacterial cells to the cover glass. The biofilms could then be visualized under a confocal microscope after a specific staining procedure (Fig. 1c, f) or directly analyzed by impedance measurements (as shown in Fig. 1c, e).

Optimal parameters for uniform biofilm formation

Our primary goal was to design a BiofilmChip with optimized capacity for growing biofilms with maximal uniformity across the different chambers of the chip. First, several prototype designs with chambers that differed in dimension and shape were fabricated and tested by growing a *P. aeruginosa* PAO1 biofilm. The different prototypes manufactured and tested are shown in Fig. 2, and the formed biofilms were established as described in Fig. 1c, stained with LIVE/DEAD dyes, and visualized under a confocal microscope. As seen in Fig. 2, the chamber geometry and height clearly impacted the biofilm formation: a rectangular chamber morphology was preferred over a square morphology. As observed in prototype b (Fig. 2b), the biofilm formed in the square chamber was nonhomogeneous, while that formed in the rectangular chamber (with a height of 150 µm) remained smooth (Fig. 2d).

P. aeruginosa cell division was impaired in the outer biofilm layers of the 50- and 100-µm height chambers, with evident cell filamentation and increased cell death (stained in red), indicated by a more significant proportion of red biomass (ratios of dead cell biomass to total biomass of 0.57, 0.26 and 0.37) (Fig. 2a–c). On the other hand, bacteria had a morphology characteristic of wild-type *Pseudomonas* in the chip with 150-µm height chambers and showed uniform green staining covering the entire surface area (a lower proportion of dead cells) (Fig. 2d, e).

Even though the optimal parameters (rectangular shape with 150 µm high) resulted in homogeneous biofilms with a low proportion of dead cells (ratio of 0.24), manual system manipulations (i.e., direct injection during inoculation and staining) caused disturbances in biofilm uniformity (Fig. 2d). There is a tremendous boost of the shear stress all along with the chamber due to the abrupt increase in the flow rate when injecting the bacteria for inoculation. (Fig. 1d). The pressure generated at the inlet was 363 ± 197 psi during manual injection[35]. At this specific pressure generated during injection, we simulated the influence of fluid velocity and chamber shape on biofilm formation using COMSOL Multiphysics software (COMSOL AB, Sweden). Supplementary Fig. 1 shows that the inclusion of a prechamber ahead of the biofilm growth chambers stabilized the flow and rendered a better distribution of velocity, minimizing the effect of sample loading. The results were confirmed by observing uniform biofilm growth in the chambers, as shown in Fig. 2e. Therefore, the prototype with a rectangular chamber, 150 µm high and with a prechamber (Fig. 2e) was chosen as the optimal design for biofilm formation and used thenceforward.

BiofilmChip robustness

We next evaluated the robustness of the BiofilmChip with the optimized conditions (rectangular chambers 2 mm wide, 10 mm long, and 150 µm high with a 2-mm prechamber diameter) (Fig. 2e) by analyzing some biofilm parameters along with the biofilm growth chamber. For these experiments, we used laboratory strains of *Pseudomonas aeruginosa* PAO1 and *Staphylococcus aureus* (ATCC12600). We compared the biofilm biomass and thickness at different locations inside a chamber (close to the inlets, the middle part and the outlet, see Fig. 3a), between sets of chambers (Fig. 3b) and finally among separate chambers of the same set (Fig. 3c). In all cases, we observed robust, homogenous biofilm formation with similar biomass and thickness values among the different locations and chambers, demonstrating the uniformity of the biofilm formed. Note that in Fig. 3c, we used two bacterial strains isolated from chronically infected cystic fibrosis patients (*P. aeruginosa* PAET1 and methicillin-resistant *S. aureus* MRSA).

As a proof of concept to evaluate the ability of our BiofilmChip to assess antimicrobial therapy, we determined whether a reduction in the biofilm biomass can be detected with our BiofilmChip, by treating a mature biofilm (72 h old) with the extensively used antibiotic ciprofloxacin (CPX). As shown in Fig.

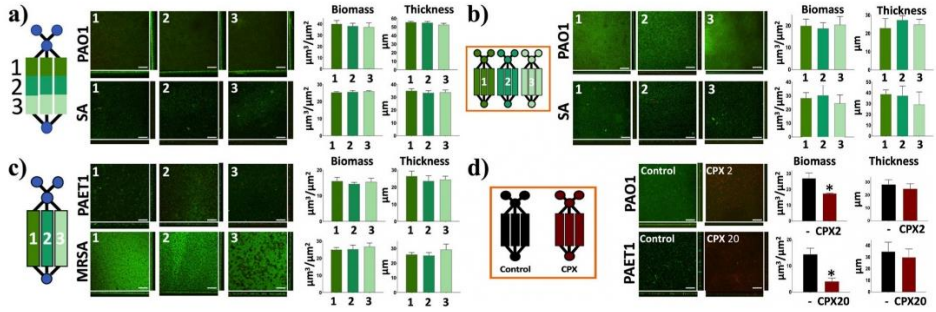

Fig. 3 BiofilmChip robustness evaluation. Uniformity in the established biofilm biomass and thickness across different chamber locations (**a**), between sets of chambers (**b**), and among chambers in the same set (**c**). Decreases in biomass and thickness after 24 h of treatment of *P. aeruginosa* PAO1 and PAET1 with ciprofloxacin (**d**). In all cases, 72-hour-old biofilms were stained and visualized by confocal microscopy (CLSM). Images represent the sum of stacked CLSM images and their corresponding orthogonal views, and bars show the quantified biofilm biomass ($\mu m^3/\mu m^2$) and average thickness (μm) with error bars of the three different replicates. Scale bar represents 50 μm. The results presented in this figure are representative of the same experiment repeated at least three times, producing similar results every time. PAO1 (*P. aeruginosa* PAO1 laboratory strain), PAET1 (*P. aeruginosa* PAET1 clinical isolate strain), SA (*S. aureus* laboratory strain), MRSA (*S. aureus* MRSA clinical isolate strain), CPX2 (ciprofloxacin 2 μg/ml), CPX20 (ciprofloxacin 20 μg/ml). *$p < 0.05$ vs. control in a *t*-test.

3d, the treatment of *P. aeruginosa* laboratory strain PAO1 and clinical *P. aeruginosa* isolate PAET1 with 2 and 20 μg/ml ciprofloxacin (10× approximately their MIC, See Supplementary Table 1), respectively, reduced the biofilm biomass (35 and 71%) and thickness (12 and 14%) after 24 h, detected by measuring their viability with the LIVE/DEAD staining. Moreover, this reduction of biofilm biomass correlates with an increase of dead cells caused by the ciprofloxacin (see results in Supplementary Table 2). Therefore, BiofilmChip was suitable for use in inhibition experiments to observe changes in biofilm biomass after specific antibiotic treatment.

BiofilmChip is a versatile system for growing biofilms directly from clinical sputum samples

The BiofilmChip prototype has been tested with laboratory and clinical strains of *P. aeruginosa* and *S. aureus* (Fig. 3) and directly from patient samples.

Sputum samples from cystic fibrosis patients (Supplementary Table 3) at different stages of *P. aeruginosa* and/or *S. aureus* chronic infection were tested. First, the sputum samples were treated with hypotonic media as described in the Material and Methods section and inoculated directly into the BiofilmChip by injecting the sample through the inlet port while the medium flow was stopped. After 2 h, the TSB media was allowed to flow for 72 h. The formed biofilm was stained and visualized under a confocal microscope.

Interestingly, our system allowed the biofilm formation and growth of different bacterial species simultaneously from the sputum samples. Figure 4 displays representative confocal microscopy images of the biofilms formed from four different sputa (I–IV) (Supplementary Table 3). Different bacterial shapes and morphologies can be seen in the enlarged image of biofilms a) and b) (Fig. 4, sputum I-II), stained with the LIVE/DEAD Viability Kit. Furthermore, the biofilms from sputum III and IV (Fig. 4c, d), stained with the Gram Stain Kit, can be distinguished on the basis of the Gram staining of the different bacteria found. Information concerning the identification and antibiotic susceptibility of the bacteria present in each sputum sample is presented in Supplementary Table 3. Sputum II and IV were found to contain *P. aeruginosa* and *S. aureus* (Supplementary Table 3), which could correspond to the bacilli and staphylococci found in the biofilm (Fig. 4b, d). However, other bacteria also grew, as observed in the confocal images. On the other hand, when the sputa was grown in agar plates at the Microbiology Service at the Vall d'Hebron Barcelona Hospital, only *P. aeruginosa* was identified in the cultures of sputum I and III (Fig. 4a, c, Supplementary Table 3), which can correspond to the bacilli found in the biofilm from sputum I, but no signs of Gram-negative bacilli were found in the biofilm from sputum III, demonstrating the existing variability between the planktonic cells used for microbiological identification and those involved in biofilm growth.

The importance of growing the biofilms directly from sputum samples before analyzing them was corroborated by directly visualizing the sputum by confocal microscopy imaging (Supplementary Fig. 2), showing that it is not possible to directly observe diverse bacteria and their interactions due to the low bacterial concentrations, the presence of eukaryotic cells and the remaining mucus.

Correlation of confocal microscopy and impedance measurements in the BiofilmChip

To validate the use of the BiofilmChip in antibiofilm drug susceptibility tests, 3-day-old biofilms of *P. aeruginosa* PAO1 (wild-type strain) and *P. aeruginosa* PAET1 (clinically isolated strain) were treated for 24 h with 2 μg/ml and 20 μg/ml ciprofloxacin, respectively. They were imaged with confocal microscopy to calculate the biofilm biomass. As shown in Fig. 3d, the treated biofilm biomass was significantly decreased compared to that of the control biofilm without treatment. Then, to evaluate whether impedance measurements could be correlated to the established confocal microscopy images for biofilm monitoring, a *P. aeruginosa* PAO1 strain encoding a green fluorescent protein (*GFP*) (MK171) was used to grow and easily visualize the biofilm during the time when staining it continuously was not necessary.

We next used BiofilmChip devices with integrated interdigitated sensors (see Fig. 1a, b and the Material and Methods). Initially, impedance was measured at frequency values between 40 Hz and 400 kHz every 12 h during the entire biofilm growth period (from before inoculation until after treatment). Measures were plotted in a Bode diagram (shown in Supplementary Fig. 3). Ward et al. proposed different mechanisms on how biofilm growth can interfere in electrode-electrolyte impedance value (i.e., production of redox compounds; biofilm material deposition onto the electrode surface; the presence of microbial cells close to electrode surface; among others)[36]. They suggested that

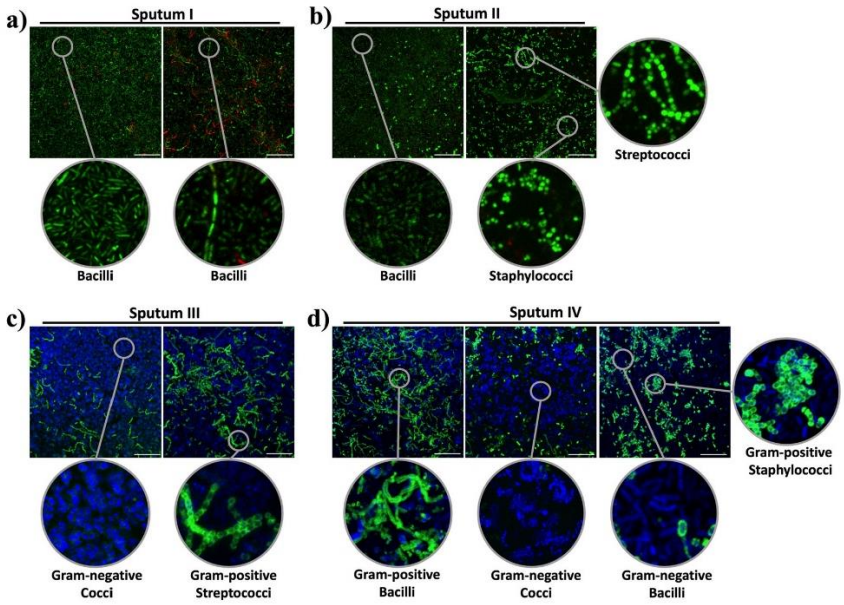

Fig. 4 Biofilms formed from four different sputum samples (I–IV) with enlarged images showing the different bacterial shapes found. Biofilms were stained with a LIVE/DEAD BacLight Bacterial Viability Kit (**a** and **b**) and with a Gram Stain Kit (**c** and **d**), which stains Gram-negative bacteria blue and Gram-positive bacteria green. Scale bar represents 20 µm. The images shown are representative of one biofilm formed per each sputa, that was repeated at least two times, yielding the same results.

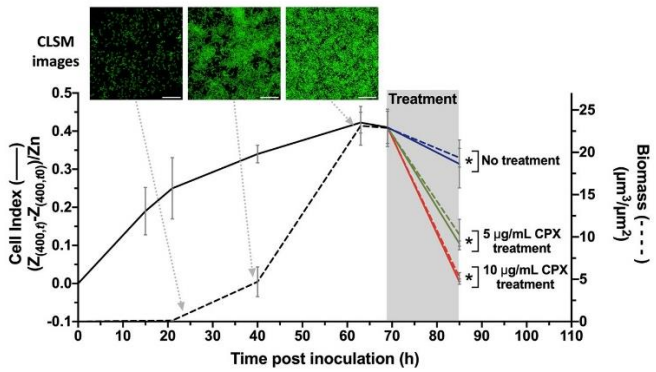

Fig. 5 Correlation in real time the biofilm formation and removal using confocal microscopy and impedance measurement. Monitored *P. aeruginosa* MK171 (expressing eGFP) biofilm growth and effect of antibiotic treatment evaluated on the basis of electrical impedance (represented as the CI, left *y*-axis, solid line) and biomass calculated from confocal microscopy images (defined as $\mu m^3/\mu m^2$, right *y*-axis, dashed line). In the shaded part, corresponding to the treatment duration, green and red lines represent 5 µg/ml and 10 µg/ml ciprofloxacin treatment, respectively, and the blue line illustrates the control without treatment. The values shown are the average of three independent experiments, and the error bars indicate the standard deviation between the experiments. Representative confocal images from three different time points are shown. Scale bar represents 20 µm. *$p < 0.05$ in a Pearson's correlation test.

measurements at low frequencies are dominated by charge transfer and mass diffusion of electroactive compounds. In concordance with their results, impedance value at 400 Hz frequency showed substantial differences in impedance at the different steps of the experiment. Accordingly, impedance measurements at 400 Hz and confocal microscopy images were performed at the same time to calculate the cell index (CI) and the biofilm biomass, respectively. CI is a normalized parameter where

the impedance value of the blank sample is subtracted from the value measured at a specific time point of the biofilm growth (see the Materials and Methods). In the early stages of biofilm formation, the cells can be imaged under a confocal microscope, but the calculated biomass is nearly zero. The CI, however, varied during the initial biofilm formation stages and thus, can better assess the cell attachment to the substrate as seen in Fig. 5. Thereafter, 69 h old biofilms were treated with ciprofloxacin at 5 µg/ml and 10 µg/ml for 16 h, and the impedance and biomass were measured. Both the CI and biomass presented the same response to the antibiotic at the two concentrations (green and red lines, Fig. 5) or the lack of treatment (blue lines, Fig. 5).

Considering the impedance changes on the basis of antibiotic treatment seen in Fig. 5, the applicability of these impedance measurements to the antibiotic sensitivity of real patient samples was tested (Supplementary Table 3, sputum V–VII). Biofilms were grown from different sputum samples having a pathogen with a known susceptibility profile, and they were treated with different antibiotics. Biofilm impedance diminished in the presence of an effective antimicrobial treatment, as proven by the difference in CI values calculated before and after antibiotic exposure of biofilms formed from sputa V–VII (Supplementary Table 3 and Supplementary Fig. 4). This CI response agrees with the response found from Fig. 5, validating the use of BiofilmChip for biofilm susceptibility testing directly from clinical samples.

DISCUSSION

Biofilm-related infections are currently a serious threat around the world. The overuse and misuse of antibiotics, along with the increase of biofilm-associated chronic infections is leading to an increasing prevalence of multi-drug resistant bacteria, resulting in a rise in the morbidity and mortality of these infections, which are expected to cause the death of ten million people by 2050[37]. The susceptibility of bacteria embedded in a biofilm to antimicrobial treatment can significantly differ from that of the same free-living bacteria, as it is known that bacteria growing in biofilms have an intrinsically higher antibiotic resistance than their planktonic counterparts due to different mechanisms[38]. Nevertheless, currently, the treatment decisions for biofilm infections are based on susceptibility tests performed in planktonic bacteria immediately after individual bacterial isolation. This makes the treatment choice inappropriate for the effective management of biofilm-associated infections[39]. Moreover, standard antimicrobial susceptibility tests are performed on individual isolates considered relevant by the microbiologist among the full range of growing microorganisms, so in case more than one pathogen is isolated, multiple tests have to be carried out. Taken together, part of the antimicrobial misuse could be attributed to the lack of tools and readily implemented technologies applied in typical microbiology laboratories to easily determine the proper treatment for biofilm infections.

The tool we developed consists of a microfluidic chamber aligned to an interdigitated electrode on which the biofilm grows. It was designed to evaluate biomass formation during the establishment of a biofilm and test antimicrobial drugs and treatments using EIS. Due to the integration of EIS into this BiofilmChip, it is unnecessary to use sophisticated technology such as advanced confocal microscopy, making it suitable for typical microbiology laboratories or industry.

The fabrication cost of the BiofilmChip once you have a specific mask fabrication is cheap (less than one US dollar) and the impedance measurement device can be fabricated easily by an electronic enterprise with cost less than four hundred US dollars. For sure extended manufacturing of all the different BiofilmChip components will reduce the price considerably.

BiofilmChip has several advantages. For example, the microfluidics better mimic growth and resemble a naturally occurring biofilm and reduce the amount of medium and reagents needed to run these continuous biofilm experiments (~16 ml of media per each set of three chambers per day, which is 90% of media reduction compared to the flow cell system). We have optimized this chip's development by producing different variants of the growth chamber geometry and dimensions to enable optimal biofilm development. It has been documented that the flow cell geometry and the shear stress in the chambers affect biofilm growth[40]. In agreement with that, we observed that both the chamber shape and height were key factors to be considered when reproducing a homogeneous biofilm. It was found that a rectangular shape and 150 µm height were optimal for this purpose, as shown in Fig. 2.

Moreover, an important feature of our device is the inclusion of a prechamber in the design (Fig. 1a), which prevents biofilm disturbances caused by manual inoculations that suddenly increase the flow rate (and consequently the shear stress) inside the chambers. The simulations of the media flow velocity inside the chambers (Supplementary Fig. 1) demonstrated that the design with a prechamber enables a more homogeneous media distribution among the three chambers of the same set, leading to a more uniform biofilm and minimizing the impact of manual injection. Although biofilms in nature are rather heterogeneous[41], homogeneity is a key factor for further reliable detection of susceptibility under different treatments. As Fig. 3d shows, significant decreases in *P. aeruginosa* PAO1 and PAET1 biofilm biomass were detected after treatment with 2 µg/ml and 20 µg/ml ciprofloxacin, respectively. To our knowledge, the prechamber is an innovative component that has never been published before; therefore, this new component represents a breakthrough in microfluidic devices, where flow rate control is critical.

It is well known that continuous biofilms produced in vitro are more reliable for antibiotic susceptibility studies[42], as they are more reproducible and similar to the in vivo infection than are in vitro static biofilms performed in microtiter plates. However, the analysis of these continuous biofilms by confocal microscopy is expensive, requires further staining and trained personnel and is extraordinarily time-consuming. We demonstrate an excellent correlation of the biofilm biomass measured via a standardized methodology involving confocal microscopy with the impedance results, which clearly validates the use of EIS to evaluate biofilm growth. Besides, the use of an EIS analyzer is quicker, simpler, and does not require any training. One interesting observation from the use of impedance measurements at 400 Hz is that such measurements can detect the attachment of bacterial cells to the substrate in the early stages of biofilm growth, when usually there aren't enough cells to be detected as a biofilm by the COMSTAT software analysis of confocal microscopy images (Fig. 5). Once a biofilm is mature, the measures under confocal microscopy are comparable to those under EIS.

Moreover, the impedimetric variations can be used to measure the response of biofilms to antibiotic exposure. In the biofilms in Fig. 5, the CI has the same pattern as the quantified biomass. For the biofilms formed from sputum samples described in Supplementary Table 3 (V–VII), the impedimetric response of the biofilms to the antibiotic was on the same wavelength as the sensitivity reported from the sputum (Supplementary Fig. 4), demonstrating the applicability of the BiofilmChip for antibiofilm testing and choosing the right personalized therapy in the future.

Interestingly, the BiofilmChip was designed to be used for growing biofilms with different characteristics. As far, it has been tested with biofilms composed of different bacterial species (from laboratory use or clinical isolates) and isolated directly from sputum samples obtained from patients suffering Cystic Fibrosis, but the applicability of the BiofilmChip can be extended to different patient samples (sputum from patients suffering from bronchiectasis, urinary infections, etc.) or hypothetically from contaminated surfaces such as medical devices (catheters, cardiac

valves, infected joints, etc.) or samples from the food industry (surfaces, etc.), among others.

Under natural conditions, most of these biofilms are formed from a polymicrobial community of bacteria[43] which interact and affect the other's pathogenicity and antibiotic susceptibility[44]. Specifically, a clear example is found in chronic infections in the cystic fibrosis lung, which is known as a polymicrobial consortium formed from different bacterial species[45,46]. Under these conditions, the antibiotic concentration needed to remove the formed biofilm is different from the needed to treat isolated planktonic bacteria or even to treat bacteria grown in a monomicrobial biofilm.

Our BiofilmChip enables the growth of polymicrobial biofilms, as it makes the growth of a biofilm directly from a patient sputum sample possible and ensures that no species are excluded, and helps determine the best treatment needed for personalized therapy. For instance, the sputum samples used to form the biofilm shown in Fig. 4b, d) are reportedly from a CF patient suffering from a lung infection by *P. aeruginosa* and *S. aureus* (sputum II and IV in Supplementary Table 3). However, when these sputum samples were directly grown in the BiofilmChip, a diverse population of other microorganisms was found, and the polymicrobial nature of these infections was demonstrated. The combination of confocal microscopy with the impedance measurements in the BiofilmChip would allow to determine which species from the polymicrobial biofilm is affected by the antibiotic, rendering a better treatment, as already described by Müsken et al.[22], where the evolution of the polymicrobial biofilms in response to different antibiotic treatments was analyzed. However, it has to be taken into account that more species would be able to grow if using different mediums and/or other growing conditions. The antibiotic treatment prescribed for these patients has probably been determined from the individual susceptibility of *P. aeruginosa* and *S. aureus* grown in isolation and planktonically, but as we have previously reported[33], antibiotic resistance can significantly change in polymicrobial biofilms[47,48]. The importance of individualized diagnostic of biofilm resistance in chronically infected patients was previously highlighted to increase the effectiveness of the treatment[49]. Ongoing work will reveal whether the BiofilmChip allows personalized treatment, ensuring a more accurate diagnosis and a better clinical outcome.

METHODS

Laboratory and clinically isolated bacterial strains and growth conditions

Wild-type *Pseudomonas aeruginosa* PAO1 strain CECT 4122 (ATCC 15692) and *Staphylococcus aureus* CECT 86 (ATCC 12600) were obtained from the Spanish Type Culture Collection (CECT). The *P. aeruginosa* PAET1 strain isolated from a cystic fibrosis patient suffering from persistant infection and *S. aureus* MRSA were from our laboratory stock[50,51]. *Pseudomonas aeruginosa* PAO1::eGFP (MK171) was kindly provided by Prof. Tim Tolker-Nielsen[52]. To obtain inocula for examination, the strains were cultured overnight at 37 °C in Luria Bertani (LB) liquid medium (Scharlab, Spain) for *P. aeruginosa* and tryptic soy broth (TSB) medium (Scharlab, Spain) for *S. aureus*. Bacterial growth was measured by reading the absorbance at 550 nm (A_{550}).

Obtaining and processing clinical sputum samples

Excess sputum samples (Supplementary Table 3) from cystic fibrosis patients were collected at the Hospital Universitari Vall d'Hebron Microbiology Department. Approval regarding human sample collection and manipulation was obtained from the Clinical Research Ethics Committee (Comitè Ètic d'Investigació Clínica, CEIC) under the number PR(AG)275/2019. Sputum samples were diluted in 10 mM Tris-HCl hypotonic buffer at pH 7.5 (Fisher Scientific, Spain) in a 1:1 ratio and incubated at 4 °C for 5 min before inoculation.

Microfluidic device design and fabrication: chip fabrication and electrode fabrication

The fabrication of the BiofilmChip (Fig. 1a) involved a multistep procedure using photolithographic and soft lithographic techniques carried out in the MicroFabSpace and Microscopy Characterization Facility, Unit 7 of ICTS "NANBIOSIS" from CIBER-BBN at IBEC. All solvents and chemicals were obtained from Sigma Aldrich unless otherwise specified. The SU-8 photoresist and developer were from MicroChem (Newton, MA). The Ordyl photoresist and developer were from Elga (Italy).

Microfluidic chambers were designed using CAD software (Autodesk, USA), and the master was built over a glass substrate (TED PELLA, Inc., USA) (75 mm × 25 mm). Briefly, the fabrication process started with three consecutive solvent baths (acetone, isopropanol, and ethanol) applied to the glass slide. Following this cleaning protocol, up to three layers of Ordyl SY 550 were laminated on top of the support material using a hot/cold laminator to obtain a smooth attached film surface (150 µm high). Then, the slide was exposed through an acetate photomask to UV light (5 s, 24 mW cm2, 345 nm) in the mask aligner and subsequently placed on a hot plate at 65 °C for 3 min.

The 3D master mold fabrication was finished by developing the Ordyl film using the developer solvent for 3 min. To replicate this mold, a poly (dimethylsiloxane) (PDMS) prepolymer mixture (a curing agent-to-PDMS ratio of 1:10, Sylgard®184, Dow Corning) was placed in a desiccator with a vacuum applied to remove bubbles. The mixture was then poured on top of the Ordyl master to fabricate a PDMS replica and heated overnight at 65 °C. The casted PDMS was peeled off carefully, and inlet and outlet holes were made using a Harris Uni-Core 0.5 mm puncher. A general view of the PDMS BiofilmChip used for biofilm growth and analysis is shown in Fig. 1a. The BiofilmChip includes several sets of independent chambers, each connected to two inlets (one for medium and one for bacterial inoculation), one prechamber, three different growth chambers (C1, C2, C3) and one outlet (Fig. 1b). Each growth chamber was 2 mm wide, 10 mm long and 150 µm high. The BiofilmChip unit was fabricated as three connected chambers (C1, C2 and C3) and considered representative with coherent replicates for straightforward analysis of a given sample.

Gold interdigitated sensors (Fig. 1b) were fabricated onto a glass coverslip to facilitate inspection under a confocal microscope and correlation to impedance measurements. The dimensions and characteristics of the interdigitated electrode were 16 pairs of gold fingers with 75 µm width and 75 µm gap between them. The design of these fingers was selected following the microfluidic chamber size (Fig. 1b). AZ5214 was spread using a spinner to create a uniform layer over the glass substrate. After that, the resin was exposed to UV light in the desired pattern. Then, it was reversed, followed by UV flood light exposure. Next, the glass coverslip was dipped into a solution of AZ Developer 400 K. Then, 20 nm chromium and 80 nm gold were thermally evaporated on glass. After this step, the glass slip was dipped into an AZ Remover 100 solution to remove the photoresist, leaving only the desired pattern's gold/chromium layer. For bonding to the PDMS microfluidic chamber, an O_2 plasma cleaner was used to activate both surfaces. PDMS slabs were carefully placed in contact with the glass slide and left on a hot plate to create permanent bonding. The PDMS microfluidic chamber chip was ready to use. Before every assay, the microfluidic device was exposed to UV/ozone for 15 min to make the surface hydrophilic and sterile. Then, the device was filled with sterile Milli-Q water.

Experimental setup

The BiofilmChip system operated in the three different biofilm formation stages (inoculation, growth and measurement). The final setup is shown in Fig. 1c. LB or TSB +0.2% glucose was stored in a 100 ml bottle connected through Tygon E-3603 tubing (1.5 mm diameter) (DD BioLab) to the microfluidic device. Tubes were attached to the chip by insertion into the inlet and outlet access holes. The medium was pumped through the system with a high-precision Ismatec IPC16 ISM933 multichannel peristaltic pump (Ismatec). Bubble traps (DTU Systems Biology, Technical University of Denmark) were added to the system to avoid the formation of bubbles inside the growth chambers. A constant flow rate of 11.4 µl/min for each set of three chambers was established. The system was filled with media through one inlet, and then, at the inoculation stage, a solution of bacteria ($A_{550} \approx 0.1$) or diluted hypotonic buffer sputum sample was pumped into the chip chamber through the other inlet.

At the start of the growth stage, the peristaltic pump was stopped for two hours to allow cell adherence to the glass surface. Then, the medium flowed through the chambers for 65–72 h. The system was previously

sterilized with 0.5% v/v sodium hypochlorite in water as previously described[53], and experiments were carried out at room temperature.

Confocal laser scanning microscopy and image analysis

Pseudomonas aeruginosa and *Staphylococcus aureus* nonfluorescent biofilms were stained with the LIVE/DEAD BacLight Bacterial Viability Kit (Thermo Scientific), consisting of SYTO9 and propidium iodide. Staining of the biofilms formed from sputum was performed with the Bacterial Viability and Gram Stain Kit (Biotium), which differentiates Gram-positive and Gram-negative bacteria. This kit comprises wheat germ agglutinin (WGA) coupled to a CF™-488 fluorophore that stains the walls of Gram-positive bacteria and the dye DAPI, which stains both Gram-negative and Gram-positive bacteria. Biofilms formed with *Pseudomonas aeruginosa* MK171 (expressing eGFP) were visualized under the microscope directly without staining.

All biofilms were visualized under a Zeiss LSM 800 confocal scanning laser microscope (CSLM) using 20X/0.80 air or 63X/1.4 oil objectives. Simulated fluorescence projections and orthogonal sections were generated using ImageJ software, and COMSTAT 2 software was used to quantify the biomass and thickness of the biofilms[54].

Biofilm treatment

Biofilms between 65 and 72 h old were treated for 16 or 24 h with different antibiotic concentrations while the medium flow was stopped. After the treatment, the flow was set at 11.4 µl/min for 30 min to wash and exclude detached bacteria affected by the antibiotic from the biofilm.

Impedance measurements and cell index calculation

We based our monitoring on the cell index (CI) parameter[55], as we wanted to use an independent, standardized parameter to compare measurements among different samples. The measurements were performed at 400 Hz as we detected bigger changes in bold diagram (see Supplementary Fig. 3).

$$CI(t) = \frac{Z_{(400,t)} - Z_{(400,t0)}}{Zn} \quad (1)$$

Where Zn is the corresponding impedance value at 400 Hz of medium with no cells, $Z_{(400,t)}$ is the measured impedance at 400 Hz at time point t of biofilm growth and $Z_{(400,t0)}$ is the background impedance 2 h after bacteria inoculation, before the biofilm started to grow.

The device used to record EIS values was an Agilent 4294 A 40 Hz–110 MHz precision impedance analyzer. This equipment allowed measuring the impedance along a range of frequencies with an oscilloscope level of 0.5 V. The impedance was measured in the module and phase format and plotted in Bode diagrams. Once the microfluidic device was connected, two impedance measurements were recorded each day, one during the morning and the second one during the afternoon.

Statistical analysis

Significant differences in biofilm biomass of the ciprofloxacin-treated biofilms vs. non-treated biofilms were calculated using an unpaired *t*-test with the GraphPad Prism 9.0 software. Correlation between Biomass and Cell Index parameters in the biofilm treatment was calculated using Pearson's correlation with the GraphPad Prism 9.0 software.

Reporting summary

Further information on research design is available in the Nature Research Reporting Summary linked to this article.

DATA AVAILABILITY

The authors declare that all relevant data supporting the findings of the study are available within the article and the Supplementary information file. Additional details are also available upon reasonable request.

Received: 9 March 2021; Accepted: 15 July 2021;
Published online: 03 August 2021

REFERENCES

1. Karunakaran, E., Mukherjee, J., Ramalingam, B. & Biggs, C. A. "Biofilmology": a multidisciplinary review of the study of microbial biofilms. *Appl. Microbiol. Biotechnol.* **90**, 1869–1881 (2011).
2. Flemming, H. C. & Wingender, J. The biofilm matrix. *Nat. Rev. Microbiol.* **8**, 623–633 (2010).
3. Lebeaux, D., Chauhan, A., Rendueles, O. & Beloin, C. From in vitro to in vivo models of bacterial biofilm-related infections. *Pathogens* **2**, 288–356 (2013).
4. Sharma, D., Misba, L. & Khan, A. U. Antibiotics versus biofilm: an emerging battleground in microbial communities. *Antimicrob. Resist. Infect. Control* **8**, 76 (2019).
5. Yebra, D. M., Kiil, S. & Dam-Johansen, K. Antifouling technology—past, present and future steps towards efficient and environmentally friendly antifouling coatings. *Prog. Org. Coat.* **50**, 75–104 (2004).
6. Lebeaux, D., Ghigo, J. M. & Beloin, C. Biofilm-related infections: bridging the gap between clinical management and fundamental aspects of recalcitrance toward antibiotics. *Microbiol. Mol. Biol. Rev.* **78**, 510–543 (2014).
7. Wolfmeier, H., Pletzer, D., Mansour, S. C. & Hancock, R. E. W. New perspectives in biofilm eradication. *ACS Infect. Dis.* **4**, 93–106 (2018).
8. Haney, E. F., Trimble, M. J., Cheng, J. T., Valle, Q. & Hancock, R. E. W. Critical assessment of methods to quantify biofilm growth and evaluate antibiofilm activity of host defence peptides. *Biomolecules* **8**, https://doi.org/10.3390/biom8020029 (2018).
9. Christensen, G. D. et al. Adherence of coagulase-negative staphylococci to plastic tissue culture plates: a quantitative model for the adherence of staphylococci to medical devices. *J. Clin. Microbiol.* **22**, 996–1006 (1985).
10. O'Toole, G. A. Microtiter dish biofilm formation assay. *J. Vis. Exp.* https://doi.org/10.3791/2437 (2011).
11. Harrison, J. J. et al. Microtiter susceptibility testing of microbes growing on peg lids: a miniaturized biofilm model for high-throughput screening. *Nat. Protoc.* **5**, 1236–1254 (2010).
12. Ceri, H. et al. The Calgary Biofilm Device: new technology for rapid determination of antibiotic susceptibilities of bacterial biofilms. *J. Clin. Microbiol.* **37**, 1771–1776 (1999).
13. Olivares, E. et al. The BioFilm ring test: a rapid method for routine analysis of *Pseudomonas aeruginosa* Biofilm formation kinetics. *J. Clin. Microbiol.* **54**, 657–661 (2016).
14. Chavant, P., Gaillard-Martinie, B., Talon, R., Hébraud, M. & Bernardi, T. A new device for rapid evaluation of biofilm formation potential by bacteria. *J. Microbiol. Methods* **68**, 605–612 (2007).
15. Sun, Y., Dowd, S. E., Smith, E., Rhoads, D. D. & Wolcott, R. D. In vitro multispecies Lubbock chronic wound biofilm model. *Wound Repair Regen.* **16**, 805–813 (2008).
16. Macia, M. D., Rojo-Molinero, E. & Oliver, A. Antimicrobial susceptibility testing in biofilm-growing bacteria. *Clin. Microbiol. Infect.* **20**, 981–990 (2014).
17. Nickel, J. C., Ruseska, I., Wright, J. B. & Costerton, J. W. Tobramycin resistance of *Pseudomonas aeruginosa* cells growing as a biofilm on urinary catheter material. *Antimicrob. Agents Chemother.* **27**, 619–624 (1985).
18. Goeres, D. M. et al. A method for growing a biofilm under low shear at the air-liquid interface using the drip flow biofilm reactor. *Nat. Protoc.* **4**, 783–788 (2009).
19. Lawrence, J. R., Swerhone, G. D. & Neu, T. R. A simple rotating annular reactor for replicated biofilm studies. *J. Microbiol. Methods* **42**, 215–224 (2000).
20. Azeredo, J. et al. Critical review on biofilm methods. *Crit. Rev. Microbiol.* **43**, 313–351 (2017).
21. Tolker-Nielsen, T. & Sternberg, C. Methods for studying biofilm formation: flow cells and confocal laser scanning microscopy. *Methods Mol. Biol.* **1149**, 615–629 (2014).
22. Musken, M., Di Fiore, S., Romling, U. & Haussler, S. A 96-well-plate-based optical method for the quantitative and qualitative evaluation of *Pseudomonas aeruginosa* biofilm formation and its application to susceptibility testing. *Nat. Protoc.* **5**, 1460–1469 (2010).
23. Rath, H., Stumpp, S. N. & Stiesch, M. Development of a flow chamber system for the reproducible in vitro analysis of biofilm formation on implant materials. *PLoS One* **12**, e0172095 (2017).
24. Musken, M. et al. Breaking the vicious cycle of antibiotic killing and regrowth of biofilm-residing *Pseudomonas aeruginosa*. *Antimicrob. Agents Chemother.*, https://doi.org/10.1128/AAC.01635-18 (2018).
25. van Duuren, J. et al. Use of single-frequency impedance spectroscopy to characterize the growth dynamics of biofilm formation in *Pseudomonas aeruginosa*. *Sci. Rep.* **7**, 5223 (2017).
26. Pires, L. et al. Online monitoring of biofilm growth and activity using a combined multi-channel impedimetric and amperometric sensor. *Biosens. Bioelectron.* **47**, 157–163 (2013).
27. Paredes, J., Becerro, S. & Arana, S. Comparison of real time impedance monitoring of bacterial biofilm cultures in different experimental setups mimicking real field environments. *Sens. Actuators B: Chem.* **195**, 667–676 (2014).

28. Sackmann, E. K., Fulton, A. L. & Beebe, D. J. The present and future role of microfluidics in biomedical research. *Nature* **507**, 181–189 (2014).
29. Benoit, M. R., Conant, C. G., Ionescu-Zanetti, C., Schwartz, M. & Matin, A. New device for high-throughput viability screening of flow biofilms. *Appl. Environ. Microbiol.* **76**, 4136–4142 (2010).
30. Zhang, X. Y., Sun, K., Abulimiti, A., Xu, P. P. & Li, Z. Y. Microfluidic system for observation of bacterial culture and effects on Biofilm formation at microscale. *Micromachines* **10**, https://doi.org/10.3390/mi10090606 (2019).
31. Straub, H. et al. A microfluidic platform for in situ investigation of biofilm formation and its treatment under controlled conditions. *J. Nanobiotechnol.* **18**, 166 (2020).
32. Janakiraman, V., Englert, D., Jayaraman, A. & Baskaran, H. Modeling growth and quorum sensing in biofilms grown in microfluidic chambers. *Ann. Biomed. Eng.* **37**, 1206–1216 (2009).
33. Cendra, M. D. M., Blanco-Cabra, N., Pedraz, L. & Torrents, E. Optimal environmental and culture conditions allow the in vitro coexistence of *Pseudomonas aeruginosa* and *Staphylococcus aureus* in stable biofilms. *Sci. Rep.* **9**, 16284 (2019).
34. Hall-Stoodley, L. & Stoodley, P. Evolving concepts in biofilm infections. *Cell Microbiol.* **11**, 1034–1043 (2009).
35. Hayward, W. A. et al. Pressure generated by syringes: implications for hydrodissection and injection of dense connective tissue lesions. *Scand. J. Rheumatol.* **40**, 379–382 (2011).
36. Ward, A. C., Connolly, P. & Tucker, N. P. *Pseudomonas aeruginosa* can be detected in a polymicrobial competition model using impedance spectroscopy with a novel biosensor. *PLoS One* **9**, e91732 (2014).
37. Inoue, H. Strategic approach for combating antimicrobial resistance (AMR). *Glob. Health Med.* **1**, 61–64 (2019).
38. Hall, C. W. & Mah, T. F. Molecular mechanisms of biofilm-based antibiotic resistance and tolerance in pathogenic bacteria. *FEMS Microbiol. Rev.* **41**, 276–301 (2017).
39. Coenye, T., Goeres, D., Van Bambeke, F. & Bjarnsholt, T. Should standardized susceptibility testing for microbial biofilms be introduced in clinical practice? *Clin. Microbiol. Infect.* **24**, 570–572 (2018).
40. Salek, M. M., Jones, S. M. & Martinuzzi, R. J. The influence of flow cell geometry related shear stresses on the distribution, structure and susceptibility of *Pseudomonas aeruginosa* 01 biofilms. *Biofouling* **25**, 711–725 (2009).
41. Wimpenny, J., Manz, W. & Szewzyk, U. Heterogeneity in biofilms. *FEMS Microbiol. Rev.* **24**, 661–671 (2000).
42. Reichhardt, C. & Parsek, M. R. Confocal laser scanning microscopy for analysis of *Pseudomonas aeruginosa* Biofilm architecture and matrix localization. *Front. Microbiol.* **10**, 677 (2019).
43. Stacy, A., McNally, L., Darch, S. E., Brown, S. P. & Whiteley, M. The biogeography of polymicrobial infection. *Nat. Rev. Microbiol.* **14**, 93–105 (2016).
44. Cendra, M. D. M. & Torrents, E. *Pseudomonas aeruginosa* biofilms and their partners in crime. *Biotechnol. Adv.* **49**, 107734 (2021).
45. Kidd, T. J. et al. Defining antimicrobial resistance in cystic fibrosis. *J. Cyst. Fibros.* https://doi.org/10.1016/j.jcf.2018.08.014 (2018).
46. Filkins, L. M. & O'Toole, G. A. Cystic fibrosis lung infections: polymicrobial, complex, and hard to treat. *PLoS Pathog.* **11**, e1005258 (2015).
47. Orazi, G. & O'Toole, G. A. *Pseudomonas aeruginosa* alters *Staphylococcus aureus* sensitivity to vancomycin in a Biofilm model of cystic fibrosis infection. *mBio* **8**, https://doi.org/10.1128/mBio.00873-17 (2017).
48. Orazi, G., Ruoff, K. L. & O'Toole, G. A. *Pseudomonas aeruginosa* increases the sensitivity of Biofilm-grown *Staphylococcus aureus* to membrane-targeting antiseptics and antibiotics. *MBio,* **10**, https://doi.org/10.1128/mBio.01501-19 (2019).
49. Musken, M. et al. Towards individualized diagnostics of biofilm-associated infections: a case study. *NPJ Biofilms Microbiomes* **3**, 22 (2017).
50. Crespo, A., Gavalda, J., Julian, E. & Torrents, E. A single point mutation in class III ribonucleotide reductase promoter renders *Pseudomonas aeruginosa* PAO1 inefficient for anaerobic growth and infection. *Sci. Rep.* **7**, 13350 (2017).
51. Blanco-Cabra, N. et al. Novel Oleanolic and Maslinic Acids derivatives as a promising treatment against bacterial biofilm in nosocomial infections: an in Vitro and in Vivo study. *ACS Infect. Dis.* https://doi.org/10.1021/acsinfecdis.9b00125 (2019).
52. Klausen, M. et al. Biofilm formation by *Pseudomonas aeruginosa* wild type, flagella and type IV pili mutants. *Mol. Microbiol.* **48**, 1511–1524 (2003).
53. Crespo, A., Blanco-Cabra, N. & Torrents, E. Aerobic vitamin B12 biosynthesis is essential for *Pseudomonas aeruginosa* class ii ribonucleotide reductase activity during planktonic and Biofilm growth. *Front. Microbiol.* **9**, 986 (2018).
54. Weiss Nielsen, M., Sternberg, C., Molin, S. & Regenberg, B. *Pseudomonas aeruginosa* and *Saccharomyces cerevisiae* biofilm in flow cells. *J. Vis. Exp.* https://doi.org/10.3791/2383 (2011).
55. Gutiérrez, D., Hidalgo-Cantabrana, C., Rodríguez, A., García, P. & Ruas-Madiedo, P. Monitoring in real time the formation and removal of Biofilms from clinical related pathogens using an impedance-based technology. *PLoS One* **11**, e0163966 (2016).

ACKNOWLEDGEMENTS

We thank Prof. Tim Tolker-Nielsen from Costerton Biofilm Center, University of Copenhagen, for providing the *P. aeruginosa* MK171 strain. This work was supported in part through grants to ET from the Ministerio de Ciencia, Innovación y Universidades (BIO2015-63557-R and RTI2018-098573-B-100) (MINECO/FEDER), the Generalitat de Catalunya (2017 SGR1079 and CERCA program), and the Spanish Cystic Fibrosis Foundation and La Caixa Foundation. The authors want to acknowledge MicroFabSpace and the Microscopy Characterization Facility, Unit 7 of ICTS "NANBIOSIS" from CIBER-BBN at IBEC. This research was supported by the Networking Biomedical Research Center (CIBER), Spain. CIBER is an initiative funded by the VI National R&D&i Plan 2008–2011, Iniciativa Ingenio 2010, Consolider Program, CIBER Actions, and the Instituto de Salud Carlos III (RD16/0006/0012), with the support of the European Regional Development Fund. This work was funded by the CERCA Programme and by the Commission for Universities and Research of the Department of Innovation, Universities, and Enterprise of the Generalitat de Catalunya (2017 SGR 1079). This work was developed in the context of AdvanceCat and Base3D with the support of ACCIÓ (Catalonia Trade and Investment; Generalitat de Catalunya) under the Catalonian ERDF operational program (European Regional Development Fund) 2014–2020. This work was funded by the Spanish Ministry of Economy and Competitiveness (MINECO) through the projects MINDS (Proyectos I+D Excelencia + FEDER): TEC2015-70104-P, CTQ2016-75870-P.

AUTHOR CONTRIBUTIONS

E.T. and J.S. conceived the idea; N.B-C., M.J.L-M., B.V.A-J. J.S. and E.T. conceived and designed the experimental studies; N.B-C., M.J.L-M., B.V.A-J. conducted the experiments; M.T.M-G supplied the clinical isolates; N.B-C., M.J.L-M., J.S. and E.T wrote the manuscript with inputs from B.V.A-J. and M.T.M-G. All authors read and approved the manuscript.

COMPETING INTERESTS

The authors declare no competing interests.

ADDITIONAL INFORMATION

Supplementary information The online version contains supplementary material available at https://doi.org/10.1038/s41522-021-00236-1.

Correspondence and requests for materials should be addressed to E.T.

Reprints and permission information is available at http://www.nature.com/reprints

Publisher's note Springer Nature remains neutral with regard to jurisdictional claims in published maps and institutional affiliations.

Material Suplementario

A new BiofilmChip device for testing biofilm formation and antibiotic susceptibility

Núria Blanco-Cabra[1,¶], Maria José López-Martínez[2,3,4,¶], Betsy Verónica Arévalo-Jaimes[1], María Teresa Martin-Gómez[5], Josep Samitier[2,3,4] and Eduard Torrents[1,6,*]

Supplementary Tables and Figures

Supplementary Table 1. Ciprofloxacin Minimal Inhibitory Concentration (MIC) for the *P. aeruginosa* strains used.

***P. aeruginosa* strains**	**Ciprofloxacin MIC (µg/ml)**
PAO1	0.25
PAET1	2

Supplementary Table 2. Percentage of dead cells (stained in red in the Live/Dead BacLight Bacterial Viability Kit) in the total biofilm biomass of the *P. aeruginosa* PAO1 and PAET1 biofilms treated with ciprofloxacin.

***P. aeruginosa* biofilm Strain**	**Treatment**	**% Dead cell biomass / Total biomass**
PAO1	0 µg/ml ciprofloxacin	10.99 % ± 1.35
	2 µg/ml ciprofloxacin	30.17 % ± 1.92
PAET1	0 µg/ml ciprofloxacin	15.94 % ± 4.58
	20 µg/ml ciprofloxacin	73.42 % ± 3.51

Supplementary Table 3. Sputum samples from cystic fibrosis patients were used to grow the biofilms, and the cell index was calculated after antibiotic treatment. Information concerning the bacterial species identified and their antibiotic sensitivity was obtained from the Microbiology Service at the Vall d'Hebron Barcelona Hospital Campus.

Sputum sample	**Bacterial species identified**	**Antibiotic treatment (sensitivity)**	**Cell Index (CI) change after antibiotic treatment**
I	*P. aeruginosa*	(Not reported)	(Not used)
II	*P. aeruginosa* and *S. aureus*	(Not reported)	(Not used)
III	*P. aeruginosa*	(Not reported)	(Not used)
IV	*P. aeruginosa* and *S. aureus*	(Not reported)	(Not used)
V	*S. aureus*	Ciprofloxacin (Susceptible) Ampicillin (Resistant)	- 0.06 + 0.07
VI	*S. aureus*	Ampicillin (Susceptible) Ciprofloxacin (Resistant)	- 0.93 + 0.72
VII	*P. aeruginosa*	Colistin (Susceptible) Ampicillin (Resistant)	- 0.07 + 0.04

Supplementary Fig. 1. Results of computational fluid dynamics (CFD) simulations to show the effect of a prechamber when loading the sample manually. Figures show contours of velocity (m/s) on the surface of the designed biofilm chip without (a) and with (b) a prechamber.

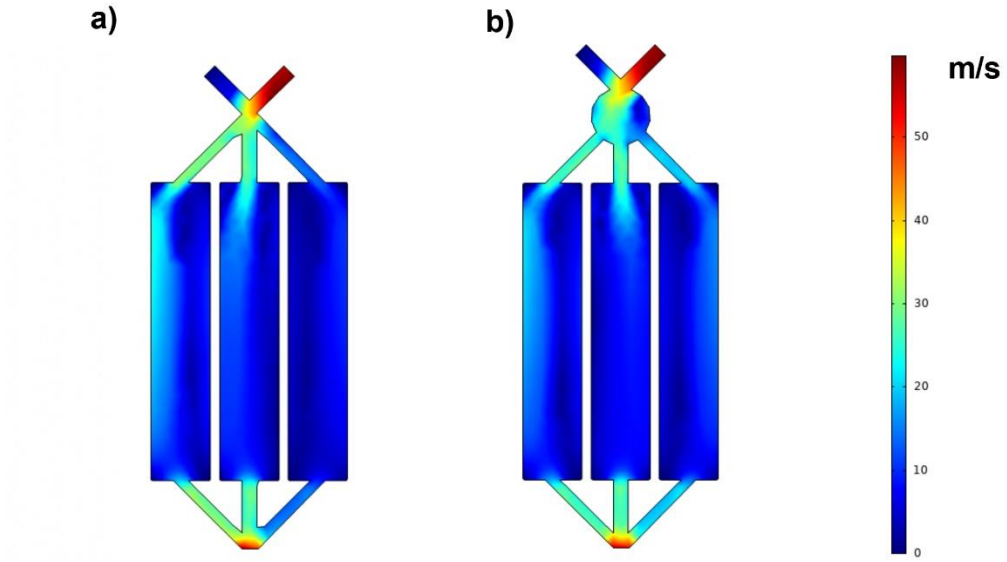

Supplementary Fig. 2. Confocal microscopy images of different sputum samples stained with the Bacterial Viability and Gram Stain Kit. Scale bars represents 10 µm.

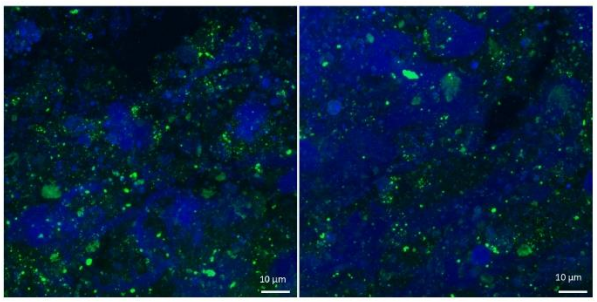

Supplementary Fig. 3. Bode diagram for a treated BiofilmChip chamber. Sweep frequency measurement was between 4 Hz - 400 kHz.

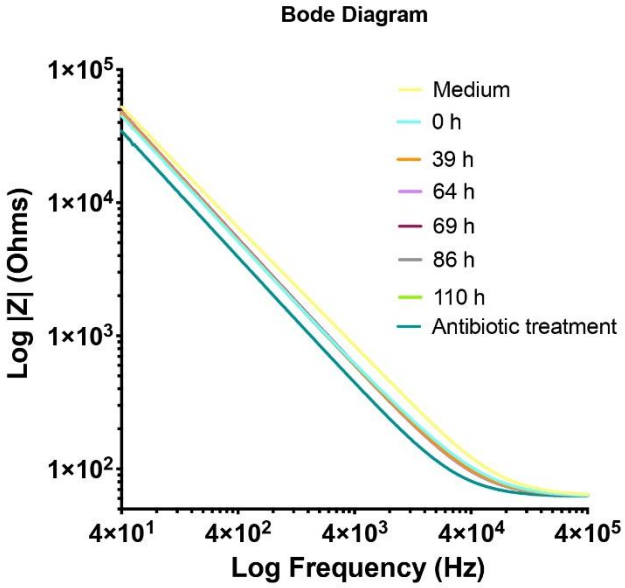

Supplementary Fig. 4. Cell Index change before and after treating the biofilms formed from cystic fibrosis patients' sputa under different antibiotics.

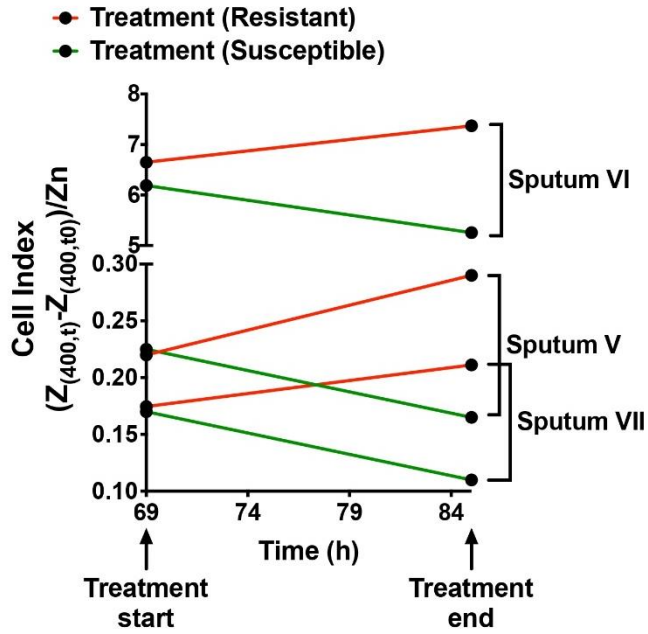

Discusión global de los resultados obtenidos

El impacto a nivel de global de los biofilms en la salud humana es indiscutible. Para el sector financiero representa una carga económica de alrededor de €350 mil millones ($380 billones) por año [68]. Para el paciente con enfermedad crónica implica visitas recurrentes al médico, múltiples rondas de tratamiento, reducción de la calidad de vida e incluso riesgo de muerte [45]. A pesar de esto, actualmente existen varias limitaciones que dificultan el manejo adecuado de las infecciones causadas por biofilms.

1. Influencia de diferentes variables en las características de biofilms monomicrobianos y polimicrobianos

La diversidad de los biofilms presentes en la naturaleza depende de muchos factores que influencian su crecimiento y composición [45]. Por ejemplo, la superficie de adhesión, la disponibilidad de nutrientes, los gradientes fisicoquímicos, las interacciones microbianas y las condiciones hidrodinámicas [45]. Esto hace que el diseño de métodos *in vitro* que recreen las condiciones ambientales naturales para el estudio de biofilms sea complicado [45]. Sin embargo, la selección rigurosa de las condiciones experimentales dará como resultado conclusiones relevantes para el manejo de las enfermedades [45, 243]. Por lo tanto, resulta imprescindible la identificación de variables que influencian la formación y, por ende, las características de los biofilms.

En el presente trabajo se demostró que variables como el medio de cultivo o el orden de colonización de las especies tienen un impacto en la virulencia de los microorganismos que crecen en biofilms, estos resultados se exponen en detalle en el artículo 1 y el artículo 2.

1.1 Impacto del medio de cultivo en la formación, susceptibilidad y virulencia de biofilms de *C. parapsilosis*

En el caso de las levaduras, una preocupación importante en el estudio de los biofilms es la inconsistencia en la selección de los medios de cultivo para su formación y crecimiento [244]. Dicha inquietud no es injustificada, ya que como se evidencia en el artículo 1, la disponibilidad de nutrientes proporcionada por el medio de cultivo tiene un impacto

importante en la patogenicidad de *C. parapsilosis,* tanto en estado plantónico como en biofilm.

Un resumen de las ventajas patogénicas específicas proporcionadas por cada medio de cultivo evaluado (RPMId, TSB, BHI y YPD) se presenta en la Tabla 1. En primer lugar, se encontró que el medio de cultivo influencia el crecimiento de *C. parapsilosis*. Medios ricos en glucosa, como YPD, favorecen una mayor acumulación de biomasa (Figura 1), pero afectan la filamentación (Figura 2) y la actividad metabólica de las células (Figura 3). Por su parte, RPMId induce un mayor número de pseudohifas en los biofilms (Figura 2). Este efecto fue más notorio cuando los biofilms se formaron al fondo del pocillo de una placa de microtitulación o en celdas de flujo, condiciones en las que las células estaban expuestas a menor disponibilidad de oxígeno y mayor tensión cortante del fluido.

También se registraron variaciones en la susceptibilidad antimicrobiana de *C. parapsilosis* asociadas con la disponibilidad de nutrientes. La MIC_{50} de la anfotericina B (AmB) en los cultivos planctónicos fue mayor en YPD (0,25 mg/mL), en comparación con los otros medios (0,125 mg/mL). Con respecto a los biofilms, la adición de AmB (1,25 mg/mL) redujo eficazmente la actividad metabólica en todos los casos, pero en distinta proporción según el medio de cultivo empleado en el proceso de formación (Figura 3). Los medios de cultivo que favorecieron una mayor producción de carbohidratos confirieron una protección superior frente la actividad de AmB (Figura 4). Biofilms formados en medio BHI presentaron un alto nivel de carbohidratos tanto en la ECM como en la pared celular, y mostraron una baja reducción de la actividad metabólica (34%) después del tratamiento con AmB (1,25 mg/mL).

Finalmente, se encontró que el crecimiento de *C. parapsilosis* en diferentes medios de cultivo influye en su virulencia, y, por consiguiente, en la supervivencia de larvas de *Galleria mellonella* infectadas con esta levadura (Figura 5). Para esto, las larvas fueron inyectadas con cultivos planctónicos y suspensiones de biofilms cultivadas en cada medio, y monitoreadas durante 48 h. Cuando el inoculo empleado fue de $5x10^7$ CFUs/mL de *C. parapsilosis*, los medios TSB y YPD aumentaron la virulencia de los cultivos plantónicos, causando una mortalidad del 29% versus el 0-7% en los demás medios. Las suspensiones de biofilm, a la misma concentración, tuvieron un efecto más pronunciado sobre la supervivencia de las larvas en todos los casos, con una tasa de mortalidad que ascendió al 40-50% para los medios RPMId, BHI y YPD, y al 71% cuando el medio empleado fue TSB.

Estos resultados confirman que las adaptaciones metabólicas juegan un papel importante en la patogenicidad de esta levadura [245]. Además, reiteran la importancia de entender cómo diferentes condiciones de crecimiento afectan a los microorganismos patógenos para poder definir protocolos para su investigación. Por ejemplo, considerando que el medio BHI estimula una mayor producción de carbohidratos en los biofilms de *C. parapsilopsis*, este puede ser empleado en el estudio de enzimas o compuestos degradadores de la ECM. De la misma manera, la identificación de condiciones ambientales importantes en el sitio de infección que influyen en la virulencia del microorganismo puede llevar a considerar nuevas aproximaciones de estudio. Teniendo en cuenta el impacto de la glucosa en los biofilms de *C. parapsilosis*, el estudio de las infecciones asociadas a catéteres causadas por esta levadura podría realizarse considerando dos escenarios diferentes: uno donde la glucosa disponible corresponde a la concentración normal en sangre (0.06-0.1%) [246], y otro donde la concentración de glucosa es alta (10-30%) debido al uso de soluciones de nutrición parenteral [247].

Es así como la investigación básica puede generar información valiosa para producir avances en el campo de los biofilms, ya que a pesar del esfuerzo de los investigadores y el aumento en el número de publicaciones (alrededor de 40000 artículos para el año 2019) [248], aún existen vacíos de conocimiento que limitan las traslación de medidas de prevención y erradicación [45]. No obstante, es importante mencionar que la mayoría de información disponible proviene de estudios de biofilms monomicrobianos, que generalmente se realizan con un microorganismo modelo [46, 51], relegando la naturaleza polimicrobiana de los biofilms en las infecciones.

1.2 Efectos de prioridad en biofilms de *C. albicans* y *P. aeruginosa* PAET1

El estudio de biofilms polimicrobianos puede representar retos únicos en los diseños experimentales, aumentando el número de variables a considerar [51]. Por ejemplo, estudios de ecología microbiana han demostrado que procesos históricos de formación de la comunidad microbiana, como el orden de llegada de las especies, influyen en las interacciones que se establecen entre sus miembros [249, 250]. Estas interacciones, denominadas efectos de prioridad, han sido poco estudiadas en el contexto de microorganismos patógenos. En la vida real es poco probable que las coinfecciones sean resultado de una colonización simultánea [251], sin embargo la mayoría de los protocolos experimentales utilizan esta aproximación.

Por esta razón, en el artículo 2 se exploraron los efectos de prioridad presentes en los biofilms polimicrobianos de *C. albicans* y *P. aeruginosa*. Para ello, tres protocolos diferentes de formación de biofilms fueron establecidos según el orden de colonización de cada especie (Figura 1): 1) 1Ca2Pa, cuando el inóculo inicial de *C. albicans* es seguido por la adición de *P. aeruginosa* 6 h después; 2) 1Pa2Ca, cuando el Inóculo inicial de *P. aeruginosa* es seguido por la adición de *C. albicans* 6 h después; y 3) CaPa, cuando el inóculo inicial contiene las dos especies, *C. albicans* y *P. aeruginosa.* Biofilms monomicrobianos de cada microorganismo fueron incluidos como controles y designados como Ca para *C. albicans* y Pa para *P. aeruginosa.* En todos los casos, ambos microorganismos fueron inoculados en la misma proporción, con una concentración que correspondía a ~10^6 CFUs/mL.

La cuantificación de CFUs permitió observar que el primer organismo en colonizar tiene la ventaja de mayor disponibilidad de superficies de adhesión, lo cual se refleja en la biomasa al final del experimento (Figura 1). Por ende, la condición 1Ca2Pa presentó la mayor abundancia relativa de *C. albicans* (13.7%), mientras que la condición 1Pa2Ca mostró una mayor cantidad de *P. aeruginosa* (97.7%), en comparación con los otros biofilms polimicrobianos.

Con el fin de elucidar si los efectos de prioridad influían en la virulencia de los biofilms, se realizaron experimentos con la línea celular de adenocarcinoma alveolar A549 (ATCC CCL-185) (Figura 3). Los protocolos de formación de biofilms fueron ligeramente modificados, reduciendo el tiempo entre los eventos de colonización (4h), la cantidad del inóculo (~10^5 CFUs/mL) y el tiempo total del experimento (24 h). También se incluyó un control adicional de cada microorganismo (Pa 2x y Ca 2x) inoculado al doble de la concentración (~10^6 CFUs/mL). De esta forma, se encontró que cuando la colonización era sucesiva se producían biofilms polimicrobianos estadísticamente más virulentos que cuando los microorganismos eran inoculados simultáneamente (Figura 4). Este efecto fue más marcado en la condición 1Ca2Pa, con una reducción en la viabilidad celular de 1 Log_{10} células/mL.

Estos resultados indican que la presencia de *C. albican*s puede afectar el resultado de las infecciones de *P. aeruginosa*. Sin embargo, la incógnita respecto a la inclusión del tratamiento antifúngico en el manejo de estas coinfecciones continúa siendo una pregunta clave por responder. El cumplimiento de este objetivo requerirá de aproximaciones que consideren y evalúen la presencia de interacciones microbianas que influencian la virulencia y susceptibilidad de los biofilms. Ya que se ha demostrado que las interacciones

entre los microorganismos influyen en la repuesta del huésped, la resistencia a los tratamientos y la progresión de la enfermedad [207].

Finalmente, se evalúo la presencia de alteraciones en la susceptibilidad antimicrobiana de los microorganismos debido a los efectos de prioridad (Figura 5). Con respecto a *P. aeruginosa*, no se encontró alteraciones en la susceptibilidad a meropenem (MER) en biofilms polimicrobianos formados tras la colonización sucesiva de los microorganismos (1Ca2Pa y 1Pa2Ca) en comparación con sus biofilms monomicrobianos (Pa). Sin embargo, la inoculación simultánea de ambas especies (CaPa) sí conlleva una reducción en la eficacia antimicrobiana del tratamiento. Adicionalmente, se demostró que la inclusión de N-acetilcisteína, como agente que afecta la estabilidad de la ECM, pueden ser una alternativa interesante en el manejo de coinfecciones, al presentar una eficacia independiente de los efectos de prioridad.

Los resultados obtenidos en este trabajo demuestran que el orden de colonización es un factor importante en el establecimiento de las interacciones entre estos microorganismos. Por ende, la evaluación de susceptibilidad de los biofilms polimicrobianos de estas dos especies frente a agentes terapéuticos, tanto actuales como en desarrollo, debería incluir esta variable. Si bien los eventos de colonización probablemente son paciente-específicos e imposibles de descifrar *a posteriori*, la elección de tratamientos cuya eficacia no se vea alterada por los efectos de prioridad aumentará la probabilidad de éxito en el manejo de las coinfecciones. En este contexto, el uso de moléculas como la N-acetilcisteína se convierten en una alternativa prometedora.

2. Interacciones microbianas inter-reino entre *C. albicans* y las bacterias patógenas *P. aeruginosa* y *S. aureus*

Adicional a los efectos de prioridad, el estudio de biofilms polimicrobianos de *C. albicans* y *P. aeruginosa* PAET1 presentado en el artículo 2 permitió identificar otros tipos de interacciones inter-reino. En primer lugar, interacciones físicas de adhesión entre la bacteria y el hongo se observaron en los biofilms polimicrobianos independiente del orden de llegada de las especies (Figura 2). Estos hallazgos recalcan la importancia de incluir hongos en el estudio de las infecciones causadas por bacterias. El gran tamaño de las células de *C. albicans* y la capacidad de *P. aeruginosa* de adherirse a ellas dio como resultado

biofilms estructuralmente diferentes a aquellos producidos únicamente por la bacteria (Figura 2).

Por otra parte, se encontró que la inoculación simultánea (CaPa) genera competencia por la superficie de adhesión, lo que resulta en biofilms con mayor mortalidad de *C. albicans* en comparación con sus biofilms monomicrobianos (Ca) (Figura suplementaria 1). Esto concuerda con la relación antagónica comúnmente descrita entre estos microorganismos, donde generalmente *P. aeruginosa* resulta como contendiente victorioso [231, 252-256]. Curiosamente, los biofilms de la condición CaPa presentaron menor virulencia en los experimentos con células A549, en comparación con los biofilms polimicrobianos formados mediante inoculación sucesiva de los microorganismos (1Ca2Pa y 1Pa2Ca) (Figura 4).

Los resultados también sugieren que la presencia de *P. aeruginosa* en los biofilms polimicrobianos puede ofrecer protección a *C. albicans* contra el antifúngico CAS (5 µg/mL) (Figura 5), independientemente del orden de colonización de las especies. Dicho efecto protector parece estar asociado con la ECM producida por *P. aeruginosa* (Figura suplementaria 3).

No obstante, las interacciones microbianas son complejas y dinámicas [257], requiriendo el uso de distintos enfoques para su completa caracterización. Por ejemplo, desde hace décadas se sabe que *C. albicans* incrementa la virulencia de *S. aureus*, por lo que la coinfección con ambas especies resulta en mayor mortalidad [240]. Hoy en día, detalles del sinergismo letal aún permanece pendientes por descifrar. Aunque recientemente se identificó a la toxina α como la molécula efectora de la virulencia de *S. aureus*, y la neutralización del medio y la depleción de ribosas como los mecanismos de activación inducidos por *C. albicans* [133, 166, 258].

En el artículo 3 se exponen los resultados del estudio de las interacciones no físicas presentes en el co-cultivo de estas dos especies. El ensayo de proximidad evaluó el crecimiento de las colonias de ambos microorganismos en agar sólido, a seis distancias diferentes y durante 9 días (Figura 1). Se encontró que la proximidad con *S. aureus* estimulaba el crecimiento de *C. albicans* (Figura suplementaria 1). A su vez, *C. albicans* indujo la formación de nuevas colonias de *S. aureus* que con el paso del tiempo cubrían y desbordaban la colonia original (Figura 1). Dicho efecto también se observó cuando *S. aureus* crecía cerca de *C. parapsilosis*, aunque en menor grado, indicando cierta restricción al género *Candida*, ya que no se produjo con ninguna de las bacterias *S. epidermidis*,

Streptococcus mutans, *E. faecalis* y *E. coli* (Figura 2). En el caso contrario, se encontró que *C. albicans* también induce la formación de estas variantes en *S. epidermidis* y *E. coli* (Figura suplementaria 2).

La aparición de los nuevos fenotipos de *S. aureus* en respuesta a la presencia de *C. albicans* requirió de disponibilidad inicial de glucosa y coincidió con la neutralización progresiva del medio por parte del hongo, aunque la manipulación artificial del pH también indujo el mismo efecto (Figura 3 y Figura 4). La neutralización del pH del medio por parte de *C. albicans* durante el crecimiento de este consorcio inter-reino ha sido asociada con la activación sostenida del sistema *agr* de *S. aureus*, y por ende con la secreción del efector citolítico α-toxina [133]. Por lo tanto, se procedió a evaluar la virulencia de las variantes fenotípicas.

Para ello, se utilizó el modelo de infección *G. mellonella* y se analizó cambios de la expresión génica mediante qPCR (Figura 5). Tras 10 días de crecimiento en un ensayo de proximidad, las colonias de *S. aureus* (Figura 5 variantes 1-6) y los respectivos controles monocultivo (Figura 5 variantes 7 y 8) fueron aislados. Nuestros estudios han demostrado que las variantes 1 y 2, son estadísticamente más patogénicas (86-100% mortalidad de las larvas) y expresan en mayor proporción *agrA* y *RNAIII*, con respecto al control 8. Estas dos variantes se generaron en la posición más próxima a *C. albicans*, y por ende estuvieron expuestas a la neutralización del medio por más tiempo. Lo que indica que *C. albicans* aumenta la virulencia de *S. aureus* mediante la inducción progresiva de variantes fenotípicas con mayor expresión de factores de virulencia.

Nuestros resultados permiten entender mejor la asociación de dos microorganismos presentes en coinfecciones de gran relevancia clínica. Por consiguiente, se propuso un modelo integrativo de las interacciones metabólicas que podrían estar favoreciendo este proceso, según la literatura actualmente disponible (Figura 6). Brevemente, se hipotetiza que en condiciones de disponibilidad de glucosa, *S. aureus* convierte el piruvato en acetato y lo secreta al medio [259], lo que disminuye considerablemente el pH [164]. *C. albicans* usa el acetato como precursor de acetil-coA en diferentes rutas metabólicas [260], lo que, sumado a la producción de amonio tras el metabolismo de GlcNAc y/o aminoácidos, ayuda a neutralizar el pH [261-263]. Por otra parte, el acetato induce estrés oxidativo en *C. albicans*, induciendo el consumo de ribosas en la ruta de las pentosas fosfato, para producir el NADPH requerido en la síntesis de glutatión [264-266]. La neutralización del pH y la

depleción de ribosa, como ha sido reportado, activan el sistema *agr* de *S. aureus*, aumentando al producción de toxina α, y por ende su virulencia [133, 166].

Por lo tanto, el sinergismo letal producto de la sociedad de *C. albicans* y *S. aureus* sería el resultado de una serie de interacciones metabólicas mediadas por cambios ambientales. Tal como lo evidencia la reversión del fenotipo de las variantes de colonia cuando son sembradas en nuevas placas de agar donde los estímulos externos generados en el co-cultivo están ausentes (Figura 5). Aunque se desconoce cuál es la ventaja adaptativa que favorece la replicación de las variantes fenotípicas de *S. aureus* sobre las colonias originales en estas condiciones, la conexión entre metabolismo y virulencia es cada vez más evidente. De hecho, en el caso de *S. aureus*, distintos reguladores metabólicos que influencian la expresión de factores de virulencia han sido descritos [259]. El sistema *agr*, es un sistema *quorum sensing* que desempeña múltiples funciones regulatorias en la virulencia de *S. aureus*, entender cómo funciona en contextos de interacciones polimicrobianas ayudará al desarrollo de nuevas opciones terapéuticas para el manejo de las coinfecciones. Al final, entre más se descifran las interacciones microbianas, más claro se vuelve el hecho de que para lograr un tratamiento efectivo de las coinfecciones es necesario atacar la comunidad como un todo [267].

3. Métodos para evaluar la eficacia de terapias antibiofilm

Por lo general, las pruebas de susceptibilidad antimicrobiana se realizan de manera rutinaria con microorganismos en estado plantónico, previo aislamiento de la especie de interés [61, 71, 268]. Aunque la necesidad de cambiar el paradigma se vuelve cada vez más irrefutable, la implementación práctica de las pruebas de susceptibilidad en biofilms requiere de plataformas y métodos confiables que permitan su ejecución. La presente tesis evaluó el funcionamiento de dos métodos diferentes para la realización de pruebas de susceptibilidad en biofilms.

3.1 Tinciones de viabilidad y vitalidad en biofilms de *C. parapsilosis*.

Una de las opciones para el estudio de biofilms son los métodos de lectura basados en fluorescencia, gracias al amplio repertorio disponible de tinciones [45]. Sin embargo, en lo que respecta a la investigación con levaduras, no existe consenso ni pautas establecidas para su aplicación.

En el artículo 4, se evaluó el rendimiento y la utilidad de dos tinciones de viabilidad, Syto 9 (S9) y Naranja de tiazol (TO, por sus siglas en inglés), y dos tinciones de vitalidad, Diacetato de fluoresceína (FDA, por sus siglas en inglés) y FUN-1, en células planctónicas de *C. parapsilosis* y biopelículas tratadas con AmB. Tras la cuantificación bioinformática de la intensidad de fluorescencia a partir de las imágenes de microscopía, se encontró que S9, TO y FDA mostraban diferencias de permeabilidad celular no asociadas con la viabilidad/vitalidad celular. Este comportamiento estuvo presente tanto en la tinción de células plantónicas como de biofilms (Figura 1, Figura 3 y Figura 4). Como resultado se obtuvieron valores de biomasa celular y porcentajes de viabilidad/vitalidad no reales de la eficacia de AmB (2.5 µg/ml) como tratamiento antibiofilm (Tabla 1). Estas irregularidades fueron detectadas gracias a la inclusión de la tinción de pared celular, Blanco de calcoflúor (CW, por sus siglas en inglés), la cual permitió corregir los valores de biomasa celular.

Los problemas de permeabilidad de S9 y TO parecen estar asociados a diferencias estructurales inherentes de cada morfotipo celular, siendo más pronunciada en las pseudohifas que las blastósporas (Figura 3). En el caso de FDA, la baja penetrabilidad fue más generalizada. Contradictoriamente, el tratamiento con AmB aumentó la permeabilidad celular, incrementando la cantidad de células teñidas en los biofilms tratados en comparación con los controles (Figura 4). Por el contrario, el colorante FUN-1 demostró un correcto funcionamiento en la determinación de células metabólicamente activas, con resultados similares al uso de PrestoBlue (37% vs 39%) (Figura 2 y Figura 4).

Estos resultados resaltan la importancia de evaluar el funcionamiento de tinciones en la especie de interés antes de su implementación, especialmente cuando se trata de levaduras con dimorfismo o polimorfismo. Para ello, se pueden realizar evaluaciones microscópicas que utilicen imágenes de campo claro o tintes de membrana o pared celular como controles de visualización. Sin embargo, la elección del control de visualización debe realizarse considerando las características del tratamiento que será empleado, ya que algunos agentes terapéuticos pueden inducir cambios en la composición y estructura de la membrana o pared celular [215, 269, 270].

Por lo general, los modelos *in vitro* dinámicos usados en el estudio de biofilms, incluyendo los dispositivos de microfluídica, son sistemas cerrados que utilizan métodos de microscopía como mecanismo de lectura [45]. En este escenario, la correcta selección de las tinciones de fluorescencia resulta imprescindible. Solo así se podría identificar de

manera confiable tratamientos efectivos para la erradicación de biofilms, o incluso desarrollar nuevos métodos para evaluar su susceptibilidad.

3.2 El BiofilmChip: Una nueva tecnología para la evaluación de la susceptibilidad de biofilms

La comunidad científica es consciente de que se necesitan nuevos modelos *in vitro* sencillos, rápidos, económicos y de fácil interpretación que puedan ser implementados en los laboratorios de diagnóstico clínico [69, 243]. Es así como constantemente nuevos dispositivos son propuestos, especialmente en el campo de la microfluídica [45]. Estas plataformas trabajan con fluidos en la microescala, lo que provee condiciones controladas de flujo laminar y reduce los requerimientos de volumen de reactivos y muestras [45]. Además, los materiales usados en el proceso de fabricación permiten flexibilidad en el diseño [45]. En este contexto, los dispositivos de microfluídica han permitido la incursión de nuevas técnicas de monitoreo de biofilms no invasivas, de fácil lectura y sin la necesidad de equipos complejos ni personal entrenado [45].

Una de las técnicas propuestas como alternativa para el monitoreo de biofilms es la Espectroscopía de Impedancia Eléctrica (EIS, por sus siglas en inglés), la cual mide cambios en la resistencia de un sistema electroquímico cuando se aplica un voltaje [271]. De esta manera, la EIS permite registrar cambios en la densidad de células adheridas a un electrodo [271]. Aunque su utilidad en el campo de los biofilms ha sido demostrada en modelos *in vitro*, estos sistemas eran estáticos [272, 273]. Se sabe que los biofilms formados en condiciones dinámicas se asemejan más a los biofilm presentes naturalmente en las infecciones, siendo una opción más realista para realizar pruebas de susceptibilidad [274].

En el artículo 5, se presenta el BiofilmChip, una plataforma de microfluídica que permitió monitorear la formación de biomasa durante el establecimiento de un biofilm y evaluar tratamientos antimicrobianos utilizando impedancia. Este dispositivo se diseñó, en colaboración con el grupo de Nanobioingienería del Instituto de Bioingeniería de Cataluña (IBEC), como un modelo dinámico que utiliza el montaje convencional de un ensayo de flujo lateral (Figura 1). Su fabricación se realizó mediante la adhesión de un cubreobjetos de vidrio a un molde de polidimetilsiloxano (PDMS) que contenía un set de cámaras a microescala (Figura 1). El vidrio incluía un electrodo interdigitado que se alineaba con las

cámaras, de manera que el biofilm se formaba en su superficie y podía ser estudiado mediante microscopía confocal o impedancia.

El diseño del BiofilmChip requirió la fabricación de 5 prototipos, en los cuáles se evaluaron modificaciones de las dimensiones y geometría de la cámara, y la inclusión de una pre-cámara. El modelo final fue seleccionado considerando la formación de biofilms uniformes y viables de la cepa de laboratorio *P. aeruginosa* PAO1 (Figura 2 y Figura suplementaria 1). Este incluyó una pre-cámara que distribuye el medio en tres cámaras que actúan como replicas técnicas. La homogeneidad de los biofilms a lo largo de la cámara, entre cámaras y entre dispositivos confirmó la robustez del diseño del BiofilmChip (Figura 3). Así mismo, la formación de biofilms monomicrobianos a partir de aislamientos clínicos y biofilms polimicrobianos a partir de muestras de esputo de pacientes con FQ, evidenció la versatilidad del dispositivo (Figura 3 y Figura 4). Esto expande su potencial aplicabilidad a otras muestras clínicas (orina, líquido cefalorraquídeo, lavados broncoalveolares, etc.) e incluso a inóculos provenientes de superficies contaminadas, como dispositivos médicos.

Por otra parte, el uso de la tinción *Live and Dead* tras el tratamiento de cepas de *P. aeruginosa* con ciprofloxacina, evidenció que el BiofilmChip permitía registrar cambios en la biomasa celular asociados a la susceptibilidad microbiana (Figura 3). Sin embargo, las técnicas de microscopía son costosas y requieren de equipo especializado y personal entrenado. Por ende, se procedió a validar el uso de impedancia como método alternativo de lectura en el BiofilmChip. Para esto se monitoreó el crecimiento y la respuesta a ciprofloxacina de un biofilm de una cepa fluorescente de *P. aeruginosa* mediante microscopía e impedancia simultáneamente, y se compararon los resultados (Figura 5). Se encontró que las variaciones impedimétricas son lo suficientemente sensibles para medir la respuesta de los biofilms a la exposición a antibióticos, en una manera dosis-dependiente. Además, en las etapas iniciales de formación del biofilm, la impedancia resultó ser un método de lectura más sensible y preciso que las técnicas de microscopía.

En conclusión, el BiofilmChip es una plataforma dinámica que permite la formación de biofilms directamente a partir de muestras clínicas, proporcionando condiciones que se asemejan a las encontradas en infecciones naturales. Además, posee un método de lectura rápido y sencillo que permite monitorear el crecimiento y los cambios de biomasa asociados a efectividad del tratamiento. Todo esto en conjunto, hace de este dispositivo una herramienta prometedora para la caracterización de biofilms en el contexto clínico, abriendo la posibilidad de evaluar la susceptibilidad de las infecciones polimicrobianas de

manera personalizada. Lo cual es sumamente relevante si se considera que el diagnóstico individualizado de la resistencia de los biofilms en pacientes con infecciones crónicas incrementa la efectividad del tratamiento [275]. Esto se logra cuando la elección del régimen terapéutico deja de ser empírica y pasa a ser basada en evidencia verídica y confiable.

4. Nuevas estrategias antibiofilm

La efectividad de un tratamiento en la erradicación de un biofilm estará limitada por el mecanismo de acción propio de la molécula. Los agentes antimicrobianos empleados actualmente fueron desarrollados contra células planctónicas, por lo que su efectividad en biofilms suele ser baja [32, 61, 62] . Esto hace que sea imprescindible desarrollar estrategias con actividad específica antibiofilm. Aunque el abordaje de esta problemática no se encuentra dentro de los objetivos de esta tesis, la sección de anexos presenta dos estudios que evalúan dos estrategias antibiofilm en bacterias.

Brevemente, en el artículo 6 se evaluó el potencial antimicrobiano de tres subtipos de la histona H1 humana: H1.0, H1.2 y H1.4. Como resultado, las tres proteínas mostraron un efecto bactericida contra células plantónicas de *P. aeruginosa* PAO1, asociado a daño en la membrana. La reducción de la biomasa celular también se encontró luego del tratamiento de los biofilms con H1.0, tanto en un modelo *in vitro* estático como en uno dinámico. Lo que sugiere un potencial terapéutico de estas biomoléculas en el tratamiento de infecciones agudas y crónicas por patógenos como *P. aeruginosa.*

La inyección de las histonas H1.0 y H1.4 en larvas de *G. mellonella* no causó ningún signo de toxicidad, y su uso en larvas infectadas con *P. aeruginosa* incrementó la supervivencia de estas, en comparación con las larvas no tratadas. Sin embargo, estudios que involucren células humanas y mamíferos como modelo animal deben validar estos resultados. El mecanismo de acción a nivel de la membrana de estas moléculas puede ocasionar reacciones adversas por interacciones inespecíficas con las células eucariotas [276, 277]. Sin embargo, el descubrimiento del ácido polisiálico como molécula capaz de reducir la citotoxicidad de las histonas H1 sin alterar su actividad antimicrobiana, abre las puertas para que estas proteínas sean utilizadas en aplicaciones biomédicas [278].

Por otra parte, la actividad antibiofilm de bacteriófagos aislados clínicamente contra biofilms de la cepa uropatogénica *E. coli* CFT073 fue demostrada en el artículo 7. Este

estudio evidenció que reducciones en la biomasa de los biofilms bacterianos pueden presentarse incluso cuando los bacteriófagos no son específicos para la cepa implicada. Dicha actividad fue confirmada en modelos *in vitro* estáticos y dinámicos. Este efecto está asociado con potencial antibacteriano y la producción de enzimas depolimerizantes.

Aunque ambas opciones pueden ser alternativas importantes en el desarrollo de terapias antibiofilm, es importante seguir explorando su efectividad y seguridad. Adicionalmente, es necesario que nuevos estudios evalúen la combinación de las histonas y los bacteriófagos con tratamientos clásicos (antibióticos) y poco convencionales (AMPs). Esto debido a que los experimentos de sinergia con antibióticos realizados en el artículo 6 y el artículo 7 no fueron concluyentes.

Conclusiones

1. La capacidad de adaptación de *C. parapsilosis* a la disponibilidad de nutrientes presente en los diferentes medios de cultivo influencia su tasa de crecimiento, morfología, susceptibilidad antimicrobiana y virulencia, tanto en estado plantónico como de biofilm.

2. Caracterizar las respuestas de los microorganismos que crecen en biofilms frente a variaciones ambientales ayudará a definir mejores protocolos para su estudio.

3. El orden de colonización de las especies afecta la composición, estructura, susceptibilidad y virulencia de biofilms polimicrobianos de *C. albicans* y *P. aeruginosa.*

4. La elección de tratamientos antimicrobianos, cuya eficacia sea independiente de los efectos de prioridad derivados del orden de colonización de las especies, aumentará la probabilidad de éxito terapéutico de las coinfecciones causadas por biofilms de *C. albicans* y *P. aeruginosa.*

5. La matriz extracelular es un factor importante en la resistencia de los biofilms, brindando protección individual, como en el caso de *C. parapsilosis* frente a la anfotericina B, o extendida, como la otorgada por *P. aeruginosa* a *C. albicans* frente a la caspofungina.

6. *C. albicans* y *S. aureus* interactúan en respuesta a cambios ambientales asociados a las disponibilidad de recursos y del pH, que resultan en nuevos fenotipos con adaptaciones metabólicas y cambios en la expresión de factores de virulencia que impactan negativamente en la supervivencia del huésped.

7. Interacciones físicas, químicas y efectos de prioridad derivados del orden de colonización de las especies presentes entre hongos y bacterias pueden aumentar el potencial patogénico de las coinfecciones.

8. La tinción específica para hongos FUN-1 permite evaluar la susceptibilidad a los antifúngicos en células de *C. parapsilosis*, tanto en estado plantónico como de biofilm.

9. El dimorfismo de *C. parapsilosis* generó variaciones en la permeabilidad de las tinciones comúnmente usadas, Syto 9 y Naranja de tiazol, resaltando la importancia de evaluar *a priori* el rendimiento de las tinciones de fluorescencia en el estudio de levaduras.

10. El BiofilmChip es un dispositivo de microfluídica robusto y versátil que permite la formación de biofilms monomicrobianos y polimicrobianos en condiciones dinámicas.

11. La medida de la impedancia es un método de lectura sensible que permite monitorear en tiempo real el proceso de formación de biofilms y la respuesta a los antibióticos.

12. Una estrategia para el desarrollo de terapias antibiofilm consiste en explotar la actividad antibacteriana presente en la naturaleza, como en el caso de los bacteriófagos y las histonas.

13. *G. mellonella* es un modelo animal que permite evaluar fácilmente diferencias fenotípicas como la virulencia de los microorganismos patógenos.

Bibliografía

1. **Dobell, C.** *Antony van Leeuwenhoek and his "little animals".* The American Journal of the Medical Sciences, 1933, 186(2): p.287.
2. **Pasteur, L.** *Mémoire sur la fermentation acétique.* Annales scientifiques de l'École Normale Supérieure, 1864, 1(1): p.113.
3. **Flemming, H.C. *et al*.** *Who put the film in biofilm? The migration of a term from wastewater engineering to medicine and beyond.* npj Biofilms and Microbiomes, 2021, 7(1): p.10.
4. **Flemming, H.C. and Wuertz, S.** *Bacteria and archaea on earth and their abundance in biofilms.* Nature Reviews Microbiology, 2019, 17(4): p.247.
5. **Høiby, N.** *A short history of microbial biofilms and biofilm infections.* APMIS, 2017, 125(4): p.272.
6. **Høiby, N. *et al*.** *Pseudomonas aeruginosa infection in cystic fibrosis. Diagnostic and prognostic significance of Pseudomonas aeruginosa precipitins determined by means of crossed immunoelectrophoresis.* Scandinavian journal of respiratory diseases, 1977, 58(2): p.65.
7. **Nickel, J.C. *et al*.** *Tobramycin resistance of Pseudomonas aeruginosa cells growing as a biofilm on urinary catheter material.* Antimicrobial Agents and Chemotherapy, 1985, 27(4): p.619.
8. **Hall-Stoodley, L. *et al*.** *Towards diagnostic guidelines for biofilm-associated infections.* FEMS Immunology & Medical Microbiology, 2012, 65(2): p.127.
9. **Alhede, M. *et al*.** *Phenotypes of non-attached Pseudomonas aeruginosa aggregates resemble surface attached biofilm.* PLoS One, 2011, 6(11): p.e27943.
10. **Sauer, K. *et al*.** *The biofilm life cycle: expanding the conceptual model of biofilm formation.* Nature Reviews Microbiology, 2022, 20(10): p.608.
11. **Penesyan, A. *et al*.** *Three faces of biofilms: a microbial lifestyle, a nascent multicellular organism, and an incubator for diversity.* npj Biofilms and Microbiomes, 2021, 7(1): p.80.
12. **Anju, V.T. *et al*.** *Polymicrobial infections and biofilms: clinical significance and eradication strategies.* Antibiotics, 2022, 11(12): p.1731.
13. **Sadiq, F.A. *et al*.** *Trans-kingdom interactions in mixed biofilm communities.* FEMS Microbiology Reviews, 2022, 46(5).
14. **Branda, S.S. *et al*.** *Biofilms: the matrix revisited.* Trends in Microbiology, 2005, 13(1): p.20.
15. **Luo, A. *et al*.** *Formation, development, and cross-species interactions in biofilms.* Frontiers in Microbiology, 2022, 12: p.757327.
16. **Li, Y.H. and Tian, X.** *Quorum sensing and bacterial social interactions in biofilms.* Sensors, 2012, 12(3): p.2519.
17. **Paula, A.J., Hwang, G., and Koo, H.** *Dynamics of bacterial population growth in biofilms resemble spatial and structural aspects of urbanization.* Nature Communications, 2020, 11(1): p.1354.
18. **Flemming, H.C. and Wingender, J.** *The biofilm matrix.* Nature Reviews Microbiology, 2010, 8(9): p.623.
19. **Mitchell, K.F., Zarnowski, R., and Andes, D.R.** *The extracellular matrix of fungal biofilms*, in *Fungal biofilms and related infections: Advances in microbiology, infectious diseases and public health volume 3*, C. Imbert, Editor. 2016, Springer International Publishing: Cham. p.21.
20. **Singh, S. *et al*.** *Bacterial exo-polysaccharides in biofilms: role in antimicrobial resistance and treatments.* Journal of Genetic Engineering and Biotechnology, 2021, 19(1): p.140.
21. **Dragoš, A. and Kovács, Á.T.** *The peculiar functions of the bacterial extracellular matrix.* Trends in Microbiology, 2017, 25(4): p.257.
22. **Karygianni, L. *et al*.** *Biofilm matrixome: Extracellular components in structured microbial communities.* Trends in Microbiology, 2020, 28(8): p.668.
23. **Moser, C. *et al*.** *Immune responses to Pseudomonas aeruginosa biofilm infections.* Frontiers in Immunology, 2021, 12: p.625597.
24. **Flemming, H.C. *et al*.** *The biofilm matrix: multitasking in a shared space.* Nature Reviews Microbiology, 2023, 21(2): p.70.
25. **Fong, J.N.C. and Yildiz, F.H.** *Biofilm Matrix Proteins.* Microbiology Spectrum, 2015, 3(2): p.201.

26. **Ibáñez de Aldecoa, A.L., Zafra, O., and González-Pastor, J.E.** *Mechanisms and regulation of extracellular DNA release and its biological roles in microbial communities.* Frontiers in Microbiology, 2017, 8: p.1390.
27. **Quan, K. *et al*.** *Water in bacterial biofilms: pores and channels, storage and transport functions.* Critical Reviews in Microbiology, 2022, 48(3): p.283.
28. **Hrynyshyn, A., Simões, M., and Borges, A.** *Biofilms in surgical site infections: Recent advances and novel prevention and eradication strategies.* Antibiotics, 2022, 11(1): p.69.
29. **Steinberg, N. and Kolodkin-Gal, I.** *The matrix reloaded: How sensing the extracellular matrix synchronizes bacterial communities.* Journal of Bacteriology, 2015, 197(13): p.2092.
30. **Koo, H. and Yamada, K.M.** *Dynamic cell–matrix interactions modulate microbial biofilm and tissue 3D microenvironments.* Current Opinion in Cell Biology, 2016, 42: p.102.
31. **Alotaibi, G.F. and Bukhari, M.A.** *Factors influencing bacterial biofilm formation and development.* American Journal of Biomedical Science and Research, 2021, 12(6): p.617.
32. **Mirghani, R. *et al*.** *Biofilms: Formation, drug resistance and alternatives to conventional approaches.* AIMS Microbiol, 2022, 8(3): p.239.
33. **Blanco-Cabra, N. *et al*.** *Nanomedicine against biofilm infections: A roadmap of challenges and limitations.* WIREs Nanomedicine and Nanobiotechnology, 2024, 16(1): p.e1944.
34. **Tolker-Nielsen, T.** *Biofilm Development.* Microbiology Spectrum, 2015, 3(2).
35. **de Beer, D. *et al*.** *Effects of biofilm structures on oxygen distribution and mass transport.* Biotechnology and Bioengineering, 1994, 43(11): p.1131.
36. **Davies, D.** *Understanding biofilm resistance to antibacterial agents.* Nature Reviews Drug Discovery, 2003, 2(2): p.114.
37. **Rumbaugh, K.P. and Sauer, K.** *Biofilm dispersion.* Nature Reviews Microbiology, 2020, 18(10): p.571.
38. **Chua, S.L. *et al*.** *Dispersed cells represent a distinct stage in the transition from bacterial biofilm to planktonic lifestyles.* Nature Communications, 2014, 5(1): p.4462.
39. **Ponde, N.O. *et al*.** *Candida albicans biofilms and polymicrobial interactions.* Critical Reviews in Microbiology, 2021, 47(1): p.91.
40. **Uruén, C. *et al*.** *Biofilms as promoters of bacterial antibiotic resistance and tolerance.* Antibiotics, 2021, 10(1): p.3.
41. **Yin, W. *et al*.** *Biofilms: the microbial "protective clothing" in extreme environments.* International Journal of Molecular Sciences, 2019, 20(14): p.3423.
42. **Jo, J., Price-Whelan, A., and Dietrich, L.E.P.** *Gradients and consequences of heterogeneity in biofilms.* Nature Reviews Microbiology, 2022, 20(10): p.593.
43. **Ciofu, O. *et al*.** *Tolerance and resistance of microbial biofilms.* Nature Reviews Microbiology, 2022, 20(10): p.621.
44. **Orazi, G. and O'Toole, G.A.** *"It takes a village": Mechanisms underlying antimicrobial recalcitrance of polymicrobial biofilms.* Journal of Bacteriology, 2019, 202(1).
45. **Alcàcer-Almansa, J. *et al*.** *Methods for studying biofilms: Microfluidics and translation in the clinical context*, in *Methods in Microbiology*, V. Gurtler and M. Patrauchan, Editors. 2023, Academic Press. p.195.
46. **Lebeaux, D. *et al*.** *From in vitro to in vivo models of bacterial biofilm-related infections.* Pathogens (Basel, Switzerland), 2013, 2(2): p.288.
47. **Azeredo, J. *et al*.** *Critical review on biofilm methods.* Critical Reviews in Microbiology, 2017, 43(3): p.313.
48. **Ceri, H. *et al*.** *The Calgary Biofilm Device: New technology for rapid determination of antibiotic susceptibilities of bacterial biofilms.* Journal of clinical microbiology, 1999, 37(6): p.1771.
49. **Bahamondez-Canas, T.F., Heersema, L.A., and Smyth, H.D.C.** *Current status of in vitro models and assays for susceptibility testing for wound biofilm infections.* Biomedicines, 2019, 7(2): p.34.
50. **Guzmán-Soto, I. *et al*.** *Mimicking biofilm formation and development: Recent progress in in vitro and in vivo biofilm models.* iScience, 2021, 24(5): p.102443.
51. **Gabrilska, R.A. and Rumbaugh, K.P.** *Biofilm models of polymicrobial infection.* Future microbiology, 2015, 10(12): p.1997.
52. **McCoy, W.F. *et al*.** *Observations of fouling biofilm formation.* Canadian Journal of Microbiology, 1981, 27(9): p.910.

53. **Wilson, C. *et al*.** *Quantitative and qualitative assessment methods for biofilm growth: A mini-review.* Research & Reviews: Journal of Engineering and Technology, 2017, 6(4).
54. **Coenye, T. and Nelis, H.J.** *In vitro and in vivo model systems to study microbial biofilm formation.* Journal of Microbiological Methods, 2010, 83(2): p.89.
55. **Kishen, A. and Haapasalo, M.** *Biofilm models and methods of biofilm assessment.* Endodontic Topics, 2010, 22(1): p.58.
56. **Del Pozo, J.L.** *Biofilm-related disease.* Expert Review of Anti-infective Therapy, 2018, 16(1): p.51.
57. **Jamal, M. *et al*.** *Bacterial biofilm and associated infections.* Journal of the Chinese Medical Association, 2018, 81(1): p.7.
58. **Lewis, K.** *Riddle of biofilm resistance.* Antimicrobial Agents and Chemotherapy, 2001, 45(4): p.999.
59. **Pragman, A.A., Berger, J.P., and Williams, B.J.** *Understanding persistent bacterial lung infections: Clinical implications informed by the biology of the microbiota and biofilms.* Clinical pulmonary medicine, 2016, 23(2): p.57.
60. **Moser, C. *et al*.** *Biofilms and host response – helpful or harmful.* APMIS, 2017, 125(4): p.320.
61. **Santos, A.L.S. *et al*.** *What are the advantages of living in a community? A microbial biofilm perspective!* Memórias do Instituto Oswaldo Cruz, 2018, 113(9): p.e180212.
62. **Di Domenico, E.G., Oliva, A., and Guembe, M.** *The Current Knowledge on the Pathogenesis of Tissue and Medical Device-Related Biofilm Infections.* Microorganisms, 2022, 10(7): p.1259.
63. **Miquel, S. *et al*.** *Anti-biofilm activity as a health issue.* Frontiers in Microbiology, 2016, 7: p.592.
64. **Arciola, C.R., Campoccia, D., and Montanaro, L.** *Implant infections: adhesion, biofilm formation and immune evasion.* Nature Reviews Microbiology, 2018, 16(7): p.397.
65. **Raoofi, S. *et al*.** *Global prevalence of nosocomial infection: A systematic review and meta-analysis.* PLoS One, 2023, 18(1): p.e0274248.
66. **Dhar, Y. and Han, Y.** *Current developments in biofilm treatments: Wound and implant infections.* Engineered Regeneration, 2020, 1: p.64.
67. **Rather, M.A. *et al*.** *Microbial biofilm: A matter of grave concern for human health and food industry.* Journal of Basic Microbiology, 2021, 61(5): p.380.
68. **Cámara, M. *et al*.** *Economic significance of biofilms: a multidisciplinary and cross-sectoral challenge.* npj Biofilms and Microbiomes, 2022, 8(1): p.42.
69. **Høiby, N. *et al*.** *ESCMID guideline for the diagnosis and treatment of biofilm infections 2014.* Clinical Microbiology and Infection, 2015, 21: p.S1.
70. **Banerjee, D. *et al*.** *A review on basic biology of bacterial biofilm infections and their treatments by nanotechnology-based approaches.* Proceedings of the National Academy of Sciences, India Section B: Biological Sciences, 2020, 90(2): p.243.
71. **Bryers, J.D.** *Medical biofilms.* Biotechnology and Bioengineering, 2008, 100(1): p.1.
72. **Mandakhalikar, K.D.** *Medical Biofilms*, in *Introduction to Biofilm Engineering*, N.K. Rathinam and R.K. Sani, Editors. 2019, American Chemical Society. p.83.
73. **Mirzaei, R. *et al*.** *The biofilm-associated bacterial infections unrelated to indwelling devices.* IUBMB Life, 2020, 72(7): p.1271.
74. **Ding, L. *et al*.** *Pulmonary biofilm-based chronic infections and inhaled treatment strategies.* International Journal of Pharmaceutics, 2021, 604: p.120768.
75. **Vestby, L.K. *et al*.** *Bacterial biofilm and its role in the pathogenesis of disease.* Antibiotics, 2020, 9(2): p.59.
76. **Hemmati, F. *et al*.** *Novel Strategies to Combat Bacterial Biofilms.* Molecular Biotechnology, 2021, 63(7): p.569.
77. **Jiang, Y., Geng, M., and Bai, L.** *Targeting biofilms therapy: Current research strategies and development hurdles.* Microorganisms, 2020, 8(8): p.1222.
78. **Fu, J. *et al*.** *Strategies for interfering with bacterial early stage biofilms.* Frontiers in Microbiology, 2021, 12: p. 675843.
79. **Paluch, E. *et al*.** *Prevention of biofilm formation by quorum quenching.* Applied Microbiology and Biotechnology, 2020, 104(5): p.1871.
80. **Rodríguez-Merchán, E.C., Davidson, D.J., and Liddle, A.D.** *Recent strategies to combat infections from biofilm-forming bacteria on orthopaedic implants.* International Journal of Molecular Sciences, 2021, 22(19): p.10243.

81. **da Silva, R.A.G., Afonina, I., and Kline, K.A.** *Eradicating biofilm infections: an update on current and prospective approaches.* Current Opinion in Microbiology, 2021, 63: p.117.
82. **Mishra, S. *et al*.** *Therapeutic strategies against biofilm infections.* Life, 2023, 13(1): p.172.
83. **Zhang, K. *et al*.** *Promising therapeutic strategies against microbial biofilm challenges.* Frontiers in Cellular and Infection Microbiology, 2020, 10: p.359.
84. **Wolfmeier, H. *et al*.** *New Perspectives in Biofilm Eradication.* ACS Infectious Diseases, 2018, 4(2): p.93.
85. **Ferriol-González, C. and Domingo-Calap, P.** *Phages for Biofilm Removal.* Antibiotics, 2020, 9(5): p.268.
86. **Asma, S.T. *et al*.** *An overview of biofilm formation–combating strategies and mechanisms of action of antibiofilm agents.* Life, 2022, 12(8): p.1110.
87. **Shamim, A. *et al*.** *Natural medicine a promising candidate in combating microbial biofilm.* Antibiotics, 2023, 12(2): p.299.
88. **Verderosa, A.D., Totsika, M., and Fairfull-Smith, K.E.** *Bacterial biofilm eradication agents: A current review.* Frontiers in Chemistry, 2019, 7.
89. **Srinivasan, R. *et al*.** *Bacterial biofilm inhibition: A focused review on recent therapeutic strategies for combating the biofilm mediated infections.* Frontiers in Microbiology, 2021, 12: p.676458.
90. **Liu, Y. *et al*.** *Nanotechnology-based antimicrobials and delivery systems for biofilm-infection control.* Chemical Society Reviews, 2019, 48(2): p.428.
91. **Tuon, F.F. *et al*.** *Pathogenesis of the Pseudomonas aeruginosa biofilm: A review.* Pathogens (Basel, Switzerland), 2022, 11(3): p.300.
92. **Van Delden, C. and Iglewski, B.H.** *Cell-to-cell signaling and Pseudomonas aeruginosa infections.* Emerging Infectious Diseases, 1998, 4(4): p.551.
93. **Strateva, T. and Mitov, I.** *Contribution of an arsenal of virulence factors to pathogenesis of Pseudomonas aeruginosa infections.* Annals of Microbiology, 2011, 61(4): p.717.
94. **Cheung, G.Y.C., Bae, J.S., and Otto, M.** *Pathogenicity and virulence of Staphylococcus aureus.* Virulence, 2021, 12(1): p.547.
95. **Lopes, J.P. and Lionakis, M.S.** *Pathogenesis and virulence of Candida albicans.* Virulence, 2022, 13(1): p.89.
96. **Yin, R. *et al*.** *Treatment of Pseudomonas aeruginosa infectious biofilms: Challenges and strategies.* Frontiers in Microbiology, 2022, 13: p.955286.
97. **Cendra, M.D.M. and Torrents, E.** *Pseudomonas aeruginosa biofilms and their partners in crime.* Biotechnology Advances, 2021, 49: p.107734.
98. **Reynolds, D. and Kollef, M.** *The epidemiology and pathogenesis and treatment of Pseudomonas aeruginosa infections: An update.* Drugs, 2021, 81(18): p.2117.
99. **Vetrivel, A. *et al*.** *Pseudomonas aeruginosa biofilm formation and its control.* Biologics, 2021, 1(3): p.312.
100. **World Health Organization.** *WHO Bacterial Priority Pathogens List, 2024: bacterial pathogens of public health importance to guide research, development and strategies to prevent and control antimicrobial resistance*. 2024.
101. **Thi, M.T., Wibowo, D., and Rehm, B.H.A.** *Pseudomonas aeruginosa Biofilms.* International Journal of Molecular Sciences, 2020, 21(22): p.8671.
102. **Sousa, A.M. and Pereira, M.O.** *Pseudomonas aeruginosa diversification during infection development in cystic fibrosis lungs - A review.* Pathogens (Basel, Switzerland), 2014, 3(3): p.680.
103. **Jurado-Martín, I., Sainz-Mejías, M., and McClean, S.** *Pseudomonas aeruginosa: An audacious pathogen with an adaptable arsenal of virulence factors.* International Journal of Molecular Sciences, 2021, 22(6): p.3128.
104. **Muggeo, A., Coraux, C., and Guillard, T.** *Current concepts on Pseudomonas aeruginosa interaction with human airway epithelium.* PLOS Pathogens, 2023, 19(3): p.e1011221.
105. **Kaminski, A. *et al*.** *Pseudomonas aeruginosa ExoS induces intrinsic apoptosis in target host cells in a manner that is dependent on its GAP domain activity.* Scientific Reports, 2018, 8(1): p.14047.
106. **Alaoui-El-Azher, M. *et al*.** *ExoS of Pseudomonas aeruginosa induces apoptosis through a Fas receptor/caspase 8-independent pathway in HeLa cells.* Cellular Microbiology, 2006, 8(2): p.326.
107. **Barbieri, J.T. and Sun, J.** *Pseudomonas aeruginosa ExoS and ExoT*, in *Reviews of Physiology, Biochemistry and Pharmacology*. 2005, Springer Berlin Heidelberg: Berlin, Heidelberg. p.79.

108. **Jia, J. *et al*.** *Expression of Pseudomonas aeruginosa toxin ExoS effectively induces apoptosis in host cells.* Infection and Immunity, 2006, 74(12): p.6557.
109. **Finck-Barbançon, V. *et al*.** *ExoU expression by Pseudomonas aeruginosa correlates with acute cytotoxicity and epithelial injury.* Molecular Microbiology, 1997, 25(3): p.547.
110. **Drenkard, E.** *Antimicrobial resistance of Pseudomonas aeruginosa biofilms.* Microbes and Infection, 2003, 5(13): p.1213.
111. **Jouenne, T. *et al*.** *Proteomics of biofilm bacteria.* Current Proteomics, 2004, 1(3): p.211.
112. **Sauer, K. *et al*.** *Pseudomonas aeruginosa displays multiple phenotypes during development as a biofilm.* Journal of Bacteriology, 2002, 184(4): p.1140.
113. **Klockgether, J. *et al*.** *Pseudomonas aeruginosa genomic structure and diversity.* Frontiers in Microbiology, 2011, 2: p.150.
114. **Moradali, M.F., Ghods, S., and Rehm, B.H.A.** *Pseudomonas aeruginosa lifestyle: A paradigm for adaptation, survival, and persistence.* Frontiers in Cellular and Infection Microbiology, 2017, 7.
115. **Aloush, V. *et al*.** *Multidrug-resistant Pseudomonas aeruginosa: risk factors and clinical impact.* Antimicrobial Agents and Chemotherapy, 2006, 50(1): p.43.
116. **Hancock, R.E. and Speert, D.P.** *Antibiotic resistance in Pseudomonas aeruginosa: mechanisms and impact on treatment.* Drug Resistance Updates, 2000, 3(4): p.247.
117. **Govan, J.R. and Deretic, V.** *Microbial pathogenesis in cystic fibrosis: mucoid Pseudomonas aeruginosa and Burkholderia cepacia.* Microbiological Reviews, 1996, 60(3): p.539.
118. **Maunders, E. and Welch, M.** *Matrix exopolysaccharides; the sticky side of biofilm formation.* FEMS Microbiology Letters, 2017, 364(13).
119. **Colvin, K.M. *et al*.** *The Pel polysaccharide can serve a structural and protective role in the biofilm matrix of Pseudomonas aeruginosa.* PLOS Pathogens, 2011, 7(1): p.e1001264.
120. **Khan, W. *et al*.** *Aminoglycoside resistance of Pseudomonas aeruginosa biofilms modulated by extracellular polysaccharide.* International Microbiology, 2010, 13(4): p.207.
121. **Billings, N. *et al*.** *The extracellular matrix component Psl provides fast-acting antibiotic defense in Pseudomonas aeruginosa biofilms.* PLOS Pathogens, 2013, 9(8): p.e1003526.
122. **Mishra, M. *et al*.** *Pseudomonas aeruginosa Psl polysaccharide reduces neutrophil phagocytosis and the oxidative response by limiting complement-mediated opsonization.* Cellular Microbiology, 2012, 14(1): p.95.
123. **Costerton, J.W., Stewart, P.S., and Greenberg, E.P.** *Bacterial biofilms: a common cause of persistent infections.* Science, 1999, 284(5418): p.1318.
124. **Kourtis, A.P. *et al*.** *Vital signs: Epidemiology and recent trends in Methicillin-Resistant and in Methicillin-Susceptible Staphylococcus aureus bloodstream infections - United States.* Morbidity and Mortality Weekly Report, 2019, 68(9): p.214.
125. **Tong, S.Y.C. *et al*.** *Staphylococcus aureus infections: Epidemiology, pathophysiology, clinical manifestations, and management.* Clinical Microbiology Reviews, 2015, 28(3): p.603.
126. **Powers, M.E. and Wardenburg, J.B.** *Igniting the fire: Staphylococcus aureus virulence factors in the pathogenesis of sepsis.* PLOS Pathogens, 2014, 10(2): p.e1003871.
127. **Otto, M.** *Staphylococcus aureus toxins.* Current Opinion in Microbiology, 2014, 17: p.32.
128. **Oliveira, D., Borges, A., and Simões, M.** *Staphylococcus aureus toxins and their molecular activity in infectious diseases.* Toxins, 2018, 10(6): p.252.
129. **Bubeck-Wardenburg, J. *et al*.** *Poring over pores: α-hemolysin and Panton-Valentine leukocidin in Staphylococcus aureus pneumonia.* Nature Medicine, 2007, 13(12): p.1405.
130. **Kitur, K. *et al*.** *Toxin-induced necroptosis Is a major mechanism of Staphylococcus aureus lung damage.* PLOS Pathogens, 2015, 11(4): p.e1004820.
131. **Kobayashi, S.D. *et al*.** *Comparative analysis of USA300 virulence determinants in a rabbit model of skin and soft tissue infection.* The Journal of Infectious Diseases, 2011, 204(6): p.937.
132. **Powers, M.E. *et al*.** *ADAM10 mediates vascular injury induced by Staphylococcus aureus α-hemolysin.* The Journal of Infectious Diseases, 2012, 206(3): p.352.
133. **Todd, O.A. *et al*.** *Candida albicans augments Staphylococcus aureus virulence by engaging the staphylococcal agr quorum sensing system.* mBio, 2019, 10(3): p.e00910.
134. **Clauditz, A. *et al*.** *Staphyloxanthin plays a role in the fitness of Staphylococcus aureus and its ability to cope with oxidative stress.* Infection and Immunity, 2006, 74(8): p.4950.

135. **Pelz, A. *et al*.** *Structure and biosynthesis of Staphyloxanthin from Staphylococcus aureus.* Journal of Biological Chemistry, 2005, 280(37): p.32493.
136. **Clements, M.O., Watson, S.P., and Foster, S.J.** *Characterization of the major superoxide dismutase of Staphylococcus aureus and its role in starvation survival, stress resistance, and pathogenicity.* Journal of Bacteriology, 1999, 181(13): p.3898.
137. **Mandell, G.L.** *Catalase, superoxide dismutase, and virulence of Staphylococcus aureus. In vitro and in vivo studies with emphasis on staphylococcal - leukocyte interaction.* The Journal of Clinical Investigation, 1975, 55(3): p.561.
138. **Cosgrove, K. *et al*.** *Catalase (KatA) and Alkyl Hydroperoxide Reductase (AhpC) have compensatory roles in peroxide stress resistance and are required for survival, persistence, and nasal colonization in Staphylococcus aureus.* Journal of Bacteriology, 2007, 189(3): p.1025.
139. **Richardson, A.R., Libby, S.J., and Fang, F.C.** *A nitric oxide–inducible lactate dehydrogenase enables Staphylococcus aureus to resist innate immunity.* Science, 2008, 319(5870): p.1672.
140. **Lai, Y. *et al*.** *The human anionic antimicrobial peptide dermcidin induces proteolytic defence mechanisms in staphylococci.* Molecular Microbiology, 2007, 63(2): p.497.
141. **Berends, E.T.M. *et al*.** *Nuclease expression by Staphylococcus aureus facilitates escape from neutrophil extracellular traps.* Journal of Innate Immunity, 2010, 2(6): p.576.
142. **Forsgren, A. and Sjöquist, J.** *"Protein A" from S. aureus: I. Pseudo-immune reaction with human γ-Globulin.* The Journal of Immunology, 1966, 97(6): p.822.
143. **Goodyear, C.S. and Silverman, G.J.** *Death by a B cell superantigen : In vivo VH-targeted apoptotic supraclonal B cell deletion by a Staphylococcal toxin.* Journal of Experimental Medicine, 2003, 197(9): p.1125.
144. **Pauli, N.T. *et al*.** *Staphylococcus aureus infection induces protein A–mediated immune evasion in humans.* Journal of Experimental Medicine, 2014, 211(12): p.2331.
145. **Atkins, K.L. *et al*.** *S. aureus IgG-binding proteins SpA and Sbi: host specificity and mechanisms of immune complex formation.* Molecular Immunology, 2008, 45(6): p.1600.
146. **Zhang, L. *et al*.** *A second IgG-binding protein in Staphylococcus aureus.* Microbiology, 1998, 144(4): p.985.
147. **Itoh, S. *et al*.** *Staphylococcal superantigen-like protein 10 (SSL10) binds to human immunoglobulin G (IgG) and inhibits complement activation via the classical pathway.* Molecular Immunology, 2010, 47(4): p.932.
148. **Rooijakkers, S.H.M. *et al*.** *Immune evasion by a staphylococcal complement inhibitor that acts on C3 convertases.* Nature Immunology, 2005, 6(9): p.920.
149. **Ko, Y.P. *et al*.** *Phagocytosis escape by a Staphylococcus aureus protein that connects complement and coagulation proteins at the bacterial surface.* PLOS Pathogens, 2013, 9(12): p.e1003816.
150. **Jongerius, I. *et al*.** *Convertase inhibitory properties of Staphylococcal extracellular complement-binding protein.* Journal of Biological Chemistry, 2010, 285(20): p.14973.
151. **Kang, M. *et al*.** *Collagen-binding Microbial Surface Components Recognizing Adhesive Matrix Molecule (MSCRAMM) of Gram-positive bacteria inhibit complement activation via the alassical pathway.* Journal of Biological Chemistry, 2013, 288(28): p.20520.
152. **Sharp, J.A. *et al*.** *Staphylococcus aureus surface protein SdrE binds complement regulator factor H as an immune evasion tactic.* PLoS One, 2012, 7(5): p.e38407.
153. **Zhang, Y. *et al*.** *Staphylococcus aureus SdrE captures complement factor H's C-terminus via a novel "close, dock, lock and latch" mechanism for complement evasion.* Biochemical Journal, 2017, 474(10): p.1619.
154. **Woehl, J.L. *et al*.** *The extracellular adherence protein from Staphylococcus aureus inhibits the classical and lectin pathways of complement by blocking formation of the C3 proconvertase.* The Journal of Immunology, 2014, 193(12): p.6161.
155. **Langley, R. *et al*.** *The staphylococcal superantigen-like protein 7 binds IgA and complement C5 and inhibits IgA-FcαRI binding and serum killing of Bacteria.* The Journal of Immunology, 2005, 174(5): p.2926.
156. **Mousavi, M.N.S. *et al*.** *The pathogenesis of Staphylococcus aureus in autoimmune diseases.* Microbial Pathogenesis, 2017, 111: p.503.

157. **Flora, M. *et al*.** *Staphylococcus aureus in chronic airway diseases: An overview.* Respiratory Medicine, 2019, 155: p.66.
158. **Cerca, N. *et al*.** *Molecular basis for preferential protective efficacy of antibodies directed to the poorly acetylated form of staphylococcal poly-N-acetyl-beta-(1-6)-glucosamine.* Infection and Immunity, 2007, 75(7): p.3406.
159. **Fournier, J.M. *et al*.** *Isolation of type 5 capsular polysaccharide from Staphylococcus aureus.* Annales de l'Institut Pasteur / Microbiologie, 1987, 138(5): p.561.
160. **Fournier, J.M., Vann, W.F., and Karakawa, W.W.** *Purification and characterization of Staphylococcus aureus type 8 capsular polysaccharide.* Infection and Immunity, 1984, 45(1): p.87.
161. **Vuong, C. *et al*.** *Polysaccharide intercellular adhesin (PIA) protects Staphylococcus epidermidis against major components of the human innate immune system.* Cellular Microbiology, 2004, 6(3): p.269.
162. **Archer, N.K. *et al*.** *Staphylococcus aureus biofilms.* Virulence, 2011, 2(5): p.445.
163. **Jenul, C. and Horswill, A.R.** *Regulation of Staphylococcus aureus virulence.* Microbiology Spectrum, 2019, 7(2).
164. **Regassa, L.B. and Betley, M.J.** *Alkaline pH decreases expression of the accessory gene regulator (agr) in Staphylococcus aureus.* Journal of Bacteriology, 1992, 174(15): p.5095.
165. **Regassa, L.B., Novick, R.P., and Betley, M.J.** *Glucose and nonmaintained pH decrease expression of the accessory gene regulator (agr) in Staphylococcus aureus.* Infection and Immunity, 1992, 60(8): p.3381.
166. **Saikat, P. *et al*.** *A fungal metabolic regulator underlies infectious synergism during Candida albicans-Staphyloccocus aureus intra-abdominal co-infection.* bioRxiv, 2024.
167. **Rothfork, J.M. *et al*.** *Inactivation of a bacterial virulence pheromone by phagocyte-derived oxidants: New role for the NADPH oxidase in host defense.* Proceedings of the National Academy of Sciences, 2004, 101(38): p.13867.
168. **Sun, F. *et al*.** *Quorum-sensing agr mediates bacterial oxidation response via an intramolecular disulfide redox switch in the response regulator AgrA.* Proceedings of the National Academy of Sciences, 2012, 109(23): p.9095.
169. **Bonesso, M.F. *et al*.** *Key role of α-toxin in fatal pneumonia caused by Staphylococcus aureus Sequence Type 398.* American Journal of Respiratory and Critical Care Medicine, 2016, 193(2): p.217.
170. **Bouiller, K. *et al*.** *Human infection of Methicillin-Susceptible Staphylococcus aureus CC398: A review.* Microorganisms, 2020, 8(11): p.1737.
171. **Lowy, F.D.** *Antimicrobial resistance: the example of Staphylococcus aureus.* The Journal of Clinical Investigation, 2003, 111(9): p.1265.
172. **Turner, N.A. *et al*.** *Methicillin-resistant Staphylococcus aureus: an overview of basic and clinical research.* Nature Reviews Microbiology, 2019, 17(4): p.203.
173. **McGuinness, W.A., Malachowa, N., and DeLeo, F.R.** *Vancomycin resistance in Staphylococcus aureus.* Yale Journal of Biology and Medicine, 2017, 90(2): p.269.
174. **Hiramatsu, K. *et al*.** *Vancomycin-intermediate resistance in Staphylococcus aureus.* Journal of Global Antimicrobial Resistance, 2014, 2(4): p.213.
175. **Schilcher, K. and Horswill, A.R.** *Staphylococcal biofilm development: Structure, regulation, and treatment strategies.* Microbiology and Molecular Biology Reviews, 2020, 84(3): p.e00026.
176. **Periasamy, S. *et al*.** *How Staphylococcus aureus biofilms develop their characteristic structure.* Proceedings of the National Academy of Sciences, 2012, 109(4): p.1281.
177. **Moormeier, D.E. and Bayles, K.W.** *Staphylococcus aureus biofilm: a complex developmental organism.* Molecular Microbiology, 2017, 104(3): p.365.
178. **Lister, J.L. and Horswill, A.R.** *Staphylococcus aureus biofilms: recent developments in biofilm dispersal.* Frontiers in Cellular and Infection Microbiology, 2014, 4.
179. **Yarwood, J.M. *et al*.** *Quorum sensing in Staphylococcus aureus biofilms.* Journal of Bacteriology, 2004, 186(6): p.1838.
180. **Boles, B.R. and Horswill, A.R.** *agr-mediated dispersal of Staphylococcus aureus biofilms.* PLOS Pathogens, 2008, 4(4): p.e1000052.
181. **Pereira, R. *et al*.** *Biofilm of Candida albicans: formation, regulation and resistance.* Journal of Applied Microbiology, 2021, 131(1): p.11.

182. **Kumamoto, C.A., Gresnigt, M.S., and Hube, B.** *The gut, the bad and the harmless: Candida albicans as a commensal and opportunistic pathogen in the intestine.* Current Opinion in Microbiology, 2020, 56: p.7.
183. **Alonso-Monge, R. *et al*.** *Candida albicans colonization of the gastrointestinal tract: A double-edged sword.* PLOS Pathogens, 2021, 17(7): p.e1009710.
184. **Talapko, J. *et al*.** *Candida albicans - The virulence factors and clinical manifestations of infection.* Journal of Fungi, 2021, 7(2): p.79.
185. **d'Enfert, C. *et al*.** *The impact of the Fungus-Host-Microbiota interplay upon Candida albicans infections: current knowledge and new perspectives.* FEMS Microbiology Reviews, 2021, 45(3).
186. **Chow, E.W.L., Pang, L.M., and Wang, Y.** *Impact of the host microbiota on fungal infections: New possibilities for intervention?* Advanced Drug Delivery Reviews, 2023, 198: p.114896.
187. **Williams, R.B. and Lorenz, M.C.** *Multiple alternative carbon pathways combine to promote Candida albicans stress resistance, immune interactions, and virulence.* mBio, 2020, 11(1).
188. **Citiulo, F. *et al*.** *Candida albicans scavenges host zinc via Pra1 during endothelial invasion.* PLOS Pathogens, 2012, 8(6): p.e1002777.
189. **Malavia, D. *et al*.** *Zinc limitation induces a hyper-adherent goliath phenotype in Candida albicans.* Frontiers in Microbiology, 2017, 8: p.2238.
190. **Crawford, A. and Wilson, D.** *Essential metals at the host–pathogen interface: nutritional immunity and micronutrient assimilation by human fungal pathogens.* FEMS Yeast Research, 2015, 15(7).
191. **Mackie, J. *et al*.** *Host-imposed copper poisoning impacts fungal micronutrient acquisition during systemic Candida albicans infections.* PLoS One, 2016, 11(6): p.e0158683.
192. **Weissman, Z. *et al*.** *The high copper tolerance of Candida albicans is mediated by a P-type ATPase.* Proceedings of the National Academy of Sciences, 2000, 97(7): p.3520.
193. **Potrykus, J. *et al*.** *Fungal iron availability during deep seated Candidiasis is defined by a complex interplay involving systemic and local events.* PLOS Pathogens, 2013, 9(10): p.e1003676.
194. **Ramanan, N. and Wang, Y.** *A high-affinity iron permease essential for Candida albicans virulence.* Science, 2000, 288(5468): p.1062.
195. **Almeida, R.S. *et al*.** *The hyphal-associated adhesin and invasin Als3 of Candida albicans mediates iron acquisition from host ferritin.* PLOS Pathogens, 2008, 4(11): p.e1000217.
196. **Ramage, G. *et al*.** *Our current clinical understanding of Candida biofilms: where are we two decades on?* APMIS, 2023, 131(11): p.636.
197. **Lee, Y. *et al*.** *Antifungal drug resistance: Molecular mechanisms in Candida albicans and beyond.* Chemical Reviews, 2021, 121(6): p.3390.
198. **Mitchell, K.F. *et al*.** *Community participation in biofilm matrix assembly and function.* Proceedings of the National Academy of Sciences, 2015, 112(13): p.4092.
199. **Fan, F. *et al*.** *Candida albicans biofilms: antifungal resistance, immune evasion, and emerging therapeutic strategies.* International Journal of Antimicrobial Agents, 2022, 60(5): p.106673.
200. **Massey, J., Zarnowski, R., and Andes, D.** *Role of the extracellular matrix in Candida biofilm antifungal resistance.* FEMS Microbiology Reviews, 2023, 47(6).
201. **Zarnowski, R. *et al*.** *Coordination of fungal biofilm development by extracellular vesicle cargo.* Nature Communications, 2021, 12(1): p.6235.
202. **Blankenship, J.R. and Mitchell, A.P.** *How to build a biofilm: a fungal perspective.* Current Opinion in Microbiology, 2006, 9(6): p.588.
203. **Zarnowski, R. *et al*.** *Novel entries in a fungal biofilm matrix encyclopedia.* mBio, 2014, 5(4).
204. **Puig-Asensio, M. *et al*.** *Epidemiology and predictive factors for early and late mortality in Candida bloodstream infections: a population-based surveillance in Spain.* Clinical Microbiology and Infection, 2014, 20(4): p.O245.
205. **Tóth, R. *et al*.** *Candida parapsilosis: from genes to the bedside.* Clinical Microbiology Reviews, 2019, 32(2): p.e00111.
206. **Govrins, M. and Lass-Flörl, C.** *Candida parapsilosis complex in the clinical setting.* Nature Reviews Microbiology, 2024, 22(1): p.46.
207. **Rodrigues, M.E., Gomes, F., and Rodrigues, C.F.** *Candida spp./bacteria mixed biofilms.* Journal of Fungi, 2020, 6(1).

208. **Ricotta, E.E. *et al*.** *Invasive candidiasis species distribution and trends, United States, 2009–2017.* The Journal of Infectious Diseases, 2021, 223(7): p.1295.
209. **Hirayama, T. *et al*.** *Virulence assessment of six major pathogenic Candida species in the mouse model of invasive candidiasis caused by fungal translocation.* Scientific Reports, 2020, 10(1): p.3814.
210. **Arastehfar, A. *et al*.** *Clonal candidemia outbreak by Candida parapsilosis carrying Y132F in Turkey: Evolution of a persisting challenge.* Frontiers in Cellular and Infection Microbiology, 2021, 11: p.676177.
211. **Mesini, A. *et al*.** *Changing epidemiology of candidaemia: Increase in fluconazole-resistant Candida parapsilosis.* Mycoses, 2020, 63(4): p.361.
212. **Daneshnia, F. *et al*.** *Worldwide emergence of fluconazole-resistant Candida parapsilosis: current framework and future research roadmap.* The Lancet Microbe, 2023, 4(6): p.e470.
213. **Yamin, D. *et al*.** *Global prevalence of antifungal-resistant Candida parapsilosis: A systematic review and meta-analysis.* Tropical Medicine and Infectious Disease, 2022, 7(8): p.188.
214. **Escribano, P. and Guinea, J.** *Fluconazole-resistant Candida parapsilosis: A new emerging threat in the fungi arena.* Frontiers in Fungal Biology, 2022, 3.
215. **Branco, J., Miranda, I.M., and Rodrigues, A.G.** *Candida parapsilosis virulence and antifungal resistance mechanisms: A comprehensive review of key determinants.* Journal of Fungi, 2023, 9(1): p.80.
216. **Soldini, S. *et al*.** *Microbiologic and clinical characteristics of biofilm-forming Candida parapsilosis isolates associated with fungaemia and their impact on mortality.* Clinical Microbiology and Infection, 2018, 24(7): p.771.
217. **Kim, S.-K., Bissati, K.E., and Mamoun, C.B.** *Amino acids mediate colony and cell differentiation in the fungal pathogen Candida parapsilosis.* Microbiology, 2006, 152(10): p.2885.
218. **Németh, T. *et al*.** *Characterization of virulence properties in the C. parapsilosis sensu lato species.* PLoS One, 2013, 8(7): p.e68704.
219. **Tóth, R. *et al*.** *Kinetic studies of Candida parapsilosis phagocytosis by macrophages and detection of intracellular survival mechanisms.* Frontiers in Microbiology, 2014, 5: p.633.
220. **Pereira, L. *et al*.** *Influence of glucose concentration on the structure and quantity of biofilms formed by Candida parapsilosis.* FEMS Yeast Research, 2015, 15(5).
221. **Lohse, M.B. *et al*.** *Development and regulation of single- and multi-species Candida albicans biofilms.* Nature Reviews Microbiology, 2018, 16(1): p.19.
222. **Pohl, C.H.** *Recent advances and opportunities in the study of Candida albicans polymicrobial biofilms.* Frontiers in Cellular and Infection Microbiology, 2022, 12.
223. **Khan, F. *et al*.** *Mixed biofilms of pathogenic Candida-bacteria: regulation mechanisms and treatment strategies.* Critical Reviews in Microbiology, 2021, 47(6): p.699.
224. **Bernard, C., Girardot, M., and Imbert, C.** *Candida albicans interaction with Gram-positive bacteria within interkingdom biofilms.* Journal de Mycologie Médicale, 2020, 30(1): p.100909.
225. **Costa-Orlandi, C.B. *et al*.** *Polymicrobial biofilms: Impact on fungal pathogenesis*, in *Understanding Microbial Biofilms*, S. Das and N.A. Kungwani, Editors. 2023, Academic Press. p.521.
226. **Kahl, L.J. *et al*.** *Interkingdom interactions between Pseudomonas aeruginosa and Candida albicans affect clinical outcomes and antimicrobial responses.* Current Opinion in Microbiology, 2023, 75: p.102368.
227. **Short, B. *et al*.** *There is more to wounds than bacteria: Fungal biofilms in chronic wounds.* Current Clinical Microbiology Reports, 2023, 10(1): p.9.
228. **Hernandez-Cuellar, E. *et al*.** *Characterization of Candida albicans and Staphylococcus aureus polymicrobial biofilm on different surfaces.* Revista Iberoamericana de Micología, 2022, 39(2): p.36.
229. **Young, T. *et al*.** *Candida albicans as an essential "keystone" component within polymicrobial oral biofilm models?* Microorganisms, 2021, 9(1): p.59.
230. **Negrini, T.d.C., Koo, H., and Arthur, R.A.** *Candida–bacterial biofilms and host–microbe interactions in oral diseases.* Oral Mucosal Immunity and Microbiome, 2019: p.119.
231. **Trejo-Hernández, A. *et al*.** *Interspecies competition triggers virulence and mutability in Candida albicans–Pseudomonas aeruginosa mixed biofilms.* The ISME Journal, 2014, 8(10): p.1974.
232. **Bergeron, A.C. *et al*.** *Candida albicans and Pseudomonas aeruginosa interact to enhance virulence of mucosal infection in transparent zebrafish.* Infection and Immunity, 2017, 85(11).
233. **Kasetty, S. *et al*.** *Pseudomonas aeruginosa and Candida albicans both accumulate greater biomass in dual species biofilms under flow.* mSphere, 2021, 6(3).

234. **Kulshrestha, A. and Gupta, P.** *Polymicrobial interaction in biofilm: Mechanistic insights.* Pathogens and Disease, 2022, 80(1).
235. **Van Dyck, K. *et al*.** *Adhesion of Staphylococcus aureus to Candida albicans during co-infection promotes bacterial dissemination through the host immune response.* Frontiers in Cellular and Infection Microbiology, 2021, 10: p.624839.
236. **Todd, O.A. and Peters, B.M.** *Candida albicans and Staphylococcus aureus pathogenicity and polymicrobial Interactions: Lessons beyond Koch's postulates.* Journal of Fungi, 2019, 5(3): p.81.
237. **Rapala-Kozik, M. *et al*.** *Living together: The role of Candida albicans in the formation of polymicrobial biofilms in the oral cavity.* Yeast, 2023, 40(8): p.303.
238. **Carolus, H., Van Dyck, K., and Van Dijck, P.** *Candida albicans and Staphylococcus species: A threatening twosome.* Frontiers in Microbiology, 2019, 10: p.2162.
239. **Eichelberger, K.R. and Cassat, J.E.** *Metabolic adaptations during Staphylococcus aureus and Candida albicans co-infection.* Frontiers in Immunology, 2021, 12.
240. **Carlson, E.** *Synergistic effect of Candida albicans and Staphylococcus aureus on mouse mortality.* Infection and Immunity, 1982, 38(3): p.921.
241. **Peters, B.M. and Noverr, M.C.** *Candida albicans-Staphylococcus aureus polymicrobial peritonitis modulates host innate immunity.* Infection and Immunity, 2013, 81(6): p.2178.
242. **Sheehan, G., Tully, L., and Kavanagh, K.A.** *Candida albicans increases the pathogenicity of Staphylococcus aureus during polymicrobial infection of Galleria mellonella larvae.* Microbiology, 2020, 166(4): p.375.
243. **Coenye, T.** *Biofilm antimicrobial susceptibility testing: Where are we and where could we be going?* Clinical Microbiology Reviews, 2023, 36(4): p.e00024.
244. **Konečná, K. *et al*.** *The impact of cultivation media on the in vitro biofilm biomass production of Candida spp.* Current Microbiology, 2021, 78(5): p.2104.
245. **Rupert, C.B. and Rusche, L.N.** *The pathogenic yeast Candida parapsilosis forms pseudohyphae through different signaling pathways depending on the available carbon source.* mSphere, 2022, 7(3): p.e00029.
246. **Dunker, C. *et al*.** *Rapid proliferation due to better metabolic adaptation results in full virulence of a filament-deficient Candida albicans strain.* Nature Communications, 2021, 12(1): p.3899.
247. **Herek, T.C. *et al*.** *Biofilm formation by blood isolates of Candida parapsilosis sensu stricto in the presence of a hyperglycidic solution at comparable concentrations of total parenteral nutrition.* Revista da Sociedade Brasileira de Medicina Tropical, 2019, 52.
248. **Rumbaugh, K.P.** *How well are we translating biofilm research from bench-side to bedside?* Biofilm, 2020, 2: p.100028.
249. **Olsen, N.M.C. *et al*.** *Priority of early colonizers but no effect on cohabitants in a synergistic biofilm community.* Frontiers in Microbiology, 2019, 10.
250. **Debray, R. *et al*.** *Priority effects in microbiome assembly.* Nature Reviews Microbiology, 2022, 20(2): p.109.
251. **Ramsay, C. and Rohr, J.R.** *The application of community ecology theory to co-infections in wildlife hosts.* Ecology, 2021, 102(3): p.e03253.
252. **Hogan, D.A. and Kolter, R.** *Pseudomonas-Candida interactions: An ecological role for virulence factors.* Science, 2002, 296(5576): p.2229.
253. **Gibson, J., Sood, A., and Hogan, D.A.** *Pseudomonas aeruginosa-Candida albicans interactions: Localization and fungal toxicity of a phenazine derivative.* Applied and Environmental Microbiology, 2009, 75(2): p.504.
254. **McAlester, G. *et al*.** *Signal-mediated interactions between Pseudomonas aeruginosa and Candida albicans.* Journal of Medical Microbiology, 2008, 57(5): p.563.
255. **Shirtliff, M.E., Peters, B.M., and Jabra-Rizk, M.A.** *Cross-kingdom interactions: Candida albicans and bacteria.* FEMS Microbiology Letters, 2009, 299(1): p.1.
256. **Morales Diana, K. *et al*.** *Control of Candida albicans metabolism and biofilm formation by Pseudomonas aeruginosa phenazines.* mBio, 2013, 4(1).
257. **Cheong, J.Z.A. *et al*.** *Priority effects dictate community structure and alter virulence of fungal-bacterial biofilms.* The ISME Journal, 2021, 15(7): p.2012.
258. **Todd, O.A., Noverr, M.C., and Peters, B.M.** *Candida albicans impacts Staphylococcus aureus alpha-toxin production via extracellular alkalinization.* mSphere, 2019, 4(6): p.e00780.

259. **Richardson, A.R.** *Virulence and metabolism.* Microbiology Spectrum, 2019, 7(2).
260. **Wijnants, S., Vreys, J., and Van Dijck, P.** *Interesting antifungal drug targets in the central metabolism of Candida albicans.* Trends in Pharmacological Sciences, 2022, 43(1): p.69.
261. **Danhof, H.A. *et al*.** *Robust extracellular pH modulation by Candida albicans during growth in carboxylic acids.* mBio, 2016, 7(6).
262. **Vylkova, S. and Lorenz, M.C.** *Modulation of phagosomal pH by Candida albicans promotes hyphal morphogenesis and requires Stp2p, a regulator of amino acid transport.* PLOS Pathogens, 2014, 10(3): p.e1003995.
263. **Vesely, E.M. *et al*.** *N-acetylglucosamine metabolism promotes survival of Candida albicans in the phagosome.* mSphere, 2017, 2(5).
264. **Bayot, J. *et al*.** *The adaptive response to alternative carbon sources in the pathogen Candida albicans involves a remodeling of thiol- and glutathione-dependent redox status.* Biochemical Journal, 2023, 480(3): p.197.
265. **Komalapriya, C. *et al*.** *Integrative model of oxidative stress adaptation in the fungal pathogen Candida albicans.* PLoS One, 2015, 10(9): p.e0137750.
266. **Wang, Y. *et al*.** *Cap1p is involved in multiple pathways of oxidative stress response in Candida albicans.* Free Radical Biology and Medicine, 2006, 40(7): p.1201.
267. **Lin, Y.J. *et al*.** *Interactions between Candida albicans and Staphylococcus aureus within mixed species biofilms.* BIOS, 2013, 84(1): p.30.
268. **Coenye, T. *et al*.** *Should standardized susceptibility testing for microbial biofilms be introduced in clinical practice?* Clinical Microbiology and Infection, 2018, 24(6): p.570.
269. **Bizerra, F.C. *et al*.** *Changes in cell wall synthesis and ultrastructure during paradoxical growth effect of caspofungin on four different Candida species.* Antimicrobial Agents and Chemotherapy, 2011, 55(1): p.302.
270. **Nunes, T.S. *et al*.** *Fungistatic action of N-acetylcysteine on Candida albicans biofilms and its interaction with antifungal agents.* Microorganisms, 2020, 8(7): p.980.
271. **Van Duuren, J. *et al*.** *Use of single-frequency impedance spectroscopy to characterize the growth dynamics of biofilm formation in Pseudomonas aeruginosa.* Scientific Reports, 2017, 7(1): p.5223.
272. **Paredes, J., Becerro, S., and Arana, S.** *Comparison of real time impedance monitoring of bacterial biofilm cultures in different experimental setups mimicking real field environments.* Sensors and Actuators B: Chemical, 2014, 195: p.667.
273. **Pires, L. *et al*.** *Online monitoring of biofilm growth and activity using a combined multi-channel impedimetric and amperometric sensor.* Biosensors and Bioelectronics, 2013, 47: p.157.
274. **Reichhardt, C. and Parsek, M.R.** *Confocal laser scanning microscopy for analysis of Pseudomonas aeruginosa biofilm architecture and matrix localization.* Frontiers in Microbiology, 2019, 10.
275. **Müsken, M. *et al*.** *Towards individualized diagnostics of biofilm-associated infections: a case study.* npj Biofilms and Microbiomes, 2017, 3(1): p.22.
276. **Li, X. *et al*.** *Histones: The critical players in innate immunity.* Frontiers in Immunology, 2022, 13: p.1030610.
277. **Hoeksema, M. *et al*.** *Histones as mediators of host defense, inflammation and thrombosis.* Future microbiology, 2016, 11(3): p.441.
278. **Zlatina, K. and Galuska, S.P.** *Polysialic acid modulates only the antimicrobial properties of distinct histones.* ACS Omega, 2019, 4(1): p.1601.

Anexos

Artículo 6 (publicación)

Antimicrobial and antibiofilm activity of human recombinant H1 histones against bacterial infections

Publicado en la revista *mSystems*

DOI: 10.1128/msystems.00704-24

29 de octubre de 2024

Categoría Microbiología 2023: 1er tercil, 1er Cuartil, IF= 5.0

Betsy V. Arévalo-Jaimes[1,2], Mónica Salinas-Pena[3], Inmaculada Ponte[4], Albert Jordan[3], Alicia Roque[4] y Eduard Torrents[1,2]

[1]Grupo Infecciones Bacterianas y Terapias Antimicrobianas (BIAT), Instituto de Bioingeniería de Cataluña (IBEC), Barcelona, España.
[2]Sección de Microbiología, Departamento de Genética, Microbiología y Estadística, Facultad de Biología, Universitat de Barcelona, Barcelona, España.
[3]Instituto de Biología Molecular de Barcelona (IBMB-CSIC), Barcelona, España.
[4]Departamento de Bioquímica y Biología Molecular, Universitat Autónoma de Barcelona, Bellaterra, España.

Cita: Areválo, B. V., Salinas-Pena, M., Ponte, I., Jordan, A., Roque, A., & Torrents, E. (2024). Antimicrobial and antibiofilm activity of human recombinant H1 histones against bacterial infections. *mSystems.* DOI: 10.1128/msystems.00704-24.

AMERICAN SOCIETY FOR MICROBIOLOGY | mSystems

| Open Peer Review | Antimicrobial Chemotherapy | Research Article

Antimicrobial and antibiofilm activity of human recombinant H1 histones against bacterial infections

Betsy Verónica Arévalo-Jaimes,[1,2] Mónica Salinas-Pena,[3] Inmaculada Ponte,[4] Albert Jordan,[3] Alicia Roque,[4] Eduard Torrents[1,2]

AUTHOR AFFILIATIONS See affiliation list on p. 16.

ABSTRACT Histones possess significant antimicrobial potential, yet their activity against biofilms remains underexplored. Moreover, concerns regarding adverse effects limit their clinical implementation. We investigated the antibacterial efficacy of human recombinant histone H1 subtypes against *Pseudomonas aeruginosa* PAO1, both planktonic and in biofilms. After the *in vitro* tests, toxicity and efficacy were assessed in a *P. aeruginosa* PAO1 infection model using *Galleria mellonella* larvae. Histones were also evaluated in combination with ciprofloxacin (Cpx) and gentamicin (Gm). Our results demonstrate antimicrobial activity of all three histones against *P. aeruginosa* PAO1, with H1.0 and H1.4 showing efficacy at lower concentrations. The bactericidal effect was associated with a mechanism of membrane disruption. *In vitro* studies using static and dynamic models showed that H1.4 had antibiofilm potential by reducing cell biomass. Neither H1.0 nor H1.4 showed toxicity in *G. mellonella* larvae, and both increased larvae survival when infected with *P. aeruginosa* PAO1. Although *in vitro* synergism was observed between ciprofloxacin and H1.0, no improvement over the antibiotic alone was noted *in vivo*. Differences in antibacterial and antibiofilm activity were attributed to sequence and structural variations among histone subtypes. Moreover, the efficacy of H1.0 and H1.4 was influenced by the presence and strength of the extracellular matrix. These findings suggest histones hold promise for combating acute and chronic infections caused by pathogens such as *P. aeruginosa*.

IMPORTANCE The constant increase of multidrug-resistant bacteria is a critical global concern. The inefficacy of current therapies to treat bacterial infections is attributed to multiple mechanisms of resistance, including the capacity to form biofilms. Therefore, the identification of novel and safe therapeutic strategies is imperative. This study confirms the antimicrobial potential of three histone H1 subtypes against both Gram-negative and Gram-positive bacteria. Furthermore, histones H1.0 and H1.4 demonstrated *in vivo* efficacy without associated toxicity in an acute infection model of *Pseudomonas aeruginosa* PAO1 in *Galleria mellonella* larvae. The bactericidal effect of these proteins also resulted in biomass reduction of *P. aeruginosa* PAO1 biofilms. Given the clinical significance of this opportunistic pathogen, our research provides a comprehensive initial evaluation of the efficacy, toxicity, and mechanism of action of a potential new therapeutic approach against acute and chronic bacterial infections.

KEYWORDS biofilm, *Galleria mellonella*, treatment, toxicity, proteins, antimicrobial peptides

Bacterial infections caused by multidrug-resistant bacteria are increasingly burdening the global healthcare system (1, 2). Bacteria have evolved various mechanisms to counteract the harmful effects of antibiotic molecules, including restriction drug uptake, upregulating efflux pumps, altering drug targets, and inactivating drugs (2). Additionally, bacteria have developed defense strategies at the multicellular level. Bacterial biofilms

Editor Adina Howe, Iowa State University, Ames, Iowa, USA

Ad Hoc Peer Reviewer Mujeeb Ur Rehman, Sichuan Agricultural University, Chengdu, Sichuan, China

Address correspondence to Eduard Torrents, etorrents@ibecbarcelona.eu, eduard.torrents@ub.edu.

The authors declare no conflict of interest.

See the funding table on p. 16.

Received 20 May 2024
Accepted 26 September 2024

are communities of bacteria growing together and working collectively to withstand threats that would kill planktonic cells (3). Cells in biofilms produce an extracellular matrix (ECM) that surrounds and protects bacteria against antimicrobials, the immune system, phages, and other attacks (3). The biofilm structure and ECM create diffusion gradients of nutrients and antimicrobial molecules, promoting metabolic adaptations that result in population heterogeneity, adding more complexity to biofilm eradication (3, 4). Consequently, biofilm-associated infections are clinically challenging and often become persistent and difficult to treat (5).

Pseudomonas aeruginosa is one of the six highly drug-resistant bacteria worldwide (2). Its metabolic adaptability, coupled with an arsenal of virulence factors, explains its prevalence in life-threatening acute and chronic infections, particularly among immunocompromised patients (6). Its ability to form biofilms with increased tolerance to antibiotics leads to the development of chronic wounds and pulmonary failure in patients with cystic fibrosis and other respiratory diseases (6, 7).

The urgent need to develop new antibiofilm strategies that can either replace or complement current alternatives has led to the identification of effective natural compounds, including phytochemicals, biosurfactants, and antimicrobial peptides (AMPs) (5). AMPs are an important part of the innate immunity of multiple species, and acquiring resistance to them is more complicated than to antibiotics (4, 8).

Histones are crucial proteins in eukaryotic DNA organization and regulation (9). However, they can be secreted passively (necrosis) or actively (apoptosis and neutrophil NETosis) into the extracellular fluid (9, 10). Their cationic characteristics lead to cell membrane damage upon interacting with phospholipids (9). Like AMPs, the antimicrobial potential of histones has been demonstrated both *in vitro* and *in vivo* by effectively killing bacteria, fungi, parasites, and viruses (10, 11).

Histone H1 is a basic protein that regulates the higher-order structure of chromatin. It has three structural domains: the N-terminal domain (NTD), the globular domain (GD), and the C-terminal domain (CTD). The CTD represents approximately half of the protein and has the highest content of basic residues (12). Human somatic cells can express up to seven H1 subtypes: H1.0-H1.5 and H1X (13, 14). Histone H1 was proposed as a component of the antimicrobial defense in the human gastrointestinal tract in the 90s (15, 16). Since then, its antimicrobial activity has been reported against various bacteria (10, 11, 17); however, its potential as antibiofilm therapy and *in vivo* efficacy remains largely unexplored.

This study aims to evaluate the activity of three human recombinant histone H1 subtypes against *P. aeruginosa* PAO1 planktonic and biofilm-growing cells. We selected two of the more abundant subtypes in mammalian cells, H1.2 and H1.4, and the subtype that increases in differentiated cells, H1.0 (full length and CTD). Furthermore, we evaluated their potential as combined treatment with antibiotics (ciprofloxacin [Cpx] and gentamicin [Gm]) and assessed their toxicity and efficacy *in vivo* using the invertebrate animal model *Galleria mellonella*.

RESULTS

Antimicrobial efficacy and synergy assessment

The antimicrobial efficacy of histones H1.0, H1.0 C-terminal domain (CTD), H1.2, and H1.4 was determined by measuring their minimal inhibitory concentration 50% (MIC_{50}) (18) in the bacterial growth of three different important pathogens (Table 1). Overall, higher antimicrobial activity was observed against both Gram-negative bacteria, *P. aeruginosa* PAO1 and *Escherichia coli* CFT073, with the first being more susceptible. Conversely, a minor effect was observed against the Gram-positive bacteria *Staphylococcus aureus*.

The biomass reduction of *P. aeruginosa* PAO1 planktonic cultures after 16 h of histone treatment at MIC_{50} (Table 1) was visualized and measured by live and dead staining (Fig. 1). A statistically significant decrease in bacterial cell number (58%–70%) was shown in all samples treated with histone H1 subtypes compared to the control (Fig. 1A and B). Furthermore, some bacteria displayed red staining, indicating cell death (compromised

TABLE 1 Antibacterial activity of the different histones

	MIC_{50}[a]		
	***P. aeruginosa* PAO1**	***E. coli* CFT073**	***S. aureus***
H1.0	55 µg/mL	154 µg/mL	>220 µg/mL[b]
	(2.5 µM)	(7 µM)	(>10 µM)
H1.0 C-ter	58 µg/mL	>116 µg/mL[b]	>116 µg/mL[b]
	(5 µM)	(>10 µM)	(>10 µM)
H1.2	111 µg/mL	222 µg/mL	>222 µg/mL[b]
	(5 µM)	(10 µM)	(>10 µM)
H1.4	46 µg/mL	98 µg/mL	>229 µg/mL[b]
	(2 µM)	(4 µM)	(>10 µM)

[a]The minimal inhibitory concentration 50% (MIC_{50}) values measured after 10 h of histones treatment are shown. Data are representative of three independent experiments.
[b]No bacterial growth inhibition was observed below the indicated concentration.

membranes). Thus, we calculated the percentage of viable cells (green stained) present in each group (Fig. 1C) and found a statistically significant reduction in samples treated with H1.4 (31%), H1.0 (27%), and H1.2 (18%) compared to the control.

Consequently, we explored the potential use of histones H1.0 and H1.4 combined with antibiotics. We evaluated the synergy with Cpx and Gm to inhibit the planktonic growth of PAO1. The results showed a synergistic effect only when histone H1.0 was combined with Cpx (Table 2), whereas the other combinations showed an additive effect.

Histone and bacterial cells interaction

Aiming to elucidate the mechanism of action behind the antimicrobial activity of the H1 histones, we evaluated their direct interaction with *P. aeruginosa* PAO1 cells. Bacterial cultures were treated with histones for 30 min followed by a centrifugation step. Subsequently, we evaluated if histones were present in the supernatant or pellet fraction (Fig. 2). A precipitation control of histones without bacteria and a negative control of bacteria without histones were included. In Figure 2A, it is observed that irrespective of the histone, if bacteria were absent, Western blot bands are observed in both pellet and supernatant. However, when mixed with bacteria, histones completely co-precipitate with them, suggesting a direct interaction of H1 histones with bacterial cells. Western blot bands were confirmed by immunoblot and post-transfer Coomassie staining (Fig. 2B), except in the case of H1.0 CTD due to unavailability of specific antibodies. Notably, upon incubation with *P. aeruginosa* PAO1, H1 histones appeared to undergo partial cleavage, producing smaller H1 forms, as indicated by the presence of multiple bands detected in the pellet by specific antibodies in the immunoblot (Fig. 2B). This suggests that H1 cleavage occurs due to interaction with *P. aeruginosa* PAO, likely mediated by secreted bacterial proteases. The cleaved form represents approximately 10%–40% of the total H1, depending on the H1 variant.

Furthermore, to assess if histone interactions caused any alteration to the bacterial cell membrane, cultures were treated with histones H1 at their *P. aeruginosa* PAO1 MIC_{50} concentration (Table 1) and were stained with the specific dyes FM-464 and DAPI (Fig. 3). Some cells with membrane damage are observed in the control samples after the centrifugation step (Fig. 3, control-zoomed images). However, very evident gaps in cell membranes were observed in all samples treated with histones (Fig. 3, histones-zoomed images) in a proportion of 5%–8% (cells with gaps in membrane/total cells). Additionally, histone H1.0 (full length and CTD) and H1.4 caused non-homogenous staining among cells, with most showing a fainter membrane compared to the control sample. This effect is less markedly in samples treated with H1.2.

The differences observed in the alteration of bacterial membrane among histone subtypes could be explained by sequence and structural differences. Therefore, we analyzed several sequence-related properties of histone H1 subtypes, finding distinct features in the two subtypes with higher antimicrobial activity. Histone H1.0 has the

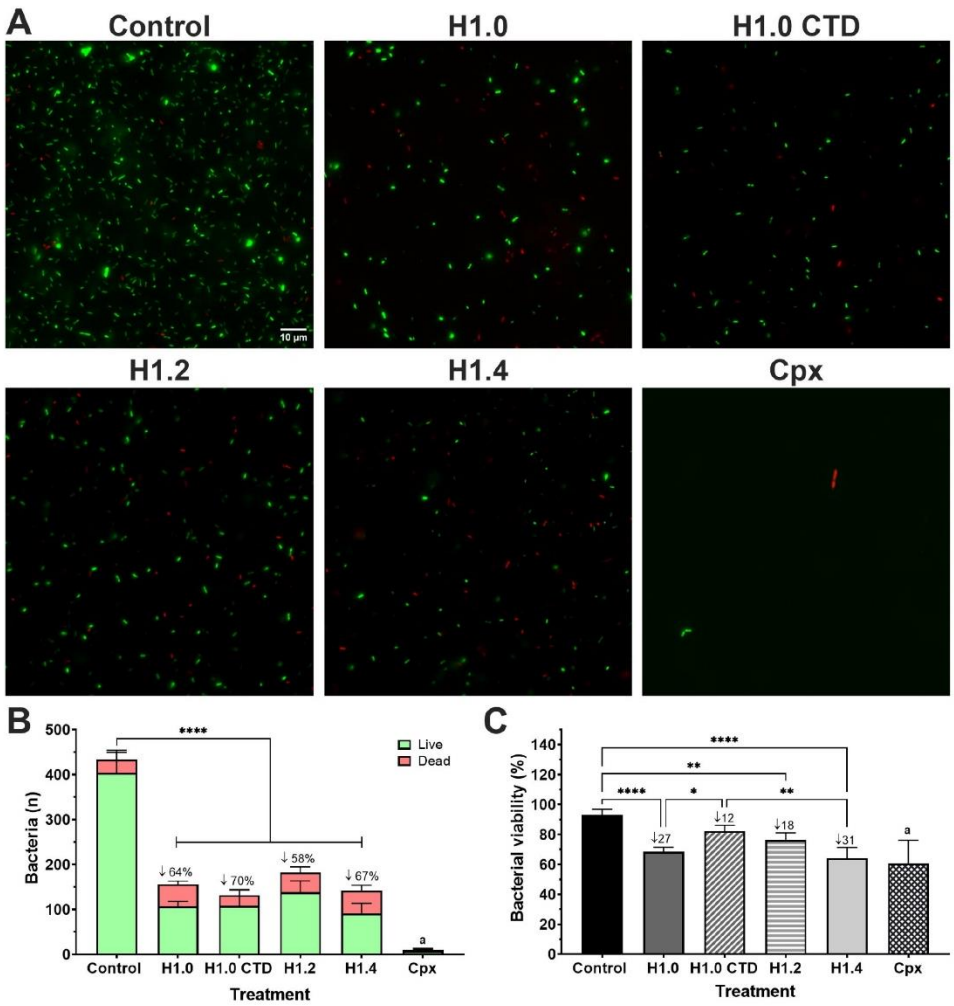

FIG 1 Bacterial viability assessment of *P. aeruginosa* PAO1 planktonic cultures after H1 histone treatment. (A) Live and dead staining using Syto 9 (green live cells) and propidium iodide (red dead cells) dyes after 16 h of treatment. Histones were used at the MIC_{50} concentration of PAO1: H1.0 at 55 µg/mL, H1.0 CTD 58 µg/mL, H1.2 at 111 µg/mL, and H1.4 at 46 µg/mL. Cpx was used at 2 µg/mL. Fluorescence images were processed with Image J. The scale bar of 10 µm is consistent for all cases. (B) Quantification of live and dead bacteria by particle counting with Image J. Numbers after ↓ symbol indicate the percentage of reduction in bacterial total cell number compared to the untreated control. Error bars display mean and standard deviation from at least four replicates. Differences in the number of total cells among groups were analyzed by a one-way ANOVA analysis with Tukey's multiple comparison test (****, *P* value < 0.0001). Letter **a** represents a statistical difference of total cell number in the Cpx group compared to the control, H1.0 and H1.2 with a *P* value < 0.0001, and H1.0 CTD and H1.4 with a *P* value < 0.001. (C) Percentage of viability of bacterial cells {[live bacteria/(live bacteria + dead bacteria)]*100}, where live bacteria is the number of particles counted in the green channel (Syto 9 stained) and dead bacteria is the number of particles counted in the red channel (propidium iodide stained). Numbers after ↓ symbol indicate the percentage of reduction compared to the control. Error bars display mean and standard deviation from at least four replicates. Differences among groups were analyzed by a one-way ANOVA analysis with Tukey's multiple comparison test (*, *P* value < 0.05; **, *P* value < 0.01; ****, *P* value < 0.0001). Letter **a** represents a statistical difference in the viability percentage of the Cpx group compared to the control with a *P* value < 0.0001, H1.0 CTD with a *P* value < 0.001, and H.12 with a *P* value < 0.05.

TABLE 2 Evaluation of synergy between histones H1.0 and H1.4 with ciprofloxacin and gentamicin on *P. aeruginosa* PAO1 growth[a]

Combination	$FIC_{Histone}$	$FIC_{Antibiotic}$	ΣFIC	Interaction
H1.0 + Cpx	0.25	0.25	0.5	Synergy
H1.0 + Gm	0.061	0.5	0.561	Additivity
H1.4 + Cpx	0.016	0.5	0.516	Additivity
H1.4 + Gm	0.012	0.5	0.512	Additivity

[a]FIC, fractional inhibitory concentration; Σ, summatory; Cpx, ciprofloxacin; Gm, gentamicin.

highest positive charge density and the lowest hydropathicity, expressed as the GRAVY index, whereas H1.4 has the highest number of basic residues per protein molecule and the highest net charge (Table 3).

Moreover, we studied the secondary structure of the recombinant proteins by bioinformatic analysis and experimental methods. Sequence predictions showed the highest values of α-helix in H1.4 followed by H1.0 and H1.2 (Table 3). The helical content and induction were studied by circular dichroism (Fig. S1). We calculated the ratio between the molar ellipticity in the minimum of the α-helix canonical spectrum at 222 nm and the minimum of the entire spectrum in the random coil region as an index of the proportion of α-helix present in each sample. The proteins were analyzed in aqueous solution, where the spectrum is clearly dominated by the random coil and in the presence of trifluoroethanol (TFE), a known stabilizer of α-helix (19). We observed that, in contrast with the predictions, the molar ellipticity ratio was higher in H1.0 than in H1.4 and H1.2 in both conditions (Table 4).

To evaluate the existence of a correlation in the variation of the parameters of positive charge, hydropathicity, and α-helix content and the differences observed in the activity of histone H1 subtypes, we performed simple linear regressions. As a result, any correlation with the antimicrobial activity of histones was found (reduction of planktonic cells after treatment). However, there is a positive correlation between the proportion of α-helix content induced in TFE and the antibiofilm activity of the histone H1 subtype against static biofilms of PAO1 ($r^2 = 1$, P value = 0.0043). Unfortunately, the low number of evaluated proteins made it impossible to perform a multiple linear regression that evaluates the effect of the parameters simultaneously.

Histone H1 antibiofilm efficacy

Recognizing the significance of biofilm-related infections, we investigated the efficacy of histones against *P. aeruginosa* PAO1 biofilms. Initially, we assessed the reduction in biofilm biomass after treatment with H1 histones using a static biofilm model (96-well plate) and the crystal violet biomass staining. As shown in Figure 4A, all histone-treated samples exhibited some degree of biomass reduction, with more pronounced effects observed when using H1.0 (28%, adjusted P value = 0.0273), followed by H1.4 (22%) and H1.2 (20%).

We selected H1.0 and H1.4 subtypes to test their antibiofilm *in vitro* efficacy in a continuous flow chamber biofilm assay, a model that better resembles *in vivo* biofilm infections. PAO1 biofilms treated with 100 µg/mL of each H1 subtype were died with the live and dead staining and imaged by confocal microscopy (Fig. 4B). As seen in Figure 4B, the orthogonal views show a significant decrease in bacterial biomass in the biofilm treated with histone H1.4 compared to the untreated control. Quantification confirmed a significant reduction in PAO1 biofilm biomass (29%) and average thickness (12%) after H1.4 treatment (Fig. 4C and D). Moreover, the dead biomass (red staining) significantly increased in the biofilm treated with H1.4 (Fig. 4E). No significant effect in the evaluated parameters was observed after H1.0 treatment. The findings obtained under this grown condition are particularly noteworthy because the resulting biofilms are highly resistant to antibiotics as seen with the Cpx treatment as positive control.

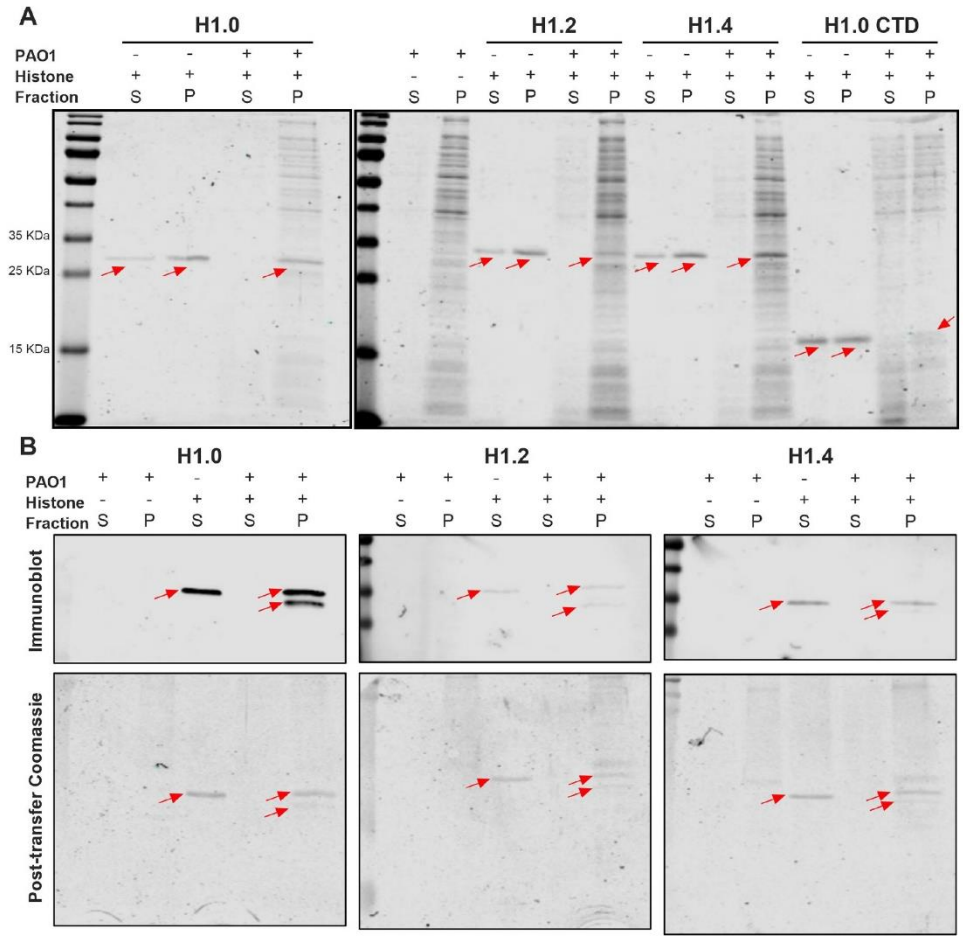

FIG 2 H1 histones precipitation assay after incubation of PAO1 planktonic cells. (A) Coomassie-stained SDS-PAGE gel of supernatant and pellet fraction from bacterial cultures, histones, and bacterial cultures treated with histones after centrifugation. Red arrows indicate the band corresponding to the respective histone subtype. (B) Immunoblot and post-transfer Coomassie staining of bands found in the supernatant and pellet fraction from bacterial cultures, histones, and bacterial cultures treated with histones after centrifugation. +, presence; –, absence; S, supernatant; P, pellet.

In vivo H1.0 and H1.4 toxicity assessment and antimicrobial efficacy

Next, we used the *G. mellonella* larvae infection model to evaluate the antimicrobial potential of histone H1. No mortality or morbidity parameters (myelinization, activity reduction, and absence of cocoon) (20) associated with toxic effects were observed in *G. mellonella* larvae for up to 60 h post-injection with H1.0 and H1.4 histones in a range of 1.25–20 mg/kg (25–400 µg/mL), indicating low toxicity and a median lethal dose (LD_{50}) higher than 20 mg/kg. In addition, the lack of morbidity or mortality in the double-injected group (PBS followed by histones at 20 mg/kg) indicated no adverse effects when histones were administered during the treatment phase of a double injection procedure.

Therefore, we proceeded to evaluate the use of histones H1.0 and H1.4 as treatments for rescuing larvae infected with *P. aeruginosa* PAO1. At 1 h post-infection, larvae were

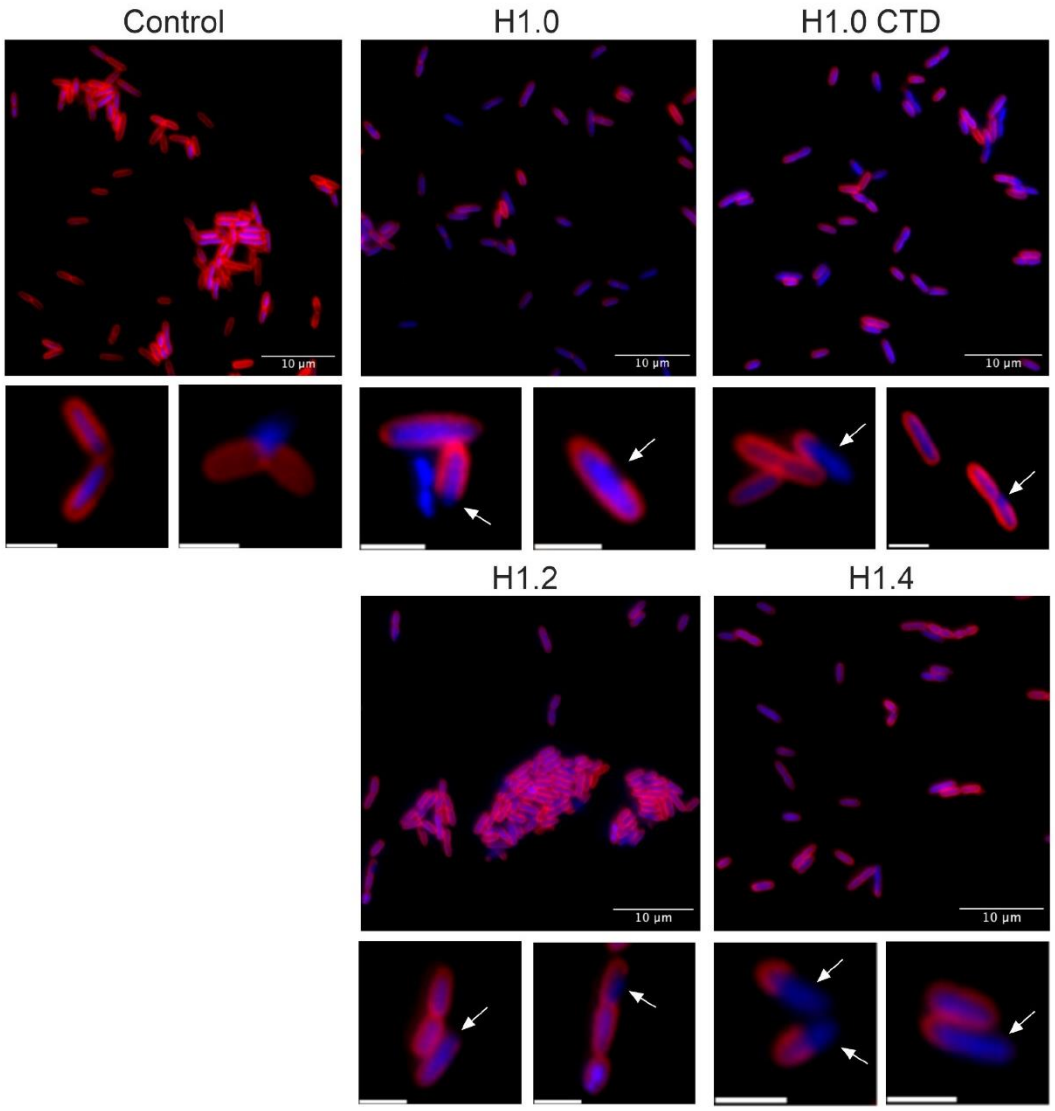

FIG 3 Assessment of membrane alterations of PAO1 cells after histone treatment. Bacteria were stained with FM-464 (red) and DAPI (blue) dyes to visualize the membrane and genetic material, respectively. Histones were used at the MIC_{50} of PAO1. Fluorescence images were processed with Image J software. Scale bars correspond to 10 µm in large images and 2 µm in zoomed images. White arrows point to gaps in cell membranes.

treated with histones (100 µg/mL) alone and in combination with Cpx (Fig. 5). Larvae survival was increased and extended when infected *G. mellonella* were treated with histones compared to those treated with PBS (negative control). Specifically, the median survival was significantly extended from 16 h in PBS-treated group to 18 and 20 h in the histone H1.0- and H1.4-treated groups, respectively. However, when comparing larvae treated with Cpx 1.5 mg/kg versus those treated with the combined therapy,

TABLE 3 Protein characteristics of H1 subtypes

Subtype	Number of basic residues	Net charge	Positive charge density	GRAVY index	Secondary structure prediction (%)			
					α-Helix	Extended strand	Random coil	Ambiguous states
H1.0	62	+53	0.32	−1.07	35.57	4.12	50	10.31
H1.2	62	+55	0.29	−0.68	32.39	2.35	55.87	9.39
H1.4	66	+59	0.30	−0.78	38.81	2.28	46.12	12.79

no significant improvement was observed. Finally, the lack of mortality in the PBS–PBS group confirmed that the observed larvae mortality in the other groups was related to bacterial infection rather than injuries associated with the double injection process.

DISCUSSION

Histones are ubiquitous across different tissues, and their antimicrobial activity had been reported in multiple species (10). Moreover, some peptide fragments derived from histones cleavage are considered AMPs (21). For instance, H1 histones secreted by human colonic epithelial cells possess antimicrobial activity (15, 22), as well as the peptides derived from the NTD of H1 histone from Atlantic salmon and the CTD of H1 histone from rainbow trout (known as Oncorhyncin II) (23, 24).

In this work, we reported the ability of three human H1 subtypes (H1.0, H1.2, and H1.4) to inhibit bacterial proliferation and induce cell death in three well-known opportunistic pathogens: *P. aeruginosa*, *S. aureus*, and *E. coli* (Table 1; Fig. 1). Our findings support the study by Jacobsen et al. (25), where the efficacy of recombinant human histone H1.2 was demonstrated against bacteria found in human wound infections (25). Similarly, Jodoin and Hincke (17) reported that histone H1 from chicken (named H5 in this animal) has antimicrobial activity against Gram-negative and Gram-positive bacteria (17).

Our results (Table 1) confirm that histones had a broad-spectrum antimicrobial effect regardless of the subtype used. However, a lower concentration of the protein is required to inhibit Gram-negative bacteria (*P. aeruginosa* PAO1 and *E. coli* CFT073). This observation is consistent with the affinity of H1 for bacterial lipopolysaccharide (LPS), the major component of the outer membrane of Gram-negative bacteria (26). Our study confirms an interaction between H1 histones and *P. aeruginosa* PAO1 cells upon mixed incubation (Fig. 2). Moreover, the fragmentation of all three histone subtypes in the precipitate fraction, alongside bacteria, suggests that bacterial proteases may degrade the histones, and their antimicrobial properties could be attributed to AMP characteristics.

The mechanism underlying histone-mediated bacteria killing remains unclear, but two primary options have been proposed: membrane disruption or cytoplasmatic targeting. H1 from the liver of Atlantic salmon causes morphological alterations that directly damage the cell surface (27). Likewise, H1 from chickens caused pore formation and content liking in *P. aeruginosa* cells (17). Conversely, Oncorhyncin II is unable to form stable channels in the membrane, suggesting an antimicrobial activity resultant from intracellular processes (24). In this study, bacterial cells treated with histone H1 subtypes displayed clear membrane gaps, indicating bacterial killing by alteration of membrane integrity (Fig. 3). Furthermore, we hypothesized that their presence in the bacterial membrane hindered FM-464 dye incorporation, resulting in less intense staining in histone-treated samples compared to the untreated control. This effect was

TABLE 4 Circular dichroism of H1 subtypes

Solvent	Molar ellipticity ratio[a]		
	H1.0	H1.2	H1.4
PBS	0.55	0.43	0.42
TFE 20%	0.63	0.56	0.57

[a]Molar ellipticity ratio was calculated as the value at 222 nm referred to the minimum of the spectrum.

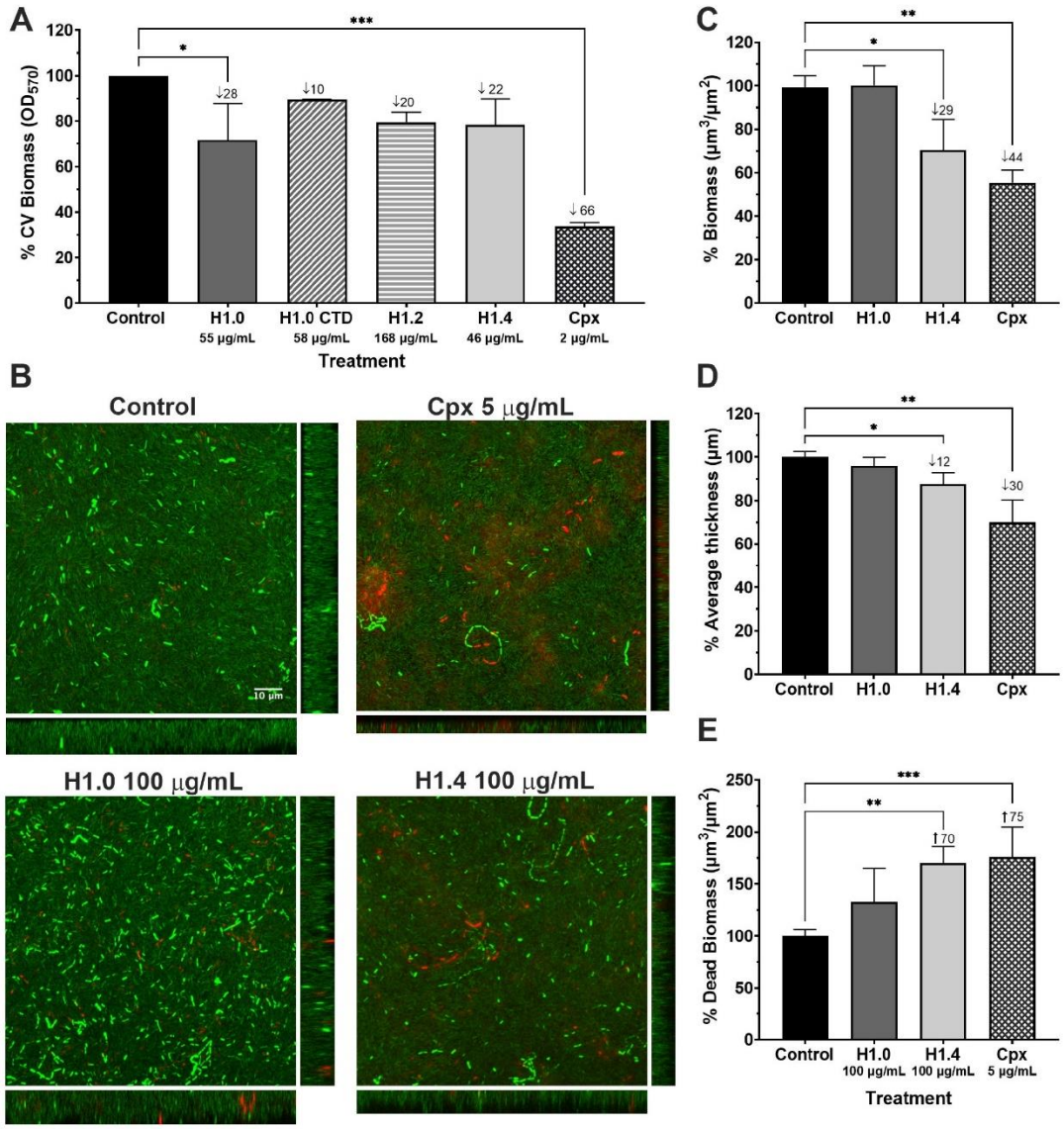

FIG 4 Antibiofilm activity of histones against PAO1 biofilms. (A) Biomass reduction of static biofilms after histone treatment. Error bars display mean and standard deviation of at least three replicates. Data differences with respect to the control group were analyzed by a one-way ANOVA analysis with Dunnett's multiple comparison test (*, *P* value < 0.05; ***, *P* value < 0.001. (B) Confocal microscopy visualization of continuous flow biofilms after treatment with H1.0 and H1.4. Biofilms were stained with Syto 9 and propidium iodide to dye live cells in green and dead cells in red. Z-stacks from confocal images with their corresponding orthogonal views are displayed. The scale bar of 10 µm is consistent across all images. Confocal image analysis of the (C) percentage reduction in biomass, (D) percentage reduction in average thickness and (E) percentage increase in dead biomass after treatment of flow biofilms with H1.0 and H1.4. Numbers after the ↓ symbol indicate the percentage of reduction compared to the control, whereas numbers after the ↑ symbol indicate the percentage of increase compared to the control. Error bars display mean and standard deviation of at least three replicates. Data differences with respect to the control group were analyzed by a one-way ANOVA analysis with Šidák's multiple comparison test (*, *P* value < 0.05; **, *P* value < 0.01; ***, *P* value < 0.001).

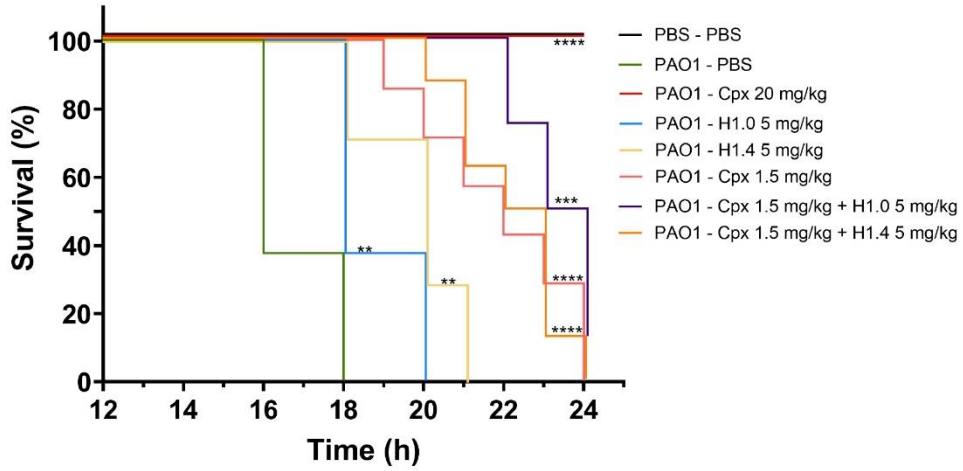

FIG 5 *In vivo* evaluation of H1 histone activity against *G. mellonella* infected with PAO1. Kaplan-Meier survival curves of *G. mellonella* larvae infected with PAO1 and treated with histones alone or in combination with Cpx. Control larvae were injected with PBS. Larval mortality was monitored for 16–24 h post-injection with observations conducted hourly. Significant differences in treatment efficacy compared to the PAO1-PBS-treated group were assessed using a log-rank test (*, *P* value < 0.05; **, *P* value < 0.01; ***, *P* value < 0.001; ****, *P* value < 0.0001). The results depicted in this figure represent an experiment replicated three times with consistent outcomes, each condition involving eight larvae.

more pronounced in the case of H1.0 and H1.4, suggesting a higher affinity of these histones with *P. aeruginosa* PAO1 membrane.

Several factors can influence how an AMP causes membrane alterations, including propensity for peptide self-assembly, net charge, and amphipathicity (21, 28). These characteristics can be found in peptides with an amphipathic α-helix structure (29, 30). We compared the positive charges, hydropathicity, and α-helix content of H1.0, H1.2, and H1.4 proteins (Tables 3 and 4). Overall, H1.0 and H1.4, the subtypes with higher antimicrobial and antibiofilm activity, exhibited higher net charge, lower gravy index (more hydrophilic), and higher α-helix content. Simple linear regression models showed a correlation between α-helix content induced in TFE and the antibiofilm activity of H1 subtypes against *P. aeruginosa* PAO1 static biofilms. However, the structural properties of the three subtypes are very similar, and more robust statistical analysis need to be conducted.

As not all the antimicrobial molecules had antibiofilm activity, we decided to test H1 histones' efficacy against *P. aeruginosa* PAO1 biofilms (Fig. 4). The urgent need for alternative molecules that can eradicate biofilms, specially from multidrug-resistant bacteria, has led to the identification of several AMPs with antibiofilm properties (see the Biofilm-active AMPs database at http://www.baamps.it/) (31). However, as far as we are aware, the ability of histones for biofilm disruption has been understudied. Jacobsen et al. showed a reduction of ~60% of bacterial burden in an *in vivo* rat burn model infected with *P. aeruginosa* after treatment with H1.2 protein (25). Likewise, the work from Jodoin and Hincke (17) reported that the minimum biofilm eradication concentration (MBEC) value of H1 from chicken against *P. aeruginosa* biofilms formed under static conditions is >128 µg/mL (17). Although the methodology used in our study is different, our data pointed to a similar MBEC value.

We used two different *in vitro* models widely employed for biofilm studies. The microtiter plate, a static model used, is easy to use and has a high throughput; and the continuous flow chamber assay is a dynamic model in which the resulting biofilms are structurally similar to those present in natural infections (32). Flow conditions stimulate the production of robust ECM, which, in the case of *P. aeruginosa* PAO1 biofilms, contain

alginate and extracellular DNA—two highly negatively charged molecules that can trap positively charged agents (33). Thus, we expected this scenario to be more challenging for histone treatment efficacy. We found higher antibiofilm activity in H1.0 in the static model compared to the other H1 subtypes (Fig. 4A). However, in the dynamic biofilm model, H1.4 has better results than H1.0 (Fig. 4B and D). H1.0 has a higher density of positive charges, lower gravy index (more hydrophilic), and higher formation of α-helix in TFE compared to H1.4 (Table 3). Similarly, H1.0 CTD, the protein region with more positive charges and less hydrophobicity (12, 34), showed reduced activity against *P. aeruginosa* PAO1 biofilms (Fig. 4A) when compared to H1.0 (full length). This could indicate that these parameters are influencing the antibiofilm activity of histones, with their effect being more markedly when biofilms are formed under dynamic conditions.

It is important to consider that the biofilm reduction assessed by the static crystal violet assay quantifies both cell and ECM biomass, whereas live and dead staining only assess differences in cell biomass. Nevertheless, we found the almost 30% reduction in cell biomass obtained after H1.4 treatment in the flow biofilm assay to be highly significant (Fig. 4B and C). Considering the reduction observed in the average biofilm thickness (Fig. 4D) and the increase in the biomass stained with propidium iodide (Fig. 4E), we proposed that the antibiofilm activity of the histone H1.4 is associated with its capacity to induce bacterial cell death.

Finally, the antimicrobial activity of H1 subtypes against *P. aeruginosa* PAO1 obtained in this study was validated in an *in vitro* animal model. It is known that the use of histones as therapeutic agents could lead to adverse effects. For instance, extracellular histones are damage-associated molecular patterns, able to induce chemokine release and cytotoxicity (10). They can induce thrombin generation and platelet aggregation, promoting thrombosis and thrombocytopenia (21). Moreover, histone interaction with cell membranes can activate adverse inflammatory responses that worsen several diseases (21).

Regarding histone H1, Oncorhyncin II and H1 from chicken do not have significant hemolysis (17, 24). Similarly, human recombinant H1.2 showed very low hemolytic activity (2%) at 250 µg/mL, but cytotoxicity against human keratinocytes at low concentrations was observed (25). In this study, we did not observe any sign of toxicity in *G. mellonella* larvae injected with histone H1.0 and H1.4 up to 20 mg/kg (400 µg/mL). Furthermore, we found an increase of the median survival rate after treatment of *G. mellonella* infected with *P. aeruginosa* PAO1 (Fig. 5).

G. mellonella larvae have an innate immune response very similar to that found in mammals, making them widely used for initial testing of the efficacy and toxicity of new antimicrobial agents, thereby reducing the use of mammalian models (35). However, we are aware that further toxicity and efficacy studies involving human cells and mammals must be conducted, but the positive results obtained against this aggressive bacterium are promising. In addition, the discovery that polysialic acid can reduce the H1-mediated cytotoxicity in eukaryotic cells without altering its antimicrobial activity creates a new alternative in biomedical applications (9).

Beyond cytotoxicity, there are still significant challenges and limitations to overcome before histone-derived AMPs, and AMPs in general, can be used clinically (36, 37). These challenges include the high cost for large-scale manufacturing of natural peptides, susceptibility to proteolytic degradation, and low bioavailability (17, 36, 38). However, new strategies are continually being proposed (39, 40), including the use of shorter peptides derived from histone sequences, structural modifications (D-amino acids, cyclic peptides, acetylation, amidation, etc.), and delivery systems (liposomes, nanoparticles, micelles, hydrogels, etc.) to increase stability (17, 36, 38, 40). In terms of formulation, most AMPs designed for clinical use are limited to local administration or intravenous injection, although lipid-based nanoparticles have been proposed to overcome the challenges associated with oral administration (36).

Another strategy to enhance clinical potential involves the concomitant use of histones with AMPs that have different modes of action, which has been shown to be

effective (41). Similarly, combining AMPs with antibiotics has been proven to enhance antibacterial activity (8). In this study, we tested the synergy between histones and two antibiotics with different mechanisms of action. First, we did not observe any improvement when combining histones with the aminoglycoside Gm. We believe Gm's ability to interact with LPS (42) may create competition for histone–bacteria interactions, diminishing their antimicrobial potential.

Second, although we observed a synergy between Cpx and H1.0 *in vitro* (Table 2), no significant difference in the median survival rate of *G. mellonella* larvae was observed with the combined treatment compared to the antibiotic alone (Fig. 5). This discrepancy may be due to a masking of the histones' antibacterial effect by Cpx in the *in vivo* test. Further experiments should include a reduced Cpx concentration (<1.5 mg/kg) where all larvae die between 19 and 21 h, as observed after *P. aeruginosa* PAO1 infection and histone treatment (Fig. 5). This would allow us to determine whether there is an extension of larval survival with the combined strategy. We acknowledge this as a limitation of our study.

In conclusion, we have demonstrated that H1.0, H1.2, and H1.4 have antimicrobial activity against *P. aeruginosa* PAO1, likely attributable to membrane disruption. H1.0 and H1.4 were the subtypes that exhibit higher antimicrobial activity with lesser concentration required. H1.4 had higher antibiofilm potential and better survival outcomes *in vivo* in an acute infection model of *P. aeruginosa* PAO1. Although we did not validate a synergistic effect of H1.0 and H1.4 with the antibiotics ciprofloxacin and gentamicin, none of the histone subtypes caused toxicity to *G. mellonella* larvae.

MATERIALS AND METHODS

Histone expression and purification

H1.0 and its CTD were cloned into pQE60 (Qiagen). The H1.0 CTD was cloned directionally into the restriction sites Nco I and Bgl II of the plasmid vector. In the case of the full-length H1.0, the pQE-60 vector was digested with Nco I, then the DNA ends were blunted with the Klenow fragment of DNA polymerase I (Roche Diagnostics) and finally digested with Bgl II. The digested plasmid was ligated to the amplification product digested with Bgl II. Recombinant H1.0 and its CTD were expressed in *E. coli* M15 (Qiagen) (43). Histones H1.2 and H1.4 were cloned into pET21a using the same cloning strategy, inserting the coding sequence between Nde I and Xho I restriction sites. Expression of H1.2 and H1.4 was carried out in *E. coli* BL21 (DE3) (Merk Millipore).

All proteins contained a His-tag at the C-terminal protein end. Recombinant proteins were expressed and purified by metal-affinity chromatography as previously described (44). Cells were grown to an OD_{600} nm of 0.8 and then induced with 1 mM IPTG, allowing expression to proceed for 4 h at 37°C. Cells were then harvested and stored at 80°C until use. Cells were lysed in lysis buffer (0.05 M NaH2PO4, 0.75 M NaCl, 0.02 M imidazole) plus 4 M guanidine hydrochloride, pH 8.0, for 15 min at room temperature. Guanidine hydrochloride was added to avoid degradation and aggregation of the expressed protein. The extract was centrifuged at 20,000 × *g* for 25 min. The supernatants were loaded on a HiTrap chelating HP column (Amersham Biosciences) equilibrated with lysis buffer. The column was washed in three steps with lysis buffer containing increasing amounts of imidazole: 40, 60, and 80 mM. Finally, the proteins were eluted with 250 mM imidazole in lysis buffer and desalted by gel filtration through Sephadex G-25 (Amersham Biosciences). Before their use, histones were thawed, vortexed, and sonicated (three cycles of 20 s) using an ultrasonic processor UP50H (Hielscher ultrasonics).

Sequence analysis and predictions

The sequences of H1.0, H1.2, and H1.4 were used to compare the positive charge density and the predicted secondary structure of the analyzed subtypes. Positive charge density

of H1.0 (P07305), H1.2 (P16403), and H1.4 (P10412) was calculated as the quotient between the number of basic residues and the protein length. The GRAVY index was calculated by the sum of hydropathy values of all amino acids divided by the protein length. Consensus secondary structure predictions were obtained at the Network Protein Sequence @nalysis (NPS@) server (https:// prabi.ibcp.fr/htm/site/web/app.php/home).

Circular dichroism

Secondary structure of H1.0, H1.2, and H1.4 was analyzed in aqueous solution (PBS) and in the presence of 20% 2,2,2 trifluoroethanol. Proteins were resuspended in the desired solvent at a final concentration of 230 ng/µL. Measurements were recorded in a J-815 spectropolarimeter (JASCO) in a continuous scanning mode, in the 190–250 nm range at a scanning speed of 200 nm/min with a bandwidth of 1 nm. Five accumulations were taken of each spectrum. Molar ellipticity was obtained by normalizing CD units by the protein concentration and the number of residues.

Bacterial strains and growing conditions

Three different bacterial strains were used in this study: *P. aeruginosa* PAO1 strain (CECT 4122 – ATCC 15692), referred to as PAO1, *S. aureus* (CECT 86 – ATCC 12600), and a uropathogenic *E. coli* CFT073 strain (ATCC 700928). Bacteria were retrieved from a −80°C stock and were cultured on Luria-Bertani media (Scharlau) for PAO1 and *E. coli* CFT073, and tryptic soy agar/broth (TSA/TSB) (Scharlau) for *S. aureus*. Overnight cultures were made by incubation at 37°C and 200 rpm. Unless specified, bacterial inoculum for each experiment was prepared by incubating 100 µL of overnight cultures in fresh TSB media until reaching the initial exponential log phase ($OD_{550\ nm} \approx 0.2–0.3$).

Antibacterial activity against planktonic bacteria

One hundred microliters of inoculum from all three bacterial strains was plated in a 96-well microtiter plate (Corning) filled with histone protein concentrations ranging from 2 to 10 µM. TSB medium was used as a negative control. Following a previously described method (18), the microtiter plate was incubated at 37°C in a SPARK Multimode microplate reader (Tecan) with 150 rpm shaking. Bacterial growth was monitored for 10 h with readings taken every 15 min.

The MIC_{50} was defined as the compound concentration that reduces bacterial growth, determined as the OD_{550}, by 50%.

Fluorescent microscopy viability test analysis

Aliquots of 500 µL from a *P. aeruginosa* PAO1 inoculum were treated with histones at a concentration equal to their MIC_{50} value of each subtype (see Table 1). Samples were treated with Cpx at 2 µg/mL, and media were included as controls. After 16 h of incubation at 37°C, 100 µL of the samples was centrifuged at 6,000 rpm for 5 min. Pellets were resuspended in 25 µL of PBS (Fisher Scientific S.L.) and stained with Syto 9 and propidium iodide (Live/Dead BacLight Bacterial Viability Kit, Thermo Fisher Scientific) following the manufacturer's instructions. Samples were visualized using a Nikon inverted fluorescent microscope ECLIPSE Ti–S/L100 (Nikon, Japan) coupled with a DS-Qi2 Nikon camera (Nikon, Japan). Images were processed and quantified by analysis of particles with Image J software. The percentage of viability was calculated according to the following formula:

$$\%Viability = \frac{Live\ bacteria}{Live\ bacteria + Dead\ bacteria} * 100$$

where live bacteria is the number of particles counted in the green channel (Syto 9 stained), and dead bacteria is the number of particles counted in the red channel (propidium iodide stained).

Antibiotic-histones synergy testing by checkerboard assay

The synergy of histones H1.0 and H1.4 in combination with Cpx and Gm was determined by the standard broth microdilution assay as described previously (43). Briefly, *P. aeruginosa* PAO1 inoculum was added in a 96-well microtiter plate with increasing concentrations of histone on one axis (0.15 - 20 µM) and increasing concentrations of antibiotic on the other (0.01–2 µg/mL of Cpx or 0.125–2 µg/mL of Gm). Plates were incubated at 37°C in a SPARK Multimode microplate reader with 150 rpm shaking for 16 h. The effect of the antimicrobial combination was defined using the lowest fractional inhibitory concentration (FIC) index (45). The formula employed for FIC calculation (43) and its interpretation (46) were as previously described:

$$\Sigma\mathrm{FIC} = \frac{\mathrm{MIC}_{100}\ \text{combination}}{\mathrm{MIC}_{100}\ \text{histone}} + \frac{\mathrm{MIC}_{100}\ \text{combination}}{\mathrm{MIC}_{100}\ \text{antibiotic}},$$

where ΣFIC ≤0.5 is defined as synergy, ΣFIC >0.5 and <4 is additivity/indifference, and ΣFIC >4 is antagonism.

Histones and bacterial cells interaction by precipitation experiments

Aliquots of 200 µL of a *P. aeruginosa* PAO1 inoculum were treated with a concentration of 10 µg/mL of each histone subtype. After 30 min of incubation at 37°C and 300 rpm in a thermomixer (Eppendorf), samples were centrifuged at 6,000 rpm for 5 min, and supernatant and pellet were collected. Histones added to TSB were used as precipitation control.

Subsequently, supernatant and pellet samples were boiled (5 min at 95°C) and exposed to SDS-PAGE (14%), followed by Coomassie staining or immunoblotting with H1 variant-specific antibodies. For immunoblotting, protein extracts were transferred to PVDF membrane, blocked with 5% non-fat milk for 1 h, and incubated overnight at 4°C with the primary antibodies anti-H1.0 (Millipore 05-629I), anti-H1.2 (Abcam ab4086), and anti-H1.4 (Invitrogen 702876). No specific antibodies against the C-terminal region of H1.0 were available. Next, samples were incubated with secondary antibodies conjugated to fluorescence (IRDye 680 goat anti-rabbit IgG or IRDye 800 goat anti-mouse IgG, Li-Cor) for 1 h at room temperature. Bands were visualized using an Odyssey Infrared Imaging System (Li-Cor). Coomassie staining was used as a loading control.

Bacterial membrane integrity after H1 incubation

Aliquots of 200 µL of a *P. aeruginosa* PAO1 inoculum were treated with histones H1.0, H1.0 CTD, H1.2, and H1.4 at a concentration of 55, 58, 111, and 46 µg/mL, respectively, which correspond to their MIC_{50} value (Table 1). After 30 min of incubation at 37°C and 300 rpm in a thermomixer (Eppendorf), samples were centrifuged at 6,000 rpm for 5 min. Pellets were resuspended in 50 µL of PBS with DAPI (Invitrogen) at 100 µg/mL and FM 4-64 (Invitrogen) at 40 µg/mL for 15 min. Samples were dropped on a slide pre-covered with agarose 1% (wt/vol) as previously described (47) and visualized with a Nikon inverted fluorescent microscope ECLIPSE Ti–S/L100 (Nikon, Japan) coupled with a DS-Qi2 Nikon camera (Nikon, Japan). Images were processed with Image J software. The percentage of cells with membrane gaps was calculated by manually counting damaged cells and dividing by the total number of cells (automated particle counting) from three different replicates, using images with a 63× magnification and ImageJ software.

Antibacterial efficacy against biofilms

For static biofilm analysis, an overnight culture from *P. aeruginosa* PAO1 was diluted to an $OD_{550\ nm} = 0.1$ in TSB supplemented with 0.2% glucose (Fisher Scientific S.L.), added in a 96-well microtiter plate, and incubated at 37°C. After 72 h, wells were washed three times with PBS and treated with the different H1 histones at PAO1 MIC_{50} (Table 1). TBS and Cpx at 2 µg/mL-treated wells were used as controls. Six hours after treatment,

three PBS washes were carried out, and wells were fixed with methanol (Fisher Scientific) for 15 min. Then, 1% (wt/vol) Crystal violet (Merck Life Science) was added for 5 min, followed by a distaining step with 30% acetic acid (Scharlau). Biofilm biomass was determined by measuring the absorbance ($OD_{570\ nm}$) using a Microplate spectrophotometer Benchmark Plus (Bio-Rad, USA).

The antibiofilm efficacy of histones H1.0 and H1.4 was also tested in a continuous PAO1 flow biofilm assay as previously described (18). Briefly, an overnight culture diluted at $OD_{550\ nm} = 1$ was inoculated into a flow chamber and was allowed to attach for 2 h. Then, fresh TSB + 0.2% glucose was continuously pumped (42 µL/min) through the flow chamber for 72 h until a mature biofilm was obtained. The mature biofilms were treated with histones at 100 µg/mL and left to act for 6 h. Treatments with TBS and Cpx at 5 µg/mL were used as controls. Finally, biofilms were stained with Syto 9 and propidium iodide according to the manufacturer's instructions and were visualized with a Zeiss LSM 800 confocal laser scanning microscope (CLSM). Image processing was performed with Image J software, and measurements of biofilm biomass (green channel), average thickness (green channel), and dead biomass (red channel) were obtained using FIJI and COMSTAT2 plugins (48).

Antibacterial efficacy and toxicology in a *G. mellonella* infection model

G. mellonella larvae were fed with an artificial diet (15% corn flour, 15% wheat flour, 15% infant cereal, 11% powdered milk, 6% brewer's yeast, 25% honey, and 13% glycerol) and maintained at 34°C in the dark (49). Larvae selected for all experiments had a weight range of 175–250 mg.

First, the toxicity of H1.0 and H1.4 histones was evaluated by injecting 10 µL of five different concentrations into the top right proleg of the larvae using a microsyringe (Hamilton): 1.25, 2.5, 5, 10, and 20 mg/kg. Considering that 2.5 mg/kg is equivalent to 50 µg/mL, the evaluated concentration range comprises ~0.5× MIC_{50} to ~8× MIC_{50} of *P. aeruginosa* PAO1 to H1 histone subtype (Table 1). PBS-treated larvae were included as negative control. Because testing histone activity against infected larvae involved a double injection protocol (infection and treatment), histone toxicity was also tested in previously injected larvae. To this end, larvae injected with PBS were treated 1 h later with 10 µL of histones at 20 mg/kg though the top left proleg. The experiment was conducted twice and included a total of five larvae per group each time. Larvae were monitored for 60 h.

Then, the antimicrobial efficacy of histones against *P. aeruginosa* PAO1 infection in *G. mellonella* was tested. Larvae were infected with *P. aeruginosa* PAO1 (5–50 CFUs/larvae) and 1 h after, 5 mg/kg of histone H1.0 and H1.4 was injected, alone and in combination with 1.5 mg/kg of Cpx. Infected larvae were also treated with PBS as a negative treatment control, Cpx 20 mg/kg as a positive control of treatment, and Cpx 1.5 mg/kg as a control of synergy effect between antibiotic and histones. Additionally, a group of larvae injected with PBS at both the infection and treatment steps was included as a control for the double injection, to rule out mortality due to consecutive injuries from the injection process. The experiment was conducted three times with eight larvae per group. Larvae were monitored from 16 to 24 h post-infection, with observations every hour.

Statistical analysis

All data were statistically analyzed using GraphPad Prism version 10.00 (GraphPad Software, USA). Normality was assessed using the Shapiro-Wilk test. Comparison of means among groups was performed using one-way analysis of variance (ANOVA) with corrections for multiple comparisons (Tukey, Dunnett, or Šidák), as specified in each figure legend. Correlations among structural parameters and the antimicrobial and antibiofilm effect of histone H1 subtypes were evaluated using simple linear regressions. Comparison of Kaplan-Meier survival curves was made by log-rank tests. A P value of <0.05 was considered statistically significant in all tests, including those with multiple comparisons (adjusted P value).

ACKNOWLEDGMENTS

This study was partially supported by grants PID2021-125801OB-100, PLEC2022-009356, and PDC2022-133577-I00 to E.T., PID2020-112783GB-C21 to A.J., and PID2020-112783GB-C22 to A.R., funded by the Spanish Ministry of Science and Innovation MCIN/AEI/10.13039/501100011033 and "ERDF A way of making Europe," the CERCA programme and *AGAUR-Generalitat de Catalunya* (2021SGR01545), the European Regional Development Fund (FEDER), and Catalan Cystic Fibrosis association. The project that gave rise to these results received the support of a fellowship from "la Caixa" Foundation (ID 100010434). The fellowship code is "LCF/BQ/DI20/11780040."

The funders had no role in the study design, data collection, and interpretation.

AUTHOR AFFILIATIONS

[1]Bacterial infections and antimicrobial therapies group, Institute for Bioengineering of Catalonia (IBEC), The Barcelona Institute of Science and Technology, Barcelona, Spain
[2]Microbiology Section, Department of Genetics, Microbiology and Statistics, Faculty of Biology, University of Barcelona, Barcelona, Spain
[3]Molecular Biology Institute of Barcelona (IBMB-CSIC), Barcelona, Spain
[4]Biochemistry and Molecular Biology Department, Universitat Autònoma de Barcelona, Bellaterra, Spain

AUTHOR ORCIDs

Betsy Verónica Arévalo-Jaimes http://orcid.org/0000-0002-3363-5403
Inmaculada Ponte http://orcid.org/0000-0002-9448-6915
Albert Jordan http://orcid.org/0000-0002-3970-8693
Alicia Roque http://orcid.org/0000-0002-6206-6481
Eduard Torrents http://orcid.org/0000-0002-3010-1609

FUNDING

Funder	Grant(s)	Author(s)
Ministerio de Ciencia e Innovación (MCIN)	PID2021-125801OB-100, PLEC2022-009356, and PDC2022-133577-I00	Eduard Torrents
Ministerio de Ciencia e Innovación (MCIN)	PID2020-112783GB-C21	Albert Jordan
Ministerio de Ciencia e Innovación (MCIN)	PID2020-112783GB-C22	Inmaculada Ponte Alicia Roque
Generalitat de Catalunya (Government of Catalonia)	2021SGR01545	Eduard Torrents
'la Caixa' Foundation ('la Caixa')	LCF/BQ/DI20/11780040	Betsy Veronica Arévalo-Jaimes

AUTHOR CONTRIBUTIONS

Betsy Verónica Arévalo-Jaimes, Conceptualization, Formal analysis, Investigation, Methodology, Software, Writing – original draft, Writing – review and editing | Mónica Salinas-Pena, Investigation, Methodology, Writing – review and editing | Inmaculada Ponte, Conceptualization, Data curation, Funding acquisition, Investigation, Methodology, Resources, Writing – review and editing | Albert Jordan, Conceptualization, Data curation, Funding acquisition, Supervision, Writing – review and editing | Alicia Roque, Conceptualization, Funding acquisition, Investigation, Methodology, Supervision, Writing – original draft, Writing – review and editing | Eduard Torrents, Conceptualization, Data curation, Formal analysis, Funding acquisition, Investigation, Methodology, Project

administration, Resources, Supervision, Validation, Writing – original draft, Writing – review and editing

ADDITIONAL FILES

The following material is available online.

Supplemental Material

Supplemental Material (mSystems00704-24-s0001.docx). Figure S1.

Open Peer Review

PEER REVIEW HISTORY (review-history.pdf). An accounting of the reviewer comments and feedback.

REFERENCES

1. Baindara P, Mandal SM. 2023. Gut-antimicrobial peptides: synergistic co-evolution with antibiotics to combat multi-antibiotic resistance. Antibiotics (Basel) 12:1732. https://doi.org/10.3390/antibiotics12121732
2. Salam MA, Al-Amin MY, Salam MT, Pawar JS, Akhter N, Rabaan AA, Alqumber MAA. 2023. Antimicrobial resistance: a growing serious threat for global public health. Healthc (Basel) 11:1946. https://doi.org/10.3390/healthcare11131946
3. Smith WPJ, Wucher BR, Nadell CD, Foster KR. 2023. Bacterial defences: mechanisms, evolution and antimicrobial resistance. Nat Rev Microbiol 21:519–534. https://doi.org/10.1038/s41579-023-00877-3
4. Shree P, Singh CK, Sodhi KK, Surya JN, Singh DK. 2023. Biofilms: understanding the structure and contribution towards bacterial resistance in antibiotics. Med Microecol 16:100084. https://doi.org/10.1016/j.medmic.2023.100084
5. Mohamad F, Alzahrani RR, Alsaadi A, Alrfaei BM, Yassin AEB, Alkhulaifi MM, Halwani M. 2023. An explorative review on advanced approaches to overcome bacterial resistance by curbing bacterial biofilm formation. Infect Drug Resist 16:19–49. https://doi.org/10.2147/IDR.S380883
6. Wood SJ, Kuzel TM, Shafikhani SH. 2023. *Pseudomonas aeruginosa*: infections, animal modeling, and therapeutics. Cells 12:199. https://doi.org/10.3390/cells12010199
7. Cendra MDM, Torrents E. 2021. *Pseudomonas aeruginosa* biofilms and their partners in crime. Biotechnol Adv 49:107734. https://doi.org/10.1016/j.biotechadv.2021.107734
8. Yasir M, Dutta D, Willcox MDP. 2020. Activity of antimicrobial peptides and ciprofloxacin against *Pseudomonas aeruginosa* biofilms. Molecules 25:3843. https://doi.org/10.3390/molecules25173843
9. Zlatina K, Galuska SP. 2019. Polysialic acid modulates only the antimicrobial properties of distinct histones. ACS Omega 4:1601–1610. https://doi.org/10.1021/acsomega.8b02222
10. Li X, Ye Y, Peng K, Zeng Z, Chen L, Zeng Y. 2022. Histones: the critical players in innate immunity. Front Immunol 13:1030610. https://doi.org/10.3389/fimmu.2022.1030610
11. Hoeksema M, van Eijk M, Haagsman HP, Hartshorn KL. 2016. Histones as mediators of host defense, inflammation and thrombosis. Future Microbiol 11:441–453. https://doi.org/10.2217/fmb.15.151
12. Roque A, Ponte I, Suau P. 2016. Interplay between histone H1 structure and function. Biochim Biophys Acta 1859:444–454. https://doi.org/10.1016/j.bbagrm.2015.09.009
13. Fyodorov DV, Zhou B-R, Skoultchi AI, Bai Y. 2018. Emerging roles of linker histones in regulating chromatin structure and function. Nat Rev Mol Cell Biol 19:192–206. https://doi.org/10.1038/nrm.2017.94
14. Millán-Ariño L, Izquierdo-Bouldstridge A, Jordan A. 2016. Specificities and genomic distribution of somatic mammalian histone H1 subtypes. Biochim Biophys Acta 1859:510–519. https://doi.org/10.1016/j.bbagrm.2015.10.013
15. Rose F, Bailey K, Keyte JW, Chan WC, Greenwood D, Mahida YR. 1998. Potential role of epithelial cell-derived histone H1 proteins in innate antimicrobial defense in the human gastrointestinal tract. Infect Immun 66:3255–3263. https://doi.org/10.1128/IAI.66.7.3255-3263.1998
16. Hecht G. 1999. Innate mechanisms of epithelial host defense: spotlight on intestine. Am J Physiol 277:C351–C358. https://doi.org/10.1152/ajpcell.1999.277.3.C351
17. Jodoin J, Hincke MT. 2018. Histone H5 is a potent antimicrobial agent and a template for novel antimicrobial peptides. Sci Rep 8:2411. https://doi.org/10.1038/s41598-018-20912-1
18. Blanco-Cabra N, Vega-Granados K, Moya-Andérico L, Vukomanovic M, Parra A, Álvarez de Cienfuegos L, Torrents E. 2019. Novel oleanolic and maslinic acid derivatives as a promising treatment against bacterial biofilm in nosocomial infections: an *in vitro* and *in vivo* study. ACS Infect Dis 5:1581–1589. https://doi.org/10.1021/acsinfecdis.9b00125
19. Clark DJ, Hill CS, Martin SR, Thomas JO. 1988. Alpha-helix in the carboxy-terminal domains of histones H1 and H5. EMBO J 7:69–75. https://doi.org/10.1002/j.1460-2075.1988.tb02784.x
20. Tsai CJ-Y, Loh JMS, Proft T. 2016. *Galleria mellonella* infection models for the study of bacterial diseases and for antimicrobial drug testing. Virulence 7:214–229. https://doi.org/10.1080/21505594.2015.1135289
21. Doolin T, Gross S, Siryaporn A. 2020. Physical mechanisms of bacterial killing by histones, p 117–133. In Duménil G, Teeffelen S (ed), Physical microbiology. Springer International Publishing, Cham.
22. Howell SJ, Wilk D, Yadav SP, Bevins CL. 2003. Antimicrobial polypeptides of the human colonic epithelium. Peptides 24:1763–1770. https://doi.org/10.1016/j.peptides.2003.07.028
23. Lüders T, Birkemo GA, Nissen-Meyer J, Andersen Ø, Nes IF. 2005. Proline conformation-dependent antimicrobial activity of a proline-rich histone h1 N-terminal peptide fragment isolated from the skin mucus of atlantic salmon. Antimicrob Agents Chemother 49:2399–2406. https://doi.org/10.1128/AAC.49.6.2399-2406.2005
24. Fernandes JMO, Molle G, Kemp GD, Smith VJ. 2004. Isolation and characterisation of oncorhyncin II, a histone H1-derived antimicrobial peptide from skin secretions of rainbow trout, *Oncorhynchus mykiss*. Dev Comp Immunol 28:127–138. https://doi.org/10.1016/s0145--305x(03)00120-4
25. Jacobsen F, Baraniskin A, Mertens J, Mittler D, Mohammadi-Tabrisi A, Schubert S, Soltau M, Lehnhardt M, Behnke B, Gatermann S, Steinau HU, Steinstraesser L. 2005. Activity of histone H1.2 in infected burn wounds. J Antimicrob Chemother 55:735–741. https://doi.org/10.1093/jac/dki067
26. Augusto LA, Decottignies P, Synguelakis M, Nicaise M, Le Maréchal P, Chaby R. 2003. Histones: a novel class of lipopolysaccharide-binding molecules. Biochemistry 42:3929–3938. https://doi.org/10.1021/bi0268394
27. Richards RC, O'Neil DB, Thibault P, Ewart KV. 2001. Histone H1: an antimicrobial protein of Atlantic salmon (*Salmo salar*). Biochem Biophys Res Commun 284:549–555. https://doi.org/10.1006/bbrc.2001.5020
28. Pasupuleti M, Schmidtchen A, Malmsten M. 2012. Antimicrobial peptides: key components of the innate immune system. Crit Rev Biotechnol 32:143–171. https://doi.org/10.3109/07388551.2011.594423
29. Huang Y, Huang J, Chen Y. 2010. Alpha-helical cationic antimicrobial peptides: relationships of structure and function. Protein Cell 1:143–152. https://doi.org/10.1007/s13238-010-0004-3

30. Lohan S, Konshina AG, Efremov RG, Maslennikov I, Parang K. 2023. Structure-based rational design of small α-helical peptides with broad-spectrum activity against multidrug-resistant pathogens. J Med Chem 66:855–874. https://doi.org/10.1021/acs.jmedchem.2c01708
31. Di Luca M, Maccari G, Maisetta G, Batoni G. 2015. BaAMPs: the database of biofilm-active antimicrobial peptides. Biofouling 31:193–199. https://doi.org/10.1080/08927014.2015.1021340
32. Alcàcer-Almansa J, Arévalo-Jaimes BV, Blanco-Cabra N, Torrents E. 2023. Methods for studying biofilms: microfluidics and translation in the clinical context
33. Blanco-Cabra N, Movellan J, Marradi M, Gracia R, Salvador C, Dupin D, Loinaz I, Torrents E. 2022. Neutralization of ionic interactions by dextran-based single-chain nanoparticles improves tobramycin diffusion into a mature biofilm. NPJ Biofilms Microbiomes 8:52. https://doi.org/10.1038/s41522-022-00317-9
34. Eisenberg D, Schwarz E, Komaromy M, Wall R. 1984. Analysis of membrane and surface protein sequences with the hydrophobic moment plot. J Mol Biol 179:125–142. https://doi.org/10.1016/0022-2836(84)90309-7
35. Moya-Andérico L, Admella J, Fernandes R, Torrents E. 2020. Monitoring gene expression during a *Galleria mellonella* bacterial infection. Microorganisms 8:1798. https://doi.org/10.3390/microorganisms8111798
36. Wang C, Hong T, Cui P, Wang J, Xia J. 2021. Antimicrobial peptides towards clinical application: delivery and formulation. Adv Drug Deliv Rev 175:113818. https://doi.org/10.1016/j.addr.2021.05.028
37. Luo X, Chen H, Song Y, Qin Z, Xu L, He N, Tan Y, Dessie W. 2023. Advancements, challenges and future perspectives on peptide-based drugs: focus on antimicrobial peptides. Eur J Pharm Sci 181:106363. https://doi.org/10.1016/j.ejps.2022.106363
38. Zhang C, Yang M. 2022. Antimicrobial peptides: from design to clinical application. Antibiotics (Basel) 11:349. https://doi.org/10.3390/antibiotics11030349
39. Rai A, Ferrão R, Palma P, Patricio T, Parreira P, Anes E, Tonda-Turo C, Martins MCL, Alves N, Ferreira L. 2022. Antimicrobial peptide-based materials: opportunities and challenges. J Mater Chem B 10:2384–2429. https://doi.org/10.1039/d1tb02617h
40. Tan P, Fu H, Ma X. 2021. Design, optimization, and nanotechnology of antimicrobial peptides: From exploration to applications. Nano Today 39:101229. https://doi.org/10.1016/j.nantod.2021.101229
41. Doolin T, Amir HM, Duong L, Rosenzweig R, Urban LA, Bosch M, Pol A, Gross SP, Siryaporn A. 2020. Mammalian histones facilitate antimicrobial synergy by disrupting the bacterial proton gradient and chromosome organization. Nat Commun 11:3888. https://doi.org/10.1038/s41467-020-17699-z
42. Yokota S, Hakamada H, Yamamoto S, Sato T, Shiraishi T, Shinagawa M, Takahashi S. 2018. Release of large amounts of lipopolysaccharides from *Pseudomonas aeruginosa* cells reduces their susceptibility to colistin. Int J Antimicrob Agents 51:888–896. https://doi.org/10.1016/j.ijantimicag.2018.02.004
43. Berenbaum MC. 1978. A method for testing for synergy with any number of agents. J Infect Dis 137:122–130. https://doi.org/10.1093/infdis/137.2.122
44. Roque A, Orrego M, Ponte I, Suau P. 2004. The preferential binding of histone H1 to DNA scaffold-associated regions is determined by its C-terminal domain. Nucleic Acids Res 32:6111–6119. https://doi.org/10.1093/nar/gkh945
45. Hindler J. 1992. Broth microdilution checkerboard and macrodilution methods. In Isenberg HD (ed), Clinical microbiology procedures handbook. American Society for Microbiology, Washington DC.
46. Eliopoulos GM, Moellering RC. 1991. Antimicrobial combinations, p 432–492. In Lorian V (ed), Antibiotics in laboratory medicine, 3rd ed. The Williams & Wilkins Co, Baltimore.
47. Sass P. 2023. Microscopy-based multiwell assay to characterize disturbed bacterial morphogenesis upon antibiotic action, p 171–190. In Sass P (ed), Antibiotics: methods and protocols. Springer US, New York, NY.
48. Heydorn A, Nielsen AT, Hentzer M, Sternberg C, Givskov M, Ersbøll BK, Molin S. 2000. Quantification of biofilm structures by the novel computer program comstat. Microbiol (Reading, Engl) 146:2395–2407. https://doi.org/10.1099/00221287-146-10-2395
49. Moya-Andérico L, Admella J, Torrents E. 2021. A clearing protocol for *Galleria mellonella* larvae: visualization of internalized fluorescent nanoparticles. N Biotechnol 60:20–26. https://doi.org/10.1016/j.nbt.2020.08.002

Material Suplementario

Fig S1 Circular dichroism spectra of histones H1 subtypes in (**A**) PBS and (**B**) TFE 20%. Represented data are derived for 5 independent measurements.

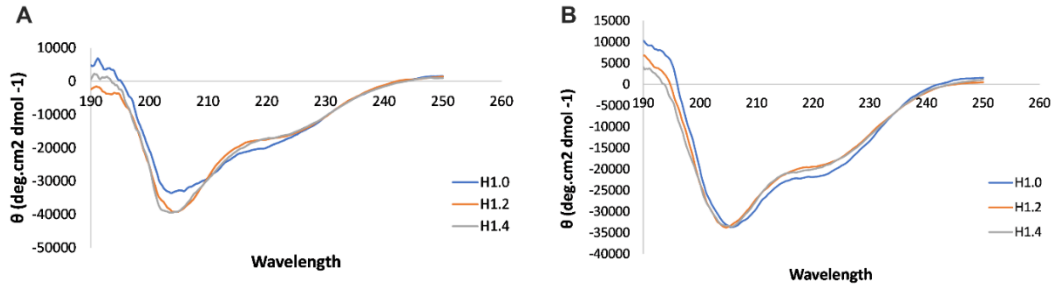

Artículo 7 (publicación)

Accessing the *In vivo* efficiency of clinically isolated phages against uropathogenic and invasive biofilm-forming *Escherichia coli* strains for phage therapy

Publicado en la revista *cells*

DOI: 10.3390/cells12030344

17 de enero de 2023

Categoría Biología celular 2023: 1er tercil, 2do Cuartil, IF= 5.1

Swapnil Ganesh Sanmukh[1,2], Joana Admella[1], Laura Moya-Andérico[1], Tamás Fehér[2], Betsy V. Arévalo-Jaimes[1], Núria Blanco-Cabra[1,3] and Eduard Torrents[1,3]

[1]Grupo Infecciones Bacterianas y Terapias Antimicrobianas (BIAT), Instituto de Bioingeniería de Cataluña (IBEC), Barcelona, España.
[2]Unidad de Biología sintética y de sistemas, Instituto de Bioquímica, Centro de investigación Biológica de la Red de investigación Eötvös Lóránd, Szeged, Hungría.
[3]Sección de Microbiología, Departamento de Genética, Microbiología y Estadística, Facultad de Biología, Universitat de Barcelona, Barcelona, España.

Cita: Sanmukh, S. G., Admella, J., Moya-Andérico, L., Fehér, T., Arévalo-Jaimes, B. V., Blanco-Cabra, N., & Torrents, E. (2023). Accessing the in vivo efficiency of clinically isolated phages against uropathogenic and invasive biofilm-forming *Escherichia coli* strains for phage therapy. *Cells*, 12(3), 344. DOI: 10.3390/cells12030344.

cells

MDPI

Article

Accessing the In Vivo Efficiency of Clinically Isolated Phages against Uropathogenic and Invasive Biofilm-Forming *Escherichia coli* Strains for Phage Therapy

Swapnil Ganesh Sanmukh [1,2,*], Joana Admella [1], Laura Moya-Andérico [1], Tamás Fehér [2], Betsy Verónica Arévalo-Jaimes [1], Núria Blanco-Cabra [1,3] and Eduard Torrents [1,3,*]

[1] Bacterial Infections: Antimicrobial Therapies Group, Institute for Bioengineering of Catalonia (IBEC), The Barcelona Institute of Science and Technology (BIST), Baldiri Reixac, 15-21, 08028 Barcelona, Spain
[2] Synthetic and Systems Biology Unit, Institute of Biochemistry, Biological Research Centre of the Eötvös Lóránd Research Network, H-6726 Szeged, Hungary
[3] Microbiology Section, Department of Genetics, Microbiology, and Statistics, Faculty of Biology, University of Barcelona, 08028 Barcelona, Spain
* Correspondence: ssanmukh@ibecbarcelona.eu or ssanmukh@brc.hu (S.G.S.); etorrents@ibecbarcelona.eu or eduard.torrents@ub.edu (E.T.)

Abstract: *Escherichia coli* is one of the most common members of the intestinal microbiota. Many of its strains are associated with various inflammatory infections, including urinary or gut infections, especially when displaying antibiotic resistance or in patients with suppressed immune systems. According to recent reports, the biofilm-forming potential of *E. coli* is a crucial factor for its increased resistance against antibiotics. To overcome the limitations of using antibiotics against resistant *E. coli* strains, the world is turning once more towards bacteriophage therapy, which is becoming a promising candidate amongst the current personalized approaches to target different bacterial infections. Although matured and persistent biofilms pose a serious challenge to phage therapy, they can still become an effective alternative to antibiotic treatment. Here, we assess the efficiency of clinically isolated phages in phage therapy against representative clinical uropathogenic and invasive biofilm-forming *E. coli* strains. Our results demonstrate that irrespective of host specificity, bacteriophages producing clear plaques with a high burst size, and exhibiting depolymerizing activity, are good candidates against biofilm-producing *E. coli* pathogens as verified from our in vitro and in vivo experiments using *Galleria mellonella* where survival was significantly increased for phage-therapy-treated larvae.

Keywords: intestinal microflora; inflammatory infections; antibiotic resistance; biofilm-forming potential; bacteriophage

Citation: Sanmukh, S.G.; Admella, J.; Moya-Andérico, L.; Fehér, T.; Arévalo-Jaimes, B.V.; Blanco-Cabra, N.; Torrents, E. Accessing the In Vivo Efficiency of Clinically Isolated Phages against Uropathogenic and Invasive Biofilm-Forming *Escherichia coli* Strains for Phage Therapy. *Cells* **2023**, *12*, 344. https://doi.org/10.3390/cells12030344

Academic Editors: Stephen T. Abedon, Katarzyna Danis-Wlodarczyk, Razi Kebriaei and Aleksandra Petrovic Fabijan

Received: 23 November 2022
Revised: 9 January 2023
Accepted: 13 January 2023
Published: 17 January 2023

1. Introduction

Approximately 80% of bacterial infections are caused by biofilms, which represents a significant problem for chronic infection treatments due to their reduced antibiotic sensitivity [1,2]. Compared with planktonic cells, biofilms confer an additional mechanism of antibiotic resistance. Therefore, the resistance of biofilms to antibiotics is 100–1000 times greater than that of planktonic bacteria [3]. Moreover, biofilms increase resistance to antimicrobial treatments and disinfectants and protect against environmental stresses [4]. Biofilm-mediated drug/antibiotic resistance is one of the major modes of drug resistance in most biofilm-forming bacteria, including *Escherichia coli* [5]. It is also the way that most biofilm-forming bacteria survive in hostile environments. It has been reported that biofilm development in *E. coli* depends not only on anaerobic conditions but also on its physiological state [6].

It has been observed that biofilm formation is an essential factor responsible for bacterial infections. Certain colonization and virulence factors, such as adhesin (protein),

and invasive behavior are critical to the initiation of its synthesis [7]. Biofilms are reported to play a key role in infections associated with enteropathogenic *E. coli* (EPEC), enterohaemorrhagic *E. coli* (EHEC), enterotoxigenic *E. coli* (ETEC), enteroaggregative *E. coli* (EAEC), enteroinvasive *E. coli* (EIEC), diffusely adherent *E. coli* (DAEC), uropathogenic *E. coli* (UPEC), and meningitis and sepsis—meningitis-associated *E. coli* (MNEC) [8,9]. The increased survival rate of UPEC in urinary tract infections is reported in TLR-4 mutant C3H/HeJ mice, lacking an intact innate immune response, following acute infection by the UPEC189 strain due to the formation of intracellular bacterial biofilm-like pods [10–12]. The AIEC strain of *E. coli* LF82, associated with Crohn's disease, demonstrates antibiotic resistance, and can survive and multiply within macrophages [13,14]. Similarly, in vitro studies involving laboratory *E. coli* K-12 reference strain MG1655 demonstrate the interaction of environmental and genetic factors in biofilm formation, which was not restricted to disease-associated clinical isolates [15,16]. The physical protection from the immune system, provided by biofilms, in addition to the ability of numerous strains to develop persister cells that survive very high antibiotic concentrations, are possibly common causes of therapeutic failure seen upon antibiotic treatment [17].

Bacteriophages have been utilized effectively for antibacterial as well as antibiofilm agents, alone or in combination with different antibiotics or antimicrobial compounds/drugs, for in vitro as well as in vivo [18–21] phage threapies. For example, studies of bacteriophage therapies in BALB/c mice and *Galleria mellonella* larvae have been reported to increase the survival capability in the infected host against different infections for possible human applications [18–21]. Additionally, phage enzymes, such as endolysins as well as depolymerases, have been explored for such applications [22]. Due to the disadvantages associated with antibiotics and their limitations due to increasing antibiotic resistance development in pathogenic bacterial strains, such as *Pseudomonas aeruginosa*, *Mycobacterium abscessus*, *Staphylococcus aureus*, and many other pathogens, it is very important to identify a suitable alternative against such biofilm-forming pathogens [19–22].

Community-acquired urinary tract infections (CAUTIs) are the most common infectious diseases affecting more than 150 million people each year globally, where UPEC is considered to be responsible for more than 80% of all CAUTIs [23–25]. *E. coli* represents one of the most common members of the normal intestinal microbiota and includes some of the strains involved in a wide range of pathogenic conditions ranging from inflammatory bowel diseases, such as Crohn's disease or ulcerative colitis [26–28], to their prevalence in lungs as an unknown pathogen [29–32]. Considering the recent report from the World Health Organization (WHO), *E. coli* strains displaying resistance against widely used fluoroquinolone antibiotics are getting more frequent, making their treatment ineffective in most parts of the world [33]. Due to such an urgent emerging situation of antibiotic resistance, alternative treatment options are sought to ensure better disease outcomes, placing phage therapy back into the game.

Biofilms are frequently considered to be a barrier for bacteriophage therapy as the extracellular polymeric matrix produced by some microbial species (i.e., *S. aureus*, *E. coli*, *Klebsiella pneumoniae*, *P. aeruginosa*, etc.) protects these cells from phage infections by forming a barrier. In addition, biofilm aging further impedes phage infection and replication due to the decreasing number of metabolically active bacterial cells [34]. Recently, bacteriophages have been explored against various infectious diseases [17,35–37] and seem to be amongst the most promising options for treating urinary tract infections (UTIs). In line with these studies, we are reporting for the first time the in vitro and in vivo efficiency assessment of selected clinically significant phages that harbour depolymerase activity against representative clinical uropathogenic and invasive biofilm-forming *E. coli* strains. We found that irrespective of their host specificity they can be a good alternative for biofilm removal/eradication, which aids the future development of effective phage therapies for UTIs.

2. Materials and Methods

2.1. Selection and Propagation of E. coli Strains

In this work, we used three different *E. coli* strains, two pathogenic (the uropathogenic CFT073 (ATCC 700928) and the adherent invasive LF82) [38], and the laboratory strain MG1655 (ATCC 700926). All *E. coli* strains were routinely grown in Tryptic soy broth (TSB) and Tryptic soy agar (TSA) media (Scharlab, S.L., Barcelona, Spain). Each strain was selectively grown overnight in TSB at 37 °C in a shaking incubator at 200 rpm. The bacterial cell concentration used for the experiments of phage isolation, in vitro biofilm assay, and one-step growth curve experiments was obtained after adjustment to a final optical density $\lambda = 550$ nm (OD_{550}) of 0.1, approximately 1×10^8 CFU/mL.

2.2. Processing of Clinical Samples for Phage Isolation

The clinical sputum samples from cystic fibrosis patients and urine pooled samples from patients with different, not defined urine infections, were processed before phage isolation. Informed consent was not required because we collected a microbiology laboratory waste product, and all comorbidity data were identified, excluding potential patient risks. Sewage samples were also obtained from the wastewater treatment plant at Prat de Llobregat, Barcelona (Spain), and screened for phage isolation. The Ethic Committee at the Vall d'Hebrón hospital has approved and signed the protocol (PR(AG)275/2019) for the transfer of clinical samples from the hospital to the IBEC lab with all ethical guarantees.

The collected samples were separately incubated in the ratio of 1:5 with the *E. coli* CFT073, LF82, and MG1655 strains in TSB broth at 37 °C overnight. After incubation, the samples were centrifuged separately at 12,000× *g* for 10 min to pellet out all suspended bacterial cell debris. The supernatant lysate was then filtered through a sterile syringe filter with a 0.22 µm pore size to remove any possible contaminant [39].

Isolation of phages against all the *E. coli* strains was carried out in the TSA medium by pour plating as per Lillehaug protocol with some modification [40,41]. For the pour plating assay, 100 µL of bacterial culture at OD_{550} ~0.1 (approximately 1×10^8 CFU/mL) was inoculated with 10 µL of processed clinical lysate separately and incubated at room temperature for 5–10 min before plating. After incubation, the mixture was slightly vortexed and later plated with the help of 1.25% Molten agar at a temperature below 45 °C and incubated at 37 °C overnight for plaque formation. Single plaque showing clear lysis zone and/or double-layered (bull-eyed) morphology were selected. Each plaque was selectively picked and enriched with its respective host, followed by plaque assay. This step was repeated for each isolated phage at least three times until uniformity in plaque formation was observed [42].

2.3. Phage Propagation and Lysate Preparation

For phage propagation, 0.5 mL of phage lysate and 5 mL of bacterial host strain at logarithmic phase were added to 5 mL of Trypticase soy broth (TSB) and incubated at 37 °C with agitation (200 rpm) for 18–24 h. At 3 h, 6 h, and 18 h the tube was visually inspected for any bacterial lysis. When bacterial lysis occurred, incubation was stopped, and the sample was centrifuged at 5000× *g* for 20 min at 4 °C. The supernatant was stored at 4 °C.

For laboratory scale propagation, 500 mL of TSB was inoculated with 5 mL of bacterial culture and incubated at 37 °C with constant shaking at 200 rpm. When the culture's optical density reached $OD_{550} = 0.5 \pm 0.1$ (approximately 1×10^8 CFU/mL), the supernatant obtained above was inoculated at 30 °C at a concentration of 1×10^7 PFU/mL with shaking until considerable lysis (OD_{550}~0.2) was observed. Later, 10% *v/v* chloroform was added to the culture with further incubation for more than 30 min at 37 °C, and then the culture was kept at 4 °C without shaking overnight. Finally, the bacterial debris was removed by centrifugation at 5000× *g* for 20 min at 4 °C, and the supernatant obtained was filtered through a 0.22 mm Millipore™ filter and stored at 4 °C as a phage stock [41].

2.4. Endotoxin Removal and Bacteriophage Purification

For phage precipitation and enrichment, two different steps of PEG precipitation were performed as previously described [38,40] with some modifications. Phage stocks were centrifuged at 10,000× *g* for 20 min to remove bacterial cells/debris. PEG-8000 (2 g/L) and NaCl (3 g/L) were then added to the resulting supernatant with proper mixing and centrifuged at 10,000× *g* for 10 min at 4 °C. Pellets and cell debris were discarded. Again, the supernatant was added to a solution containing PEG (9 g/L) and NaCl (2.9 g/L) with proper mixing and left at 4 °C overnight (or −20 °C for 1–2 h). The lysate was centrifuged at 10,000× *g* for 20 min at 4 °C to pellet all phage. At this stage, the pellet can be resuspended in 1 mL of 1X PBS buffer. Endotoxin removal was performed using the ToxOut™ Rapid Endotoxin Removal Kit (Thermofisher, Waltham, MA, USA) according to the manufacturer's protocol. This protocol was repeated several times to keep endotoxin levels below 0.05 EU/mL. Further traces of endotoxin were removed by diluting these purified phages. Purified phages were later analyzed to determine their titer, and purified bacteriophage stocks were further diluted and used for in vivo studies [43–45].

2.5. Cross Infectivity among Isolated Phages

For the spot test, 200 µL overnight culture of each *E. coli* strain was poured plated with TSA agar and kept for 45–60 min to solidify. After solidifying, 10 µL of each isolated phage with a titer greater than 10^8 PFU (plaques forming units)/mL was spotted on the plate to check the cross-reactivity. The plates were left to dry and were incubated at 37 °C. The plates were visually inspected for lysis zones [41]. For phage isolation, the spot test was performed in triplicate following their inclusion in the IBEC library. Phages showing consistent lysis events were considered for the experiments, and plaque characteristics, such as clear lysis zone and/or double layer (bull-eyed), latent period, and high burst size, were some of the factors used for phage selection. Special importance was given to the phages exhibiting double layer (bull-eyed) property, which is a representation of phage-bound depolymerase activity.

2.6. Phage One-Step Growth Characteristics

The one-step growth curves of the selected phages were performed as described previously, along with some modifications [42]. The different multiplicity of infection (MOI) within the range of 0.1 to 0.0001 were selected to determine the effective phage-host concentration for understanding the latent period and the burst size of phages against their respective hosts. All the experiments were performed in triplicate, and the results are the mean ± standard deviation. The latent period and burst size of these phages was determined by observing the number of phage particles' changes during the experiments. Based on the number of PFU/mL, the latent period and the burst size were determined by dividing the average PFU/mL of the latent period by the average PFU/mL of the last three time points of the experiment, as reported previously [46,47].

2.7. Scanning Electron Microscopy (SEM) for Studying the Lytic Phage Activity

Scanning electron microscopy was performed to observe the phage-mediated bacterial lysis. For sample processing, 50 mL of each *E. coli* strain grown overnight at OD_{550} = 0.1 (approximately 1×10^8 CFU/mL) was inoculated with its respective phage at a minimum concentration of 10^6 PFU/mL and incubated overnight at 37 °C with constant shaking condition at 200 rpm in 100 mL falcon flasks. Following incubation, the flasks were kept at room temperature to let the lysed bacterial debris settle at the bottom for 20–30 min. The coverslips (Thermofisher, Waltham, MA, USA) of 20 × 20 mm were first sterilized with 70% ethanol and later wiped with milli-Q water with the help of tissue paper. For each phage, 100 µL lysate was equally spread on the coverslip with another thin coverslip slide in one direction to form a homogeneous smear. The coverslips were dried in sterile conditions, preferably in Petri-plates. The coverslips were washed twice by submerging them in 0.1 M PBS pH 7.4 and were fixed with the help of 2.5% glutaraldehyde (Sigma, Spain) diluted in

0.1 M PBS pH 7.4 for 2–3 h. After fixation, the coverslips were again washed 3–4 times with 0.1 M PBS pH 7.4. Dehydration steps were performed by emerging the fixed coverslips in different concentrations of ethanol (Sigma Spain) (from 50%, 60%, 70%, 80%, 90%, and 100%) and were placed over filter paper and dried in a Petri plate upside down before observation with the help of NOVA NanoSEM 230TM through-the-lens detector of the secondary electron (TLD-SE) to obtain images of ultra-high resolution.

2.8. Transmission Electron Microscopy (TEM) of Bacteriophages

For sample processing for transmission electron microscopy, 30 µL of purified bacteriophages from samples with a concentration of around 10^8 PFU/mL in 1x PBS solution were placed on a paraffin tape initially cleaned with 70% ethanol. A carbon-coated copper grid was placed over the sample drop to absorb for 25–30 min and later removed. The excess sample around the grid was released with the help of filter paper without disturbing the mesh. The same side of the grid was placed over the 30 µL of 2% uranyl acetate (Sigma, Spain) staining solution for 30 s, and again the excess solution was removed with the help of filter paper. The grids were placed over filter paper and dried under a Petri plate upside down to avoid contact with the wet surface. They were later observed with the help of J-1010 (Jeol) coupled with a CCD camera Orius (Gatan) with software Digital Micrograph (Gatan) at an 80 kV accelerating voltage.

2.9. Static and Continuous Flow Biofilm Assay

For the in vitro static biofilm assay, 200 µL of each bacterial suspension at OD_{550} = 0.1 (approximately 1×10^8 CFU/mL) was inoculated in 96-well polystyrene plates with a flat bottom (Corning 3596 Polystyrene Flat Bottom 96 Well Corning, NY, USA) in triplicates and incubated overnight in TSB medium + glucose 0.5% at 37 °C without shaking. At different time points (24, 48, and 72 h), the media was removed, and wells were washed three times with 1X PBS pH = 7.5 (Fisher Scientific, Madrid, Spain) at 70 rpm for 3 min. After 72 h, formed biofilms were treated with 200 µL of phage sample with a concentration of 1×10^6 PFU/well in triplicate with control and incubated again at 37 °C for 24 h. Here, the phages used for the treatment were diluted in TSB broth, also used in control wells. After treatment, the wells were washed three times with 1x PBS and stained with 200 µL of 0.1% (*w/v*) Crystal violet for 5 min. Then, 200 µL/well of 30% acetic acid (Sigma, Madrid, Spain) was used to elute the Crystal violet, and biomass was determined by measuring the absorbance (OD_{570}) using the SPARK Multimode microplate reader (Tecan, Männedorf, Switzerland). The formed biofilms were categorized depending on their biofilm formation as per Stepanović et al. [48].

For the continuous flow biofilm assay, flow-cell chambers were employed according to the protocol previously described [49]. Briefly, the biofilms were grown in Luria Bertani (LB) broth 0.1× enriched with 0.002% glucose and pumped through the flow-cell system using a peristaltic pump (Ismatec ISM 943, Ismatec) at a constant rate of 42 µL/min. An inoculum of 250 µL of the pathogenic CFT073 strain, the best biofilm former, at OD_{550} = 0.1 (approximately 1×10^8 CFU/mL) was introduced to the system, and 2 h of static conditions were provided to favor the attachment step. Afterward, the flow was restored for 96 h, and the mature biofilms were treated for 12 h with 200 µL of tested phages at a concentration of 1×10^7 PFU/mL. LB broth and Ciprofloxacin (CPX) 1 µg/mL treated channel were implemented as negative and positive controls, respectively. Finally, biofilms were stained with the LIVE/DEAD BacLight Bacterial Viability kit (Thermofisher, Waltham, MA, USA) to image with the 20×/0.8 air objective of a Zeiss LSM 800 confocal laser scanning microscope (CLSM). The obtained data were visualized and analyzed by Image J. Biomass ($\mu m^3/\mu m^2$) and Thickness (µm) measurements of biofilms were calculated from live cells data (green channel) by COMSTAT2 analysis software

2.10. In Vivo Phage Therapy Efficacy in the Galleria Mellonella Infection Model

The *G. mellonella* larvae were maintained and injected, as previously reported by our laboratory [50]. Bacteriophage samples were prepared using ToxOut™ Rapid Endotoxin Removal Kit (Thermofisher, Waltham, MA, USA) to effectively eliminate endotoxins up to <0.05 EU/mL in solutions containing proteins or pharmacologically important components as per the manufacturer's protocol with some modifications as discussed above. For this experiment, a single *E. coli* strain (CFT073) producing high biofilm and high-biofilm-disrupting phages (IBEC 40 and IBEC 77) were selected for studying in vivo survival in *G. mellonella* according to the in vitro biofilm assays (static and in-flow biofilm assays).

The bacterial culture was centrifuged at 1500× *g* for ten minutes and resuspended with 1X PBS during three washes to remove any possible toxins from the overnight culture. Phage toxicity of endotoxin-free diluted purified phages was first assessed by injecting larvae with 10 µL of different phage concentrations from 10^3 to 10^5 PFUs/larva prepared in 1X PBS. All solutions were prepared in 1X PBS. To determine treatment efficiency, larvae were injected with 10 µL of either 1X PBS or the selected *E. coli* CFT073 strain as controls. For the phage treatment group, larvae were injected with 10 µL of *E. coli* CFT073 (10^6 CFUs/mL). One hour post-infection, purified bacteriophages were injected with 10^4 PFUs/larva. A second reminder phage dose was also tested five hours post-infection.

After bacterial infection, an antibiotic control group was injected with one dose of ciprofloxacin (CPX) (20 mg/kg larva) [51,52]. Additionally, the mixed combination of ciprofloxacin with each respective phage was tested one hour post-infection. Another group injected with ciprofloxacin at one hour post-infection was followed with the injection of the respective phage 5 h post-infection. All experiments contained 8 larvae per condition. Larvae were incubated at 37 °C throughout the experiments. Following injection, the larvae were frequently observed to survive up to 48 h or 55 h.

2.11. Statistical Analysis

The statistical analysis of all the experiments was performed using values expressed as mean ± standard deviation (SD) in GraphPad Prism 9.00 (GraphPad Software, San Diego, CA, USA) software package. All the experiments performed were repeated at least three times. The *p*-values of < 0.05 were considered significant.

3. Results

3.1. Isolation and Selection of Phages

For the isolation of *E. coli* phages, the clinical (urine and sputum) and sewage sources were tested against the three different *E. coli* host strains (CFT073, LF82, and MG1655) to detect the available phages specific against each host. The detection of phages was dependent upon their availability in these sources and their host specificity; hence, different numbers of phages were selected for each strain from different sources based on the plaque morphology. The source of isolation and plaque characteristics like turbidity, plaque diameter, and double-layered and/or bull-eyed morphologies were considered crucial for phage isolation and selection. All 21 phages were isolated against the three *E. coli* strains. For uropathogenic *E. coli* CFT073, 3 phages, namely, IBEC 77, IBEC 78, and IBEC 98; against the adherent invasive *E. coli* LF82, 5 phages, namely, IBEC 36 through IBEC 40; whereas against the laboratory strain *E. coli* MG1655, 13 phages, namely, IBEC 41 through IBEC 53, were selectively isolated as represented in Table 1. Phage selection was based on plaque morphology involving phages that produce distinct and visually distinguishable plaques when applied to a bacterial lawn. Plaque characteristics includes turbidity (clear or blur), and specific properties like formation of double layered or bull eyed plaques as represented in Table 1.

Table 1. Different phages were isolated from clinical and environmental samples.

Phage Number	Host Strain	Source	Specific Property	Turbidity	Plaque Diameter	Geographical Location
IBEC 36	*E. coli* LF82	Urine	NO	Clear	Large (>1 cm)	Barcelona (Spain)
IBEC 37	*E. coli* LF82	Urine	NO	Blur	Large (>1 cm)	Barcelona (Spain)
IBEC 38	*E. coli* LF82	Urine	NO	Blur	Large (>1 cm)	Barcelona (Spain)
IBEC 39	*E. coli* LF82	Sputum	NO	Clear	Large (>1 cm)	Barcelona (Spain)
IBEC 40	*E. coli* LF82	Sputum	Double-layered, Bull-eyed	Clear	Small (<0.5 cm)	Barcelona (Spain)
IBEC 41	*E. coli* MG1655	Sewage	NO	Clear	Small (<0.5 cm)	Barcelona (Spain)
IBEC 42	*E. coli* MG1655	Sewage	NO	Clear	Small (<0.5 cm)	Barcelona (Spain)
IBEC 43	*E. coli* MG1655	Sewage	NO	Clear	Small (<0.5 cm)	Barcelona (Spain)
IBEC 44	*E. coli* MG1655	Sewage	NO	Clear	Large (>1 cm)	Barcelona (Spain)
IBEC 45	*E. coli* MG1655	Sewage	NO	Clear	Small (<0.5 cm)	Barcelona (Spain)
IBEC 46	*E. coli* MG1655	Sputum	NO	Blur	Small (<0.5 cm)	Barcelona (Spain)
IBEC 47	*E. coli* MG1655	Sputum	NO	Blur	Small (<0.5 cm)	Barcelona (Spain)
IBEC 48	*E. coli* MG1655	Urine	Double-layered, Bull-eyed	Clear	Large (>1 cm)	Barcelona (Spain)
IBEC 49	*E. coli* MG1655	Urine	NO	Clear	Medium (0.5–1 cm)	Barcelona (Spain)
IBEC 50	*E. coli* MG1655	Urine	NO	Clear	Small (<0.5 cm)	Barcelona (Spain)
IBEC 51	*E. coli* MG1655	Sputum	NO	Clear	Large (>1 cm)	Barcelona (Spain)
IBEC 52	*E. coli* MG1655	Sputum	NO	Clear	Medium (0.5–1 cm)	Barcelona (Spain)
IBEC 53	*E. coli* MG1655	Sputum	NO	Clear	Small (<0.5 cm)	Barcelona (Spain)
IBEC 77	*E. coli* CFT073	Urine	Double-layered, Bull-eyed	Clear	Medium (0.5–1 cm)	Barcelona (Spain)
IBEC 78	*E. coli* CFT073	Sewage	NO	Clear	Medium (0.5–1 cm)	Barcelona (Spain)
IBEC 98	*E. coli* CFT073	Urine	Double-layered, Bull-eyed	Clear	Medium (0.5–1 cm)	Barcelona (Spain)

Note: Average plaque diameter was determined after overnight incubation at 37 °C and were classified into small, medium, and large plaques for differentiating plaques by plaque morphology.

3.2. Spot Test and Cross-Infectivity among Isolated Phages

The spot test was performed to determine the cross-infectivity of 21 isolated phages against non-specific *E. coli* hosts. It was observed that the original host against which the phages were isolated was not as cross-reactive as observed after performing the spot test assay a minimum of three times. Considering the common differences, plaques were first categorized based on their diameter sizes ranging from small (<0.5 cm), medium (0.5–1 cm), and large (>1 cm) and later based on turbidity (from blur to clear). Considering the importance of phage-bound depolymerase enzymes in biofilm removal, plaques showing double-layered or bull-eyed plaque morphology representing depolymerase activity were considered.

The selection of phages for the experiments was based on these three selection criteria; clear plaque morphology, double halo formation (bull-eyed morphology), and/or both, as these properties were reported to be effective in dispersing biofilm and making phage therapy effective as reported in different bacterial pathogens [53–55]. As all these features were observed in the clinical phage isolates, IBEC 36, IBEC 40, IBEC 48, and IBEC 77 phages were selected for further in vitro and in vivo studies. The plaque morphology figures are provided in Supplementary Figures S1 and S2.

The sole cross-infective phage was IBEC 40, which was isolated against *E. coli* LF82 and could also infect *E. coli* MG1655 but not the *E. coli* CFT073 strain. Since its plaques showed depolymerase activity and had clear morphology, it was considered an effective candidate phage for further in vivo studies as a neutral (non-infective) phage-nanoparticle-carrying bound depolymerase. The cross-reactivity of all the isolated phages observed from the spot test is provided in Table 2. As the sources of the isolated phages varied, so did their host specificity and plaque morphologies. The plaques showing intermediate lytic activity based on the plaque turbidity or blur morphology were not considered lytic to avoid false positive results and lysogen formation.

Table 2. Cross-infective phages against different *E. coli* clinically isolated strains. Original host strains (clear zone of lysis, OH: blue), susceptible bacterial strains (clear zone of lysis, S: green), and resistant strains (no zone of lysis, R: red) against phage infection.

Bacteriophage Number	Original Host	*E. coli* LF82	*E. coli* MG1655	*E. coli* CFT073
IBEC 36	*E. coli* LF82	OH	R	R
IBEC 37	*E. coli* LF82	OH	R	R
IBEC 38	*E. coli* LF82	OH	R	R
IBEC 39	*E. coli* LF82	OH	R	R
IBEC 40	*E. coli* LF82	OH	S	R
IBEC 41	*E. coli* MG1655	R	OH	R
IBEC 42	*E. coli* MG1655	R	OH	R
IBEC 43	*E. coli* MG1655	R	OH	R
IBEC 44	*E. coli* MG1655	R	OH	R
IBEC 45	*E. coli* MG1655	R	OH	R
IBEC 46	*E. coli* MG1655	R	OH	R
IBEC 47	*E. coli* MG1655	R	OH	R
IBEC 48	*E. coli* MG1655	R	OH	R
IBEC 49	*E. coli* MG1655	R	OH	R
IBEC 50	*E. coli* MG1655	R	OH	R
IBEC 51	*E. coli* MG1655	R	OH	R
IBEC 52	*E. coli* MG1655	R	OH	R
IBEC 53	*E. coli* MG1655	R	OH	R
IBEC 77	*E. coli* CFT073	R	R	OH
IBEC 78	*E. coli* CFT073	R	R	OH
IBEC 98	*E. coli* CFT073	R	R	OH

Note: For the cross infection studies, the average repeates performed for each *E. coli* strain against each isolated IBEC phages were minimum of 3 times. Here, the phages which formed blur or turbid plaques were not considered as cross infective for this studies for selection of the best candidate phages for further studies. The spot test for cross-infectivity study were determined after overnight incubation at 37 °C.

3.3. Phage One-Step Growth Curve

The one-step growth curve for the IBEC 36, IBEC 48, and IBEC 77 were performed to find out the latent period and average burst size while infecting their original hosts. For IBEC 36 and IBEC 77, a multiplicity of infection (MOI) used to determine their one-step growth curve was 0.0001, whereas for IBEC 48, the MOI was 0.001 due to its long latent period and small burst size. The observed average burst size of IBEC 36 was approximately 250 PFU/cell, IBEC 48 was about 25 PFU/cell, and IBEC 77 was around 150 PFU/cell following primary propagation and enrichment with their original hosts (Figure 1).

3.4. Scanning Electron Microscopy Studies

The scanning electron microscopy revealed the lytic activity of IBEC 36, IBEC 48, and IBEC 77 against *E. coli* LF82, *E. coli* MG1655, and *E. coli* CFT073, respectively, as represented in Figure 2. The control for each cell is provided in Supplementary Figure S3. The specific phages were selective against their hosts, and no-cross reactivity was observed and was confirmed by spot assays.

3.5. Transmission Electron Microscopy Studies

Transmission electron microscopy revealed the morphology of the three phages, namely IBEC 36, IBEC 48, and IBEC 77, used in this study (Figure 3). IBEC 36 and IBEC 48 were morphologically similar and belong to the Myoviridae family, whereas IBEC 77 belongs to the Podoviridae family as per preliminary observation through TEM analysis.

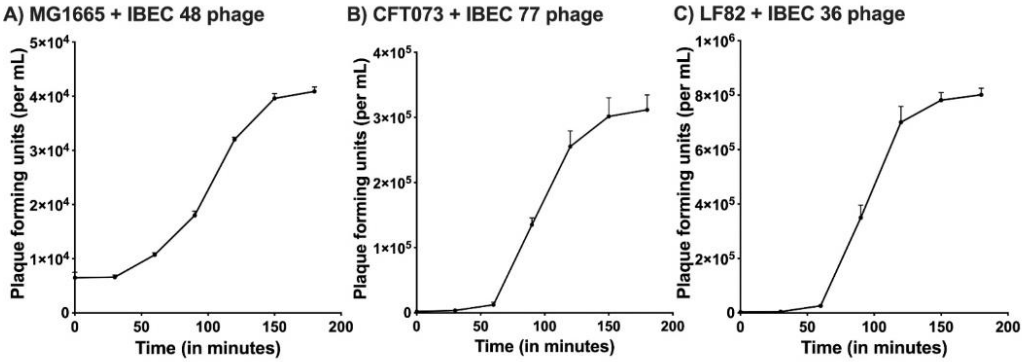

Figure 1. One-step growth curve of (**A**) IBEC48 phage, (**B**) IBEC77 phage, and (**C**) IBEC36 phage. One-step growth curves were obtained by growing IBEC 48, IBEC 77, and IBEC 36 with there exponentially growing culture of *E. coli* MG1655, *E. coli* CFT073, and *E. coli* LF82 strains respectively. Data points indicate the PFU/mL at different time points. Each data point represents the mean of three independent experiments.

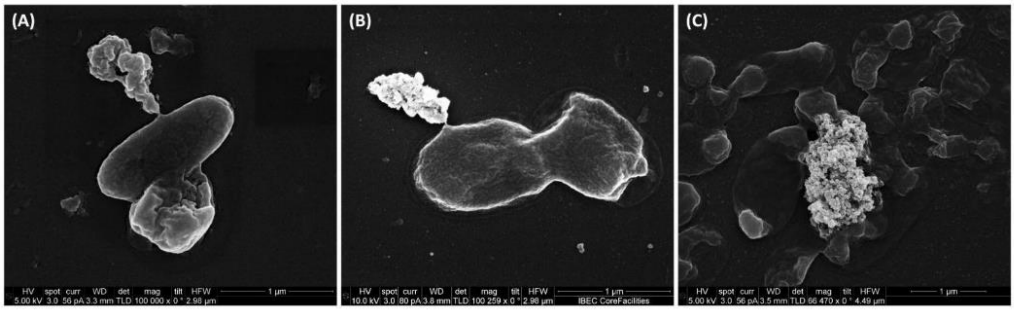

Figure 2. Representative scanning electron microscopy images of (**A**) *E. coli* CFT073, (**B**) *E. coli* LF82, and (**C**) *E. coli* MG1655 lysed by IBEC 77, IBEC 36, and IBEC 48 phage, respectively, and releasing its intracellular content as observed in these images. Bar = 1 µm.

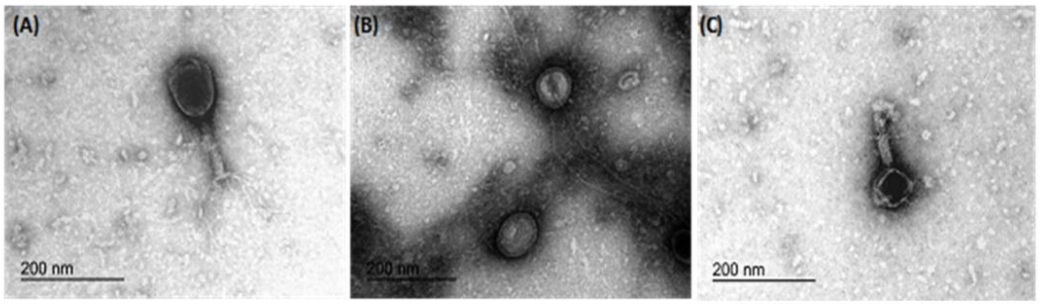

Figure 3. Representative transmission electron microscopy micrographs of bacteriophages (**A**) IBEC 36, (**B**) IBEC 77, and (**C**) IBEC 48 isolated from clinical samples against *E. coli* LF82, *E. coli* CFT073, and *E. coli* MG1655, respectively. All were only active against the representative strains and were not cross-reactive. (Bar = 200 nm).

3.6. In Vitro Biofilm Assay

Next, we evaluated the antibiofilm activity in static conditions of the three selected phages, IBEC 36, IBEC 48, and IBEC 77, which showed promising characteristics based on their plaque morphology and lytic activity depending on their source of isolation as well as depolymerase production capacity against *E. coli* strains LF82, MG1655, and CFT073, respectively. The classification of in vitro biofilm formation after 72 h of incubation was carried out as per Stepanović et al. (2000) and, as expected, it was observed that *E. coli* CFT073 forms a more robust biofilm in vitro followed by *E. coli* MG1655, which forms moderate, and *E. coli* LF82, which produces weaker biofilms [48].

As seen in Figure 4, the IBEC 36, IBEC 48, and IBEC 77 phages significantly reduced the biofilm formed after 72 h of incubation. However, in the case of *E. coli* CFT073, a considerable reduction in the biofilm formed was observed (68%) as compared to the *E. coli* LF82 (47%) and *E. coli* MG1655 strains (40%). As IBEC 77 is a depolymerase-enzyme-producing phage, these results suggest the cumulative effectiveness of phages and their enzymes against the biofilm produced by uropathogenic *E. coli* CFT073 strain. The effective minimum concentration used to obtain the significant reduction in all three strains was 10^6 PFU/mL for all the three phages after 24 h of incubation ($p < 0.0001$) (Figure 2).

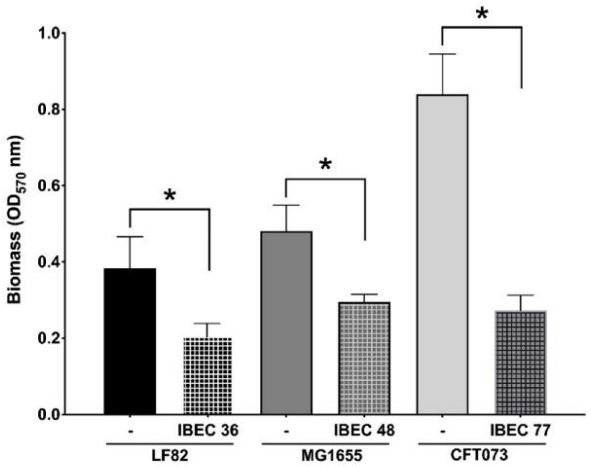

Figure 4. Effect of relative in vitro biofilm reduction in *E. coli* CFT073, *E. coli* LF82, and *E. coli* MG1655 by IBEC77, IBEC36, and IBEC48 phages, respectively, with phage concentration of 1×10^6 pfu/mL after 3-day-old biofilm (72 h) growth in 96-well plates at 37 °C. Standard deviations are indicated. (*) Statistically significant differences representing (* $p < 0.0001$) were determined by unpaired *t*-test (GraphPad Prism v.9).

Then, we selected the *E. coli* strain CFT073 due to its characteristic of high biofilm production and two phages (IBEC 40 and IBEC 77). IBEC 40 phage was randomly selected to verify if the non-specific effect of phage-bound lytic enzymes, such as depolymerases, have antibiofilm effects (in vitro) and/or enhance bacterial survival in vivo. The effects of the phages IBEC 40 and IBEC 77 were tested against biofilms formed under flow conditions because of the better representation of a real infection obtained in this model in comparison with microtiter plates. In concordance with our previous results, IBEC 77 phage significantly reduced the thickness and the biomass of *E. coli* strain CFT073 dynamic biofilms (Figure 5). However, since IBEC 40 is not cross-infective towards this strain, a lesser decrease in thickness and biomass probably associated with the bound depolymerases activity is observed, which validates our hypothesis that bacteriophages with high burst size and

depolymerase activity have antibiofilm activity regardless of their specificity towards the biofilm-producing host specie.

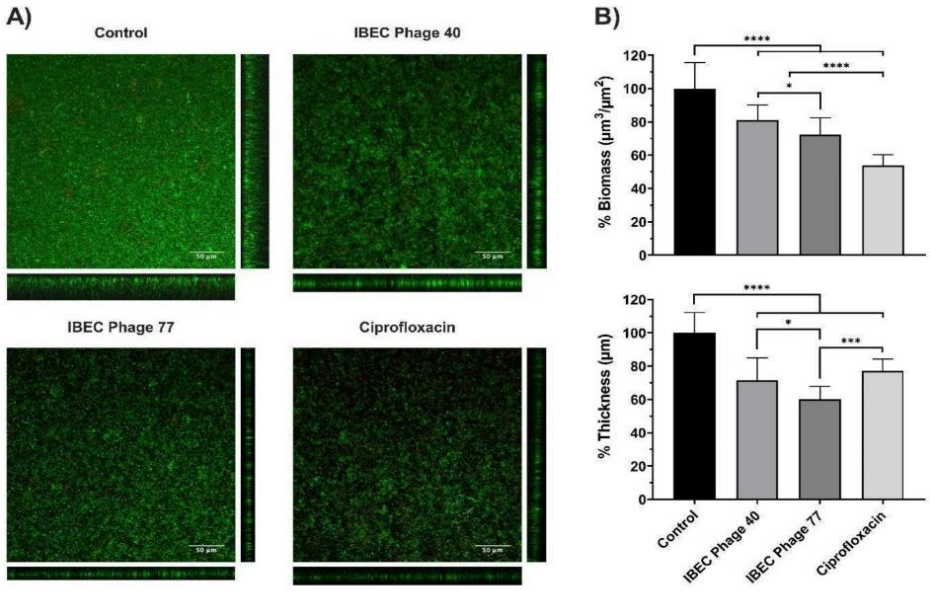

Figure 5. The relative effect of *E. coli* CFT073 specific IBEC77 and *E. coli* CFT073 non-specific IBEC 40 against 96 h biofilms formed under flow conditions. Phages at 1×10^7 pfu/mL, Ciprofloxacin 1 µg/mL, and LB Broth were employed as treatments. (**A**) Confocal microscopy images (sum and orthogonal views) of stained biofilms and (**B**) biomass and average thickness reduction with respect to control. Standard deviations of data from two different replicates are indicated. Statistically significant differences (* $p < 0.05$, *** $p < 0.001$, **** $p < 0.0001$) were determined by an ordinary one-way ANOVA (GraphPad Prism v.9).

3.7. In Vivo Phage Therapy in G. mellonella Infection Model

For in vivo studies, initially, IBEC40 (non-specific for *E. coli* CFT073) and IBEC 77 (specific) were selected to determine the efficiency of endotoxin removal on the survival of *G. mellonella* larvae at 10^3 and 10^5 PFU concentrations. Later, following confirmation of endotoxin removal and toxicity for each phage, they were tested against a high-biofilm-producing *E. coli* CFT073 strain at the different host and phage concentrations. Effective phage and host concentration for prolonged survival was determined compared to the *E. coli* CFT073 strain alone in *G. mellonella* larvae.

It was observed that out of the two phages used for the in vivo experiments, IBEC 40 was not cross-infective towards the *E. coli* CFT073 strain. Similarly, endotoxin removal was successfully achieved to determine the effective survival rate in the *G. mellonella* infection model as per the Moya-Andérico protocol, as shown in Figure 6 [50]. It was observed that the *E. coli* CFT073 strain alone was toxic to *G. mellonella* larvae at a concentration of 4.3×10^5 CFU and above (data not shown). Since IBEC 77 phage and IBEC 40 were not toxic to the *G. mellonella* larvae alone at 1×10^3–10^5 PFU concentration for over 48 h (Figure 6A), this phage stock was used for further in vivo phage therapy experiments. The effective survival of *G. mellonella* larvae was increased significantly for phage-treated larvae compared to the bacterial host alone, as shown in Figure 6B. For *E. coli* CFT073, the time where 50% of larvae had already died was 22 h. In the case of IBEC77 (×1), this time was increased up until 38 h, while for IBEC77 (×2) it increased to 50.5 h. For IBEC40 (×1) we are talking of

28.5 h, while for IBEC40 (×2) it is reduced in this case to 23 h. Therefore, we reaffirm that the most effective phage is IBEC77, with two doses.

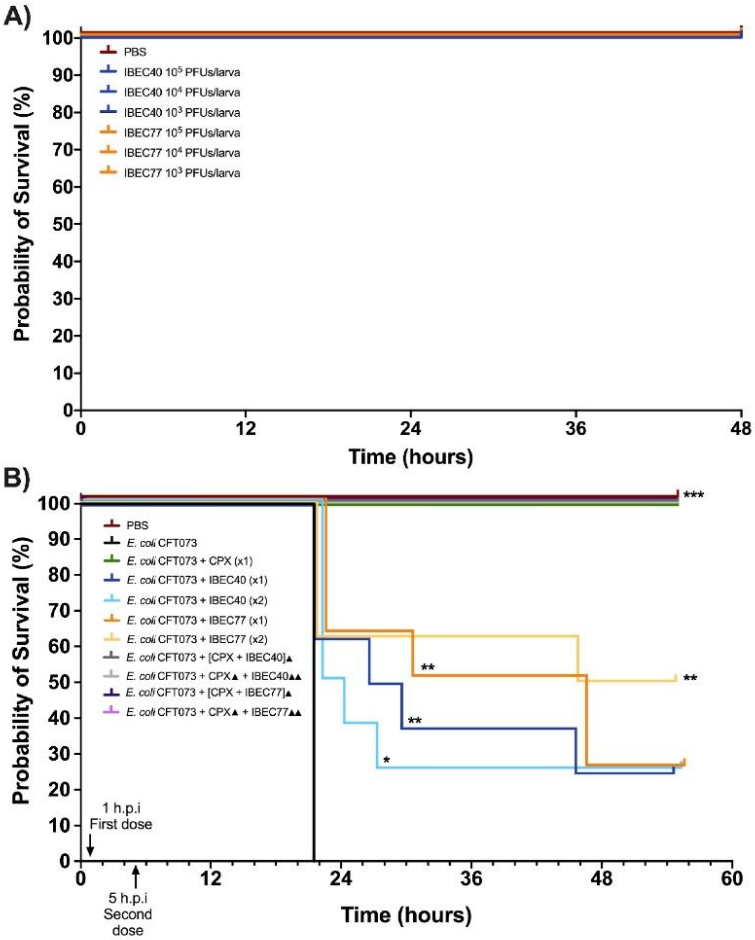

Figure 6. In vivo toxicity of *E. coli* CFT073, IBEC 40, and IBEC 77 in *G. mellonella* larvae and effective survival concentration for in vivo phage therapy. (**A**) Different concentrations of IBEC 40 and IBEC 77 phages showed no toxic effects on the survival of *G. mellonella* larvae over 48 h of inoculation. (**B**) Survival curve of *G. mellonella* larvae with effective concentrations of *E. coli* CFT073 and IBEC 40 and IBEC 77 phages alone and in different combinations with ciprofloxacin (20 mg/kg larva) for studying the prolongation of larvae survival, compared with the bacterial host strain alone. For the individual treatments of phages, the clarification x1 indicates one dose at 1 h post-infection (h.p.i) and the clarification ×2 indicates two doses (the first dose at 1 h.p.i and the second dose at 5 h.p.i). In the combined treatments of phages with the antibiotic, the ▲ clarification in the legend indicates one dose at 1 h.p.i and ▲▲ indicates 2 h.p.i. Larvae were monitored up until 55 h after inoculation. Graphs were plotted with GraphPad Prism version 9.0. Statistically significant differences (* $p < 0.05$, ** $p < 0.01$, *** $p < 0.001$) between all treatments and the *E. coli* CFT073 were determined with GraphPad Prism version 9.0, by using the Long-rank test and Gehan–Breslow–Wilcoxon test.

After validating the effect of non-specific phage IBEC 40 by a significant reduction in thickness and biomass in the in-flow biofilm experiment and demonstrating the anti-biofilm activity of naturally available phage-bound depolymerases (acting as natural enzyme-phage bioconjugates), we aimed to evaluate if the efficiency of phage therapy can be improved through the synergistic effect of phage–antibiotic combinations. Therefore, we tested the IBEC 40 and IBEC 77 phages in combination with ciprofloxacin antibiotic against the high-biofilm-producing *E. coli* CFT073 strain in vivo. It was observed that the combination of both ciprofloxacin with the phages (IBEC 40 or IBEC 77) in all tested possibilities (see Section 2.10 and Figure 6B) improves *G. mellonella* survival as 100% of larvae survived for the 55 h that were monitored. However, ciprofloxacin on its own already maintains 100% larva survival. For future studies, new treatment combinations with lower doses of antibiotics and higher phage concentration should be tested.

4. Discussion

Considering the importance of alternatives for multi-drug-resistant pathogens and increasing interest in the development of effective in vivo phage therapy approaches, we have reported some of the critical factors limiting phage therapies for in vivo applications. In the last few decades, phage therapy has been significantly explored as an alternative treatment option for antibiotics along with phage lysin-derived engineered peptides [56] as well as phage lytic enzymes [57]. Additionally, due to the newly reported studies, the internalization of phages due to the internalizing peptide available on their surface also restricts efficient applications of in vivo phage therapies [58] and for various clinical applications, including phage therapy in cancer patients [59,60].

Our work highlights the selection and optimization of phages for in vivo phage therapeutic applications. We demonstrated this by isolating effective phages from different sources, including urine, sputum, and sewage, against biofilm-forming selective uropathogenic and invasive biofilm-forming *E. coli* strains, namely *E. coli* CFT073, *E. coli* LF82, and *E. coli* MG1655. We classified the biofilm-forming potential of these selected strains into strong, moderate, and weak as per Stepanović et al. [48], and based on plaque morphology, we selected IBEC 36, IBEC 40, IBEC 48, and IBEC 77 as the candidate phages for further studies. The selection was also based on the specific properties of selected phages, such as the clear and double-layered bull-eyed plaque formation observed for IBEC 40 and IBEC 77. Since this is an indication of depolymerase activity associated with phages, they were considered to be potentially most effective against biofilm-producing pathogens. As biofilms are barriers to bacteriophage therapy and biofilm aging further hinders phage lytic activity as reported previously [34], our work validates that the phages which demonstrate plaque depolymerase activity with high burst size are effective candidates for biofilm disruption as well as infection therapy as observed from our in vitro as well as in vivo experiments with IBEC 40 and IBEC 77 against stronger biofilm-forming host *E. coli* CFT073.

The importance of plaque morphology in the selection of phages for in vivo applications is less well known. The use of phages for in vivo applications, e.g., to treat bacterial infections in animals or humans, requires a detailed understanding of the plaque morphology of the phages used. This is because plaque morphology can provide important information about the virulence and efficacy of phages, as well as their potential for adverse effects, as observed in our in vivo studies with *G. mellonella* larvae.

Clear plaques are generally considered the most desirable for in vivo applications because they are formed by virulent phages that efficiently lyse bacterial cells, which can lead to rapid clearance of infection [61], but the double-layered/bull-eyed morphology of phages is less explored for phage therapies. It should be noted that in vivo applications of phages are still being explored in a controlled manner and there are many unknowns regarding their safety and efficacy as therapeutic agents. It is also important to note that the criteria for selecting phages suitable for in vivo applications are not limited to plaque

morphology [62]; other factors such as host range, specificity, stability, and survivability in the host environment must also be considered [61].

To avoid false-positive and false-negative results during in vivo studies [63], endotoxins were eliminated from purified and enriched phages. For this, the endotoxin levels were kept far below 0.05 EU/mL for the concentrated phages, which were further diluted with the help of sterilized phosphate buffer (or any suitable buffer and/or water) to eliminate any traces of detectable endotoxins (if present). Since Gram-negative bacterial pathogens are reported to constitute most of the endotoxins, which are even associated with phages following enrichment, endotoxin removal is a mandatory step for successful phage therapies in clinical settings [64]. It is known that even after successful phage therapies against Gram-negative bacterial pathogens, endotoxins are released and are responsible for instigating pro-inflammatory and infusion-related reactions (i.e., hypersensitivity and cytokine release syndromes) and are thus responsible for endotoxic shock. Hence, quantification of endotoxin is very crucial before the implementation of bacteriophage therapy in vitro [61], in animal models as well as in clinical settings to avoid [63–65].

Furthermore, bacterial debris and biofilms' aging can contribute significantly to the endotoxin levels following phage lytic activity, which was responsible for the instantaneous death of *G. mellonella* larvae (within a few minutes) based on the growing stages of *E. coli* host strains. Hence, it is always recommended to quantify endotoxins depending upon the Gram-negative bacterial pathogen responsible for their production, as in the case of *E. coli* strains, which are already reported to produce varying lipopolysaccharide (LPS) complexes in their outer membrane by responding to the factors hindering viability [66–68]. Biofilms account for over 80% of human chronic infections and provide resistance against antibiotics and immune response, as they help avoid phagocytosis [1,2]. Since phages and their enzymes are reported to be effective antibiofilm agents [34], phages showing depolymerase activities as reported in this study seem to be a good alternative for biofilm dispersal and antibacterial potential. We believe the effect of phages over the biofilm is similar to the antibiotic treatment by eliminating the bacterial cells located on the biofilm surfaces to produce clear zones in the extracellular biofilm matrix that increase their cell removal in the overall structure.

Both IBEC 40 and IBEC 77 bacteriophages have a positive effect in the treatment of infected *G. mellonella* larvae with the uropathogenic strain *E. coli* CFT073 as they significantly increase the survival of larvae in comparison with the larvae only infected with the bacteria. An interesting fact was the complete and quick melanization of all infected larvae, mainly due to the high bacterial dose of infection. Thus, infected larvae were also more compromised as more doses (which means more punctures) were received. For this, two doses did not always give better results than one single dose. Previously, we had already tested these therapies with three doses (data not shown), but the same phenomena occurred.

Although these phages alone cannot completely avoid larvae mortality, excellent results were obtained with the different combinations of the phages with ciprofloxacin, as it resulted in the total survival of larvae. Being in the spotlight, phage therapy is, therefore, a promising approach. However, further in vivo studies are necessary to understand the synergistic effects of phage-antibiotics treatment therapies to know their effects on biofilm-producing Gram-negative bacterial pathogens for biofilm dispersal and eradication of infections.

5. Conclusions

Clinically isolated bacteriophages IBEC40 and IBEC77 demonstrated efficient removal of biofilm produced by *E. coli* CFT073 strain during in vitro in-flow biofilm, and they also showed prolonged survival in *G. mellonella* larvae after 55 h. Our work demonstrates that bacteriophages with high burst size and depolymerase activity can be a good alternative for treating uropathogenic and invasive biofilm-forming *E. coli* pathogens. Further studies are necessary to understand if the efficiency of phage therapy in vivo in biofilm-producing

bacterial pathogens can be improved synergistically in combination with antibiotics. Additionally, in line with our hypothesis, phage-bound enzymes must be explored for their antibiofilm as well as antibacterial activity irrespective of their specificity towards their hosts.

Supplementary Materials: The following supporting information can be downloaded at: https://www.mdpi.com/article/10.3390/cells12030344/s1, Figure S1: The cross-infectivity of selected clinically isolated phages against *E. coli* CFT073 biofilm-producing strain used for in vitro and in vivo studies in *Galleria mellonella*. Only IBEC77 shows lytic activity against the *E. coli* CFT073 strain; Figure S2: The plaque morphology of (A) IBEC 36, (B) IBEC 40, (C) IBEC 48, and (D) IBEC 77 isolated from clinical samples against *E. coli* LF82 (IBEC 36), *E. coli* MG1655 (IBEC 40 and IBEC 48), *E. coli* CFT073 (IBEC 77) biofilm-producing strain and used for in vitro and in vivo studies in *Galleria mellonella*; Figure S3: The control for scanning electron microscopy for phage uninfected *E. coli* LF82, *E. coli* MG1655, and *E. coli* CFT073 biofilm-producing strain.

Author Contributions: S.G.S. and E.T. designed the study. S.G.S., L.M.-A., J.A., B.V.A.-J. and N.B.-C. conducted most of the experiments and analyses. All authors analyzed the data, wrote the paper, and read and approved the final version. E.T. supervised the project. All authors have read and agreed to the published version of the manuscript.

Funding: This work is funded by the European Commission under Horizon 2020's Marie Skłodowska Curie Actions COFUND scheme (Grant Agreement No. 712754) and by the Severo Ochoa program of the Spanish Ministry of Science and Competitiveness (SEV-2014-0425 (2015–2019). ET was supported by grants from the Ministerio de Economia, Industria y Competitividad (MINECO), and Agencia Estatal de Investigación (AEI), Spain, co-funded by Fondo Europeo de Desarrollo Regional (FEDER), European Union (RTI2018-098573-B-100, PID2021-125801OB-100 and PDC2022-133577-I00), the CERCA program and AGAUR-Generalitat de Catalunya (2017SGR-1079), the European Regional Development Fund (FEDER), Catalan Cystic Fibrosis Federation, and Obra Social "La Caixa". JA is thankful to Generalitat de Catalunya, for its financial support through the FI program (2021FI_B00118). BVA-J is thankful to La Caixa Foundation (ID 100010434) for its Ph.D. grant (LCF/BQ/DI20/11780040).

Institutional Review Board Statement: The study approved by the Ethic Committee at the Vall d'Hebrón hospital (protocol code PR(AG)275/2019).

Informed Consent Statement: Not applicable.

Data Availability Statement: Data is contained within the article or Supplementary Material. The data presented in this study are available in the article or Supplementary Material.

Acknowledgments: This article represents part of an MSCA-COFUND-funded work awarded to S.G.S. at the Institute for Bioengineering of Catalonia (IBEC), Barcelona, Spain. We thank the European Commission under Horizon 2020's Marie Skłodowska Curie Actions COFUND scheme for the financial support received (Grant Agreement No. 712754). The authors also would like to thank Darren Smith and Adnan Tariq for the phage genome sequencing at NU-OMICS DNA-Sequencing research facility, Northumbria University, Newcastle upon Tyne, NE1 8ST.

Conflicts of Interest: The authors declare that there is no conflict of interest regarding the publication of this paper.

References

1. Sharma, D.; Misba, L.; Khan, A.U. Antibiotics versus biofilm: An emerging battleground in microbial communities. *Antimicrob. Resist. Infect. Control* **2019**, *8*, 76. [CrossRef]
2. Sharma, G.; Sharma, S.; Sharma, P.; Chandola, D.; Dang, S.; Gupta, S.; Gabrani, R. *Escherichia coli* biofilm: Development and therapeutic strategies. *J. Appl. Microbiol.* **2016**, *121*, 309–319. [CrossRef] [PubMed]
3. Ito, A.; Taniuchi, A.; May, T.; Kawata, K.; Okabe, S. Increased Antibiotic Resistance of *Escherichia coli* in Mature Biofilms. *Appl. Environ. Microbiol.* **2009**, *75*, 4093–4100. [CrossRef] [PubMed]
4. Sanchez-Vizuete, P.; Orgaz, B.; Aymerich, S.; Le Coq, D.; Briandet, R. Pathogens protection against the action of disinfectants in multispecies biofilms. *Front. Microbiol.* **2015**, *6*, 705. [CrossRef] [PubMed]

5. Chen, X.P.; Ali, L.; Wu, L.-Y.; Liu, C.; Gang, C.X.; Huang, Q.F.; Ruan, J.H.; Bao, S.Y.; Rao, Y.P.; Yu, D. Biofilm Formation Plays a Role in the Formation of Multidrug-Resistant Escherichia coli Toward Nutrients in Microcosm Experiments. *Front. Microbiol.* **2018**, *9*, 367. [CrossRef]
6. Farkas, A.; Crăciunaș, C.; Chiriac, C.; Szekeres, E.; Coman, C.; Butiuc-Keul, A. Exploring the Role of Coliform Bacteria in Class 1 Integron Carriage and Biofilm Formation During Drinking Water Treatment. *Microb. Ecol.* **2016**, *72*, 773–782. [CrossRef]
7. Luterbach, C.L.; Forsyth, V.S.; Engstrom, M.D.; Mobley, H.L.T. TosR-Mediated Regulation of Adhesins and Biofilm Formation in Uropathogenic Escherichia coli. *Msphere* **2018**, *3*, e00222-18. [CrossRef]
8. Kaper, J.B.; Nataro, J.P.; Mobley, H.L.T. Pathogenic Escherichia coli. *Nat. Rev. Microbiol.* **2004**, *2*, 123–140. [CrossRef]
9. Hancock, V.; Witsø, I.L.; Klemm, P. Biofilm formation as a function of adhesin, growth medium, substratum and strain type. *Int. J. Med. Microbiol.* **2011**, *301*, 570–576. [CrossRef]
10. Mulvey, M.A.; Schilling, J.D.; Hultgren, S.J. Establishment of a Persistent *Escherichia coli* Reservoir during the Acute Phase of a Bladder Infection. *Infect. Immun.* **2001**, *69*, 4572–4579. [CrossRef]
11. Anderson, G.G.; Palermo, J.J.; Schilling, J.D.; Roth, R.; Heuser, J.; Hultgren, S.J. Intracellular Bacterial Biofilm-Like Pods in Urinary Tract Infections. *Science* **2003**, *301*, 105–107. [CrossRef] [PubMed]
12. Chervy, M.; Barnich, N.; Denizot, J. Adherent-invasive *E. coli*: Update on the lifestyle of a troublemaker in Crohn's disease. *Int. J. Mol. Sci.* **2020**, *21*, 3734. [CrossRef] [PubMed]
13. Bringer, M.A.; Billard, E.; Glasser, A.L.; Colombel, J.F.; Darfeuille-Michaud, A. Replication of Crohn's disease-associated AIEC within macrophages is dependent on TNF-α secretion. *Lab. Investig.* **2012**, *92*, 411–419. [CrossRef] [PubMed]
14. Prudent, V.; Demarre, G.; Vazeille, E.; Wery, M.; Quenech'Du, N.; Ravet, A.; Dauverd-Girault, J.; van Dijk, E.; Bringer, M.A.; Descrimes, M.; et al. The Crohn's disease-related bacterial strain LF82 assembles biofilm-like communities to protect itself from phagolysosomal attack. *Commun. Biol.* **2021**, *4*, 627. [CrossRef] [PubMed]
15. Ghigo, J.-M. Natural conjugative plasmids induce bacterial biofilm development. *Nature* **2001**, *412*, 442–445. [CrossRef] [PubMed]
16. Reisner, A.; Krogfelt, K.A.; Klein, B.M.; Zechner, E.L.; Molin, S. In Vitro Biofilm Formation of Commensal and Pathogenic *Escherichia coli* Strains: Impact of Environmental and Genetic Factors. *J. Bacteriol.* **2006**, *188*, 3572–3581. [CrossRef]
17. Michiels, J.E.; Bergh, B.V.D.; Verstraeten, N.; Michiels, J. Molecular mechanisms and clinical implications of bacterial persistence. *Drug Resist. Updat.* **2016**, *29*, 76–89. [CrossRef]
18. Seed, K.D.; Dennis, J.J. Experimental Bacteriophage Therapy Increases Survival of *Galleria mellonella* Larvae Infected with Clinically Relevant Strains of the *Burkholderia cepacia* Complex. *Antimicrob. Agents Chemother.* **2009**, *53*, 2205–2208. [CrossRef]
19. Abedon, S.T.; Kuhl, S.J.; Blasdel, B.G.; Kutter, E.M. Phage treatment of human infections. *Bacteriophage* **2011**, *1*, 66–85. [CrossRef]
20. Vahedi, A.; Dallal, M.M.S.; Douraghi, M.; Nikkhahi, F.; Rajabi, Z.; Yousefi, M.; Mousavi, M. Isolation and identification of specific bacteriophage against enteropathogenic Escherichia coli (EPEC) and in vitro and in vivo characterization of bacteriophage. *FEMS Microbiol. Lett.* **2018**, *365*, fny136. [CrossRef] [PubMed]
21. Dedrick, R.M.; Guerrero-Bustamante, C.A.; Garlena, R.A.; Russell, D.A.; Ford, K.; Harris, K.; Gilmour, K.C.; Soothill, J.; Jacobs-Sera, D.; Schooley, R.T.; et al. Engineered bacteriophages for treatment of a patient with a disseminated drug-resistant Mycobacterium abscessus. *Nat. Med.* **2019**, *25*, 730–733. [CrossRef] [PubMed]
22. Pallavali, R.R.; Degati, V.L.; Narala, V.R.; Velpula, K.K.; Yenugu, S.; Durbaka, V.R.P. Lytic Bacteriophages Against Bacterial Biofilms Formed by Multidrug-Resistant *Pseudomonas aeruginosa*, *Escherichia coli*, *Klebsiella pneumoniae*, and *Staphylococcus aureus* Isolated from Burn Wounds. *Phage* **2021**, *2*, 120–130. [CrossRef] [PubMed]
23. Flores-Mireles, A.L.; Walker, J.N.; Caparon, M.; Hultgren, S.J. Urinary tract infections: Epidemiology, mechanisms of infection and treatment options. *Nat. Rev. Microbiol.* **2015**, *13*, 269–284. [CrossRef] [PubMed]
24. Öztürk, R.; Murt, A. Epidemiology of urological infections: A global burden. *World J. Urol.* **2020**, *38*, 2669–2679. [CrossRef] [PubMed]
25. Katongole, P.; Nalubega, F.; Florence, N.C.; Asiimwe, B.; Andia, I. Biofilm formation, antimicrobial susceptibility and virulence genes of Uropathogenic Escherichia coli isolated from clinical isolates in Uganda. *BMC Infect. Dis.* **2020**, *20*, 453. [CrossRef] [PubMed]
26. Xavier, R.J.; Podolsky, D.K. Unravelling the pathogenesis of inflammatory bowel disease. *Nature* **2007**, *448*, 427–434. [CrossRef]
27. Frank, D.N.; St Amand, A.L.; Feldman, R.A.; Boedeker, E.C.; Harpaz, N.; Pace, N.R. Molecular-phylogenetic characterization of microbial community imbalances in human inflammatory bowel diseases. *Proc. Natl. Acad. Sci. USA* **2007**, *104*, 13780–13785. [CrossRef]
28. Kaur, N.; Chen, C.-C.; Luther, J.; Kao, J.Y. Intestinal dysbiosis in inflammatory bowel disease. *Gut Microbes* **2011**, *2*, 211–216. [CrossRef]
29. Barillova, P.; Tchesnokova, V.; Dübbers, A.; Küster, P.; Peters, G.; Dobrindt, U.; Sokurenko, E.V.; Kahl, B.C. Prevalence and persistence of *Escherichia coli* in the airways of cystic fibrosis patients—An unrecognized CF pathogen? *Int. J. Med. Microbiol.* **2014**, *304*, 415–421. [CrossRef]
30. Edwards, B.; Greysson-Wong, J.; Somayaji, R.; Waddell, B.; Storey, D.; Surette, M.; Rabin, H.; Parkins, M. 1481. Clinical Outcomes of Escherichia coli Infections in Cystic Fibrosis (CF) Patients. *Open Forum Infect. Dis.* **2018**, *5* (Suppl. 1), S458. [CrossRef]
31. Edwards, B.D.; Somayaji, R.; Greysson-Wong, J.; Izydorczyk, C.; Waddell, B.; Storey, D.G.; Rabin, H.R.; Surette, M.G.; Parkins, M.D. Clinical Outcomes Associated with Escherichia coli Infections in Adults with Cystic Fibrosis: A Cohort Study. *Open Forum Infect. Dis.* **2019**, *7*, ofz476. [CrossRef] [PubMed]

32. Izydorczyk, C.; Waddell, B.; Edwards, B.D.; Greysson-Wong, J.; Surette, M.G.; Somayaji, R.; Rabin, H.R.; Conly, J.M.; Church, D.L.; Parkins, M.D. Epidemiology of E. coli in Cystic Fibrosis Airways Demonstrates the Capacity for Persistent Infection but Not Patient-Patient Transmission. *Front. Microbiol.* **2020**, *11*, 475. [CrossRef] [PubMed]
33. Available online: https://www.who.int/news-room/fact-sheets/detail/antimicrobial-resistance (accessed on 30 June 2022).
34. Ferriol-González, C.; Domingo-Calap, P. Phages for Biofilm Removal. *Antibiotics* **2020**, *9*, 268. [CrossRef] [PubMed]
35. Vandenheuvel, D.; Lavigne, R.; Brüssow, H. Bacteriophage Therapy: Advances in Formulation Strategies and Human Clinical Trials. *Annu. Rev. Virol.* **2015**, *2*, 599–618. [CrossRef]
36. Voelker, R. FDA Approves Bacteriophage Trial. *JAMA* **2019**, *321*, 638. [CrossRef] [PubMed]
37. Brives, C.; Pourraz, J. Phage therapy as a potential solution in the fight against AMR: Obstacles and possible futures. *Palgrave Commun.* **2020**, *6*, 100. [CrossRef]
38. Dreux, N.; Cendra, M.D.M.; Massier, S.; Darfeuille-Michaud, A.; Barnich, N.; Torrents, E. Ribonucleotide Reductase NrdR as a Novel Regulator for Motility and Chemotaxis during Adherent-Invasive Escherichia coli Infection. *Infect. Immun.* **2015**, *83*, 1305–1317. [CrossRef]
39. Khairnar, K.; Raut, M.P.; Chandekar, R.H.; Sanmukh, S.G.; Paunikar, W.N. Novel bacteriophage therapy for controlling metallo-beta-lactamase producing Pseudomonas aeruginosa infection in Catfish. *BMC Vet. Res.* **2013**, *9*, 264. [CrossRef]
40. Lillehaug, D. An improved plaque assay for poor plaque-producing temperate lactococcal bacteriophages. *J. Appl. Microbiol.* **1997**, *83*, 85–90. [CrossRef]
41. Khairnar, K.; Sanmukh, S.; Chandekar, R.; Paunikar, W. A simple and novel modification of comet assay for determination of bacteriophage mediated bacterial cell lysis. *J. Virol. Methods* **2014**, *203*, 33–38. [CrossRef]
42. Yazdi, M.; Bouzari, M.; Ghaemi, E.A.; Shahin, K. Isolation, Characterization and Genomic Analysis of a Novel Bacteriophage VB_EcoS-Golestan Infecting Multidrug-Resistant Escherichia coli Isolated from Urinary Tract Infection. *Sci. Rep.* **2020**, *10*, 7690. [CrossRef] [PubMed]
43. Sayers, J.R.; Eckstein, F. Properties of overexpressed phage T5 D15 exonuclease. Similarities with *Escherichia coli* DNA polymerase I 5′-3′ exonuclease. *J. Biol. Chem.* **1990**, *265*, 18311–18317. [CrossRef] [PubMed]
44. Bonilla, N.; Rojas, M.I.; Cruz, G.N.F.; Hung, S.-H.; Rohwer, F.; Barr, J.J. Phage on tap–a quick and efficient protocol for the preparation of bacteriophage laboratory stocks. *Peerj* **2016**, *4*, e2261. [CrossRef] [PubMed]
45. Luong, T.; Salabarria, A.-C.; Edwards, R.A.; Roach, D.R. Standardized bacteriophage purification for personalized phage therapy. *Nat. Protoc.* **2020**, *15*, 2867–2890. [CrossRef] [PubMed]
46. Buttimer, C.; Hendrix, H.; Lucid, A.; Neve, H.; Noben, J.-P.; Franz, C.; O'Mahony, J.; Lavigne, R.; Coffey, A. Novel N4-Like Bacteriophages of Pectobacterium atrosepticum. *Pharmaceuticals* **2018**, *11*, 45. [CrossRef]
47. Milho, C.; Silva, M.D.; Alves, D.; Oliveira, H.; Sousa, C.; Pastrana, L.M.; Azeredo, J.; Sillankorva, S. Escherichia coli and Salmonella Enteritidis dual-species biofilms: Interspecies interactions and antibiofilm efficacy of phages. *Sci. Rep.* **2019**, *9*, 18183. [CrossRef] [PubMed]
48. Stepanović, S.; Vuković, D.; Dakić, I.; Savić, B.; Švabić-Vlahović, M. A modified microtiter-plate test for quantification of staphylococcal biofilm formation. *J. Microbiol. Methods* **2000**, *40*, 175–179. [CrossRef]
49. Vilela, D.; Blanco-Cabra, N.; Eguskiza, A.; Hortelao, A.C.; Torrents, E.; Sanchez, S. Drug-Free Enzyme-Based Bactericidal Nanomotors against Pathogenic Bacteria. *ACS Appl. Mater. Interfaces* **2021**, *13*, 14964–14973. [CrossRef]
50. Moya-Andérico, L.; Admella, J.; Torrents, E. A clearing protocol for Galleria mellonella larvae: Visualization of internalized fluorescent nanoparticles. *New Biotechnol.* **2020**, *60*, 20–26. [CrossRef]
51. Aperis, G.; Fuchs, B.B.; Anderson, C.A.; Warner, J.E.; Calderwood, S.B.; Mylonakis, E. Galleria mellonella as a model host to study infection by the Francisella tularensis live vaccine strain. *Microbes Infect.* **2007**, *9*, 729–734. [CrossRef]
52. Thomas, R.J.; Hamblin, K.A.; Armstrong, S.J.; Müller, C.M.; Bokori-Brown, M.; Goldman, S.; Atkins, H.S.; Titball, R.W. Galleria mellonella as a model system to test the pharmacokinetics and efficacy of antibiotics against Burkholderia pseudomallei. *Int. J. Antimicrob. Agents* **2013**, *41*, 330–336. [CrossRef] [PubMed]
53. Gutiérrez, D.; Briers, Y.; Rodríguez-Rubio, L.; Martínez, B.; Rodríguez, A.; Lavigne, R.; García, P. Role of the Pre-neck Appendage Protein (Dpo7) from Phage vB_SepiS-phiIPLA7 as an Anti-biofilm Agent in Staphylococcal Species. *Front. Microbiol.* **2015**, *6*, 1315. [CrossRef] [PubMed]
54. Guo, Z.; Huang, J.; Yan, G.; Lei, L.; Wang, S.; Yu, L.; Zhou, L.; Gao, A.; Feng, X.; Han, W. Identification and Characterization of Dpo42, a Novel Depolymerase Derived from the Escherichia coli Phage vB_EcoM_ECOO78. *Front. Microbiol.* **2017**, *8*, 1460. [CrossRef] [PubMed]
55. Knecht, L.E.; Veljkovic, M.; Fieseler, L. Diversity and Function of Phage Encoded Depolymerases. *Front. Microbiol.* **2020**, *10*, 2949. [CrossRef] [PubMed]
56. Thandar, M.; Lood, R.; Winer, B.Y.; Deutsch, D.R.; Euler, C.W.; Fischetti, V.A. Novel Engineered Peptides of a Phage Lysin as Effective Antimicrobials against Multidrug-Resistant Acinetobacter baumannii. *Antimicrob. Agents Chemother.* **2016**, *60*, 2671–2679. [CrossRef]
57. Abdelrahman, F.; Easwaran, M.; Daramola, O.I.; Ragab, S.; Lynch, S.; Oduselu, T.J.; Khan, F.M.; Ayobami, A.; Adnan, F.; Torrents, E.; et al. Phage-Encoded Endolysins. *Antibiotics* **2021**, *10*, 124. [CrossRef]

58. Bichet, M.C.; Chin, W.H.; Richards, W.; Lin, Y.-W.; Avellaneda-Franco, L.; Hernandez, C.A.; Oddo, A.; Chernyavskiy, O.; Hilsenstein, V.; Neild, A.; et al. Bacteriophage uptake by mammalian cell layers represents a potential sink that may impact phage therapy. *Iscience* **2021**, *24*, 102287. [CrossRef]
59. Sanmukh, S.G.; dos Santos, N.J.; Barquilha, C.N.; Cucielo, M.S.; de Carvalho, M.; dos Reis, P.P.; Delella, F.K.; Carvalho, H.F.; Felisbino, S.L. Bacteriophages M13 and T4 Increase the Expression of Anchorage-Dependent Survival Pathway Genes and Down Regulate Androgen Receptor Expression in LNCaP Prostate Cell Line. *Viruses* **2021**, *13*, 1754. [CrossRef]
60. Sanmukh, S.G.; Santos, N.J.; Barquilha, C.N.; dos Santos, S.A.A.; Duran, B.O.S.; Delella, F.K.; Moroz, A.; Justulin, L.A.; Carvalho, H.F.; Felisbino, S.L. Exposure to Bacteriophages T4 and M13 Increases Integrin Gene Expression and Impairs Migration of Human PC-3 Prostate Cancer Cells. *Antibiotics* **2021**, *10*, 1202. [CrossRef]
61. Khan Mirzaei, M.; Nilsson, A.S. Isolation of phages for phage therapy: A comparison of spot tests and efficiency of plating analyses for determination of host range and efficacy. *PLoS ONE* **2015**, *10*, e0118557. [CrossRef]
62. Ramesh, N.; Archana, L.; Madurantakam Royam, M.; Manohar, P.; Eniyan, K. Effect of various bacteriological media on the plaque morphology of Staphylococcus and Vibrio phages. *Access Microbiol.* **2019**, *1*, e000036. [CrossRef] [PubMed]
63. Suh, G.A.; Lodise, T.P.; Tamma, P.D.; Knisely, J.M.; Alexander, J.; Aslam, S.; Barton, K.D.; Bizzell, E.; Totten, K.M.C.; Campbell, J.L.; et al. Considerations for the Use of Phage Therapy in Clinical Practice. *Antimicrob. Agents Chemother.* **2022**, *66*, e0207121. [CrossRef] [PubMed]
64. Liu, S.; Tobias, R.; McClure, S.; Styba, G.; Shi, Q.; Jackowski, G. Removal of Endotoxin from Recombinant Protein Preparations. *Clin. Biochem.* **1997**, *30*, 455–463. [CrossRef] [PubMed]
65. Liu, D.; Van Belleghem, J.D.; de Vries, C.R.; Burgener, E.; Chen, Q.; Manasherob, R.; Aronson, J.R.; Amanatullah, D.F.; Tamma, P.D.; Suh, G.A. The Safety and Toxicity of Phage Therapy: A Review of Animal and Clinical Studies. *Viruses* **2021**, *13*, 1268. [CrossRef] [PubMed]
66. Klein, G.; Raina, S. Regulated Assembly of LPS, Its Structural Alterations and Cellular Response to LPS Defects. *Int. J. Mol. Sci.* **2019**, *20*, 356. [CrossRef]
67. Klein, G.; Wieczorek, A.; Szuster, M.; Raina, S. Checkpoints That Regulate Balanced Biosynthesis of Lipopolysaccharide and Its Essentiality in *Escherichia coli*. *Int. J. Mol. Sci.* **2021**, *23*, 189. [CrossRef] [PubMed]
68. Tyulenev, A.V.; Smirnova, G.V.; Muzyka, N.G.; Oktyabrsky, O.N. Study of the early response of Escherichia coli lpcA and ompF mutants to ciprofloxacin. *Res. Microbiol.* **2022**, *173*, 103954. [CrossRef]

Material Suplementario

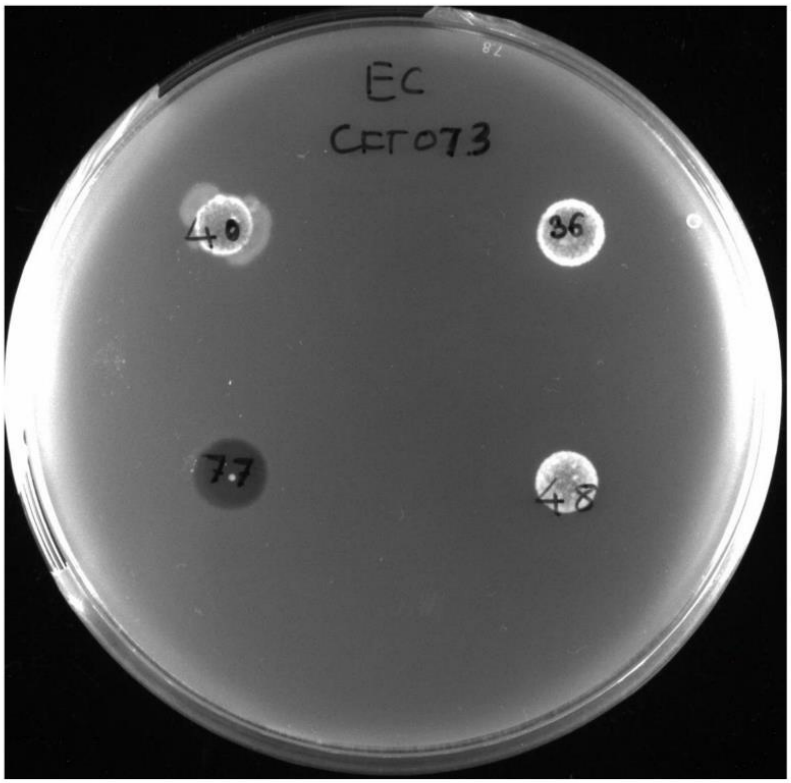

Figure S1. The cross-infectivity of selected clinically isolated phages against *E. coli* CFT073 biofilm-producing strain used for *in vitro* and *in vivo* studies in *Galleria mellonella*. Only IBEC77 shows lytic activity against the *E. coli* CFT073 strain.

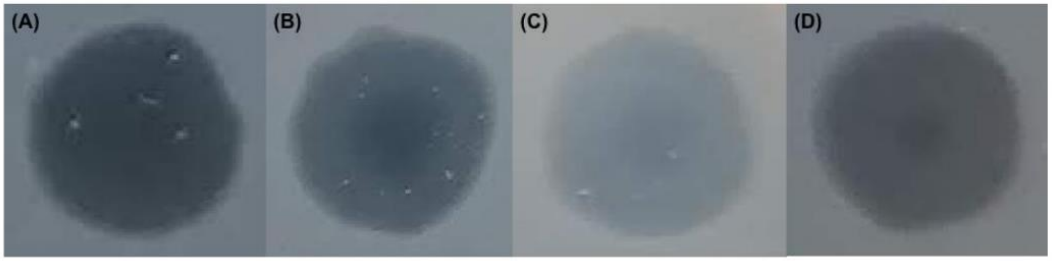

Figure S2. The plaque morphology of (A) IBEC 36, (B) IBEC 40, (C) IBEC 48, and (D) IBEC 77 isolated from clinical samples against *E. coli* LF82 (IBEC 36), *E. coli* MG1655 (IBEC 40 and IBEC 48), *E. coli* CFT073 (IBEC 77) biofilm-producing strain and used for *in vitro* and *in vivo* studies in *Galleria mellonella*.

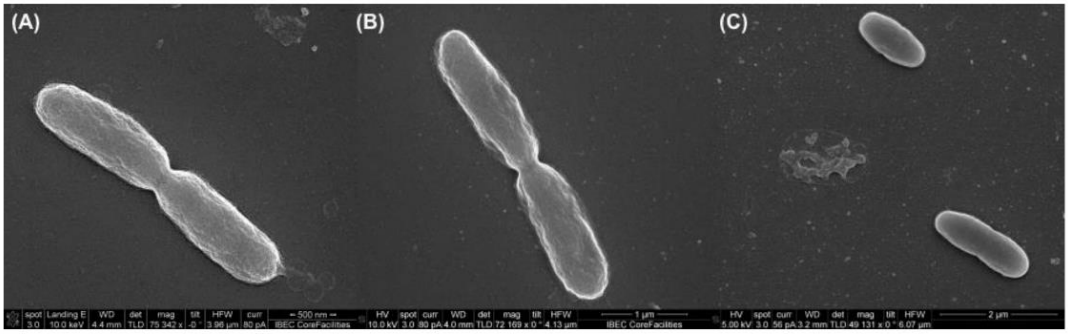

Figure S3. The control for scanning electron microscopy for phage uninfected (A) *E. coli* LF82, (B) *E. coli* MG1655, and (C) *E. coli* CFT073 biofilm-producing strain.

Artículo de Revisión (publicación)

Nanomedicine against biofilm infections: A roadmap of challenges and limitations

Publicado en la revista *Wiley Interdisciplinary Reviews: Nanomedicine and Nanobiotechnology*

DOI: 10.1002/wnan.1944

25 de febrero de 2024

Categoría Nanociencia y nanotecnología 2023: 1er tercil, 1er Cuartil, IF= 6.9

Núria Blanco-Cabra[1,2], Júlia Alcàcer-Almansa[1,2†], Joana Admella[1,2†], Betsy V. Arévalo-Jaimes[1,2†] and Eduard Torrents[1,2]

[1]Grupo Infecciones Bacterianas y Terapias Antimicrobianas (BIAT), Instituto de Bioingeniería de Cataluña (IBEC), Barcelona, España.
[2]Sección de Microbiología, Departamento de Genética, Microbiología y Estadística, Facultad de Biología, Universitat de Barcelona, Barcelona, España.

[†]Estos tres autores, citados en orden alfabético, contribuyeron de forma equitativa en este trabajo

Cita: Blanco-Cabra, N., Alcàcer-Almansa, J., Admella, J., Arévalo-Jaimes, B. V., & Torrents, E. (2024). Nanomedicine against biofilm infections: A roadmap of challenges and limitations. *Wiley Interdiscip. Rev. Nanomed. Nanobiotechnol.*, 16(1), e1944. DOI: 10.1002/wnan.1944.

Received: 18 October 2023 | Revised: 28 November 2023 | Accepted: 27 January 2024

DOI: 10.1002/wnan.1944

ADVANCED REVIEW

WIREs NANOMEDICINE AND NANOBIOTECHNOLOGY WILEY

Nanomedicine against biofilm infections: A roadmap of challenges and limitations

Núria Blanco-Cabra[1,2] | **Júlia Alcàcer-Almansa**[1,2] | **Joana Admella**[1,2] | **Betsy Verónica Arévalo-Jaimes**[1,2] | **Eduard Torrents**[1,2]

[1]Bacterial Infections and Antimicrobial Therapy Group (BIAT), Institute for Bioengineering of Catalonia (IBEC), The Barcelona Institute of Science and Technology (BIST), Barcelona, Spain

[2]Microbiology Section, Department of Genetics, Microbiology and Statistics, Faculty of Biology, University of Barcelona, Barcelona, Spain

Correspondence
Núria Blanco-Cabra and Eduard Torrents, Bacterial Infections and Antimicrobial Therapy Group (BIAT), Institute for Bioengineering of Catalonia (IBEC), The Barcelona Institute of Science and Technology (BIST), Barcelona, Spain.
Email: nuriablanco@ub.edu, nblanco@ibecbarcelona.eu and eduard.torrents@ub.edu, etorrents@ibecbarcelona.eu

Funding information
Departament d'Innovació, Universitats i Empresa, Generalitat de Catalunya, Grant/Award Number: 2021SGR-01545; 'la Caixa' Foundation, Grant/Award Numbers: FQxxx01, LCF/BQ/DI20/11780040; Ministerio de Ciencia e Innovación, Grant/Award Numbers: PLEC2022-009356, PDC2022-133577-I00, PID2021-125801OB-100, PRE2021-098703; European Regional Development Fund (FEDER); Catalan Cystic Fibrosis Association; European Union-Next Generation EU; Generalitat de Catalunya, Grant/Award Number: 2021FI_B00118

Edited by: Silvia Muro, Associate Editor and Gregory Lanza, Editor-in-Chief

Abstract

Microbial biofilms are complex three-dimensional structures where sessile microbes are embedded in a polymeric extracellular matrix. Their resistance toward the host immune system as well as to a diverse range of antimicrobial treatments poses a serious health and development threat, being in the top 10 global public health threats declared by the World Health Organization. In an effort to combat biofilm-related microbial infections, several strategies have been developed to independently eliminate biofilms or to complement conventional antibiotic therapies. However, their limitations leave room for other treatment alternatives, where the application of nanotechnology to biofilm eradication has gained significant relevance in recent years. Their small size, penetration efficiency, and the design flexibility that they present makes them a promising alternative for biofilm infection treatment, although they also present set-backs. This review aims to describe the main possibilities and limitations of nanomedicine against biofilms, while covering the main aspects of biofilm formation and study, and the current therapies for biofilm treatment.

This article is categorized under:

Therapeutic Approaches and Drug Discovery > Nanomedicine for Infectious Disease

Toxicology and Regulatory Issues in Nanomedicine > Toxicology of Nanomaterials

Toxicology and Regulatory Issues in Nanomedicine > Regulatory and Policy Issues in Nanomedicine

KEYWORDS

antimicrobials, bacteria, biofilm, infectious diseases, microorganisms

Capítulo de libro (publicación)

Methods for studying biofilms: Microfluidics and translation in the clinical context

Publicado en el volumen 53 Biofilms de la revista *Methods in Microbiology*

DOI: 10.1016/bs.mim.2023.04.002

30 de mayo de 2023

Júlia Alcàcer-Almansa[1,2†], Betsy V. Arévalo-Jaimes[1,2†], Núria Blanco-Cabra[1,2†] and Eduard Torrents[1,2]

[1]Grupo Infecciones Bacterianas y Terapias Antimicrobianas (BIAT), Instituto de Bioingeniería de Cataluña (IBEC), Barcelona, España.
[2]Sección de Microbiología, Departamento de Genética, Microbiología y Estadística, Facultad de Biología, Universitat de Barcelona, Barcelona, España.

[†]Estos tres autores, citados en orden alfabético, contribuyeron de forma equitativa en este trabajo

Cita: Alcàcer-Almansa, J., Arévalo-Jaimes, B. V., Blanco-Cabra, N., & Torrents, E. (2023). Methods for studying biofilms: Microfluidics and translation in the clinical context, in Methods in Microbiology. V. Gurtler and M. Patrauchan, Editors. 53, 195-233. DOI: 10.1016/bs.mim.2023.04.002.

Methods for studying biofilms: Microfluidics and translation in the clinical context

Júlia Alcàcer-Almansa[a,†], Betsy Verónica Arévalo-Jaimes[a,†], Núria Blanco-Cabra[a,b,*,†], and Eduard Torrents[a,b,*]

[a]*Bacterial Infections and Antimicrobial Therapy Group (BIAT), Institute for Bioengineering of Catalonia (IBEC), The Barcelona Institute of Science and Technology (BIST), Barcelona, Spain*
[b]*Microbiology Section, Department of Genetics, Microbiology and Statistics, Faculty of Biology, University of Barcelona, Barcelona, Spain*
[*]*Corresponding authors: e-mail address: nuriablanco@ub.edu; nblanco@ibecbarcelona.eu; etorrents@ibecbarcelona.eu; eduard.torrents@ub.edu*

Abbreviation

AMICI	Anti-Microbial Coating Innovations
ASTM	American Society for Testing and Materials
BCoD	bacterial-culture-on-disc
CBD	Calgary biofilm device
CBE	US Center for Biofilm Engineering
CDC	Centers for Disease Control
CFU	colony forming unit
CLSM	confocal laser scanning microscopy
COC	cyclo-olefin copolymer
COST	EU Cooperation in Science and Technology
eDNA	extracellular DNA
EIS	electrochemical impedance spectroscopy
EPS	exopolysaccharide matrix
hpBIOM	Human Plasma Biofilm Model
MP	microtiter plate
NBIC	National Biofilms Innovation Centre
PC	polycarbonate
PDMS	poly(dimethylsiloxane)
PJI	periprosthetic joint infections

[†]These three authors, listed in alphabetical order, contributed equally to this work.

Methods in Microbiology, ISSN 0580-9517, https://doi.org/10.1016/bs.mim.2023.04.002

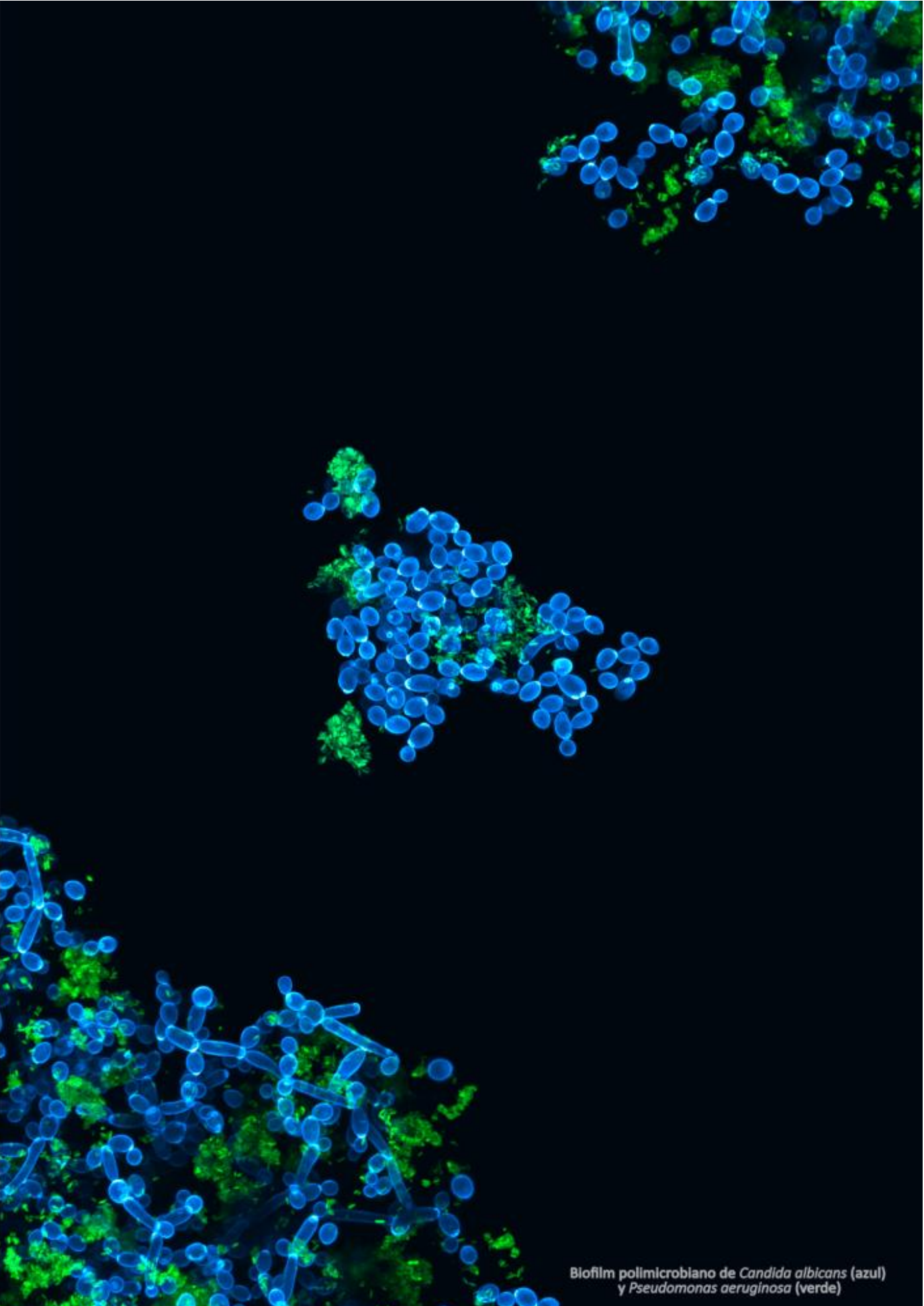

Biofilm polimicrobiano de *Candida albicans* (azul) y *Pseudomonas aeruginosa* (verde)